The Fundamental Thickening Mechanism Of Associative Polymers In Latex Systems: A Rheological Study.

Order Number 9119355

The fundamental thickening mechanism of associative polymers in latex systems: A rheological study

Jenkins, Richard D., Ph.D.

Lehigh University, 1991

U·M·I
300 N. Zeeb Rd.
Ann Arbor, MI 48106

The Fundamental Thickening Mechanism of Associative Polymers in Latex Systems: A Rheological Study

by

Richard D. Jenkins

A Dissertation

Presented to the Graduate Committee
of Lehigh University
in Candidacy for the Degree of

Doctor of Philosophy

in

Chemical Engineering

Lehigh University
October, 1990

Dedication

For my instructors, who have taught me best by example,

but especially:

Donald, who taught me self-discipline
Jeanne, who taught me patience
Gary, who taught me dignity
Mary, who taught me empathy

and

Collin, who gave me hope.

Certificate of Approval

Approved and recommended for acceptance as a dissertation in partial fulfillment of the requirements of the degree of Doctor of Philosophy.

Professor in Charge

Accepted 11/27/90

Special Committee directing the doctoral work of Richard D. Jenkins

Dr. Cesar A. Silebi, Chairman

Dr. David R. Bassett

Dr.Mohamed S. El-Aasser

Dr. Daniel C. Hong

Dr.H. Daniel Ou-Yang

Dr.John W. Vanderhoff

Acknowledgments

This dissertation represents the successful culmination of many years of hard and deliberate labour on a chemical engineering research project that would not have been possible without the efforts of many other people on my behalf.

In particular, I am indebted to Professor Cesar Silebi for his thoughtful and frank advice, and continuous encouragement during the course of this study and my graduate work. I could always count on him to help me see things from another point of view, and to foster my personal development.

I must also thank Professor Mohamed El–Aasser for his untiring efforts in support of my research. He persuaded me to attend Lehigh, provided me with the finances to stay there, and to travel extensively in the self – promotion of my work.

I am also grateful to Dr. David Bassett of Union Carbide Corporation in Charleston, West Virginia, who brought this project, and the model associative polymers, to Lehigh in the first place. His enthusiastic support of this project, as manifested in financing our annual associative polymers symposium, has helped the program to expand considerably during the past several years. Talking to David Bassett is like receiving a shot of adrenalin; he compels you to action.

I also thank Professors Daniel Ou-Yang, Daniel Hong, and John Vanderhoff, for their interest and support in serving on the Dissertation Committee, and for meaningful and stimulating discussions on the physics of polymers and colloids.

I thank Professor Ron Darby of Texas A&M University, whose example has provided me with a role model of the successful engineer. Even though we were separated by over 1800 miles, he was still able to encourage me, and to aid me with practical advice on rheological measurements.

I appreciate the assistance of Mehdi Durali of the Emulsion Polymers Institute in obtaining the data presented in Figures 3.25 and 5.1.

I must also thank Martha Collins at Union Carbide Corporation in Charleston, West Virginia, for the use of her poly(oxyethylene) standards at a crucial moment during the completion of this work.

I would be remiss if I failed to acknowledge numerous discussions with my colleagues at scientific meetings and other gatherings. These discussions shaped the interpretation of the experimental data in a significant way.

Finally, I express my heartfelt gratitude to my parents, whose financial support allowed me to further my education in the first place, and to my wife Mary, who supported me through all of the lean times, both physical and emotional.

Table of Contents

List of Tables

List of Figures

Nomenclature

Roman

A	Area of latex surface. [cm^2]
$B(T)$	Second virial coefficient. [cm^3]
B_o	A constant in Equation (2.34). [cm^3]
C_m	Flory's constant given in Equation (2.16). [dimensionless]
C_{feed}	Concentration of associative polymer in the reservoir. [parts per million]
C_{in}	Concentration of associative polymer in the input stream.[parts per million]
C_{out}	Concentration of associative polymer in the efflux stream. [parts per million]
C_2	Concentration of polymer solute [g/cm^3].
C^*	Conventional polymer coil overlap parameter. [moles/liter]
$\bar{C}$	Molar concentration of polymer. [moles/liter]
$\tilde{C}$	Mass of polymer not in an association network. [moles]
$D_{aggregate}$	Diffusion coefficient of an aggregate. [cm^2/s]
$\underline{\underline{D}}$	Rate of deformation tensor. [s^{-1}]
D_p	Partial diameter [nm].
$F(X)$	Function of the Kirkwood-Riseman draining parameter given by the tables of Kurata and Yamakawa [63]. [dimensionless]
G'	Elastic component of the complex shear modulus (i.e., the storage modulus). [$dyne/cm^2$]
G''	Viscous component of the complex shear modulus (i.e., the loss modulus). [$dyne/cm^2$]
G_{en}^o	Pseudo - equilibrium modulus.[$dyne/cm^2$]

$G(\underline{x},N)$	Junction creation potential. [s^{-1}]
$H(x)$	Heaviside's unit step function. [dimensionless]
I_m	m^{th} moment of the molecular weight distribution.
J'	Elastic component of the complex compliance. [cm^2/dyne]
J''	Viscous component of the complex compliance.[cm^2/dyne]
K'	Huggins parameter. [dimensionless]
K''	Kraemer parameter. [dimensionless]
K_{MH}	Mark-Houwink constant given by Equation (2.8). [dl/g]
K_A, K^*_n	Equilibrium reaction constants.[dimensionless]
L	Rate coefficient for the junction creation potential.[s^{-1}]
M_c	Molecular weight of the entangled portion of a polymer chain. [grams/mole]
M_n	Number average molecular weight. [grams/mole]
M_v	Viscosity average molecular weight. [grams/mole]
M_w	Weight average molecular weight. [grams/mole]
M_z	Z average molecular weight. [grams/mole]
N	Number of statistical segments in a polymer chain. [dimensionless]
N_c	Critical chain length required for Gaussian chain statistics. [dimensionless]
N_A	Avogadros number: 6×10^{23} [molecules/mole].
N_i	Depending on context, either the number of segments in a polymer chain, or number of species. [dimensionless]
N_{Γ^*}	Dimensionless adsorption number given by Equation (5.9).
N_{C^*}	Dimensionless concentration number given by Equation (5.9).
P_J	Extent of reaction J. [dimensionless]
R_h	Hydrodynamic radius of the associative polymer coil. [cm]
$R(\underline{h},\theta,\phi)$	Integrand of Equation (4.30). [dimensionless]

R	In a chemical structure: denotes a hydrophobe. elsewhere: denotes the gas constant [8.314 J/mole °K].
$\underline{R}$	Polymer chain end-to-end distance vector. [cm]
T	Absolute temperature. [degrees Kelvin]
$\underline{\underline{T}}$	Tensor of eigenvectors. [dimensionless]
$\underline{\underline{V}}$	Diagonalized velocity gradient tensor. [s^{-1}]
V_{cell}	Volume of the serum replacement cell. [grams of water]
V_{dead}	Volume of the membrane support chamber in serum replacement cell. [grams of water]
V_{hydro}, V_h	Hydrodynamic volume of the associative polymer coil. [cm^3]
V_s,V_1	Molar volume of solvent. [cm^3/mole]
V_p	Molar volume of polymer.[cm^3/mole]
X	Kirkwood-Riseman draining parameter. [dimensionless]
Y_J	Mole fraction of species J. [dimensionless]
Z	Excluded volume parameter given by Equation (2.9). [dimensionless]

$A^{\pm}(t^*)$, $B(t^*)$, $Q(t^*)$,$Z(t^*)$,$D^{\pm}(t^*)$, $K^{\pm}(t^*)$, $C(t^*)$, $H(t^*)$, $I(t^*)$, $M(t^*)$, $P(t^*)$, $U(t^*)$, $J(t^*)$, $V(t^*)$, $W(t^*)$, $Y(t^*)$	Various time dependent functions in the statistical averages given by the conformation dependent junction breakage potential. [dimensionless]

a	Mark-Houwink exponent. [dimensionless]
a_T	Williams - Landel - Ferry time-temperature superposition factor. [dimensionless]

b_e	Length of a bond. [cm]
d_p	Density of the polymer. [grams/cm^3]
f(r,N,t)	Distribution of end-to-end distances. [dimensionless]
f	Mole fraction of hydrophobes in a given polymer chain. [dimensionless]
$g(\alpha)$	Excluded volume function given by Equation (2.11). [dimensionless]
g_n	Equation resulting from the combining a mass balance with an equilibrium reaction expression. [dimensionless]
g*	Stockmayer-Zimm function for the effect of branching on intrinsic viscosity. [dimensionless]
h	Dummy variable of integration. [dimensionless]
k	Boltzmann's constant. [1.38 x 10^{-23} J/°K mole]
m_s	molecular weight of a chain segment. [grams/mole]
n_w	Number of branch points in a given polymer by weight.
$<n>$	normalized junction concentration. [dimensionless]
$<n>_o$	normalized junction concentration at rest. [dimensionless]
q	cumulative mass efflux from a serum replacement cell. [grams]
q_1*	Cumulative mass efflux from the serum replacement cell at the end of the adsorption phase of the experiment. [grams]
q_n	Correction factor for polydispersity. [dimensionless]
$<r^2>^{1/2}$	Root mean square end-to-end distance of the polymer chain. [cm]
$<r^2>_o^{1/2}$	Unperturbed root mean square end-to-end distance of the polymer chain. [cm]
t*	dimensionless time given by the product of time and the relaxation time constant.

$\underline{x}$	End-to-end distance vector made dimensionless with respect to the fully extended length of the polymer chain.
x	Chapter II: volume fraction of associative polymers in solution. Chapter IV: axis in the laboratory coordinate frame (x,y,z).

Greek

$\underline{\underline{\Gamma}}$	Velocity gradient tensor. [s^{-1}]
Γ	Mass of associative polymer adsorbed on an unit area of latex surface. [grams/cm^2]
ΔF	Free energy change of a volume element of solvent that contains polymer. [Joules]
ΔF^o_a	Standard free energy of association. [Joules/mole]
ΔH_A	Standard enthalpy of the association reaction. [Joules/mole]
ΔH_1	Enthalpy of dilution.[Joules/mole]
ΔS_1	Entropy of dilution.[Joules/mole °K]
$\Delta\mu^o$	Chapter V: standard molar free energy of adsorption.[Joules/mole]
$\Delta\mu$	Chemical potential of a hydrophobe. [Joules/mole]
Θ	Ideal Flory temperature. [degrees Kelvin]
$\Lambda(t^*), \Xi(t^*)$	Various time dependent functions in the statistical averages given by the conformation dependent junction breakage potential. [dimensionless]
Φ	Universal Flory-Fox constant whose values is 2.1 x 10^{21} when intrinsic viscosity has units of dl/g.
Φ'	A constant in Equations (2.6) and (2.7).
Φ_2	Particle volume fraction. [dimensionless]
Ψ_1	Chapter II: entropy of dilution parameter. [dimensionless]

	Chapter IV: first normal stress difference coefficient. [dyne s^2/cm^2]
Ψ_2	Second normal stress difference coefficient. [dyne s^2/cm^2]
α	Chapter II: Expansion coefficient of the polymer coil given by Equation (2.5). [dimensionless]
	Chapter IV: Weissenberg number given by γ/β_o. [dimensionless]
β	Excluded volume of a pair of chain segments.
β_o	Probability of rupturing a junction in a network at rest. [s^{-1}]
$\beta(\underline{x},N)$	Junction breakage potential.[s^{-1}]
γ	Shear rate. [s^{-1}]
γ_e	rate of elongation in an extensional flow field. [s^{-1}]
δ_s, δ_p	Solubility parameters of solvent and polymer, respectively. [$cal^{1/2}/cm^{3/2}$]
ε	"Breakage index", given by $2\sigma/3N$. [dimensionless]
ε_∞	"Breakage index" for a Gaussian network. [dimensionless]
η	Simple shear viscosity of a solution. [Poise, i.e, dyne s/cm^2]
η'	Viscous component of the complex viscosity. [dyne s/cm^2]
$\eta_{reduced}$	Reduced viscosity. [dl/g]
$\eta_{inherent}$	Inherent viscosity. [dl/g]
$\eta_{specific}$	Specific viscosity. [dimensionless]
$\bar{\eta}$	Extensional viscosity.[dyne s/cm^2]
$[\eta]$	Intrinsic viscosity or limiting viscosity number [dl/g].
θ	Polar angle in spherical coordinates.
λ	Chapters III, and VI: relaxation time constant. [s]

	Chapter IV: specifies flow field: 0 denotes simple shear; 1 denotes extensional shear.
μ	Solvent viscosity. [dyne s/cm^2]
μ_1	Chemical potential of solvent. [Joules/mole]
μ_1^o	Chemical potential of solvent in the standard state. [Joules/mole]
ν	Chapters III and VI: Molar density of network junctions by association. [mole/liter]
	Chapter IV: eigenvalue.[dimensionless]
ν_2, $\bar{\nu}$	Chapter II: partial molar specific volume of polymer.[dimensionless]
ξ	"Slip" coefficient that describes the degree of deviation from affine deformation. [dimensionless]
ρ	transformed coordinate frame (ρ,η,z).
σ	Chapter II: steric hindrance parameter.[dimensionless]
	Chapter IV: ratio of the maximum end-to-end distance of the network chain to the length scale over which $\beta(x)$ changes.[dimensionless]
$\underline{\underline{\tau}}_p$	Polymer network stress tensor. [dyne/cm^2]
ϕ	Chapter II: valence angle.
	Chapter IV: Azimuthal angle in spherical coordinates.
$\phi(\sigma)$	Debye-Bueche solvent permeability function.[dimensionless]
χ, χ_1	Flory interaction parameter. [dimensionless]
ω	Chapter III: frequency of forced oscillation (rad/sec).
	Chapter IV: vorticity given by $(1-\lambda)/(1-\xi)(1+\lambda)$. [dimensionless]

Subscripts

A	Denotes adsorption.
D	Denotes desorption.
I	Denotes initial concentration.
Ref	Denotes reference state of a variable.
o	Denotes value of a variable at zero shear.
m	Denotes monolayer saturation.
s	Denotes solvent.
Θ	Evaluated at ideal (Flory theta) conditions.

Superscripts

*	Denotes a dimensionless variable.

Brackets

[x]	Denotes concentration of variable x.
<x>	Denotes statistical average of variable x.

Acronyms

AP	Associative polymer.
BC	Butyl Carbitol, a diethylene glycol monobutyl ether.
PDI	Polydispersity index.
SDS	Sodium dodecyl sulfate.

Abstract

To elucidate the mechanism by which associative polymers interact to modify the rheological properties of thickened dispersions, we measured the solution and dispersion rheologies, colloidal stability, and the adsorption behavior of model associative polymers - linear water-soluble poly(oxyethylene) backbones of molecular weights 16,600-100,400 that have been capped with hydroxyl, dodecyl, or hexadecyl end- groups.

From the intrinsic viscosities of the model associative polymers in water, We estimated the diameter of associative polymer coil in solution as 100-300 Å . The dependence of the viscosity - concentration relationships on molecular weight and hydrophobe length qualitatively agreed with a kinetic model for the association process.

The magnitude of the viscosity of the solutions and stable dispersions thickened with associative polymers scaled with the molar density of network junctions created by association, as determined from the entanglement plateau in the storage modulus. The steady shear viscosity profiles of solutions of the hexadecyl terminated model associative polymers, measured with a Bohlin Rheometer and a Weissenberg Rheogoniometer, exhibited dramatic shear-thickening prior to shear- thinning. Agreement between the viscosity data of the associative polymer solutions and a statistical mechanical network model indicated that the shear- thickening resulted from extension of the association network under shear, and that shear- thinning resulted from both the physical rupture of the network and from the non-affine deformation of the network.

A minimum amount of associative polymer was required to flocculate the dispersion by bridging; a certain degree of networking among the associative polymers was needed to span the interparticle distance. Restabilization occurred at larger concentrations of associative polymer, whereupon a homogeneous network of associative polymer and latex particles formed. The molecular areas of adsorption calculated from adsorption

isotherms, obtained using a modified serum replacement technique, suggested that this restabilization coincided with the full coverage of the particle surface by associative polymer. The rheological properties of these stable dispersions paralleled those of associative polymer solutions in the magnitude of viscosity, the influence of surfactants and cosolvents, and in the dependence of the properties on steady and dynamic shear. Physical interpretation of the rheological properties suggested a qualitative association mechanism.

Chapter I

An Introduction to Associative Polymers and Their Thickening Mechanism in Latex Dispersions

Motivation for Associative Polymers

The performance of a latex paint is evaluated by its non–Newtonian viscosity profile, which should satisfy the following criteria [1]. The paint should possess an apparent yield stress of at least 10 dyne/cm^2 , and a low shear viscosity of nearly 500 poise to retard sedimentation or flocculation of the latex and pigment particles during storage. At application shear rates of nearly 10,000 sec^{-1}, the latex paint should thin to about 2 poise to promote good film build for one coat hiding. After shearing, the paint's low shear viscosity should decrease to 250 poise to enhance levelling of brush marks and surface irregularities without sagging before drying. (It should be thixotropic). Without some sort of rheology modifier, the rheological properties inherent in polymer dispersions make them poorly suited for use as a paint or coating.

Until the early 1980's, the predominant commercial rheology modifiers for latex paints were high molecular weight cellulose derivatives. However, latex dispersions that contain cellulose derivatives are extremely shear thinning, and this makes it difficult to produce a paint with a high shear viscosity that is large enough to produce good film build-up and hiding properties, while simultaneously maintaining a low shear viscosity that is low enough to allow good leveling. In addition, the chain entanglements that are present in solutions of high molecular weight polymers produce viscoelastic effects, which cause roller spatter [2 - 4]. Associative polymers were developed to replace cellulosic thickeners to eliminate these undesirable application characteristics [5].

Definition of an Associative Polymer

Associative thickeners are defined as thickeners that build a rheological structure in solution by interacting with themselves and with other formulation components within a latex paint. These products range from those that thicken by linking together to form a microstructure, (clay platelets, for example), to those with "relative surfaces", (silica spheres, for example), which form networks through hydrogen bonding [6 - 8]. Associative polymers are hydrophobically modified water soluble block copolymers composed of both water soluble and water insoluble components; the water insoluble components interact in solution and adsorb onto latex particles to form a microstructure that improves the rheological properties of a latex paint. We prefer the nomenclature "associative polymers" over "associative thickeners" in referring to these polymers to distinguish them from the other types of associative thickeners.

Although in principle any water soluble polymer can be modified to produce an associative polymer, the three most popular types are hydrophobically modified alkali-swellable polymers, hydrophobically modified hydroxyethyl cellulose, and hydrophobically modified ethoxylated urethane polymers [9]. An alkali - swellable associative polymer is a hydrophobically modified carboxylic acid containing copolymer, with a molecular weight of usually several hundred thousand, that swells in aqueous media upon neutralization [10]. These polymers thicken both through association, and from the expansion of the polymer backbone at high pH due to coulombic repulsions between the neutralized carboxylic acids. The hydrophobically modified urethane based associative polymers most commonly have a linear poly(oxyethylene) backbone, and have hydrophobes distributed along the backbone, and at the backbone termini [11]. This review focuses mainly on the more commonly used non-ionic hydrophobically modified ethoxylated urethane associative polymers; excellent reviews on hydrophobically modified

alkali- swellable thickeners and hydrophobically modified hydroxyethyl cellulose thickeners may be found elsewhere [10, 12 - 14].

Benefits and Limitations

Associative polymers alter the rheological properties of latex paints by interacting with themselves and with other solutes in the aqueous dispersion medium to build a shear sensitive association network. Surfactants and cosolvents can disrupt this association process, which permits the formulator to independently manipulate a paint's high shear and low shear viscosities to achieve a satisfactory combination of film build and leveling properties [15]. Because the low shear viscosity depends on the degree of association by the associative polymer, the formulator can add enough associative polymer to achieve the desired high shear viscosity, and then add enough surfactant or cosolvent to reduce the low shear viscosity to an acceptable level. The result is a more Newtonian and desirable viscosity profile than can be achieved with cellulosic thickeners, which imparts improved flow and leveling, improved film build in pad, brush, or roller application, spray pattern and bubble release, and reduced roller spatter in the latex paint.

Besides rheological benefits, associative polymers also improve the colloidal stability of latex paints, which produces films of lower permeability and higher gloss. Because cellulosic polymers do not adsorb to latex particles and are usually of high molecular weight, they are excluded from the region between two approaching latex particles. This exclusion produces a local concentration gradient of polymer, which produces an osmotic force that drives the particles together [16 - 18]. The flocculation gives the latex paint a noticeable yield stress, and compromises the paint's protective ability by making microscopic channels in the dried film. Associative polymers avoid this volume restriction flocculation by adsorbing onto latex particles, and because they have a relatively low molecular weight. Although associative polymers can flocculate a latex by a bridging

mechanism, the concentration of associative polymer that is commonly used in latex paints usually exceeds the concentration at which this phenomenon occurs [19]. The result is a paint with a lower yield stress, and a dried film with a lower permeability [20, 21]. Gloss is influenced by the surface roughness of the paint film. The surface roughness may be split into two types: macro-roughness, which results from surface defects of greater than one micrometer, and micro-roughness, which results from defects of less than 0.6 micrometer [22]. Because paints thickened with associative polymers are resistant to pigment flocculation (which produces micro-rough surfaces), and are able to cover surface defects due to improved leveling characteristics, paints thickened with associative polymers have a much higher gloss as compared to paints thickened with cellulose derivatives.

Although associative polymers are the state of the art tools for the rheological control of latex dispersions, they do suffer from some limitations, the principle one being cost. Indeed, an active area of current research is to devise more efficient associative polymers or make them from less expensive raw materials. Alkali - swellable associative polymers are one example of these less expensive associative polymers, although the water sensitivity of the dried latex films that contain them primarily limits their use to interior coatings [14]. Even though associative polymers are more expensive than cellulosics, their use in formulation of latex paints may actually result in a raw material cost savings for the entire latex paint, because the thicker and smoother films produced by associative polymers permit the paint to contain a smaller concentration of titanium dioxide pigment without sacrificing hiding power [23]. In an effort to optimize thickener cost and paint quality, some paint formulators have blended cellulose thickeners together with associative polymers [24]. Nonetheless, the superior paint rheologies and the flexibility in formulation imparted by associative polymers make them the rheology control agents of choice.

Another difficulty in formulating with associative polymers is that they do not replace cellulosics on a one - to - one basis in existing latex paint recipes. The associative polymers can interact with other formulation ingredients in an unpredictable way, and slight deviations in the formulation recipe or in the order in which the ingredients are added can have a dramatic effect on the physical properties of the paint. We are aware of one dramatic example in which the viscosity of a latex paint changed by an order of magnitude from simply changing the length of the hydrophobe of a surfactant molecule by one carbon atom [25]. As a result, the latex formulator must carefully observe the influence of each component to optimize paint rheology, and must sometimes redevelop the latex paint recipe. (Nonetheless, it is worth it.) Understanding the association mechanism and how it relates to the molecular structure of the thickener molecule would aid in the prediction of the properties of paints containing associative thickeners. The literature compares the performance of associative polymers and conventional thickeners in common latex paint formulations [23, 26 - 28], and provides practical latex paint formulation strategies [29,30].

Early Investigations into the Thickening Mechanism

Although it is generally accepted that the hydrophobic portions of associative polymers interact to alter the rheology of latex dispersions, relatively little is known about the fundamental physics behind the association process, or the relationships between associative polymer structure and latex paint rheology. Most of the hypothesized associative mechanisms can be placed into one of two categories: particle bridging theories, and associative cluster bridging theories. The difference between the two groups lies in the importance of the adsorption of the associative polymer at the particle surface relative to the association of the associative polymer hydrophobe in the dispersion medium. The particle bridging theory asserts that the latex - thickener interaction controls the rheological

properties of latex dispersions. This interaction builds the network structure, and surfactants and cosolvents influence the rheological properties of latex paints by influencing the adsorption of the associative polymer. (for example, see reference [15]). However, this theory does not explain the ability of associative polymers to thicken solutions without latex [11, 31]. In analogy to low molecular weight surfactants, the associative cluster bridging theory asserts that once the concentration of associative polymer in solution exceeds a critical concentration, the hydrophobes from a given associative polymer can exist simultaneously in two different associative clusters to effectively cross- link the solution. This theory implies that no adsorption of the associative polymer is needed to thicken the latex dispersion. However, this theory cannot explain the influence of latex particle size on the rheological properties of the latex paint. (The particles do more than simply act as inert fillers in the association network structure.) These two mechanisms represent extremes in points of view; elements of both are undoubtedly true, the degree of which probably depends on the exact structure of the associative polymer. Even though no association mechanism may be universal, fundamental knowledge about how associative polymer structure governs the association mechanism would aid in the formulation of latex paints with associative polymers, and aid in the design of improved associative polymers.

As a first approach to investigating the association mechanism, a number of studies used an experimental design approach with commercial associative polymers to determine the effect of the following parameters on the rheological properties of fully formulated coatings: associative polymer molecular weight and structure; latex particle type, surface characteristics, and particle size distribution; pigment surface characteristics and volume concentration; surfactant type and concentration; and cosolvent type and concentration. (For example, see reference [32]). Unfortunately, this kind of study does not reveal much about the fundamental association mechanism because of the multiplicity of interactions among associative polymers and other paint formulation components, and because

commercial associative polymers are made in a variety of architectures and molecular weights and are shipped pre-dispersed in mixtures of water and cosolvent. However, they were successful in developing paint formulation strategies, and in identifying the key variables that control the rheology of latexes thickened with associative polymer.

Such studies on commercial thickeners point out the complexity of the technology, and motivate studies on model associative polymers to produce a fundamental understanding of the association phenomenon and of the nature of the interactions among associative polymers and latex paint formulation components.

Use of Model Systems

Scrutiny of the cited literature reveals that a thorough investigation into the rheological properties of model systems that contain model associative polymers of known structure should reveal considerable insight into the association mechanism. We start with "stripped- down" systems (what we call model systems), and systematically build up the complexity of the model systems as we gain an understanding of the association phenomenon in the simpler systems. Our investigation into the relationships between the dynamics of an association network and rheology consists of four sequential phases: measurement of the dilute solution viscosities of aqueous associative polymer solutions, measurement and statistical mechanical modeling of the steady shear viscosity and linear viscoelastic properties of concentrated associative polymer solutions, measurement of the adsorption isotherms of associative polymer on monodisperse polystyrene latexes, and measurement of the rheological properties of monodisperse polystyrene latexes that contain model associative polymer. The use of model associative polymer systems to investigate the association phenomenon has become popular in recent years, and we review the literature pertinent to the behavior of associative polymers later in this dissertation: the rheological properties of model associative polymer solutions are reviewed in the

Introduction to Chapter III; the adsorption of model associative polymer to latex is reviewed in the Introduction to Chapter V; and the rheological properties of model polymers in latex systems are reviewed in the Introduction to Chapter VI. Because of the complexity and sensitivity of the association phenomenon, the scientific investigation of the association phenomenon has moved away from an experimental design approach toward an examination of model systems.

Our model associative polymers, kindly supplied by Union Carbide Corporation, consist of linear water–soluble poly(oxyethylene) backbones of molecular weight 16,600–100,400 with hydroxyl, dodecyl, or hexadecyl end- groups. Each type of end-group comes in six molecular weight fractions, which allows us to study simultaneously the influence of the length of the hydrophobic end-group, and thickener molecular weight (i.e., the spacing between end- groups). The hydroxyl terminated polymers form the control group in these studies. Table 2.1 presents the structure of the model polymers in more detail.

The simplest stripped down system is a dilute solution of associative polymer. Chapter II presents the results of the intrinsic viscosity experiments: estimates of the dimensions of the polymer chains in solution, semi- quantitative information on the dilute solution thermodynamics of associative polymers, and measurements of the concentration at which significant networking begins. Also, the molecular weight of the molecularly dispersed model polymers were verified by intrinsic viscosity measurements in a cosolvent system. Appendix A presents the size exclusion chromatograms obtained for the model associative polymers in tetrahydrofuran.

A concentrated solution of model associative polymer is the simplest stripped down system that serves as a control system for comparison with latex systems. The concentrations of associative polymer studied are of the same order of magnitude as those found in typical latex paints, and are large enough that a rheologically significant network has developed. In Chapter III, we study the unusual rheology of concentrated associative

polymer solutions in steady and dynamic shear. We observed shear- thickening prior to shear- thinning in steady shear viscosity profile, and we turned to a statistical mechanical network model to help us interpret this behavior (Chapter IV). The agreement between the model and the viscosity data is satisfying.

With Chapters II through IV as a foundation, we can introduce a colloidal species into the model system. The first interaction to understand is the adsorption of the associative polymer at the particle interface, and as shown in Chapter V, we examine the influence of particle size and polymer structure on this interaction. We also consider the influence of the model associative polymers on the colloidal stability of latexes.

Using the results of Chapters III through V, we can interpret the rheological behavior of latex systems, in the presence and absence of surfactants and cosolvents, in terms of a physical mechanism, as summarized in qualitative two- dimensional schematics of the association network. Chapter VI presents data that shows that the rheological properties of latexes and concentrated associative polymer solutions are quite similar, and it examines the synergistic interactions between associative polymers, surfactants, and latex particles.

And finally, Chapter VII concludes the dissertation with recommended extensions of the current work.

Chapter II

Dilute Solution Behavior of Model Associative Polymers

Introduction

Motivation

We have several reasons to measure how the relative viscosity of associative polymers in dilute solution depends on concentration. First, we want to verify that the molecular weights of the model polymers provided by Union Carbide Corporation are near the target molecular weights, and are self-consistent within a given series. Second, we hope to deduce at what concentration associative polymers begin to network, and to discern the boundaries between the dilute, semi-dilute, and concentrated solution states. The practical control of the rheological properties of a latex paint requires knowing at what thickener concentration significant network formation begins, and this information is needed to correctly design rheological experiments that involve concentrated solutions (Chapter III) and latex dispersions that contain model associative polymers (Chapter VI). Third, we need an estimate of the size of the polymer coil in solution to select the appropriate operating conditions for the adsorption experiments (Chapter V). In addition, analysis of the dilute solution viscosity data yields semi-quantitative information on the thermodynamic properties of associative polymer solutions. It would be useful to compare our estimate of the size of the dissolved associative polymer coil to that obtained from dynamic light scattering experiments. In short, these reasons have prompted us to measure the dilute solution viscosity behavior of the model associative polymers.

Corresponding States: Scaling Behavior of Polymer Solutions

The definition of intrinsic viscosity has its roots in the Einstein equation for the relative viscosity of a dilute suspension of unsolvated spherical particles:

$$\frac{\eta}{\mu} = 1 + \frac{5}{2}\Phi_2 \tag{2.1}$$

where η is the viscosity of the suspension, μ is the viscosity of the solvent, Φ_2 is the particle volume fraction given by N_2V_h/V, and N_2 is the number of particles, each of which has hydrodynamic volume of V_h , in the total suspension volume V. Polymers in solution likewise enhance the viscosity of the solvent due to their hydrodynamic size, that is, the volume that a polymer coil in solution excludes from neighboring polymer coils. If a polymer in solution is analogous to a particle, then N_2 equals V c_2 N_A/M_2 , and the relative viscosity is then:

$$\frac{\eta}{\mu} = 1 + \frac{5}{2}\frac{4\pi}{3}\frac{N_A c_2 \bar{R}_h^3}{M_2} \tag{2.2}$$

where V_h equals $(4\pi/3)R_h^3$, c_2 is the polymer concentration in grams/cm^3, N_A is Avogadro's number, and M_2 is the molecular weight of the polymer. Extrapolation of the specific viscosity $[\eta/\mu - 1]$ defines the intrinsic viscosity, or limiting viscosity number $[\eta]$, as a measure of the hydrodynamic volume of the polymer coil in solution:

$$\lim_{c_2 \to o} \frac{\left[\frac{\eta}{\mu} - 1\right]}{c_2} = \frac{5}{2}\frac{4\pi}{3}\frac{N_A}{M_2} R_h^3 \equiv [\eta] \tag{2.3}$$

In general, the viscosity theories for polymers in solution are less well developed than those for colloidal particles in suspension, mainly due to the compressibility of the polymer coils at moderate concentrations, entanglement effects, and the formation of polymer aggregates. The dependence of solution viscosity on polymer coil size and

concentration are often expressed in terms of empirical master correlations of the form $\eta/\mu = f(c[\eta])$ [33 - 35]. One such equation is the Huggins equation:

$$\frac{\eta}{\mu} = 1 + c[\eta] + K'c^2[\eta]^2 + \ldots \qquad (2.4)$$

where η/μ is the relative viscosity, $c[\eta]$ is the overlap parameter (i.e., a dimensionless coil volume), and the constant K' characterizes the first effects of polymer interaction on the viscosity. The Huggins' parameter K' is usually independent of polymer molecular weight for long polymer chains, and has a value of about 0.4 for polymers in good solvents without interaction effects and a value of about 0.8 for polymers in theta solvents [36, 37] . Equations like Equation (2.4) often unify viscosity data over a broad range of molecular weights for a given dilute polymer-solvent system where polymer-polymer interactions do not dominate.

The overlap concentration c* denotes the concentration where polymer coils begin to interpenetrate in solution, and distinguishes between the different solution states: dilute ($c<c^*$), semi–dilute ($c\approx c^*$), and concentrated ($c>>c^*$). It is commonly assumed that c* occurs when the overlap parameter $c[\eta]$ approximately equals 1. However, this neglects changes in coil dimensions with concentration: for polymers that contract to theta dimensions before they interpenetrate, $c^*=.74/[\eta]$ [38,39]. In the semi-dilute concentration regime, interaction occurs among many polymer chains so that solution viscosity no longer follows scaling laws that were derived for isolated polymer chains. de Gennes [40] showed that rheological data of semi-dilute polymer solutions scale as a power of the reduced variable $\bar{c}/c^*$, where the overbar denotes molar concentration. For a real chain following a self-avoiding random walk, c* scales with molecular weight to the -4/5 power. Thus, we can use these scaling laws to determine the boundaries of the various solution states, and to identify the concentrations at which networking begins from scaling.

Polymer Chain Dimensions from Intrinsic Viscosity

Despite the empiricism that is used to determine the concentration dependence of the relative viscosity of polymer solutions, the dimensions of flexible linear macromolecules in solution can still be extracted from the relationship between intrinsic viscosity and molecular weight. The dimensions of polymer coils in solution are determined by short range and long range interactions. Short range interactions, which occur between atoms that are separated by only a few bond lengths, produce torques that inhibit internal rotation about bonds, and hence govern the flexibility of the polymer coil. Long range interactions, which occur between segments of the polymer chain that are separated by many valence bonds, result from van der Waals interactions. These long range interactions produce an osmotic swelling of the polymer coil through polymer-solvent interactions, so that the volume of the solvent swollen polymer increases over that for a polymer that is unperturbed by the solvent. An expansion coefficient α, which is the ratio of the root mean square end-to-end distance of the polymer coil in the solvent $\langle r^2 \rangle^{1/2}$ relative to the root mean square end-to-end distance in the unperturbed state $\langle r^2 \rangle_o^{1/2}$ describes this effect:

$$\alpha = \frac{\langle r^2 \rangle^{1/2}}{\langle r^2 \rangle_o^{1/2}} \tag{2.5}$$

In a Flory "theta" solvent, long range interactions are absent, and the polymer chain assumes its unperturbed dimensions. Thus, α characterizes the "goodness" of solvent for the polymer: $\alpha < 1$ for a poor solvent, $\alpha = 1$ in a theta solvent, and $\alpha > 1$ in a good solvent.

With these considerations, the hydrodynamic volume of the polymer coil given in Equation (2.2) can be written as $V_h = (V_h)_\theta \alpha^q$, where $(V_h)_\theta$ is the volume assumed by the unperturbed coil, and q depends on the chain's conformation: 2.43 for a spherical coil and 2.18 for an elliptical coil. Then the intrinsic viscosity in Equation (2.3) becomes:

$$[\eta] = \frac{5}{2} N_A (V_h)_\Theta \frac{\alpha^q}{M_2} = \frac{5}{2} N_A \Phi' \left(\frac{< r^2 >_o}{M_2} \right)^{3/2} M^{1/2} \alpha^q = K M^{1/2} \alpha^q \quad (2.6)$$

where Φ' is a proportionality factor between the radius of gyration and the hydrodynamic volume, and K is

$$K = \frac{5}{2} N_A \Phi' \left(\frac{< r^2 >_o}{M_2} \right)^{3/2} = \Phi \left(\frac{< r^2 >_o}{M_2} \right)^{3/2} \quad (2.7)$$

Experiments have shown that Φ does not depend on the constitution or configuration of the polymer or solvent, but only on the relative expansion of the coil in solution, and that Φ equals 2 - 2.5 x 10^{21} when traditional units of (dl/g) are used for the intrinsic viscosity. Chain statistics that consider the finite thickness of the polymer chain and interaction between segments of the polymer show that $<r^2> \sim M^{1+\varepsilon}$ when in non-theta solvents. When this is substituted into the previous expression, there results the Kuhn-Mark-Houwink-Sakurada equation:

$$[\eta] = K_{MH} M^a \quad (2.8)$$

where 'K_{MH}' and the exponent 'a' are constants obtained by calibration with standards of known molecular weight. The exponent 'a' is related both to the solvent quality and to the conformation of the polymer chain: a=0 for unsolvated spheres, a=2 for rigid rods, and a= 1/2 for polymer coils in a theta solvent.

To determine unperturbed chain dimensions from intrinsic viscosity data, the relative contributions of long range interactions, which determine α, and short range interactions, which determine $<r^2>_o$, to total volume of the polymer coil must be

uncoupled. One obvious way to do this is to measure the intrinsic viscosity in a theta solvent. Then the right hand side of Equation (2.7) calculates the unperturbed dimensions: $K_\theta = \Phi[\langle r^2\rangle_o/M]^{3/2}$. Even if a theta solvent for the polymer in question is not known, the unperturbed dimensions from intrinsic viscosity measurements in a non-ideal (i.e. non-theta) solvent can still be estimated, provided that the correct allowance for the excluded volume of the polymer chain due to long range interactions is made in the expansion coefficient α.

Most theories that are used to calculate the perturbation in chain dimensions that results from the excluded volume effect start by representing the interactions among non-bonded segments of the polymer chain with the binary cluster integral (i.e., they assume pairwise interactions). As a result, the expansion coefficient depends only on the excluded volume parameter z:

$$z = \frac{\beta m_s^2}{(4\pi)^{3/2}} \left(\frac{\langle r^2 \rangle_o}{M} \right)^{-3/2} \sqrt{M} \qquad (2.9)$$

where β is the excluded volume of a pair of chain segments that have a molecular weight m_s. This is related to the second virial coefficient B(T) via $B = \beta m_s^2/(6\pi)^{3/2} = \bar{v}^2 (1-2\chi_1)/V_1 N_A$, where χ_1 is the familiar Flory interaction parameter. Hence at the Flory theta temperature, where no long range interactions exist, the excluded volume parameter is zero.

A number of expressions have been postulated to relate the excluded volume parameter to chain dimensions; the result is a large number of extrapolation equations that were designed to determine the unperturbed dimensions from intrinsic viscosity measurements made in good solvents. The reader should consult references [41] through [45] for examples of some of the various equations in use. We have chosen to use two

equations that were derived explicitly for polymers in good solvents, namely the Kurata-Stockmayer equation [45], and the Stockmayer-Fixman equation [46]. Kurata and Stockmayer suggested the approximate equation $\alpha^3-\alpha = C\, g(\alpha)\, z$, where $g(\alpha) = 8\alpha^3/(3\alpha^2+1)^{3/2}$ and C is a constant, for the relationship between excluded volume and the expansion coefficient of the polymer coil. In terms of intrinsic viscosities α^3 is:

$$\alpha^3 = \frac{\langle r^2 \rangle^{3/2}}{\langle r^2 \rangle_0^{3/2}} = \frac{[\eta]}{[\eta]_\theta} = \frac{[\eta]}{K_\theta \sqrt{M}} \tag{2.10}$$

which is the ratio of the intrinsic viscosity of the polymer in the solvent of interest to the intrinsic viscosity of the polymer in a theta solvent. When these two equations are combined, there results:

$$\frac{[\eta]^{2/3}}{M^{1/3}} = K_\theta^{2/3} + 0.363\, \Phi\, B \left[g(\alpha) \frac{M^{2/3}}{[\eta]^{1/3}} \right] \tag{2.11}$$

Equation (2.11) is applied by first plotting $[\eta]^{2/3}/M^{1/3}$ against $M^{2/3}/[\eta]^{1/3}$, while ignoring $g(\alpha)$ to determine an approximate value of K_θ. This value of K_θ is used to calculate $g(\alpha)$, and $[\eta]^{2/3}/M^{1/3}$ is now plotted against $g(\alpha)M^{2/3}/[\eta]^{1/3}$ to find an improved estimate of K_θ. The method is applied iteratively until convergence, and the final value of K_θ determines the unperturbed dimensions of the polymer coil from $K_\theta = \Phi[\langle r^2 \rangle_o/M]^{3/2}$. Stockmayer and Fixman used $\alpha^3=1+ 2z$ to derive an algebraically explicit equation that applies to flexible chains that immobilize solvent:

$$\frac{[\eta]}{\sqrt{M}} = K_\theta + .51 \Phi B \sqrt{M} \tag{2.12}$$

According to Equation (2.12), plotting the intrinsic viscosity divided by the square root of the number average molecular weight against the square root of number average molecular weight yields a line where the intercept is K_θ. Despite their entirely different origins, Equations (2.11) and (2.12) usually yield similar results.

A brief examination of Equations (2.11) and (2.12) reveals the benefit of measuring the intrinsic viscosities of a series of polymers that vary systematically in molecular weight at a variety of temperatures: the ideal Flory theta temperature Θ is that temperature at which the slope of the line in a plot of either the Kurata-Stockmayer equation or the Stockmayer-Fixman is zero. The next section shows in more detail how the enthalpy and entropy of dilution may be calculated for polymer solutions from intrinsic viscosity measurements.

Thermodynamic Parameters

Even though the intrinsic viscosity is measured from a non-equilibrium experiment, thermodynamic properties (i.e. equilibrium properties) of a polymer-solvent system can be calculated from it. What is needed is an equation that relates the free energy change in the polymer coil upon swelling to the expansion coefficient; the Flory swelling equation [47] is one example of such an equation. The free energy change of a volume element of solvent upon dissolution of a polymer is the sum of contributions from the free energy change due to changes in the polymers conformation upon mixing ΔF_{el} and the free energy change due to mixing the polymer segments with the solvent ΔF_m:

$$\Delta F = \Delta F_{el} + \sum_{j \text{ segments}} \Delta F_m \qquad (2.13)$$

Other terms may be added to represent the change in free energy due to other phenomena, such as hydrophobic association between polymers [48]. At equilibrium, the change in free energy is zero:

$$\left[\frac{\partial \Delta F}{\partial \alpha}\right]_{T,P} = 0 = \left[\frac{\partial \Delta F_{el}}{\partial \alpha}\right]_{T,P} + \sum_{j \text{ segments}} \left[\frac{\partial \Delta F_m}{\partial \alpha}\right]_{T,P} \quad (2.14)$$

Flory assumed a Gaussian distribution of polymer chain segments to derive expressions for the elastic and mixing contributions to the change in free energy. Substitution of these expressions into Equation (2.14) results in the Flory swelling equation:

$$\alpha^5 - \alpha^3 = 2\, C_m\, \psi_1\, [1-\Theta/T]\, \sqrt{M} \quad (2.15)$$

where

$$C_m = \left(\frac{27}{2^{5/2}\, \pi^{3/2}}\right)\left(\frac{\bar{v}_2^2}{N_A\, V_1}\right)\left(\frac{< r^2 >_o}{M}\right)^{-3/2} \quad (2.16)$$

V_1 is the molar volume of the solvent, $\bar{v}_2$ is the partial specific volume of the polymer, and ψ_1 is the entropy of dilution parameter. The enthalpy of dilution is $\Delta H_1 = RT\kappa_1 v_2^2$, where the enthalpy of dilution parameter κ_1 equals $\psi_1\Theta/T$, and the entropy of dilution is $\Delta S_1 = R\psi_1 v_2^2$. These parameters characterize the thermodynamic interactions between polymer and solvent. According to Equation (2.15), plotting α^5-$\alpha^3/\sqrt{M}$ against 1/T yields a line with an intercept equal to $2C_m\psi_1$ and a slope equal to $-2C_m\psi_1\Theta$. Thus, measurement of α via intrinsic viscosity (Equation (2.10) permits calculation of the ideal theta temperature Θ, and the enthalpy ΔH_1 and entropy ΔS_1 of dilution.

This chapter begins by examining the intrinsic viscosities and scaling behavior of associative polymers in water. This is followed by an estimation of the dimensions of the polymer coil in solution by way of the thermodynamic analysis described above and through some classical models for the intrinsic viscosity. This analysis results in some

semi-quantitative information of the thermodynamic properties of associative polymer solutions. The chapter concludes with a physical kinetic model derived to simulate the concentration dependence of the relative viscosity of associative polymer solutions.

Experimental Detail

Table I presents the structure of the model associative polymers kindly provided by Union Carbide Corporation [25]. The model polymers' structures consist of linear water–soluble poly(oxyethylene) backbones of number average molecular weight 16,600–100,400 with hydroxyl, dodecyl, or hexadecyl linear alkyl end- groups. The hydroxyl terminated polymers serve as a control group by which we can measure the influence of the presence of linear alkyl hydrophobic end- groups on solution and latex rheology. The notation C_{n-m}, where n represents the number of carbon atoms in the alkyl end- group and m represents the polymer number average molecular weight in thousand Daltons, describes the structure of the polymer molecule. Appendix A presents the details of molecular weight determinations by gel permeation chromatography in tetrahydrofuran and by intrinsic viscosity measurements in a water miscible cosolvent mixture. The calculations presented in this chapter and throughout this dissertation are based on the number average molecular weights calculated from reaction stoichiometry.

Table 2.1: Structure and Nomenclature of Model Associative Polymers§

R-O-(DI-PEG)Y-DI-O-R **

Reference*	Structure		Calculated†
	R	Y	Mole. Wt.
C_{12}-17	$C_{12}H_{25}$	2	17,400
C_{12}-34	$C_{12}H_{25}$	4	34,200
C_{12}-51	$C_{12}H_{25}$	6	50,700
C_{12}-68	$C_{12}H_{25}$	8	67,700
C_{12}-85	$C_{12}H_{25}$	10	84,500
C_{12}-100	$C_{12}H_{25}$	12	99,900
C_{16}-18	$C_{16}H_{33}$	2	17,500
C_{16}-34	$C_{16}H_{33}$	4	34,200
C_{16}-51	$C_{16}H_{33}$	6	51,000
C_{16}-68	$C_{16}H_{33}$	8	67,600
C_{16}-84	$C_{16}H_{33}$	10	84,300
C_{16}-100	$C_{16}H_{33}$	12	100,400
C_0-17	H	2	16,600
C_0-33	H	4	33,400
C_0-50	H	6	50,200
C_0-67	H	8	67,000
C_0-84	H	10	84,000
C_0-100	H	12	100,400

§ Kindly provided by Union Carbide Corporation.

** DI is isophorone diisocyanate, and PEG is Carbowax® 8000 with a nominal molecular weight of 8200.

* The first subscript indicates the length of the alkyl end- group, denoted R, and the second subscript indicates the molecular weight of the model associative polymer in thousands.

† Number average molecular weight calculated from reaction stoichiometry [25].

Stock solutions of five percent by weight associative polymer for the experimental work described in this chapter, and for the rheological and adsorption experiments described later in this dissertation, were prepared by adding a weighed amount of solid polymer to distilled deionized (DDI) water. Because poly(oxyethylene) degrades by a free radical mechanism [49], we added 5-20 ppm of hydroquinone inhibitor to these solutions, and stored them out of light, to stabilize them against degradation. The solid model polymers contain additional stabilizers, and are stored in a refrigerator at 4°C to promote their long term stability. The model associative polymer solutions exhibit an upper critical solution temperature, where solutions of the lower molecular weight associative polymers would phase separate upon cooling. Because such phase separated systems are inconvenient to handle, and because we were concerned about the effects of thermal history on the properties of the solutions, the stock solutions were stored at room temperature. Appendix B details our solution preparation procedure and experimental studies on the effect of degradation on the solution rheology of the model associative polymers.

The intrinsic viscosities of the associative polymers were measured with Ubbelohde dilution viscometers situated in a thermostated bath. A description of the anatomy and use of the dilution viscometer can be found in any competent textbook on polymer science, and so, is not repeated here. (For example, see reference [50]). The efflux time for the solvents were large enough to ignore the Hagenbach - Couette kinetic energy correction, and the densities of the solutions were nearly those of the solvents. Thus, the efflux times of the solutions were converted to reduced viscosity and inherent viscosities from the following definitions:

$$\eta_{reduced} = \frac{\eta_{specific}}{C} = \frac{t-t_0}{Ct_0} \; ; \quad \eta_{inherent} = \frac{\ln(\eta_{relative})}{C} = \frac{\ln(t/t_0)}{C} \qquad (2.17)$$

where t_o is the solvent efflux time, and the resulting reduced and inherent viscosities were plotted against concentration in the traditional units of g/dl. Extrapolation of the linear regions of the reduced and inherent viscosity curves for $1.2 \leq \eta_{relative} \leq 1.6$ to zero concentration with the familiar Huggins and Kraemer equations:

$$\eta_{reduced} = [\eta] + K'[\eta]^2C \; ; \; \eta_{inherent} = [\eta] + K''[\eta]^2C \qquad (2.18)$$

produced intrinsic viscosities in units of dl/g that were equivalent within the precision of the experiment. Rheological measurements on concentrated solutions with a Bohlin Rheometer (Chapter III) indicated that solutions that contained less than 0.5% associative polymer by weight were Newtonian at shear rates from 40 sec^{-1} to 8000 sec^{-1}. Recent measurements made with a Zimm viscometer, which is better adapted for the measurement of low viscosity fluids than the Bohlin rheometer, suggest that the solutions of the model associative polymers with the hydrophobic alkyl end- groups are weakly shear thinning and reach a limiting Newtonian viscosity at shear rates near 100 sec^{-1} [51]. Because the shear rates at which the dilute solutions reach Newtonian behavior are similar in magnitude to the shear rate at the wall in our Ubbelohde viscometer, no shear rate correction was applied to the measured intrinsic viscosities.

Results and Discussion

Intrinsic Viscosities

Figures 2.1 a,b, and c, compare how the reduced and inherent viscosity functions depend on concentration for hydroxyl, dodecyl, and hexadecyl end- groups, respectively. As seen in Figure 2.1a, the reduced viscosity of a hydroxyl terminated model associative

polymer remains linear over the measured concentration range, and has a value of K' near 0.35, which is the classical value for most conventional polymer–solvent pairs. In contrast, the model polymers with the alkyl end- groups interact at extremely small concentrations to produce a rapid increase in reduced viscosity, which deviates from the linear behavior predicted by the Huggins equation. Figures 2.1b and 2.1c show how the specific viscosity, which measures the specific capacity of the polymer to enhance viscosity, increases as both concentration and alkyl end- group length increase. The viscosity enhancement becomes quite dramatic at concentrations that exceed 0.5 g/dl, which heralds the formation of an extensive association network in solution, and shows that the rate of addition of associative polymer to the network with respect to polymer concentration increases as the length of the hydrophobic end- group relative to the polymer backbone increases. This concentration is less than the polymer coil overlap concentration, which is on the order of 1 - 3 g/dl, as estimated from the reciprocal of the intrinsic viscosity data given in Table 2.2. Thus, an interaction occurs between hydrophobes at a concentration that is less than that required to make the polymer coils physically touch. This suggests that we should define a new critical network concentration c^*_h as the concentration at which the associative polymers hydrophobic end- groups first interact to form a rheologically significant network [52]. For hydrophobically modified hydroxyethylcellulose, this concentration is distinct, and distinguishes between the limited aggregation that occurs in the dilute regime from the more extensive aggregation at larger concentrations that lead to an association network [13]. In contrast, the shape of the curves in Figure 2.1 suggests that the network builds up over a range in concentrations, rather than at a particular critical micellar concentration as in the case of ordinary surfactants or hydrophobically modified hydroxyethylcellulose.

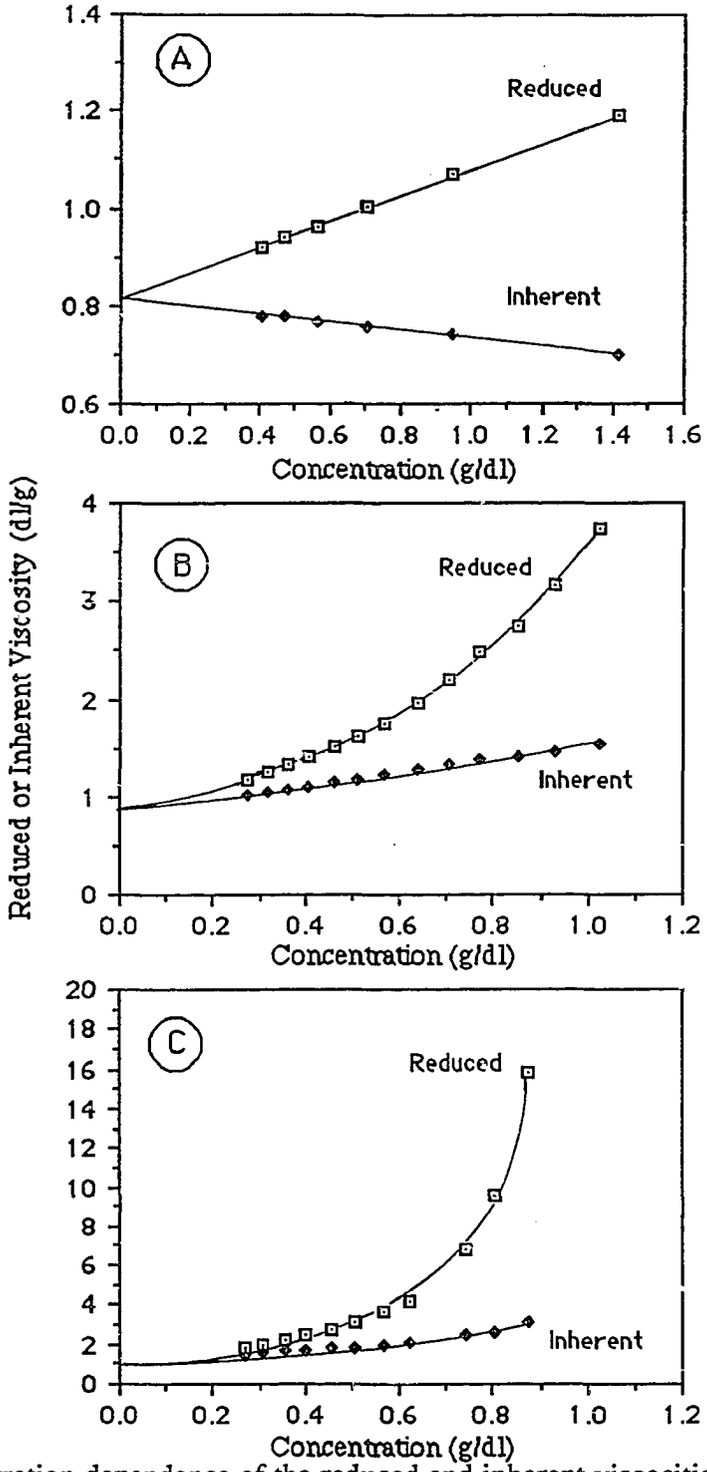

Figure 2.1: Concentration dependence of the reduced and inherent viscosities at 30°C of model associative polymers of 67,000 number average molecular weight terminated with either (a) hydroxyl, (b) dodecyl, or (c) hexadecyl end- groups.

Table 2.2: Intrinsic Viscosities (dl/g) of Model Associative Polymers in Water

Structure	30°C	40°C	50°C	60°C
$C_{0\text{-}17}$	.360	.346	.330	.315
$C_{0\text{-}33}$	.526	.488	.462	.455
$C_{0\text{-}50}$	.773	.715	.619	.563
$C_{0\text{-}67}$	.815	.744	.656	.625
$C_{0\text{-}84}$	.870	.779	.728	.658
$C_{0\text{-}100}$	1.05	.956	.841	.758
$C_{12\text{-}17}$	.355	.337	.325	.312
$C_{12\text{-}34}$	.538	.507	.473	.427
$C_{12\text{-}51}$	.710	.635	.567	.516
$C_{12\text{-}68}$	.823	.698	.647	.562
$C_{12\text{-}85}$	.885	.827	.751	.637
$C_{12\text{-}100}$	.960	.860	.760	.676
$C_{16\text{-}18}$	.456	.435	.427	.411
$C_{16\text{-}34}$	.665	.602	.570	.569
$C_{16\text{-}51}$	.850	.764	.700	.673
$C_{16\text{-}68}$	.981	.922	.819	.797
$C_{16\text{-}84}$	1.15	1.00	.951	.917
$C_{16\text{-}100}$	1.24	1.10	1.07	.972

Table 2.3: Huggins Parameter of Model Associative Polymers in Water

Structure	30°C	40°C	50°C	60°C
$C_{0\text{-}17}$	.56	.44	.32	.34
$C_{0\text{-}33}$	.46	.42	.30	.20
$C_{0\text{-}50}$	.37	.42	.46	.50
$C_{0\text{-}67}$	.40	.42	.50	.41
$C_{0\text{-}84}$	.42	.42	.40	.42
$C_{0\text{-}100}$	.34	.40	.48	.47
$C_{12\text{-}17}$	9.7	8.8	4.9	6.4
$C_{12\text{-}34}$	6.1	5.7	5.0	1.6
$C_{12\text{-}51}$	3.0	3.0	2.9	2.5
$C_{12\text{-}68}$	2.0	2.2	2.0	2.3
$C_{12\text{-}85}$	1.7	1.5	1.4	1.3
$C_{12\text{-}100}$	1.1	1.1	1.1	1.4
$C_{16\text{-}18}$	16	14	11	10
$C_{16\text{-}34}$	4.8	4.0	3.2	5.8
$C_{16\text{-}51}$	4.6	3.5	4.7	1.4
$C_{16\text{-}68}$	3.3	2.7	2.2	1.4
$C_{16\text{-}84}$	1.4	1.1	1.4	1.6
$C_{16\text{-}100}$	1.1	1.1	1.7	1.6

Table 2.4: Mark–Houwink Parameters of Model Associative Polymers in Water †

End-group	Temp (°C)	K_{MH} x 10^3 (dl/g)	a
H	30	1.29	.581
	40	1.71	.547
	50	2.38	.508
	60	3.31	.471
C12	30	1.32	.576
	40	1.84	.539
	50	2.09	.518
	60	4.07	.445
C16	30	1.59	.579
	40	2.18	.541
	50	2.48	.524
	60	3.08	.500

† $[\eta] = K_{MH} M^a$

As shown in Table 2.3, the Huggins parameters K' for solutions of model associative polymer with the hexadecyl and dodecyl end- groups are abnormally large and vary between 1 and 16. In general, the Huggins parameter decreases as molecular weight increases, as hydrophobe length decreases, and as temperature increases. This behavior is usually attributed to the association phenomenon [53]. Brown and Glass [54] used absorbance measurements on model star shaped associative polymers to find that large values of K' for associative polymer solutions corresponded to the formation of a hydrophobic domain in solution. Hence, the large values of K' in Table 2.3, and the rapid increase in specific viscosity with increasing polymer concentration in Figure 2.1 indicate association of the model polymers with dodecyl and hexadecyl end- groups, and suggest that the free energy of association becomes larger in magnitude as the length of the hydrophobic end- group increases relative to the hydrophilic polymer backbone. The decrease in the Huggins parameter, and its approach to the value expected for a polymer-theta solvent system as temperature increases, is not surprising. It is well known that poly(oxyethylene) contracts on heating because the hydrogen bonds between the ether oxygens and water molecules are disrupted [55]. This compression of the polymer coil helps to suppress interactions between neighboring coils, and thus lower K'. We discuss these and other thermodynamic features in another section of this chapter; here we simply note that the effect of temperature and associative polymer structure on K' is consistent with the dependence of the chemical potential of the associative polymers' hydrophobes on these same variables. The chemical potential of a hydrophobe $\Delta\mu$ can be estimated from Scott-Hildebrand theory [11]:

$$\Delta\mu = 2RT - \frac{V_s + V_p}{2}(\delta_s - \delta_p)^2 x^2 \qquad (2.19)$$

where R is the gas constant, T is the absolute temperature, V_S and V_P are the molar volumes of the solvent and hydrophobe respectively, δ_S and δ_p are the solubility parameters of the solvent and hydrophobe respectively, and x is the volume fraction of the hydrophobe in solution. As discussed by Hoy et al. [11], the driving force for forming and sustaining intermolecular associations increases as the chemical potential of the hydrophobic groups becomes more negative. Increasing the temperature of an associative polymer solution, decreasing the size of the hydrophobe, matching the solubility parameter of the solvent to that of the hydrophobe, or increasing molecular weight (which decreases the volume faction of hydrophobes for a given mass concentration) should decrease the degree of intermolecular association. Thus, the Huggins parameter is an indicator for the degree of intermolecular association.

Figures 2.2 through 2.5 show the dependence of the intrinsic viscosities of the model associative polymers on molecular weight and temperature. The molecular weight dependence of the intrinsic viscosities of the model polymers is nearly the same regardless of hydrophobe length, and the intrinsic viscosities of the model polymers are similar in value to those presented by Bailey and Koleske [55] and Amu [41] for poly(oxyethylene) in water. The intrinsic viscosities decrease as temperature increases irrespective of hydrophobe length, and as was discussed in the previous paragraph, this results from a decrease in coil dimensions as temperature increases. The intrinsic viscosities of the polymers with hexadecyl hydrophobes are slightly larger than those of the other polymers, which is noteworthy because the intrinsic viscosity of a hydrophobically modified polymer is usually lower than that of the corresponding homopolymer due to intramolecular associations that contract the chain dimensions [37]. This suggests that the larger intrinsic viscosities possibly result from measuring the hydrodynamic volume of an aggregate, rather than that of a molecularly dispersed associative polymer. Undoubtedly, the

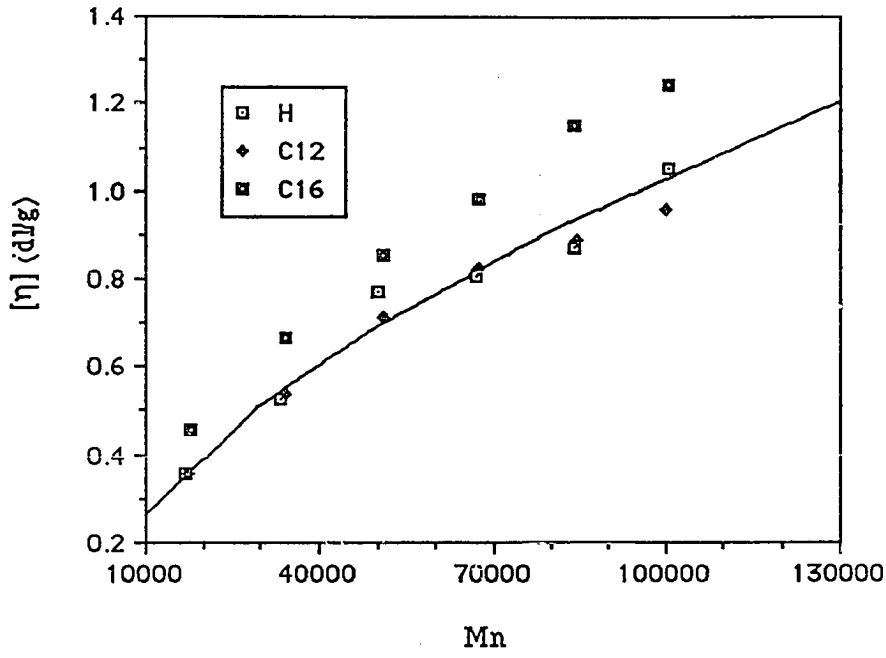

Figure 2.2: Intrinsic viscosities of model associative polymers in water at 30°C. The line represents the Mark-Houwink equation as applied to the hydroxyl terminated polymers. See Table 2.4 for the parameters of the equation.

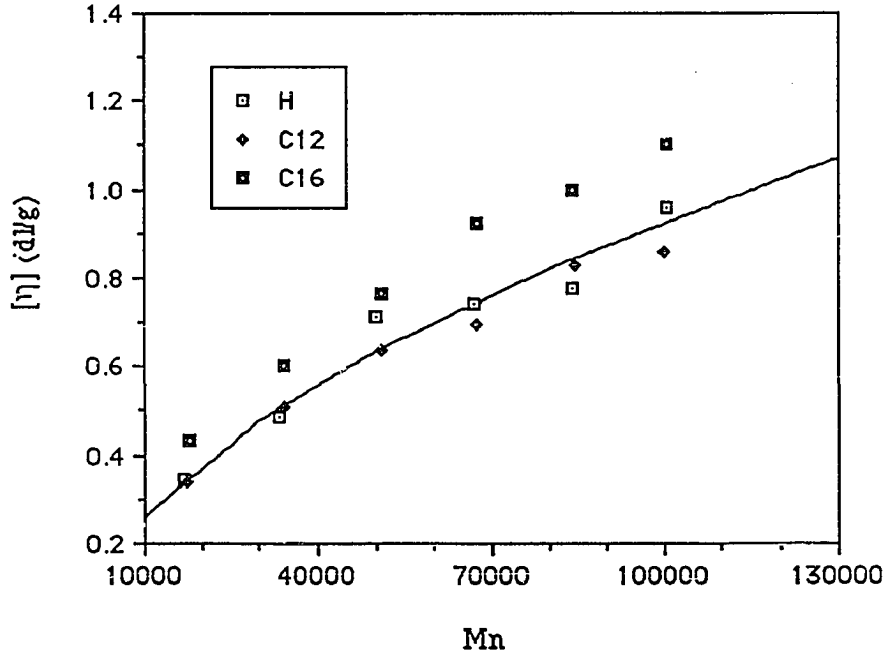

Figure 2.3: Intrinsic viscosities of model associative polymers in water at 40°C. The line represents the Mark-Houwink equation as applied to the hydroxyl terminated polymers. See Table 2.4 for the parameters of the equation.

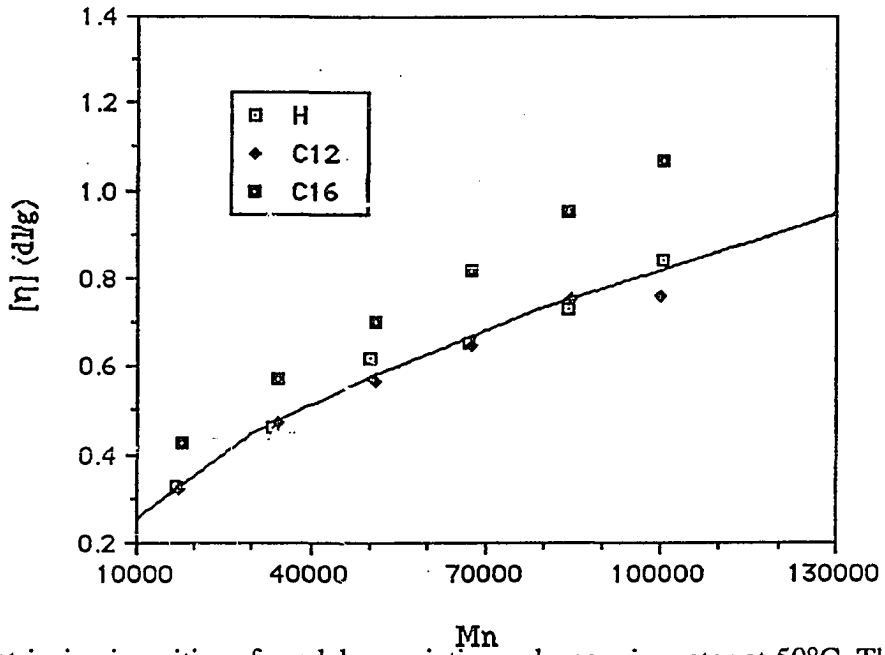

Figure 2.4: Intrinsic viscosities of model associative polymers in water at 50°C. The line represents the Mark-Houwink equation as applied to the hydroxyl terminated polymers. See Table 2.4 for the parameters of the equation.

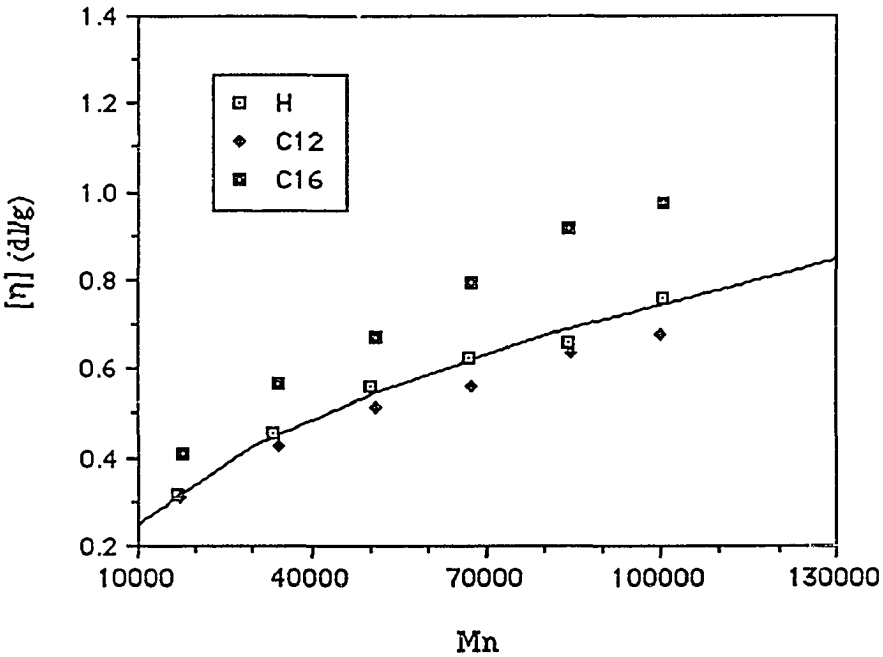

Figure 2.5: Intrinsic viscosities of model associative polymers in water at 60°C. The line represents the Mark-Houwink equation as applied to the hydroxyl terminated polymers. See Table 2.4 for the parameters of the equation.

solutions contain a distribution of species: some polymers that are aggregated, and some that are not. This distribution will depend on associative polymer concentration, structure, and solution temperature. Indeed, we make use of this fact later in this chapter to derive a physical kinetic model for the concentration dependence of relative viscosity. However, aggregation cannot be a major contribution to the intrinsic viscosities reported here for two reasons. First, the intrinsic viscosities of the hexadecyl terminated polymers are systematically larger in a solvent composed of 40 percent Butyl Carbitol and 60 percent water. The next section of this chapter shows that the associative polymers do not intermolecularly associate in this solvent mixture. Second, as shown in Appendix A, the molecular weight distributions are polydisperse, resulting in some uncertainty in the number average molecular weight. These facts indicate that the discrepancies in the intrinsic viscosities between polymers with different end- groups are probably due to differences in model polymers' molecular weight distributions. This conclusion should be tested by repeating these experiments with either monodisperse associative polymers (if it is possible to synthesize such samples), or with fractionated samples of our model associative polymers obtained either by dialysis or by precipitation from benzene with isooctane via Moacanin's method [56]. In any event, the intrinsic viscosity results show that the average molecular weights of the model associative polymer samples increase systematically in the way expected from reaction stoichiometry, and that the molecular weights of the different hydrophobe series are indeed close.

Scaling Behavior

How the rheological properties of associative polymers scale with concentration and molecular weight depends on the solvent medium, and on associative polymer structure and concentration. Dilute solution theories adequately describe the viscosity behavior of aqueous solutions of the hydroxyl terminated model associative polymers, even up to

concentrations of 5% polymer by weight. This is shown in Figure 2.6, where the relative viscosity data for all six molecular weights of the hydroxyl terminated model associative polymers in water at 30°C superimpose to form a master curve when plotted against the overlap parameter $c[\eta]$. The master curve follows the Huggins equation (Equation 2.4) when a value of 0.4 is used for K'. In contrast, dilute solution theories cannot adequately represent the viscosity data for aqueous solutions of model associative polymers with hexadecyl or dodecyl end- groups: $c[\eta]$ fails to standardize data because significant interaction occurs among the hydrophobic alkyl end- groups. Instead, the data scale via the de Gennes c* theorem for semi-dilute solutions: $\eta_o/\mu_s = F[\bar{c}/c^*]$, where $\bar{c} = c/M$ molar concentration of associative polymer, and c* is proportional to $M^{-4/5}$ for polymer chains that follow a self–avoiding random walk in a good solvent. Figure 2.7 shows the resulting standardization, where the relative viscosities of the model polymers with either dodecyl or hexadecyl hydrophobes in concentration between .2% and .8% by weight superimpose to a set of master viscosity curves, one for the dodecyl terminated polymers (open symbols) and one for the hexadecyl terminated polymers (closed symbols). These curves have more scatter than the curve in Figure 2.6, which results from the uncertainty in the number average molecular weights of the polymers due to their broad molecular weight distributions. Also, solutions of hexadecyl terminated polymers are non-Newtonian when the polymer concentration exceeds 0.5%, and the relative viscosity depends on the shear rate in the capillary. This causes additional scatter in the data in the curve at the larger polymer concentrations. The important conclusion from these two figures is that interactions among associative polymer hydrophobes in water cause significant non-classical rheological behavior, even when the concentrations are dilute enough that an unmodified homopolymer of identical molecular weight exhibits single chain behavior.

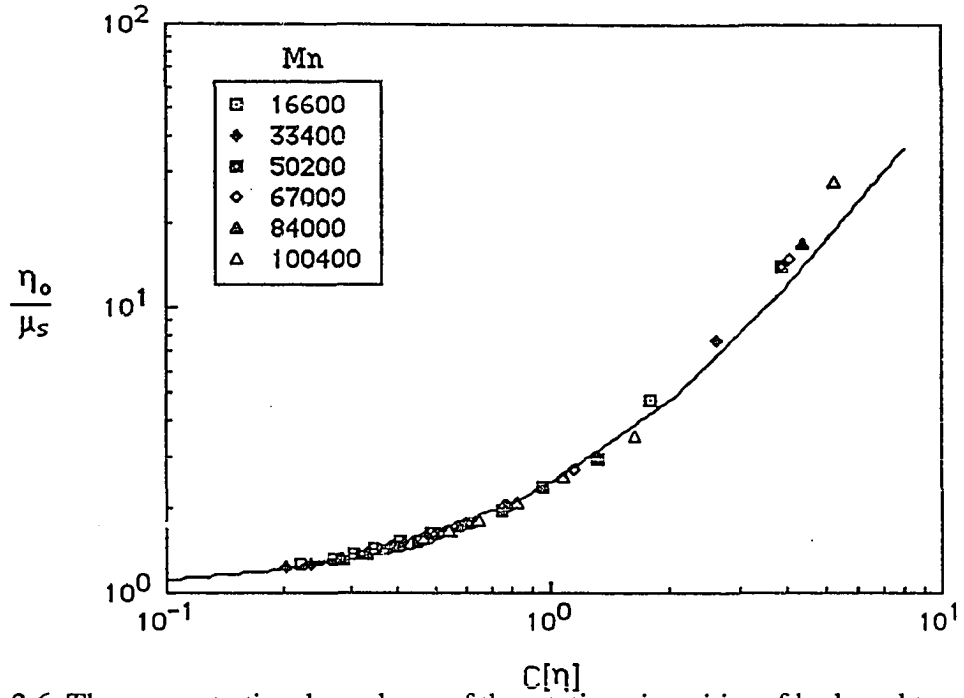

Figure 2.6: The concentration dependence of the relative viscosities of hydroxyl terminated model associative polymers in water at 30°C. The line in the Figure is Equation (2.4) with the Huggins parameter K' equal to 0.4.

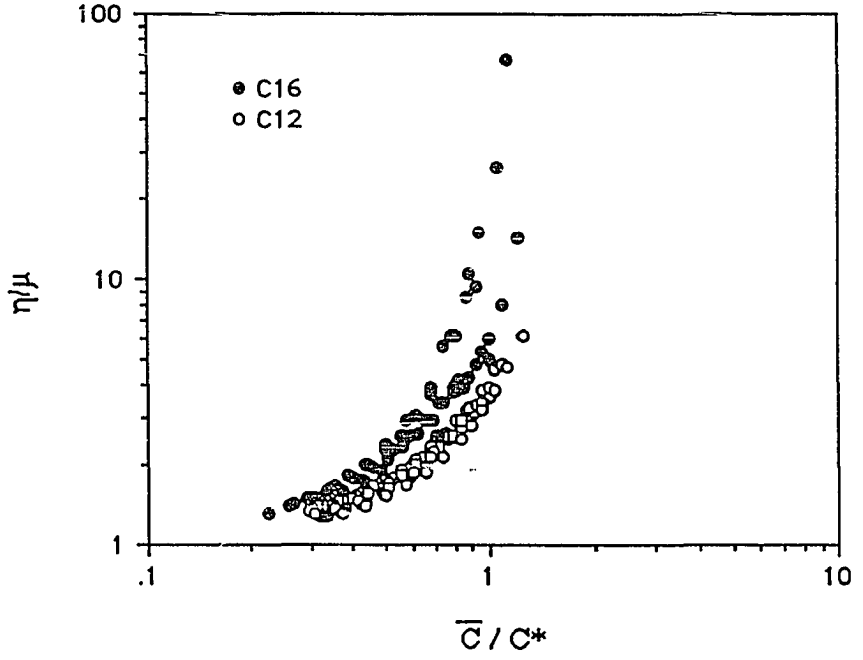

Figure 2.7: The semi-dilute scaling behavior of the relative viscosities of dodecyl (open symbols) and hexadecyl (closed symbols) terminated model associative polymers in water at 30°C.

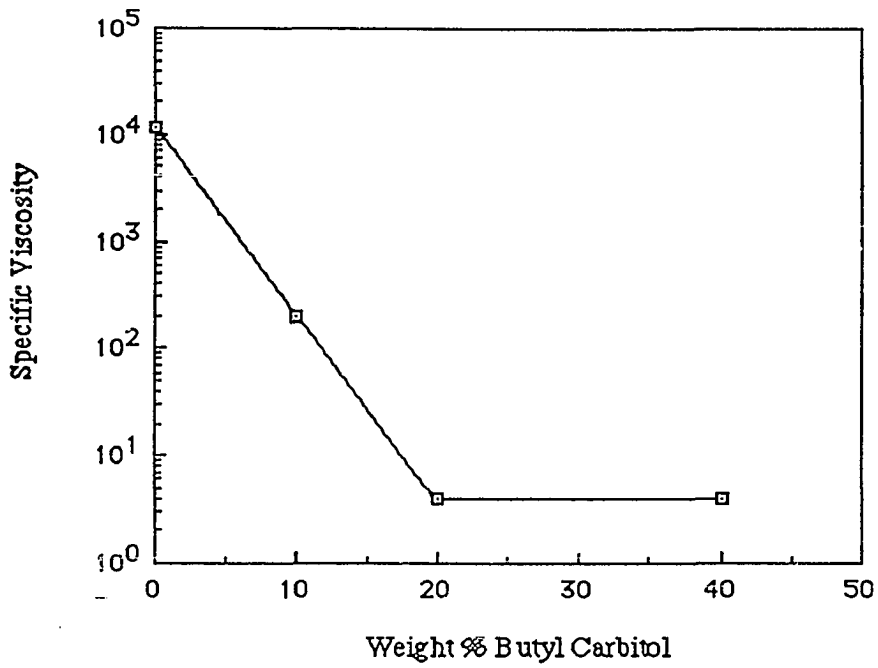

Figure 2.8: The influence of diethylene glycol monobutyl ether (Butyl Carbitol) on the specific viscosity of 2.5% by weight hexadecyl terminated associative polymer with a number average molecular weight of 51,000 at 24.5°C.

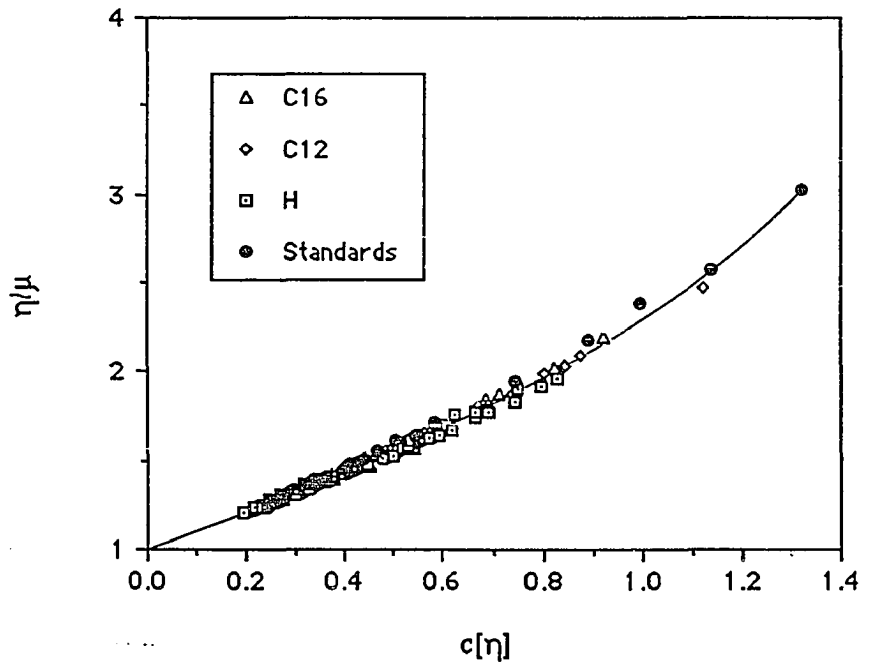

Figure 2.9: The dilute scaling behavior of model associative polymers and monodisperse poly(oxyethylene) standards in a mixed solvent system composed of 40% diethylene glycol monobutyl ether (Butyl Carbitol) and 60% water at 30°C.

Apparently, intermolecular interactions between hydrophobes in water occur at extremely dilute concentrations, definitely at concentrations on the order of a few tenths of a weight percent.

Figure 2.8 shows the effect of adding Butyl Carbitol, a diethylene glycol monobutyl ether water miscible cosolvent manufactured by Union Carbide Corporation, on the specific viscosity of a 2.5 weight percent aqueous solution of a hexadecyl terminated associative polymer with a number average molecular weight of 51,000. Because Butyl Carbitol has a relatively large viscosity on its own, the specific viscosity of the polymer in solution is used to eliminate the variation in the viscosity of the solvent mixture from the comparison. The specific viscosity decreases sharply as the concentration of Butyl Carbitol increases up to 20% by weight in the solvent mixture, whereupon it reaches a plateau where additional Butyl Carbitol has no effect on the specific viscosity. This plateau suggests that association has been minimized; however, it is not until we examine the scaling behavior of the polymers in solvent mixture that contain 40% Butyl Carbitol and 60% water by weight that we can conclude that association has been eliminated. As shown in Figure 2.9, the relative viscosities of model associative polymers, both hydroxyl and hydrophobe terminated, and poly(oxyethylene) standards in the solvent mixture collapse to a single master curve. The rheological properties of the model polymers are indistinguishable from those of the poly(oxyethylene) standards, and this indicates that the association has been eliminated. This behavior is anticipated from Equation (2.19). The solubility parameter of water is 23.4, the solubility parameter of Butyl Carbitol is 9.78, and the solubility parameter of the hexadecyl alkyl groups are approximately 8; the addition of Butyl Carbitol lowers the solubility parameter of the solvent so that it more nearly matches that of the hydrophobe to reduce the free energy of association. Therefore, the non-classical behavior in water described in the previous paragraphs can only be from association among associative polymer hydrophobes.

Molecular Dimensions

As described in the Introduction, we can use the analysis developed by Kurata and Stockmayer (Equation (2.11)) and by Stockmayer and Fixman (Equation (2.12)) to estimate the unperturbed dimensions of the associative polymer coil in solution. Figures 2.10 through 2.15 show the the intrinsic viscosity data plotted by this analysis for the model associative polymers; all of the plots have two features in common. First , regardless of the temperature of the solution, the lines in each figure extrapolate to the same intercept K_θ , which measures the unperturbed dimension of the model polymers in water from $K_\theta = \Phi[\langle r^2\rangle_0/M]^{3/2}$. Second, the lines in the figures have positive slopes, and thus positive second virial coefficients at room temperature, and these slopes decrease to zero as the temperature increases. This section describes the calculations made to determine the molecular dimensions of the model associative polymer in solution; the next section describes the thermodynamic implications of the temperature dependence of the slopes of the lines in Figures 2.10 through 2.15.

As shown in Table 2.5, the two different extrapolation equations, as applied to model associative polymers of a given length for the alkyl end- group, provide similar estimates of K_θ. Because we used number average molecular weights in the extrapolation equations, and because the model associative polymers are not monodisperse, we must correct the intercepts for the polydispersity before we can calculate the unperturbed dimensions of the model polymers from them. This is done by multiplying K_θ in Equations (2.11) and (2.12) with q_n , which is a correction factor that depends on the shape of the molecular weight distribution [45, 57, 58]. The equation of Newman et al. [57] estimates the correction factor directly from the moments of the molecular weight distribution:

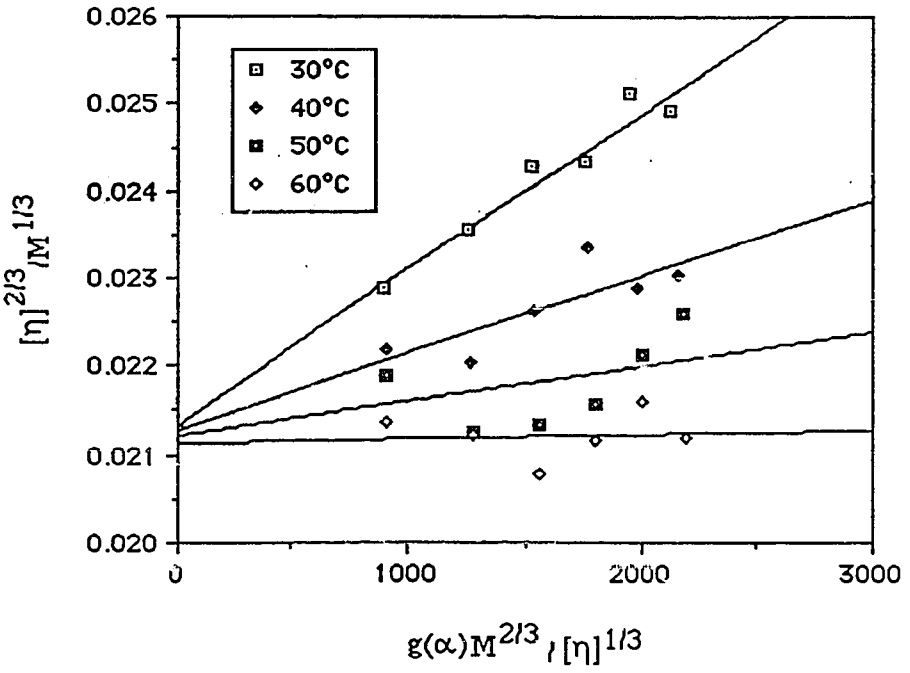

Figure 2.10: Plot of the Kurata-Stockmayer equation (Equation 2.11) as applied to hexadecyl terminated model associative polymers in water.

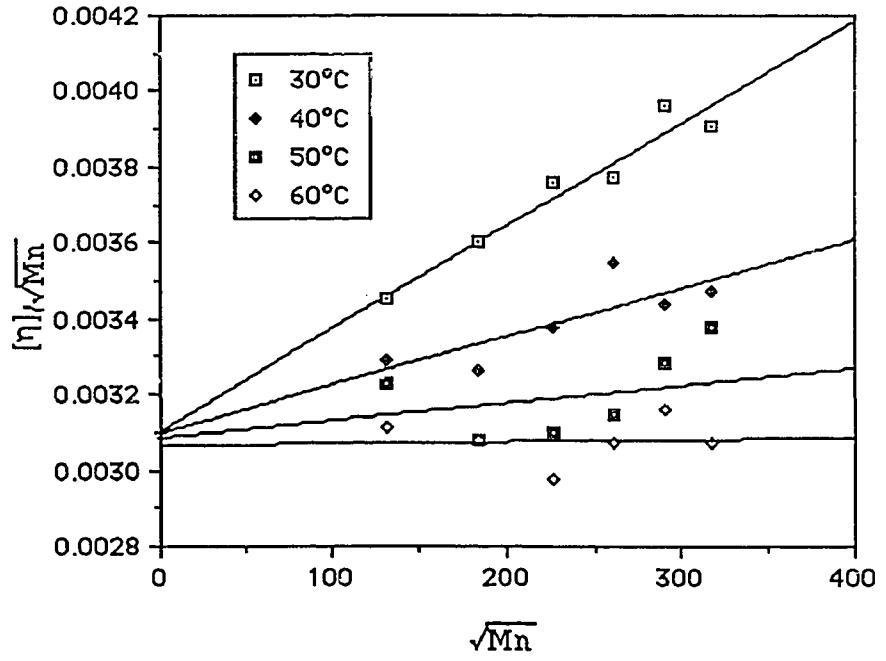

Figure 2.11: Plot of the Stockmayer-Fixman equation (Equation 2.12) as applied to hexadecyl terminated model associative polymers in water.

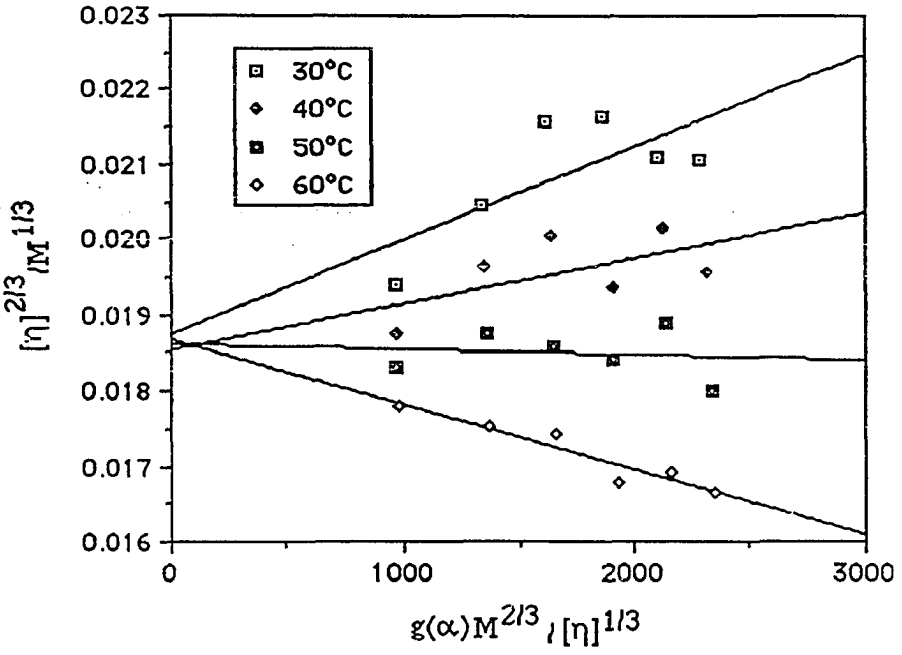

Figure 2.12: Plot of the Kurata-Stockmayer equation (Equation 2.11) as applied to dodecyl terminated model associative polymers in water.

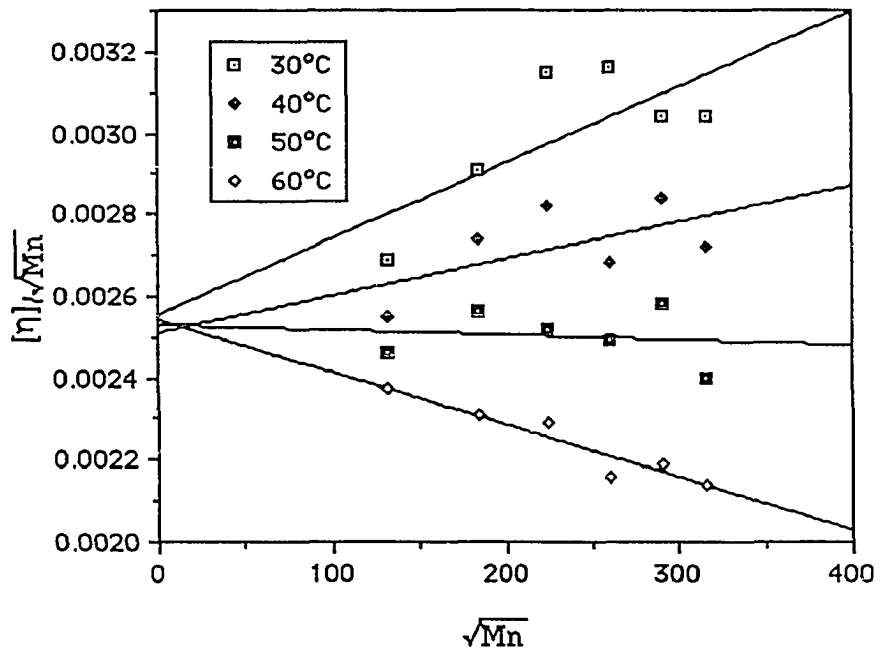

Figure 2.13: Plot of the Stockmayer-Fixman equation (Equation 2.12) as applied to dodecyl terminated model associative polymers in water.

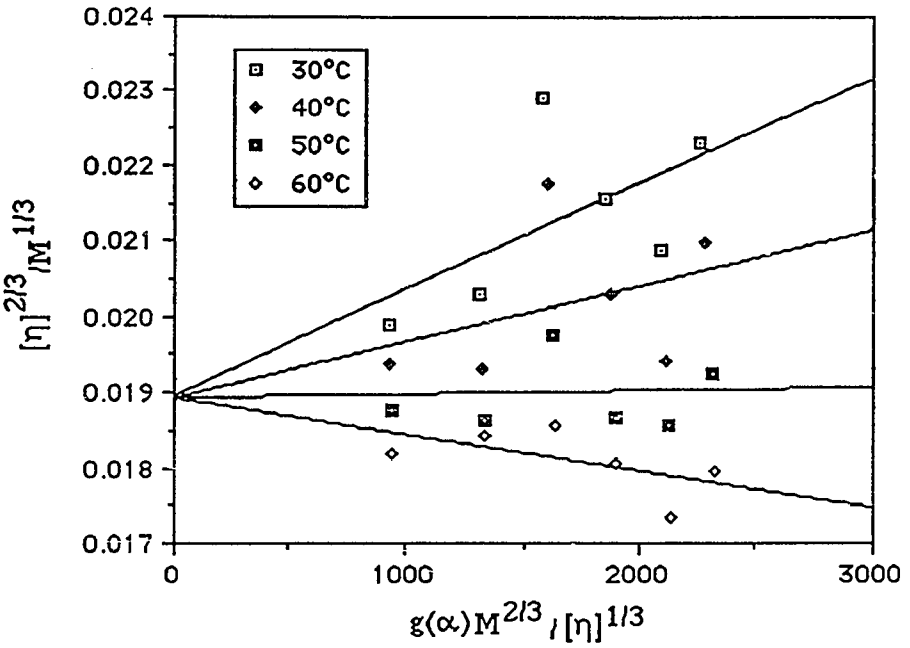

Figure 2.14: Plot of the Kurata-Stockmayer equation (Equation 2.11) as applied to hydroxyl terminated model associative polymers in water.

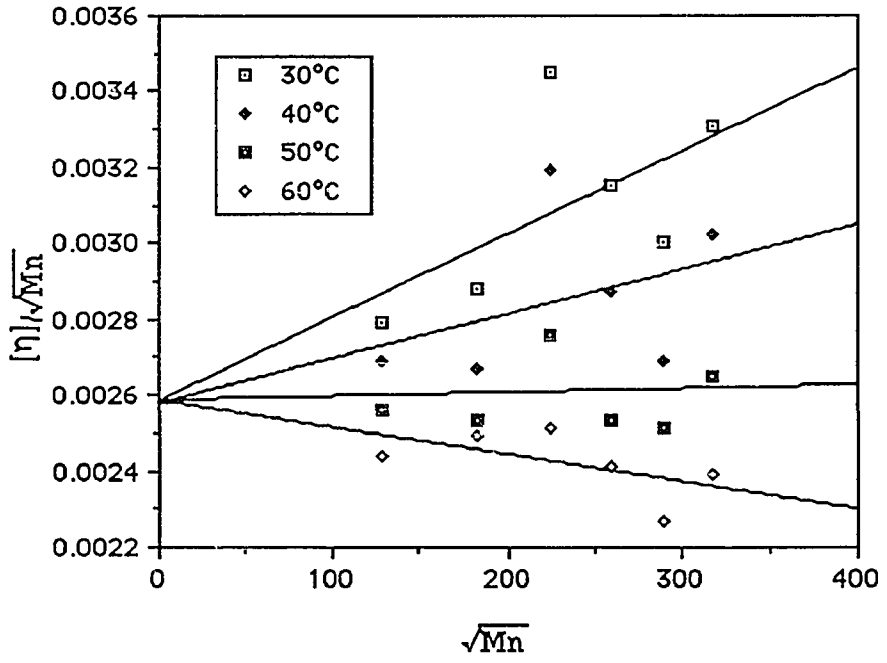

Figure 2.15: Plot of the Stockmayer-Fixman equation (Equation 2.12) as applied to hydroxyl terminated model associative polymers in water.

Table 2.5: Thermodynamic Parameters of Model Associative Polymers in Water†

Item	End-group: C16	C12	H
$K_\theta \times 10^3$ (dl/g) (SF)	3.10	2.37	2.54
$K_\theta \times 10^3$ (dl/g) (KS)	3.10	2.57	2.60
$K_\theta \times 10^3$ (dl/g) (Corrected)*	1.48	1.12	1.21
$B_O \times 10^{27}$ (cm^3) (SF)	-2.67	-3.06	-2.77
$B_O \times 10^{27}$ (cm^3) (KS)	-2.66	-2.87	-2.58
Θ (°C) (SF)	58.1	55.4	53.0
Θ (°C) (KS)	60.0	50.9	51.7
Θ (°C) (MH)	60.6	51.9	53.7
Θ (°C) (FF)	52.5	54.5	58.4

† Letters in Parenthesis indicate method of evaluation:
SF = via Stockmayer-Fixman analysis
KS = via Kurata-Stockmayer analysis
MH = via interpolation on the Mark-Houwink exponent
FF = via Flory-Fox analysis

* Average experimental value, corrected for polydispersity with Equation (2.20)

Table 2.6: Root Mean Square End–To–End Distances of Model Associative Polymers in Water

End-group	M_n	$\langle r^2 \rangle_o^{1/2}$ (Å)	$\langle r^2 \rangle^{1/2}$ (Å) 30°C	40°C	50°C	60°C
H	16600	108	110	109	107	106
	33400	152	158	154	151	150
	50200	187	207	201	191	186
	67000	216	231	225	215	211
	84000	243	255	246	240	232
	100400	264	288	279	268	259
C12	17400	107	112	110	108	107
	34200	150	161	158	154	149
	50700	183	201	194	186	181
	67700	211	232	220	215	205
	84500	236	257	251	243	230
	99900	257	278	268	257	248
C16	17500	118	122	120	119	118
	34200	164	172	167	164	164
	51000	200	214	207	200	197
	67600	231	246	242	232	230
	84300	257	279	267	262	259
	100400	282	304	292	289	280

$$q_n \cong \frac{I_1^2 I_3^{3/2}}{I_{3/2} I_2^{5/2}} \tag{2.20}$$

where

$$I_m = \sum_i M^m N_i \tag{2.21}$$

For a Gaussian distribution, q_n is approximately equal to the the ratio of the weight average molecular weight to the number average molecular weight. Fortunately, the method should provide a fair estimate of the chain dimensions even though the correction factor for the model polymers is rather large (about 2.1), because the linear unperturbed dimensions are only proportional to $K_\theta^{2/3}$. Table 2.6 lists the unperturbed dimensions of the model associative polymers in water that are corrected in this manner. The unperturbed root mean square end–to–end distances of the model polymers in water are on the order of one hundred to three hundred angstroms, which are similar to the dimensions of poly(oxyethylene) that were obtained by other workers [43, 55, 56, 59].

Once the dimensions of the unperturbed coil are known, the effect of short range interactions on the thermodynamic flexibility of the polymer chain can be estimated through the "steric hindrance" parameter σ: $\sigma^2 = \langle r^2 \rangle_o / \langle r^2 \rangle_{o,\,free}$, where

$$\langle r^2 \rangle_{o,\,free} = N b_e^2 \left(\frac{1 - \cos\phi}{1 + \cos\phi} \right) \tag{2.22}$$

is the dimension of a polymer with completely free rotation about its bonds, and N is the number of bonds of length b_e and valence angle ϕ in the polymer backbone. Because steric or electrostatic interaction among segments prevent a polymer coil from sampling all of the possible internal bond rotations available to it, the coil expands to dimensions that are

larger than those that the coil would assume in the absence of steric hindrance. Thus the steric hindrance parameter is greater than one, and usually has a value of between 1.5 to 2.5 for most polymers. In poly(oxyethylene), the internal resistances are steric rather than electrostatic, and the chain is relatively flexible about its ether oxygens due to the absence of hydrogen atoms substituents [45]. Neglecting the presence of the isophorone diisocyanates in the associative polymer backbone, and assuming a carbon-carbon bond length of 1.54Å , a carbon-oxygen bond length of 1.43Å, and tetrahedral bonds in the polymer backbone, the steric hindrance parameter for the associative polymer is 1.47. This is consistent with values of 1.4 through 1.6 calculated from the data of poly(oxyethylene) from other workers [43, 45, 55,56, 59]. The ratio of the fully extended length of the polymer coil L_{max} to the calculated end-to-end distance $\langle r^2 \rangle_o^{1/2}$ provides an estimate for the degree of coiling of the polymer coil in solution. Assuming again that poly(oxyethylene) approximates the associative polymers' molecular structure, the fully extended length of the model associative polymer monomer unit is 3.6Å, and the ratio of the fully extended polymer chain to the end-to-end distance of the polymer coil is over 12 for the lowest molecular polymer, and over 30 for the highest molecular weight polymer. These calculations indicate that the model associative polymers are flexible, highly coiled chains in solution, and can be modelled in dilute solution as having a Gaussian segment distribution.

During the last several decades, many models that account for the intensity of interaction between the polymer and solvent have been developed for the conformation of the polymer coil in solution: non-draining coils for polymers that interact strongly with solvent molecules, and free draining coils for polymers that interact weakly with the solvent. The molecular theories of Debye and Bueche [60] , Kirkwood and Riseman [61], and Peterlin [62] can infer the dimensions of such a polymer chain in solution. Debye and Bueche modeled the polymer coil as a solvent permeable sphere that has a constant polymer

Table 2.7: Theoretical Root Mean Square End–To–End Distances of Model Associative Polymers in Water at 30°C

		$\langle r^2 \rangle^{1/2}$ (Å)			
End-group	Mn	Stockmayer-Fixman	Peterlin	Kirkwood-Riseman	Debye-Bueche
H	16600	110	136	136	94
	33400	158	195	194	135
	50200	207	255	253	176
	67000	231	285	283	197
	84000	255	314	312	217
	100400	288	355	353	246
C12	17400	112	137	137	95
	34200	161	197	197	136
	50700	201	247	247	170
	67700	232	286	285	197
	84500	257	316	315	217
	99900	278	344	342	228
C16	17500	122	150	149	103
	34200	172	213	212	147
	51000	214	264	262	182
	67600	246	304	302	210
	84300	279	345	343	238
	100400	304	375	373	259

segment distribution function (i.e. a sieve-like permeable equivalent sphere), and solved the resulting hydrodynamic problem. Their result is:

$$< r^2 >^{1/2} (cm) = \left(\frac{36}{10}\right)^{1/2} \left(\frac{3\,M\,[\eta]}{4\pi N_A\,\phi(\sigma)}\right)^{1/3} \qquad (2.23)$$

where $[\eta]$ has the units cm^3/g, and the function $\phi(\sigma)$ accounts for the permeability of the equivalent sphere and depends on the Mark-Houwink exponent. When the solvent and polymer do not interact strongly, the polymer only slightly inhibits the flow of the solvent through the polymer coil with the result that the average velocity of the solvent differs from that of the polymer coil. Kirkwood and Riseman model the polymer chain as a "pearl necklace" where the frictional resistance of the polymer was concentrated in beads spaced along a completely flexible polymer backbone, and expressed the hydrodynamic interaction between beads given with the Oseen tensor. Their result is :

$$< r^2 >^{1/2} (cm) = \left[\frac{36\,M\,[\eta]}{N_A \sqrt{6\pi^3}\; XF(X)}\right]^{1/3} \qquad (2.24)$$

where the intrinsic viscosity has the units cm^3/g, X is the "draining parameter" found from the Mark-Houwink exponent, and the function F(X) is given in the revised tables of Kurata and Yamakawa [63]. Peterlin modeled the polymer as a random coil that had a high segment density at its center that partially immobilized the solvent. His result for the root mean square end–to–end distance is:

$$< r^2 >^{1/2} (cm) = 1.21 \times 10^{-8} \left[\frac{[\eta]\,M}{(1-a)}\right]^{1/3} \qquad (2.25)$$

where "a" is the Mark–Houwink exponent, and the intrinsic viscosity has units of cm^3/g. Table 2.7 compares the root mean square end–to–end distances calculated by these theories to those determined by experiment (i.e., the Kurata-Stockmayer and Stockmayer-Fixman analyses). Although the models have various deficiencies and simulate the polymer coil with varying degrees of realism [34, 45], the dimensions calculated from them agree fairly well with those calculated from the extrapolation equations. The draining characteristics of the polymer coils calculated from these models are small; thus, all of the theories indicate a large degree of solvent inhibition by the polymer backbone in solution.

Thermodynamic Parameters

The second virial coefficient, Flory theta temperature, and the enthalpy and entropy of dilution parameters quantify the degree of polymer-solvent interaction. For solutions of model associative polymers, Ballard et al. [48] cleverly modified Flory-Fox theory [47] to account for the effects of association on these parameters by including a term in the free energy due to association $\Delta F_{association}$:

$$\Delta F = \Delta F_{el} + \sum_{j\ segments} \Delta F_m + \Delta F_{association} \tag{2.26}$$

ΔF_{el} and ΔF_m are calculated from the Flory's familiar expressions. To derive an expression for contribution of association to the overall free energy, Ballard et al. assumed that the kinetics of association followed:

$$m + m \underset{\leftarrow}{\rightarrow} d \tag{2.27}$$

where 'm' and 'd' represent monomers and dimers respectively. The equilibrium constant for this reaction is given by:

$$K_A = [d]/[m]^2 \tag{2.28}$$

and is related to the standard molar free energy of association ΔF_a^o through:

$$\Delta F_a^o = -RT \ln K_A \tag{2.29}$$

By assuming dilute conditions, which are valid for small degrees of association, and by assuming that the polymers coils are Gaussian, they derived the contribution of association to the overall free energy:

$$\Delta F_{association} = -2\, kT\, C_m\, (d_p^2\, V_1\, f^2\, K_A \ln K_A / m_s^2)\, M^{1/2}\, \alpha^{-3} \tag{2.30}$$

where k is Boltzmann's constant, C_m is given by Equation (2.16), d_p is the density of the polymer, and f is the mole fraction of hydrophobes in the associative polymer. When Equation (2.30) is substituted into Equation (2.26) along with Flory's expressions for ΔF_{el} and ΔF_m, there results:

$$\alpha^5 - \alpha^3 / M^{1/2} = 2\, C_m (\psi_1 - \Theta/T - f^2\, d_p^2\, V_1\, K_A \ln K_A / m_s^2) \tag{2.31}$$

which reduces to the Flory swelling equation when no association is present.

Equation (2.31) states that association, as reflected in positive values of K_A, actually decreases the dimensions of the polymer coil. As discussed previously, this is ostensibly due to intramolecular association. A plot of $\alpha^5 - \alpha^3/\sqrt{M}$ against $1/T$ should then produce a family of parallel lines with equal slopes that are proportional to the Flory theta

temperature and with intercepts that decrease as the free energy of association increases. Although the quantity $\alpha^5-\alpha^3/\sqrt{M}$ should not depend on molecular weight, it is well known that it does because of the approximate nature of the Flory swelling equation [45]. For the model associative polymers, $\alpha^5-\alpha^3/\sqrt{M}$ passes through a maximum in the middle of the molecular weight series. Hence, when we plot the results for our model polymers according to Equation (2.31) in Figure 2.16, we use the average value of $(\alpha^5-\alpha^3)/\sqrt{M}$ that is obtained from the series of molecular weights for a given alkyl end- group. The error bars in Figure 2.16 mark the extremes of the values used to obtain this average. It is not clear in Figure 2.16 that the length of the alkyl end- group has made any difference at all. As an interesting aside, if the data are regressed separately by hydrophobe type, what results are lines that have nearly the same intercepts and slopes that depend on the length of the alkyl end- group. This suggest that the equilibrium constant for association depends on

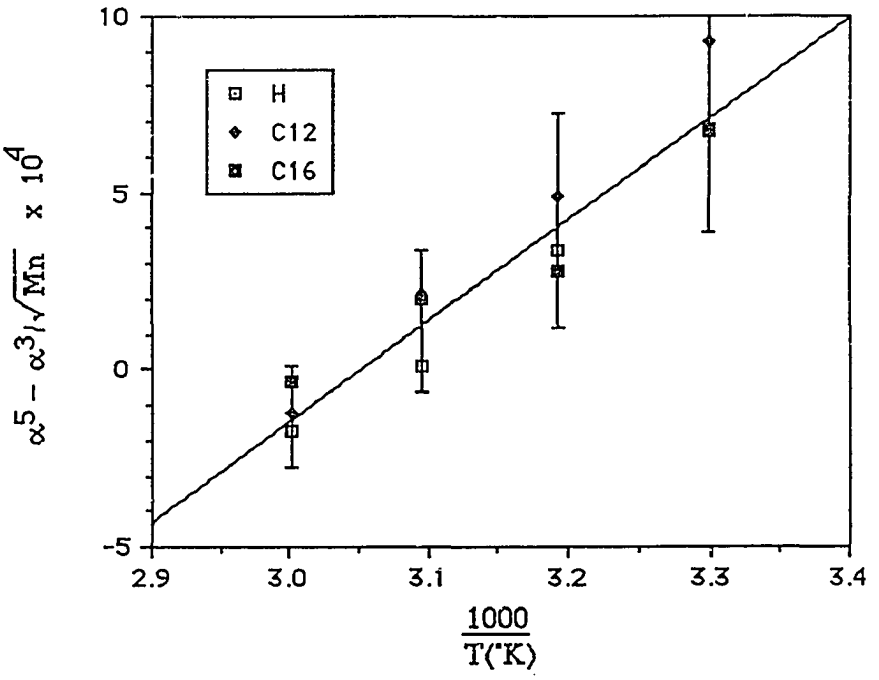

Figure 2.16: Flory-Fox plot for model associative polymers in water.

temperature, $K_A = F(T)$. In classical thermodynamics, the Gibbs-Helmholtz equation expresses the effect of temperature on an equilibrium reaction :

$$\frac{\partial[\frac{\Delta F_a^o}{T}]}{\partial T} = -R\frac{\partial \ln K_A}{T} = -\frac{\Delta H_A}{T^2} \qquad (2.23)$$

where ΔH_A is the standard enthalpy of reaction: it is negative for an exothermic reaction and positive for an endothermic reaction. Substitution of Equation (2.32) into Ballard's analysis results in:

$$\alpha^5 - \alpha^3 / M^{1/2} = 2\, C_m[\psi_1 - \Theta/T + \frac{f^2 V_1}{v_2^2 m_s^2}\frac{\Delta H_A}{RT} e^{-\Delta H_A/RT}] \qquad (2.33)$$

If the standard enthalpy of the association reaction is small, and the exponential can be approximated by its Taylor series, then a plot of Equation (2.33) should produce a line whose slope depends on the standard enthalpy of association. If the enthalpy of association is larger, then a curve results. Like Ballard's equation, Equation (2.33) indicates that the standard enthalpy of association is negative, and the association is therefore spontaneous, the effect of association is to contract the dimensions of the polymer coil. Equation (2.33) can be considered the generalization of Ballard's equation to include the effect of temperature on the distribution of aggregates at equilibrium in solution.

Unfortunately, it is difficult to unambiguously distinguish between the various data for polymers with different termini in Figure 2.16 because the polymers have broad molecular weight distributions. We are thus resigned to the fact that the equations described above must be applied to well - fractionated samples before they can produce a

precise analysis of effect of hydrophobe on dilute solution thermodynamics. In addition, Equation (2.19) asserts that the free energy of association, and hence K_A, depends both on concentration and temperature so that it might be difficult to measure the free energy of association from data obtained from extrapolation to infinite dilution. As elegant as Ballard's analysis is, we must look elsewhere for a means to estimate free energy of association.

In the meantime, we settle for a semi - quantitative evaluation of the enthalpy and entropy of dilution parameters from classical Flory-Fox analysis, which means that we set ΔH_A in Equation (2.33) to zero, and draw a single line of best fit through all of the data in Figure 2.16. This assumption does not affect the signs on the enthalpy and entropy of dilution parameters that we calculate. Due to the assumptions made in the Flory-Fox theory, the absolute values of the enthalpy and entropy of dilution parameters may differ in absolute magnitude from those obtained by osmotic pressure or light scattering measurements. However, as pointed out by Flory and Fox [47], the relative contributions of ψ_1 and κ_1 to the thermodynamic interactions between polymer and solvent are correct. The slope of the line in Figure 2.16 equals $-2C_m\psi_1\Theta$, and its intercept equals $2C_m\psi_1$. Since the slope of the line is positive, and since Θ is positive, the entropy of dilution parameter ψ_1 is negative. Although a negative entropy of dilution parameter is opposite in sign to those of most polymer-solvent systems, it is typical of water soluble polymers, and of poly(oxyethylene) [41]. The negative entropy of dilution parameter results from orientation effects produced by the hydrogen bonding between water molecules and the ether oxygens in the model polymer backbone [45], and indicates that the dissolved polymer deswells on heating. This was observed as a decrease in the intrinsic viscosities of the model associative polymers on heating, as was presented in Figures 2.2 through 2.5. Calculation of a number value for the entropy of dilution parameter from the the line in Figure 2.16 requires a numerical value for the partial specific volume of the model

polymers so that C_m can be calculated from Equation (2.16). Although this is unknown at present, it can be estimated since the model polymers have a composition similar to poly(oxyethylene), which has $\nu_2 = 0.846$ [64]. The partial specific volume should not vary appreciably from this value, and the values of ψ_1 and κ_1 relative to each other are not affected by this assumption. The enthalpy and entropy of dilution parameter for the models associative polymers estimated in this manner are 164/T(°K) and -0.5, respectively.

Because K_θ does not depend on temperature, the slopes of the lines in Figures 2.10 through 2.15 are proportional to $(1/2-\chi)$ [45], and the Flory equation can be used to determine Θ:

$$B(T) = B_o[1-\Theta/T] \tag{2.34}$$

where absolute temperature is used. As shown in Table 2.5, these values of the theta temperature agree well with those obtained from interpolation of the exponent in the Mark–Houwink equation as a function of temperature (Table 2.4), and with that obtained from the slope of the line in Figure 2.16. B_o is negative because the entropy of dilution parameter is negative. The model associative polymers form irregular solutions with water, as demonstrated by the negative enthalpy and entropy of dilution parameters. (Recall that $\kappa_1=\psi_1\Theta/T$). Since ψ_1 is negative, the Flory–Huggins interaction parameter:

$$\chi = 1/2 + \psi_1[\Theta/T-1] \tag{2.35}$$

is less than 1/2 for $T < \Theta$, which confirms that water at room temperature is a good solvent for the model associative polymers. This also means that the chemical potential of the solvent in the polymer volume element μ_1 is less than that of pure liquid water μ_1^0 for $T < \Theta$, as shown by the excess chemical potential of the solvent:

$$(\mu_1-\mu_1^0)_E = -RT\psi_1(1-\Theta/T) \qquad (2.36)$$

Thus, water swells the model polymer at room temperature in response to a chemical potential gradient. As temperature increases, an increase in the excess entropy of mixing compensates for the favorable enthalpy of mixing, which reduces the chemical potential gradient and dehydrates the polymer backbone. This shows that water is a good solvent for the model polymers at room temperature, and the solvent quality decreases as temperature increases.

Our conclusion from this discussion is that either the interactions between the alkyl hydrophobic end- groups do not alter the behavior of the associative polymers at infinite dilution enough to invalidate using the classical Flory-Fox analysis, or that the molecular weight distributions of the samples prevent us from seeing such effects. In any event, we must consider a different analysis that accounts for the increase in free energy of association with concentration before we can estimate the free energy of association among the hydrophobic groups in dilute solution.

Kinetic Model

In view of the difficulties in the analysis presented in the previous section on determining the influence of the free energy of association on the viscosity of a dilute solution of associative polymer, Equation (2.19) and the data in Figures 2.17 and 2.18 inspire us to estimate free energy of association by examining the influence of length of the alkyl end-group (Figure 2.17) and molecular weight of the model polymer (Figure 2.18) on the concentration dependence of the relative viscosity. It is self-evident that the differences

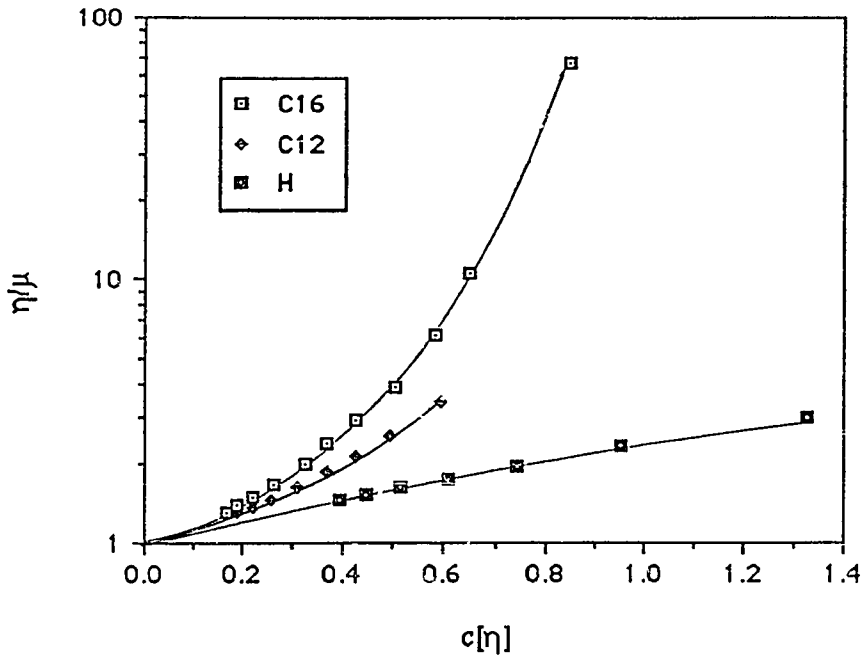

Figure 2.17: Influence of the length of the alkyl end- group on the relative viscosity of model associative polymers with a number average molecular weight of 51,000 in water at 30°C.

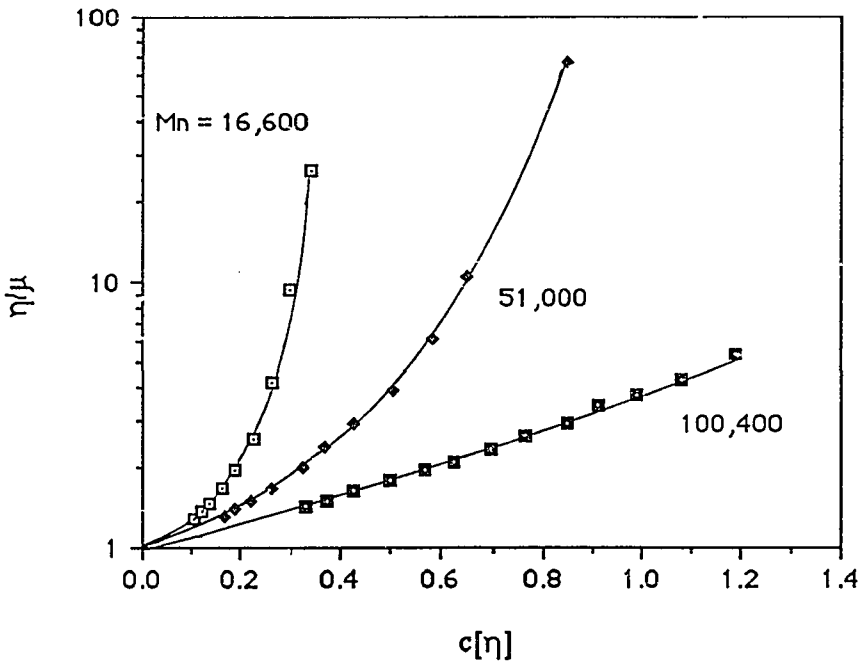

Figure 2.18: Influence of molecular weight on the relative viscosity of hexadecyl terminated model associative polymers in water at 30°C.

in the viscosity -concentration curves for the hydroxyl terminated polymers and the hexadecyl and dodecyl terminated polymers plotted in Figure 2.16 must result from an association among the alkyl end- groups. This was discussed in a previous section of this chapter in terms of the influence of associative polymer structure on the Huggins parameter K'. The results of that section indicated that the driving force for association increased as the length of the alkyl end- group increased and as the molecular weight of the associative polymer decreased (Figure 2.18). The association built up a pseudo-high-molecular weight in solution, which resulted in a large value for the Huggins parameter and a sharp increase in the relative viscosity with concentration. From these ideas, we build a physical model for the concentration dependence of the relative viscosity.

Like Ballard et al., we model the reaction kinetics of the association process as a reversible equilibrium step polymerization in a closed reaction vessel. Thus, the reaction kinetics are:

Reaction Number	Reaction	extent of reaction	
1	$m + m \underset{\leftarrow}{\rightarrow} (m + 1)\ mer$	p_1	(2.37)
2	$(m + 1)mer + m \underset{\leftarrow}{\rightarrow} (m + 2)\ mer$	p_2	(2.38)
o	o	o	
o	o	o	
o	o		
		o	
J	$(m + J - 1)mer + m \underset{\leftarrow}{\rightarrow} (m + J)\ mer$	p_J	(2.39)

which may be written in general form as:

$$n = 1 \ldots J \qquad (n - 1)mer + m \underset{\leftarrow}{\rightarrow} (n)\ mer \qquad (2.40)$$

where "m" denotes an unassociated polymer. These equations are general up to any arbitrary number of association reactions n = J. In this section, the notation "monomer" refers to the unaggregated associative polymer, and "dimer", "trimer", "n-mer" and etc., refer to aggregate composed of two, three and n associative polymer chains. Weissberg et al. [65] have taken a similar approach in modelling the influence of aggregation of polymers on the concentration dependence of the relative viscosities of dilution solutions, although they restricted their reaction kinetics to dimer and trimers, and the context of our model is different. It is not difficult to show that reactions like dimer + dimer, or dimer + trimer , are simply linear combinations of Equations (2.37) to (2.40), and are therefore not needed to completely describe the association process. Our model also differs from the model developed by Bieleman et. al. in that we do not assume the existence of a micellar network in solution [31], an assumption that applies better to more concentrated solutions.

The equilibrium constants for the reactions expressed by Equations (2.37) through (2.40) are given by:

$$K_1^* = \frac{[\,(m+1)\text{mer}]}{[m]^2} \tag{2.41}$$

$$K_n^* = \frac{[(m+n)\ \text{mer}\,]}{[m]\ [(m+n-1)\text{mer}\,]}\ ,\ n= 2...J \tag{2.42}$$

The equilibrium constant depends on the standard molar free energy of association, as was given before in Equation (2.29), and on the molecular weight of the growing aggregate because it is more difficult for the aggregate to diffuse and participate in the reaction. The

relationship between the size of a polymer in dilute solution and the diffusion coefficient is modelled by the Hookean dumbbell of polymer kinetic theory:

$$D_{Aggregate} = \frac{\langle r^2 \rangle_o}{M} \frac{N_A k T}{6 \mu} \frac{1}{[\eta]} = \left(\frac{K_\theta}{\Phi} \right)^{2/3} \frac{N_A k T}{6 \mu} \frac{1}{K_{MH} M^a} \tag{2.43}$$

where the molecular weight used in Equation (2.43) is the molecular weight of the aggregate. Here we make the physically reasonable and intuitive assumption that the association reaction is diffusion limited so that the equilibrium constants depend on molecular weight in the same way. Thus, Brownian processes build up a dynamic network that can never grow to infinite extent unless the free energy of association is infinite. The formation of a dynamic network of finite extent is consistent with rheological properties of concentrated solutions presented in Chapter III of this dissertation.

A mass balance on the associative polymer in solution yields:

$$[m] = [m]_i - p_1[m]_I - p_2[m]_I - \ldots - p_J[m]_I = [m]_I \left(1 - \sum_{L=1}^{J} P_L \right) \tag{2.44}$$

$$[(m + n)\text{mer}] = p_n [m]_I \tag{2.45}$$

$$[(m+n-1)\text{mer}] = p_{n-1}[m]_I - p_n[m]_I \tag{2.46}$$

where p_i is the extent of reaction i, and $[m]_I$ is the initial molar concentration of unassociated polymers. Combining these mass balances with the reaction kinetics given in Equations (2.41) and (2.42) yields:

$$K_1^* = \frac{p_1}{[m]_I \left(1 - \sum_{L=1}^{J} p_L\right)^2} \tag{2.47}$$

$$K_n^* = \frac{p_n}{[m]_I \left(1 - \sum_{L=1}^{J} p_L\right)(p_{n-1} - p_n)} \quad , n = 2...J \tag{2.48}$$

Thus, if the equilibrium constants are known from the free energy of association, the extent of reaction and the distribution of species in solution can be calculated.

Equations (2.47) and (2.48) represent J coupled non-linear algebraic equations:

$$1 - 2\sum_{L=1}^{J} p_L + \sum_{L=1}^{J} p_L \sum_{L=1}^{J} p_L - \frac{p_1}{K_1^*[m]_I} = 0 \quad n = 1 \tag{2.49}$$

$$p_n \sum_{L=1}^{J} p_L - p_n - \frac{p_n}{K_n^*[m]_I} - p_{n-1} \sum_{L=1}^{J} p_L + p_{n-1} = 0 \quad n = 2...J \tag{2.50}$$

which we solve numerically via the Newton-Raphson method. Note that increasing the initial concentration of unassociated polymers in solution has the same effect as increasing the free energy of association; increasing either drives the equilibrium reaction toward completion. To apply the method, we rewrite Equation (2.49) as

$$g_1(p_1, p_2, ...p_J) = 0 \qquad n = 1 \tag{2.51}$$

and Equation (2.50) as

$$g_n(p_1, p_2, ... p_J) = 0 \qquad n = 2... J \tag{2.52}$$

and expand Equations (2.51) and (2.52) in terms of their Taylor series to linearize them:

$$- g_1(p_1^i, p_2^i, \ldots p_J^i) = \Delta p_1 \frac{\partial g_1(p_1^i, p_2^i, \ldots p_J^i)}{\partial p_1} + \Delta p_2 \frac{\partial g_1(p_1^i, p_2^i, \ldots p_J^i)}{\partial p_2} + \ldots$$

$$\ldots + \Delta p_J \frac{\partial g_1(p_1^i, p_2^i, \ldots p_J^i)}{\partial p_J} \qquad n = 1$$

...(2.53)

$$- g_n(p_1^i, p_2^i, \ldots p_J^i) = \Delta p_1 \frac{\partial g_n(p_1^i, p_2^i, \ldots p_J^i)}{\partial p_1} + \Delta p_2 \frac{\partial g_n(p_1^i, p_2^i, \ldots p_J^i)}{\partial p_2} + \ldots$$

$$\ldots + \Delta p_J \frac{\partial g_n(p_1^i, p_2^i, \ldots p_J^i)}{\partial p_J} \qquad n = 2 \ldots J$$

...(2.54)

and define

$$\Delta p_n = p_n^{i+1} - p_n^i \tag{2.55}$$

where the superscript on the extent of reaction indicates the iteration number. These equations may be represented in matrix form as:

$$\begin{bmatrix} \frac{\partial g_1}{\partial p_1} & \cdots & \frac{\partial g_1}{\partial p_J} \\ \vdots & & \vdots \\ \frac{\partial g_J}{\partial p_1} & \cdots & \frac{\partial g_J}{\partial p_J} \end{bmatrix} \begin{bmatrix} \Delta p_1 \\ \vdots \\ \Delta p_J \end{bmatrix} = \begin{bmatrix} -g_1 \\ \vdots \\ -g_J \end{bmatrix} \tag{2.56}$$

where the partial derivatives in the Jacobian are:

$$\frac{\partial g_1}{\partial p_1} = 2p_1 - \left(2 + \frac{1}{K_1^*[m]_I} - 2\sum_{L=2}^{J} p_L\right)$$

$$\frac{\partial g_1}{\partial p_n} = 2p_1 + 2\sum_{L=2}^{J} P_L - 2 \qquad n = 2 \ldots J$$

$$\frac{\partial g_n}{\partial p_n} = \sum_{L=1}^{J} P_L - 1 - \frac{1}{K_n^*[m]_I} + p_n - p_{n-1}$$

$$\frac{\partial g_n}{\partial p_{n-1}} = 1 - \sum_{L=1}^{n-1} p_L - \sum_{L=n+1}^{J} p_L - p_{n-1} \qquad (2.57)$$

$$\frac{\partial g_n}{\partial p_{n-2}} \cdots \frac{\partial g_n}{\partial p_{n-J}} = p_n - p_{n-1}$$

$$\frac{\partial g_n}{\partial p_{n+1}} \cdots \frac{\partial g_n}{\partial p_J} = p_n - p_{n-1}$$

The method is as follows. We start by assuming an initial set of extent of reactions p_n^i, and use these to calculate the partial derivatives and the functions in the solution vector in Equations (2.56) and (2.57). These values are used to then calculate the correction in the extent of reactions Δp_i in Equation (2.56) by inverting the matrix using LU decomposition.

Then a new set of extents of reaction p_n^{i+1} are found from Equation (2.55), and the process is repeated until the correction Δp_i becomes negligible.

Once the extents of reaction have been calculated, the mole fractions Y_n, where the n represents the product of the nth reaction, are calculated from:

$$Y_o = \frac{1 - \sum_{L=1}^{J}}{1 - \sum_{L=2}^{J}}; \quad Y_1 = \frac{p_1 - p_2}{1 - \sum_{L=2}^{J}} \; ; \; Y_{J-1} = \frac{p_{J-1} - p_J}{1 - \sum_{L=2}^{J}} \; ; \; Y_J = \frac{p_J}{1 - \sum_{L=2}^{J}} \qquad (2.58)$$

where Y_0 is the mole fraction of unassociated polymer. The number average and weight average molecular weights of the distribution are then calculated from:

$$\frac{<M>_n}{M_o} = \frac{\sum_{i=o}^{J} Y_i(i+1)}{\sum_{i=o}^{J} Y_i} \; ; \quad \frac{<M>_w}{M_o} = \frac{\sum_{i=0}^{J} Y_i (i+1)^2}{\sum_{i=0}^{J} Y_i (i+1)} \qquad (2.59)$$

where M_0 is the molecular weight of the unassociated polymer. The ratio of the number average molecular weight to the molecular weight of the unassociated polymer is also the average number of associations in the solution. The total free energy from the association process can simply be calculated from the product of number average of associations and the free energy change for one association given by Equation (2.29).

The next step is to relate the distribution of aggregate sizes to solution viscosity. Because no analytical theory is available for this, we use the corresponding states principles developed earlier in this chapter, namely Equation (2.4). Here we assume that the hydrodynamic volume of a dimer composed of two monomers of molecular weight M_0 is

the same as a single monomer of molecular weight $2M_o$. This neglects branching in the network, and does not account for the functionality of the network junction; however, we can relax this assumption momentarily. This assumption also implies that the enhancement in solution viscosity comes completely from individual clusters that grow as concentration increases, and does not consider the interactions that occur between aggregates. This is a serious flaw, but there is no easy way to mathematically incorporate these interactions into the model. Thus, we can expect no more than qualitative agreement with the data. With this assumption, we can calculate the effective intrinsic viscosity of the aggregate from the Mark-Houwink equation, and then calculate the relative viscosity of the solution from :

$$\frac{\eta}{\mu} = 1 + c[\eta]_{effective} + K'c^2[\eta]^2_{effective} + \ldots \qquad (2.60)$$

where $[\eta]_{effective}$ equals:

$$[\eta]_{effective} = K_{MH} M_o^a \sum_{i=o}^{J} Y_i I^a \qquad (2.61)$$

Thus, we can calculate how viscosity - concentration relationship for associative polymers in dilute solution varies with the free energy of association.

Figures 2.19 and 2.20 show the effect of varying the free energy of association and the molecular weight of the unassociated polymer on the viscosity - concentration relationships calculated by the model. As the free energy of association increases, the number average molecular weight of the aggregated species in solution grows to larger and larger values, which results in a solution viscosity that increases sharply as concentration increases. Here we have used free energies that are comparable to the free energy of micellization of nonionic surfactants. When the free energy of association is zero, the

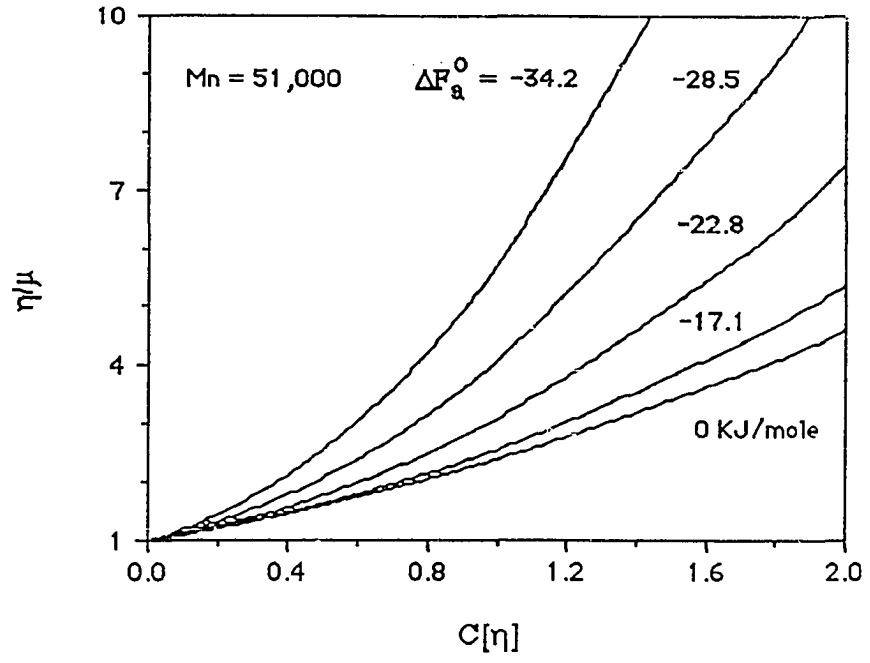

Figure 2.19: Influence of the free energy of association (Equation 2.29) on the kinetic model's viscosity-concentration relationship of associative polymers with a number average molecular weight of 51,000.

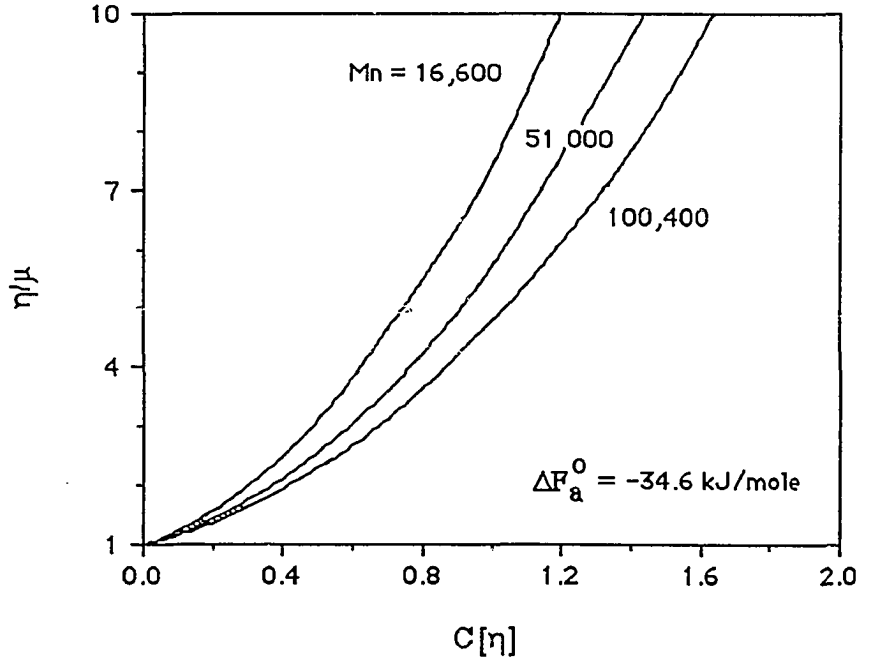

Figure 2.20: Influence of molecular weight on the kinetic model's viscosity-concentration relationship of associative polymers with a free energy of association of -34.6 KJ/Mole.

model follows the Huggins equation, and when the free energy of association is non-zero, the viscosity - concentration relationship becomes more dramatic. For a fixed free energy of association, the viscosities of solutions that contain small molecular weight associative polymer are more sensitive to changes in concentration than are solutions that contain large molecular weight associative polymers. Both effects mimic experimental data, where the unmodified polymer followed the Huggins equation, and the hydrophobically modified polymers had large values of K' that depended on lengths of both the associative polymer backbone and the alkyl end- groups. Thus, the model indicates that the free energy of association of the model associative polymers increases as molecular weight decreases, and as the length of the hydrophobic end- group increases.

Although the qualitative agreement between the model and the data is pleasing, the model has neglected many things. First, it has neglected the influence branching on the hydrodynamic resistance of the aggregate. As shown by Zimm and Stockmayer [66], branched macromolecules have a higher average segment density than linear macromolecules of the same molecular weight, and therefore have a lower coil volume. The effect of branching on the chain dimensions is expressed by:

$$\frac{[\eta]_{branched}}{[\eta]_{linear}} = g^{*3/2} = \frac{\langle r^2 \rangle_{branched}}{\langle r^2 \rangle_{linear}} \tag{2.62}$$

where g* depends on the functionality and number of the branching sites. For example, for a polymer with tetrafunctional branches, g* is:

$$g^*_4 = (1/n_w) \ln (1 + n_w) \tag{2.63}$$

where n_w is the number of branch points per molecule by weight. Thus the resistance of a branched polymer in solution is less than the resistance of an unbranched polymer of similar molecular weight. When Equations (2.62) and (2.63) are used in the model, the growth in the viscosity tapers off at large concentrations. This also is observed experimentally, as shown in Figure 3.2 of the next chapter, where the rate of increase of the viscosity enhancement by the associative polymer tapers off at large concentrations. Second, the model neglects polydispersity in the unassociated polymers. Third, the model has assumed that the aggregates are like unassociated polymers in that they assume a spherical or Gaussian segment distribution in solution. It does not consider that the aggregates might be non-spherical in shape. Fourth, the current model also neglects the increase of the local viscosity on the diffusion of the growing aggregates. The effect would be to retard the growth of the aggregate, and we can account for this by using the local solution viscosity in Equation (2.43) rather than the solvent viscosity. This effect will keep the aggregate from growing into an infinite cluster, and causes the viscosity enhancement to taper off at large concentrations. Hence concentrated solutions of associative polymer are not true gels, although they are gel-like. These effects are better probed through rheology, as shown in Chapter III.

We have also neglected interactions between neighboring aggregates, which should build a network that has striking rheological properties. At a certain critical concentration between one half and one weight percent, solutions of associative polymers exhibit remarkable and strongly non-Newtonian rheologies. Chapters III and IV show that these solution rheologies are best and most naturally interpreted and modelled with network theories. So it is not surprising that although the model predicts a sharper increase in the solution viscosity as concentration, the experimental data exhibit an even larger viscosity enhancement than the model can predict using the values we have used for the free energy

of association. Thus, much of the enhancement in viscosity in the data must be due to multi - body interactions between aggregates.

In short, we have constructed a physical model for viscosity - concentration relationship of dilute associative polymer solutions that is based on equilibrium kinetics of association. Because we are unaware of any theory that has been derived from fundamental origins on how solution viscosity relates to associative polymer structure, we have used a principle from corresponding states to connect molecular weight to occupied volume to viscosity. The model incorporates the effects of diffusion and branching of the aggregates through physically reasonable, but somewhat ad hoc, assumptions. The most serious shortcomings in the model as it now stands are its inability to account for multi - body interactions among aggregates, and its inability to predict the formation of a coherent network. When these features are introduced into the model, it should represent the data better. Nonetheless, the model does correctly predict the qualitative influence of the structure of the associative polymer on the viscosity - concentration relationship in dilute solution.

Conclusions

Analysis of the data presented in this chapter has yielded some useful information, even if some of it is semi-quantitative because of the polydispersity of the model associative polymer samples. We have estimated the dimensions of the associative polymer coils in solution, which are needed to select the correct membrane pore size for the adsorption apparatus. We have measured the signs and relative magnitudes of heat and entropy of dilution, and have demonstrated that water miscible cosolvents can disrupt the networking behavior of associative polymers by modifying the solubility characteristics of the solvent. This has allowed us to verify the molecular weights of the model polymers, and to prove that the dramatic enhancement of solution viscosity by associative polymers, and the

dependence this enhancement on polymer structure, are due to association behavior. We have constructed a physical model based on equilibrium kinetics for the association process, and have used it to monitor how the free energy of association influences the distribution of aggregates in solution. Although the model neglects some important features, and is therefore only qualitative, it does exhibit the correct dependence of viscosity on molecular weight and concentration, and indicates that the free energy of association must become larger as the length of the alkyl end- groups becomes larger relative to the hydrophilic backbone. Combination of the results of this chapter with those obtained from dynamic light scattering measurements will provide complimentary characterizations of the associative polymer in dilute solution.

Because some of the analysis presented in the chapter depends on having samples of monodisperse polymers of known molecular weight, it can be improved by fractionating the model associative polymer sample. This can be achieved either through dialysis, or through precipitation of the associative polymer from benzene with isooctane [56].

Setting questions on polydispersity aside, the dilute solution viscosity behavior shows that once the concentration of associative polymer exceeds the overlap concentration, water excludes the hydrophobes from solution to form a hydrophobic domain. This concentration is less than the coil overlap concentration. This congregation of hydrophobes, which we call an association cluster, consists of the approximate aggregation of two or more hydrophobes from different model polymers to form an association network. The three dimensional shear sensitive association network increases the apparent molecular weight of the associative polymer in solution to enhance rheological properties. The next chapter examines the consequences of this behavior in concentrated solutions.

Chapter III

Steady Shear and Linear Viscoelastic Material Properties of Concentrated Model Associative Polymer Solutions

Introduction

Motivation

The concentration of associative polymer used in commercial latex paints is usually on the order of a few weight percent, which is large enough to be considered concentrated by the standards set forth in Chapter II. To understand the influence of associative polymer structure on the rheology of such systems, we must uncouple the influence of aqueous phase self-association of the associative polymer from its interaction with particle surfaces. This means that we should examine the rheological behavior of associative polymers in concentrated solutions, as we do in this chapter, as well as the adsorption behavior of the associative polymer, as we do in Chapter V. In the same way that the dilute solution studies of the previous chapter serve as a control group for concentrated solution studies of this chapter, the concentrated solutions serve as a control group for the latex rheology studies presented in Chapter VI.

As discussed in Chapter I, most of the early research on the influence of associative polymers on latex rheology sought to examine systems that closely approximated commercial paints. (see reference [32] for example) The goal of this kind of research was to aid in paint formulation, so that comparatively little attention was devoted to the aqueous phase self-association. What little experimental work on solution rheology that had been published in the open literature concerned itself with the influence of associative polymer structure on low shear viscosity; the traditional proof of the existence of the association

network came from how the low shear viscosity dramatically depended on the nature of the hydrophobic component of the associative polymer. Nevertheless, the influence of the association mechanism on the entire viscosity profile and on the frequency dependence of the viscoelastic properties of neat associative polymer solutions were often neglected. This is surprising, especially given the apparent influence of the aqueous phase network on the rheological properties of the latex paints, and the fundamental nature of such experiments. We do not disparage the importance of the early studies; we only suggest that experiments that were useful for determining formulation strategies were not necessarily the best experiments for revealing fundamental aspects of the association mechanism.

Rheology of Associative Polymer Solutions

The early studies on latexes pointed out the complexity of associative polymer technology, and motivated rheological studies on the influence of polymer structure on viscous and elastic properties of concentrated associative polymer solutions. As the following literature reveals, contemporary research on associative polymer solutions encompasses a range of associative polymer types. Despite the structural differences in associative polymers, some rheological characteristics, such as viscoelasticity and a shear thickening region in the viscosity profile, are common among many associative polymer solutions. This suggests that rheological properties of associative polymer solutions result from the dynamics of an association network under shear.

Because any microstructure possessed by a fluid imparts solid-like elastic properties to the fluid, solutions of associative polymer have elastic properties. By measuring the frequency dependence of these viscoelastic properties, we can uncover fundamental molecular information on the association mechanism. Lundberg et al. [67] studied the viscoelastic properties of solutions that contained one of the following four

hydrophobically modified urethane-ethoxylate model associative polymers: a linear polymer of number average molecular weight between 8,700 to 24,000 with either octyl, dodecyl, or nonylphenol hydrophobic end- groups, or a trimer with a number average molecular weight of 10,500 and with nonylphenol hydrophobic end- groups. They concluded that the placement and number of hydrophobes on the associative backbone were critical in determining elasticity, and that linear polymers with large hydrophobic end- groups form a strongly elastic network in solution. Goodwin et al. [13] characterized the viscoelastic properties of a hydrophobically modified cellulose of number average molecular weight of 100,000. They monitored, by an inflection in the loss modulus with respect to frequency, the aggregation and disaggregation of the polymers in the solution. Flynn and Goodwin [68] measured the shear wave rigidity moduli and the pyrene fluorescence emission spectra of acrylamide dodecyl methacrylate copolymers in saline solution to determine the functionality of the association network formed by the polymers. They calculated that a given network junction contained roughly ten associative polymer hydrophobes. These studies show that the viscoelasticity of solutions reflects the functionality and strength of association network junctions.

Because the quality of a paint is judged by how its viscosity depends on shear rate, it seems natural that we should measure the entire viscosity profile of a given associative polymer solution, and not just its viscosity at one or two shear rates. We can deduce the dynamics of the association network under shear from the influence that associative polymer structure exerts on the viscosity profile. Bock et al. [53] synthesized copolymers of alkylacrylamide and acrylamide with weight average molecular weights of 3×10^6, and probed the effect of hydrophobe structure and electrolyte concentration on the steady shear viscosity. They observed a shear - thickening region in the viscosity profile, the magnitude of which depended on level and type of hydrophobe content, polymer concentration, and

solvent quality. Because the relaxation times for the polymer solution increased in the shear - thickening region of the viscosity profile, they concluded that the shear - thickening resulted from a change in the relative amounts of intramolecular to intermolecular associations. They also pointed out that quantifying the relationships between associative polymer structure and solution rheology via scaling laws would be useful in associative polymer design. Maerker and Sinton [69] used poly(vinyl alcohol) and polysaccharide with sodium borate at low pH as a model associating polymer system. They measured steady shear viscosity profiles and dynamic mechanical properties to investigate the flow structures induced by shear, and used nuclear magnetic resonance to determine number of association complexes in their solutions. Like Maerker and Sinton, they related the shear - thickening regions in the viscosity profiles of their solutions to a shift from intramolecular to intermolecular association as polymer chains extend. Ballard et al. [48] extended Flory's thermodynamic treatment of dilute solutions to polymers that can associate intermolecularly. Their model assumed that extension during simple shear breaks intramolecular associations to form intermolecular associations, and they fit their model to rheological data obtained for a shear - thickening commercial polymer made from t-butylstyrene and methacrylic acid to obtain the strength of the association. These results make a strong case for the argument that shear -thickening results from the formation of intermolecular associations at the expense of intramolecular associations under shear; nevertheless, as we show later in this chapter, the shear-thickening we observe in the viscosity profiles of our model associative polymer solutions results from a different mechanism.

A review of the cited literature shows that a thorough investigation of the rheological properties of solutions of model associative polymers of known structure, which vary systematically in hydrophobe length and molecular weight, should give

considerable insight into the aqueous phase self-association. Our work studies the self–association mechanism, and the relationship between network dynamics and solution rheology, by measuring viscosity profiles and linear viscoelastic properties over a broad range of shear rates and frequencies. Only when we understand the behavior of the model associative polymers in pure water, we can more easily understand the effect of surfactants, cosolvent, latex particles, and their complex interactions, on dispersion rheology.

Experimental Detail

Stock solutions of five percent by weight associative polymer were prepared by adding a weighed amount of solid polymer and hydroquinone inhibitor to distilled deionized water, as described in Appendix B. Table 2.1 on the previous chapter lists the structure and nomenclature of the model associative polymers. Solutions whose associative polymer concentrations were less than five percent model polymer were made by dilution of the stock solutions; after dilution, the solutions were gently agitated and allowed to stand for several days to form a homogeneous solution. A Bohlin VOR rheometer equipped with a set of Mooney – Couette concentric cylinders and a 1 degree angle cone and plate measured the steady shear and oscillatory shear responses of solutions of one-half to five percent model polymer by weight. The Mooney – Couette measuring system has an inner bob of diameter 25 mm located within an outer rotating cup of diameter 27.5 mm, and the bob's cone angle and gap depth are sized so that shear rate under the bob's cone is the same as that in the annular gap and is independent of radial position. A cover on the cup, which did not interfere with torque measurement, prevented evaporation of the solutions during testing. All viscosity profiles were measured at a temperature of 24.5°C. We verified the calibration of the instrument by measuring the viscosity profiles of several Newtonian oil standards. Superposition of viscosity data collected from the

different geometries yielded viscosity profiles in a shear rate range of 10^{-3} to 10^{4} sec^{-1}. Expulsion of the more concentrated solutions from the testing chamber in both the cone and plate and Couette geometries by normal stresses during the measurement sometimes dictated an upper limit on the shear rate that could be used in this study. To measure the viscoelastic response of the solutions over an effectively broader range of imposed frequencies of oscillation, the viscoelastic properties of the solutions were measured in the temperature range of 15°C to 60°C , and shifted relative to a reference temperature of 24.5°C using the time - temperature superposition principle. (In the figures, a_T is the Williams - Landel - Ferry shift factor). Unlike the strain hardening solutions of hydrophobically modified cellulose of Goodwin et. al. [13], solutions of our model associative polymer are linearly viscoelastic over almost the entire range of small applied strains available to the Bohlin rheometer (Figure 3.1). The experimental techniques and pitfalls in measuring and interpreting rheological properties are covered in many classical texts, and are therefore not repeated here [70 - 72].

Results and Discussion

Steady Shear Viscosity Profiles

Figure 3.2 compares the influence of the length of the alkyl hydrophobic end-group on the relationship between low shear relative solution viscosity and associative polymer concentration for model associative polymers of equivalent molecular weight. (The viscosity of water at the measurement temperature is approximately 0.01 Poise.) At large polymer concentrations, the difference between the low shear viscosities of the unmodified polymer and the hexadecyl terminated polymer is over four orders of magnitude. This is the traditional proof that some sort of interaction between the

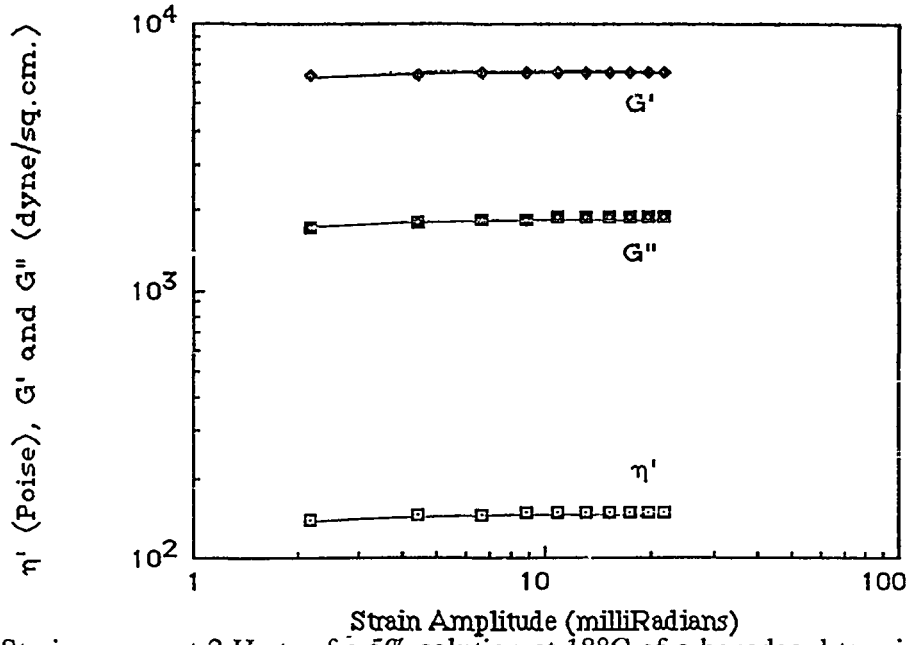

Figure 3.1: Strain sweep at 2 Hertz of a 5% solution at 18°C of a hexadecyl terminated model associative polymer with a number average molecular weight of 34,200.

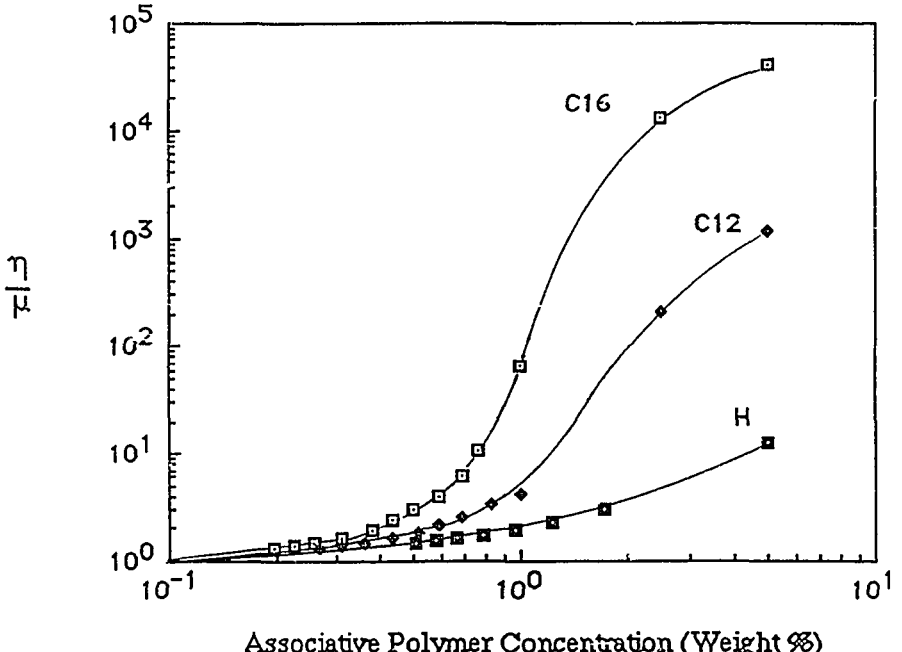

Figure 3.2: Comparison of the relative viscosity by alkyl end- group length of model associative polymers that have a number average molecular weight of 51,000. The hydroxyl terminated polymers served as a control group to measure the influence of the presence of linear alkyl hydrophobe on solution properties.

hydrophobic end- groups of associative polymers enhances low shear viscosity of solutions. The proof that this viscosity enhancement results from a network can only come from viscoelastic measurements or some other direct measurement of network structure; a large viscosity by itself does not necessarily imply the existence of a network. The rate of increase of viscosity with respect to concentration begins to slow down at large polymer concentrations, which implies that although the network imparts gel-like qualities to the solution, the network produces a highly viscous and viscoelastic solution rather than a true gel. As described in the following text, the rheological properties of these concentrated solutions are non-Newtonian.

Figure 3.3 through 3.8 display the viscosity profiles of aqueous solutions of the hexadecyl terminated model polymers. The solutions are Newtonian at low concentrations and become non–Newtonian as polymer concentration increases. The non–Newtonian viscosity profiles consist of a limiting low shear viscosity, a shear – thickening region at moderate shear rates, and a shear – thinning region at high shear rates, which is similar to the data of Bock et al. and of Maerker and Sinton for their model associating systems. The concentration of associative polymer that maximizes the magnitude of the shear-thickening region decreases as molecular weight decreases. We reproduced these shear -thickening viscosity profiles on another Bohlin rheometer and on a Weissenberg rheogoniometer; the shear thickening is a real phenomenon and is not an experimental artifact. These viscosity profiles are in contrast to those of solutions of the dodecyl terminated polymers, which are Newtonian until they begin to thin at large shear rates (Figure 3.9), and to solutions of the hydroxyl terminated polymers, which have viscosities which are independent of shear rate

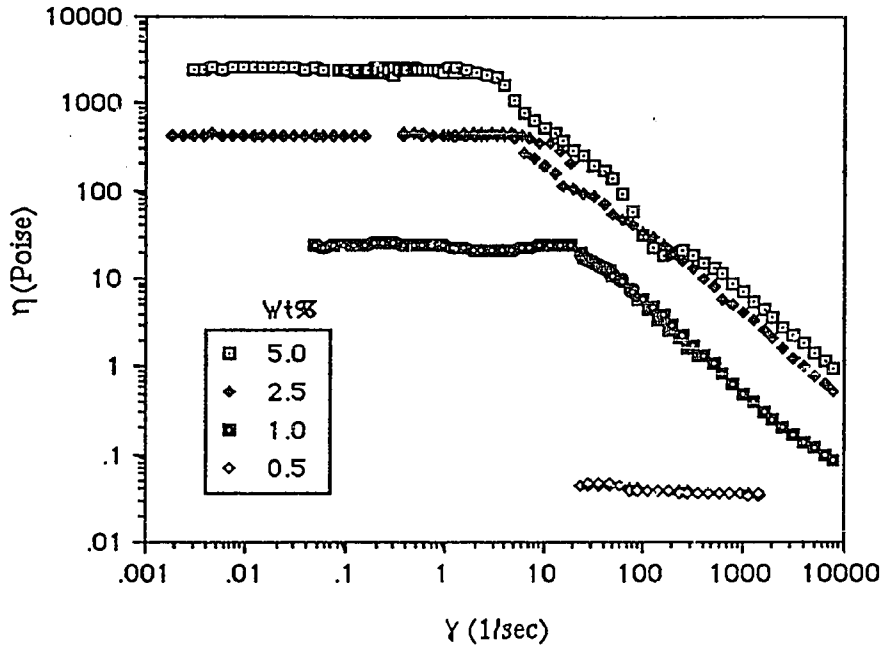

Figure 3.3: Steady shear viscosity profiles of a hexadecyl terminated model associative polymer with a number average molecular weight of 17,500.

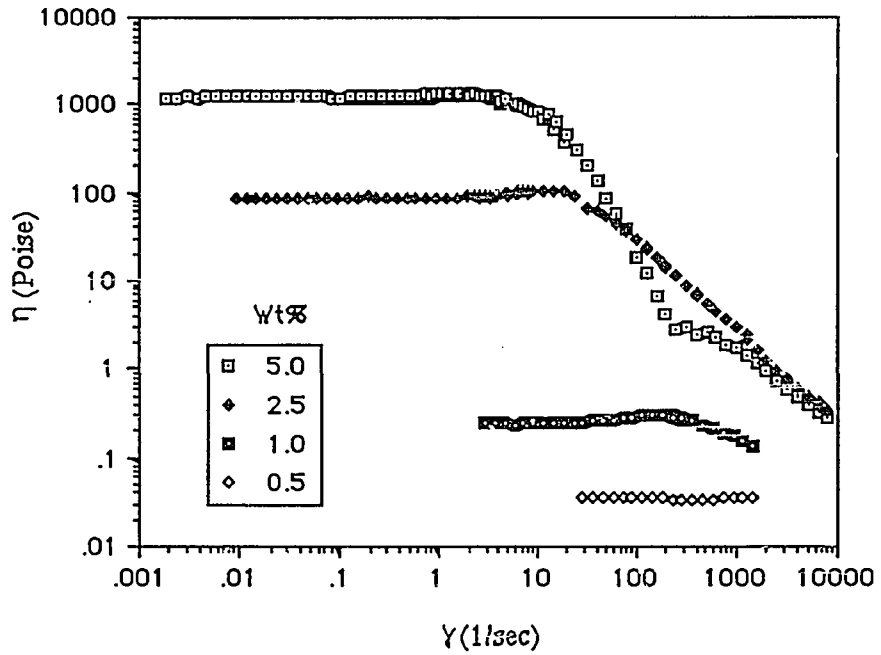

Figure 3.4: Steady shear viscosity profiles of a hexadecyl terminated model associative polymer with a number average molecular weight of 34,200.

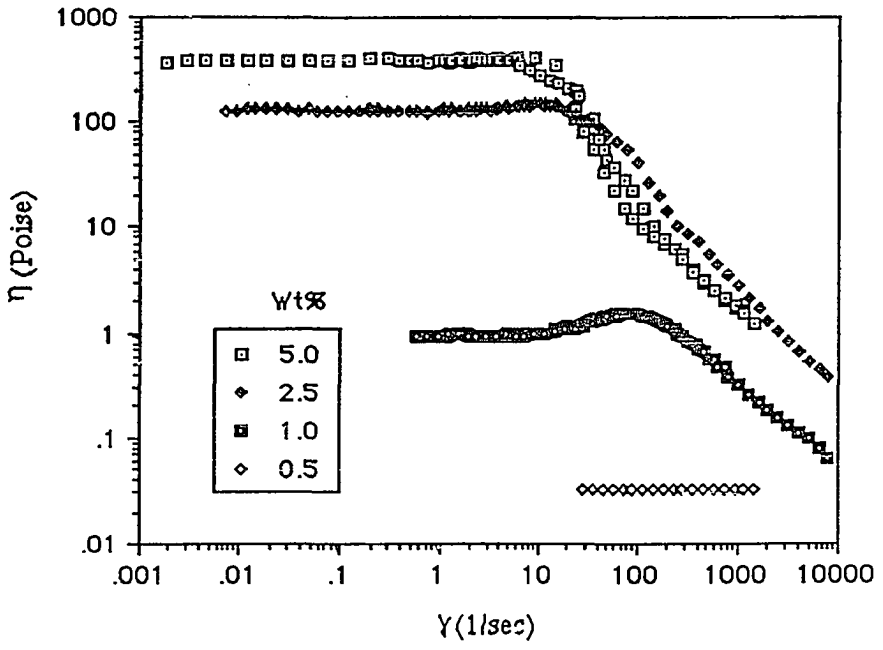

Figure 3.5: Steady shear viscosity profiles of a hexadecyl terminated model associative polymer with a number average molecular weight of 51,000.

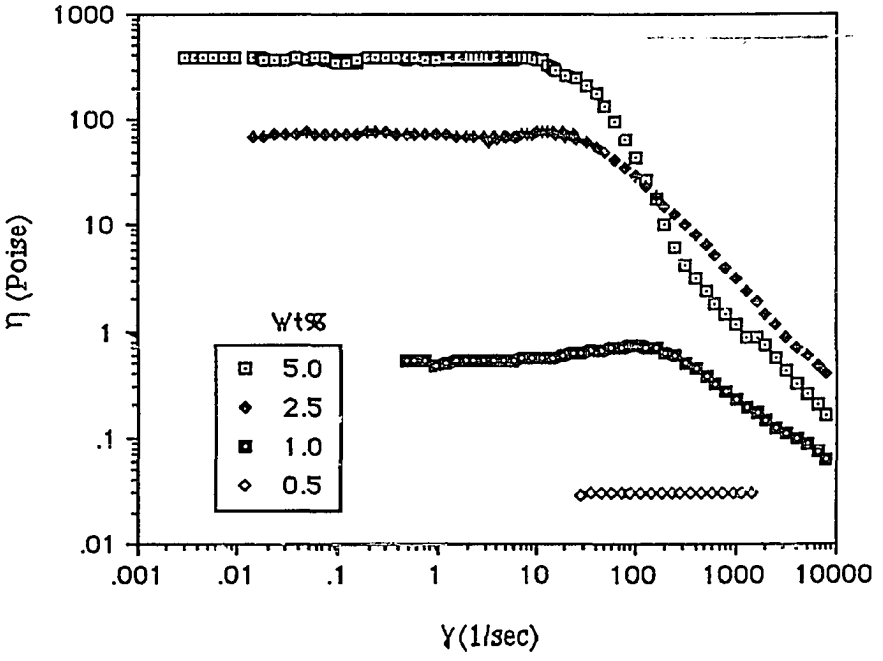

Figure 3.6: Steady shear viscosity profiles of a hexadecyl terminated model associative polymer with a number average molecular weight of 67,600.

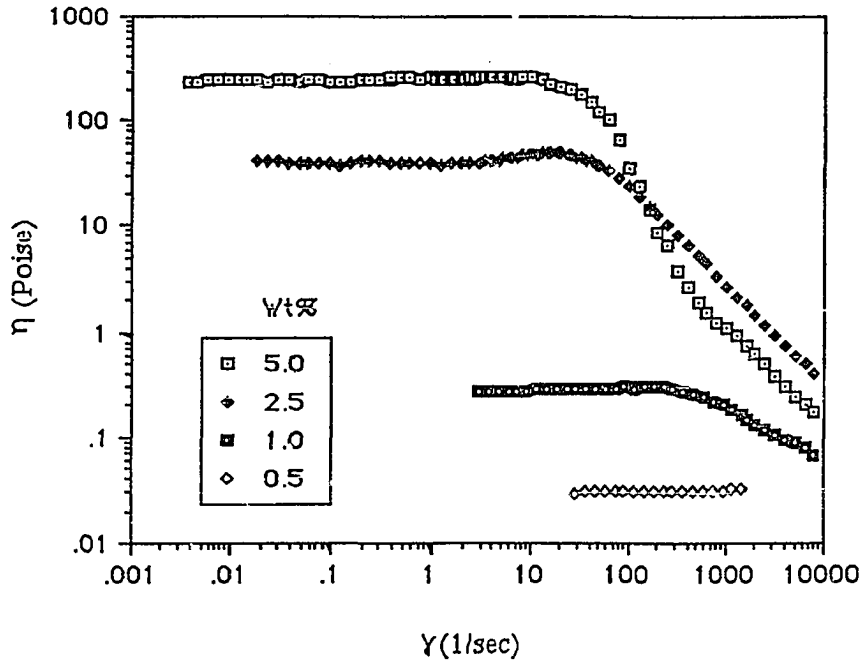

Figure 3.7: Steady shear viscosity profiles of a hexadecyl terminated model associative polymer with a number average molecular weight of 84,000.

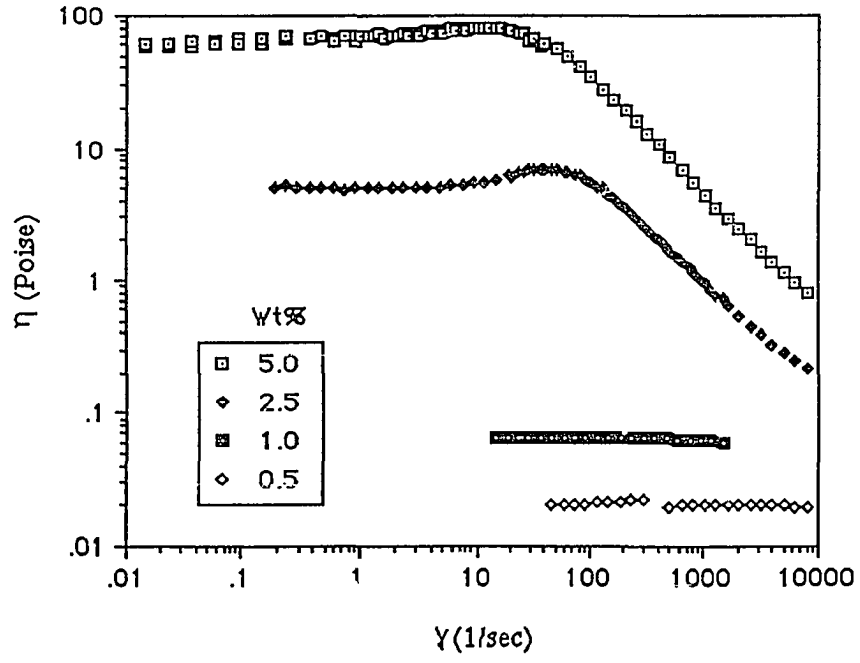

Figure 3.8: Steady shear viscosity profiles of a hexadecyl terminated model associative polymer with a number average molecular weight of 100,400.

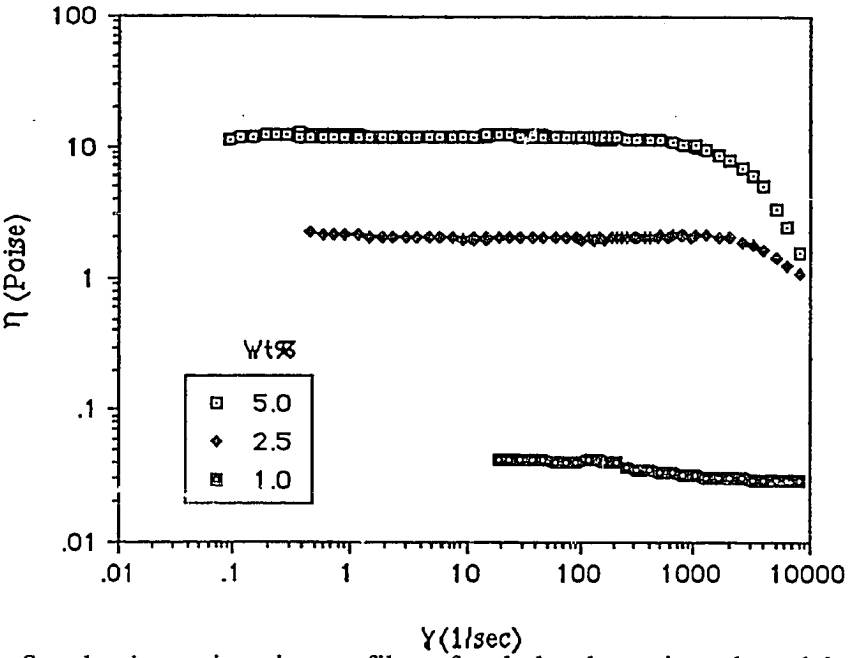

Figure 3.9: Steady shear viscosity profiles of a dodecyl terminated model associative polymer with a number average molecular weight of 50,700.

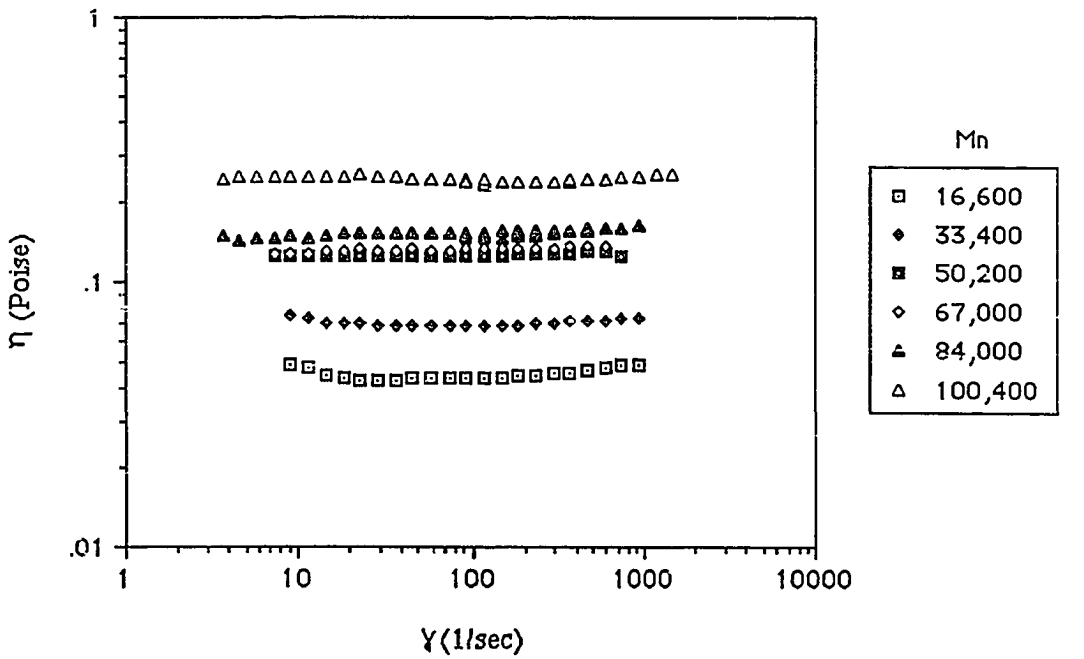

Figure 3.10: Steady shear viscosity profiles of 5 weight % aqueous solutions of hydroxyl terminated model associative polymers of various number average molecular weights.

for the polymer concentrations and molecular weights used in this study (Figure 3.10). It is interesting to note that the low shear viscosity of a 0.5% solution of a hexadecyl terminated model polymer of molecular weight 17,500 is nearly the same as a 5% solution of the the hydroxyl terminated associative polymer of similar molecular weight. At the highest shear rates observed in this study, the high shear viscosities of solutions of model polymers terminated with hydrophobic end- groups are still greater than those of solutions of the hydroxyl terminated model polymers, which indicates that the shear forces have yet to completely disrupt the hydrophobic intermolecular associations. In some of the figures for the hexadecyl terminated polymers, the viscosity of a five weight percent solution in the shear-thinning region of the viscosity profile appears to dip below that of a two and one-half percent solution. This results because the five percent solutions are so highly elastic that the solutions exit the gap during measurement, and hence, the measured viscosity for the five percent solutions are artificially low in this region of the viscosity profile. Also, at any given shear rate, the strength of the flow field and its ability to deform the association network, as measured by the product of the characteristic relaxation time constant and the shear, is larger for the more highly concentrated solutions because their relaxation time constants are larger. We interpret these viscosity profiles in terms of the dynamics of the association network under shear in the following discussion.

The lack of an apparent yield stress in the viscosity profile, which would cause the viscosity to become infinite as shear rate is decreased to zero, indicates that either the network is of finite extent or that the hydrophobic junctions which make up the network are constantly forming, breaking, and reforming by Brownian motion during shear. Otherwise, if the network junctions were permanent, or if the network was large enough to consider it a single cluster in solution, the solution would exhibit a yield stress. If such a yield stress exists, it is too small to measure with the available equipment. As in Witten

and Cohen's theory on the shear-thickening behavior of ionomers [73], a dynamic network can support stress and appear to have properties similar to that of a permanent network when the lifetime of an association junction is nearly as long as the hydrodynamic relaxation time of the association unit.

The shear–thickening region that occurs at a shear rate of nearly 10 sec^{-1} in the viscosity profiles detailed in Figure 3.11 is not surprising, because shear–thickening occurs at nearly the same shear rate as in the data for model associating systems presented by Bock et al. and by Maerker and Sinton. Much later, it was reported that solutions of commercial urethane based nonionic associative polymers also exhibited shear-thickening region in their viscosity profiles at similar shear rates [74]. Georgelos and Torkelson studied the shear - thickening viscosity profiles of solutions of high molecular weight poly(oxyethylene) [75]. The apparent shear-thickening in their solutions occurred at shear rates of 10^5 through 10^6 sec^{-1}, which are orders of magnitude larger than the shear rates where the shear -thickening occurs in our solutions. They concluded that the shear - thickening resulted when the aggregates of poly(oxyethylene) stretched and interacted with the flow field. This happens in a large straining flow, where the product of the relaxation time constant of the solution and the shear rate is greater than one. Thus, the shear thickening results from more than just coil-stretch transition, but also from the stretching of aggregated systems or micronetworks from their equilibrium conformations.

The molecular network theory used by Vrahopoulou and McHugh [76] qualitatively predicts such a shear thickening region in the steady shear viscosity profile, and also predicts that the magnitude of viscosity enhancement in the shear–thickening region increases as the polymer molecular weight decreases, as seen in Figure 3.11. According to this theory, the shear–thickening region of the viscosity curve results from the extension of network chains under shear, which provides an additional energy dissipation mechanism.

Since smaller chains reach the limit of their extensibility before longer chains, networks with smaller chains should exhibit larger increases in viscosity by this mechanism. The magnitude of the absolute increase in viscosity in the shear–thickening region shown in Figure 3.11 decreases with increasing polymer concentration, and, as Maerker and Sinton have also observed in their solutions, the shear rate at which shear–thickening begins decreases with increasing polymer concentration. Witten and Cohen , and the other papers

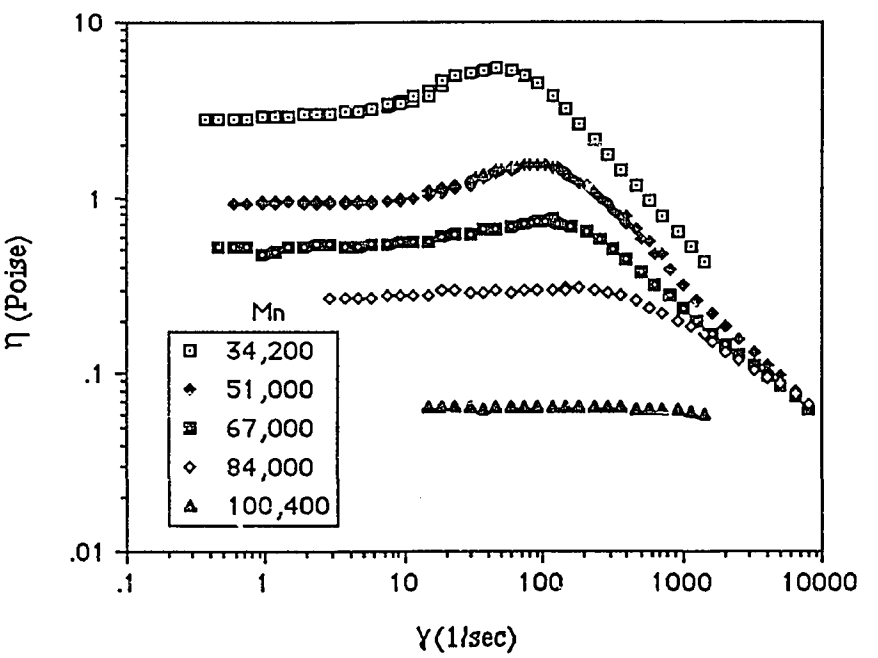

Figure 3.11: Detail of shear-thickening viscosity profiles of 1 weight % aqueous solutions hexadecyl terminated model associative polymers of various number average molecular weights.

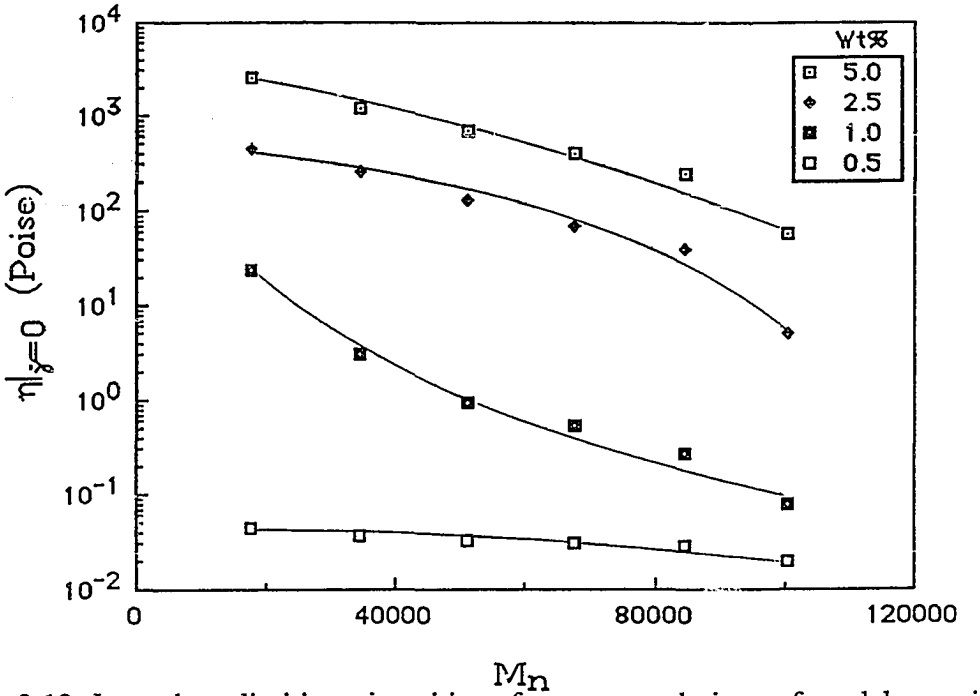

Figure 3.12: Low shear limiting viscosities of aqueous solutions of model associative polymers terminated with hexadecyl hydrophobic end- groups.

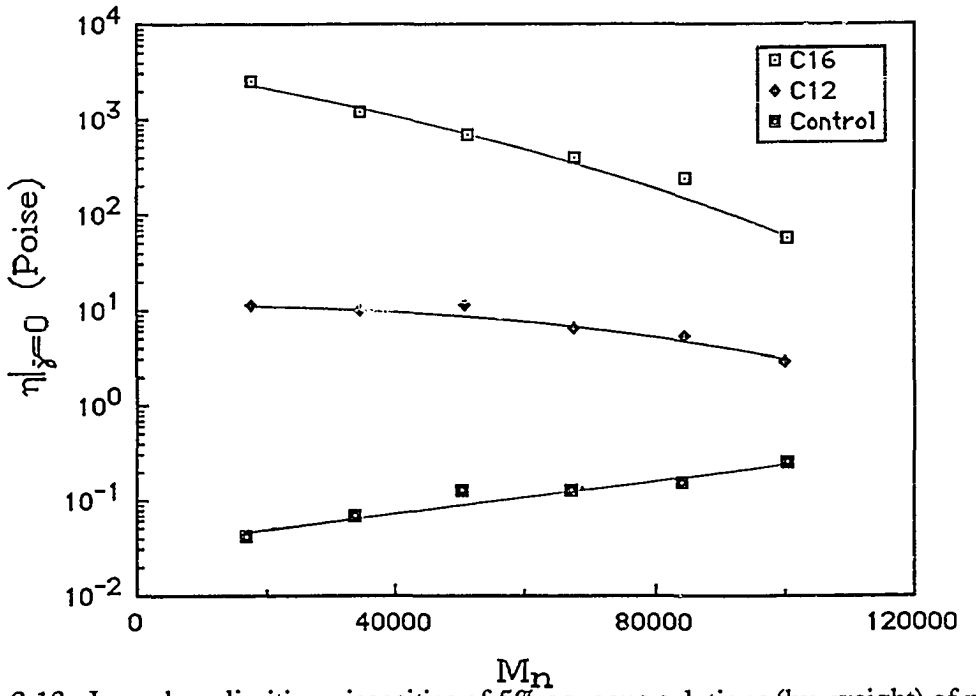

Figure 3.13: Low shear limiting viscosities of 5% aqueous solutions (by weight) of model associative polymers with alkyl end- groups (C16 or C12). The control polymers do not have alkyl end- groups.

reviewed in the Introduction to this chapter, attributed the shear–thickening viscosity, and the decrease in the shear rate required to induce it as polymer concentration increases, to a change from intramolecular to intermolecular association as molecules elongate under shear. According to this theory, many of the association junctions in a network at rest are intramolecular. During flow, shear forces stretch the polymer chains and break some of the intramolecular associations, allowing intermolecular junctions to form at the expense of intramolecular junctions to enhance viscosity. Since the shear rate required to produce a given degree of elongation decreases as solution viscosity increases, the shear rate at which shear thickening begins decreases as solution viscosity increases. Likewise, the magnitude of shear thickening decreases as solution viscosity increases because the relative number of intermolecular to intramolecular associations increases. Thus, the two proposed mechanisms for the shear-thickening differ on the fate of the intermolecular junctions under shear: one theory (Vrahopoulou and McHugh [76]) claims that the shear- thickening results without a change in the concentration of intermolecular junctions, while the other (Witten and Cohen [73]) claims that an increase in the concentration of intermolecular network junctions is responsible for the shear- thickening. We must therefore measure how the number of association clusters depends on shear rate to determine which mechanism is responsible for the shear thickening behavior of our model associative polymer solutions. We address this issue shortly, when we discuss the viscoelastic properties of the model polymer solutions.

Figures 3.12 and 3.13 illustrate how the low shear viscosities of the model polymer solutions depend on polymer concentration, molecular weight, and the length of the alkyl end- groups. The low shear viscosities, obtained by using least squares regression to extrapolate the viscosity profiles to zero shear rate, depend upon the amount of network structure in the solution at rest. The inverse viscosity– molecular weight relationship shown

by solutions of the model polymers with hydrophobic end- groups in Figures 3.12 and 3.13 becomes more pronounced as polymer concentration increases: the low shear viscosity depends upon polymer concentration as c^{β}, where β is greater than unity and increases with increasing ratio of alkyl chain length to polymer molecular weight. Although the isophorone diisocyanates that connect the poly(oxyethylene) units in backbone of the model associative polymers are slightly hydrophobic, the primary hydrophobicity of the model polymer comes from its alkane end- groups. Thus, the viscosity behavior depicted in Figures 3.12 and 3.13 indicates that the driving force for intermolecular association increases with increasing length of the alkane end- group relative to the hydrophilic polymer backbone, and that interaction between the hydrophobic end- groups of the polymer molecules increases the apparent molecular weight of the polymer in solution.

Viscoelastic Material Properties

Figures 3.14 through 3.19 present storage $G'(\omega)$ and loss $G''(\omega)$ moduli of concentrated solutions of the hexadecyl terminated model polymers. All of the solutions were tested in the region of linear viscoelasticity, where the measured properties did not depend upon the amplitude of the oscillating shear strain. Hence, the measurements did not significantly perturb the network from its equilibrium rest state, and did not change the number of effective physical crosslinks in the association network. In the figures, $G'(\omega)$ has a slope of 2 and $G''(\omega)$ has a slope of 1 at low frequencies on a doubly logarithmic plot. This indicates that the response is viscous at low frequencies of the imposed oscillation since the complex viscosity tends toward the zero shear limiting viscosity in this region, (i.e. the response approaches the "terminal" region). At higher frequencies, $G'(\omega)$ increases to cross $G''(\omega)$ and reach an entanglement plateau, and $G''(\omega)$ passes through a maximum. Maerker and Sinton observed a similar plateau in $G'(\omega)$ between 6 and 300

rad/s for their solutions due to entanglement coupling. This behavior means that, at high frequencies, the time scale of deformation has become smaller than the time scale required for the polymers to change their conformation or to withdraw from an association network junction, and the fluid responds as an elastic solid, (i.e. the Deborah number is greater than 1). Thus, the range of frequencies used in our experiments encompasses the longest relaxation times in the relaxation spectrum of our solutions. As indicated by the theory of Witten and Cohen, the hydrodynamic relaxation time measured by this method is characteristic of the lifetime of the association junction because the association network acts as a single rheological unit.

This viscoelasticity results from the association between the hexadecyl alkyl groups, since solutions of the hydroxyl terminated model polymers of similar molecular weight and similar concentrations lack viscoelasticity. As shown in Figure 3.20, solutions of the dodecyl terminated model polymers exhibit a great deal less elasticity. Their response is primarily viscous, and it is not possible to measure the entanglement plateau within the frequency ranges available on the Bohlin rheometer. We have tested solutions as high as 20% polymer by weight, and still this behavior persists. This leads us to conclude that the strength of the network, if one indeed forms with the dodecyl terminated polymers, is much less strong than that formed by the hexadecyl terminated polymers.

Since, as a first approximation the relaxation spectrum $H(\tau)$ equals $\frac{2}{\pi}G''(\omega)|_{\tau=1/\omega}$, the maximum in $G''(\omega)$ results from the longest relaxation times of the relaxation spectrum associated with the network, which we can use to calculate ν, the average molar density of network junctions by association [72, p.404]. In analogy to rubber elasticity, the pseudo–equilibrium modulus (G^o_{en}) is:

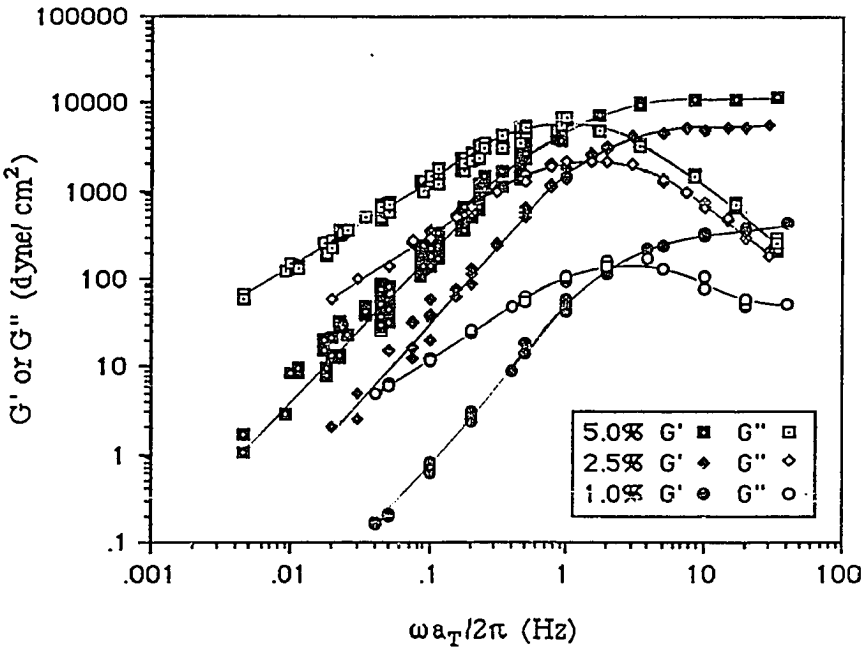

Figure 3.14: Shear moduli of aqueous solutions of a hexadecyl terminated model associative polymer with a number average molecular weight of 17,500.

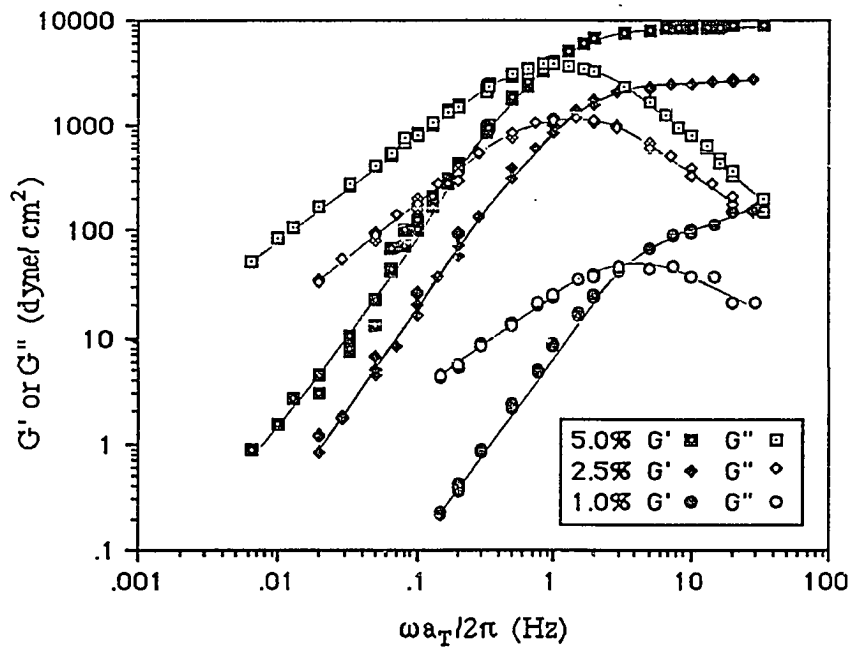

Figure 3.15: Shear moduli of aqueous solutions of a hexadecyl terminated model associative polymer with a number average molecular weight of 34,200.

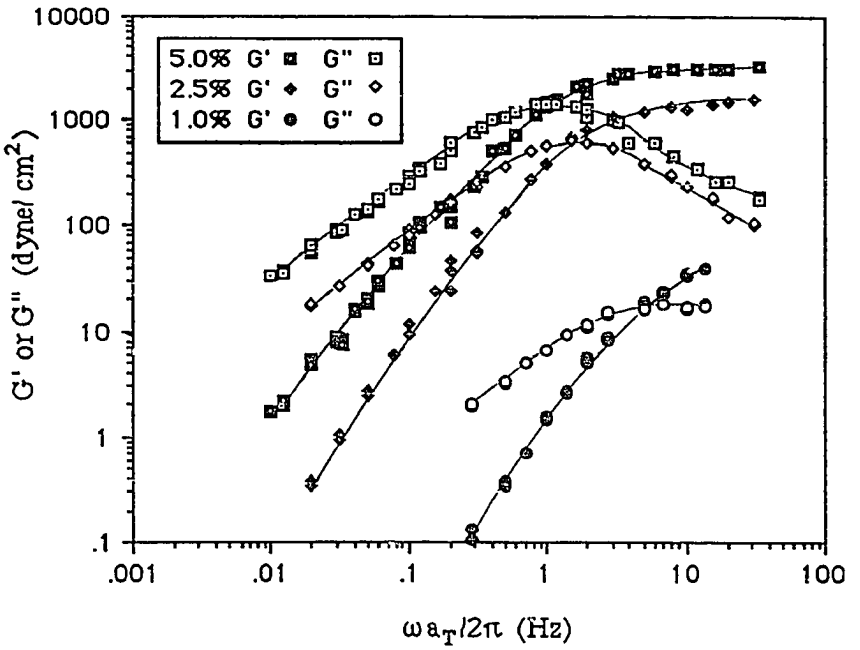

Figure 3.16: Shear moduli of aqueous solutions of a hexadecyl terminated model associative polymer with a number average molecular weight of 51,000.

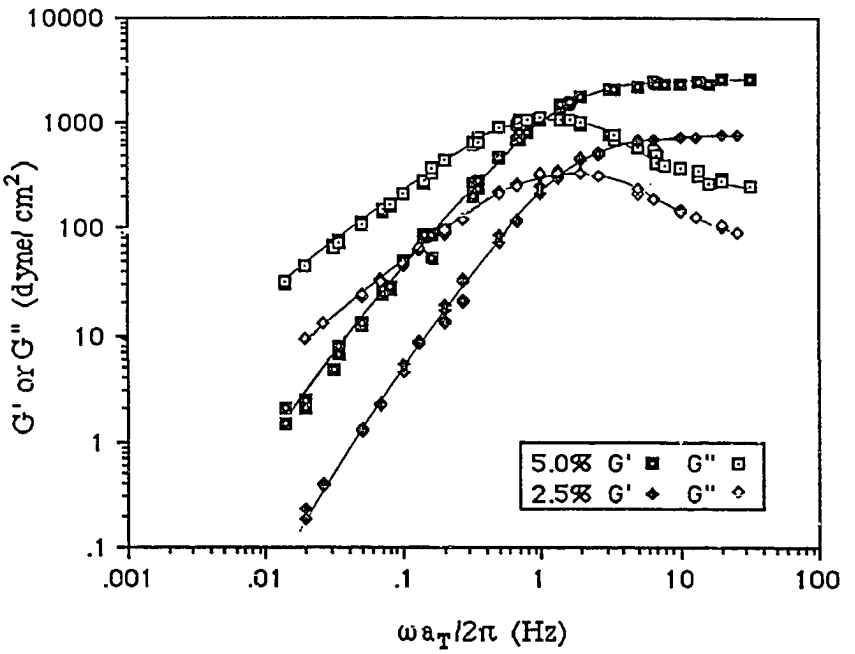

Figure 3.17: Shear moduli of aqueous solutions of a hexadecyl terminated model associative polymer with a number average molecular weight of 67,600.

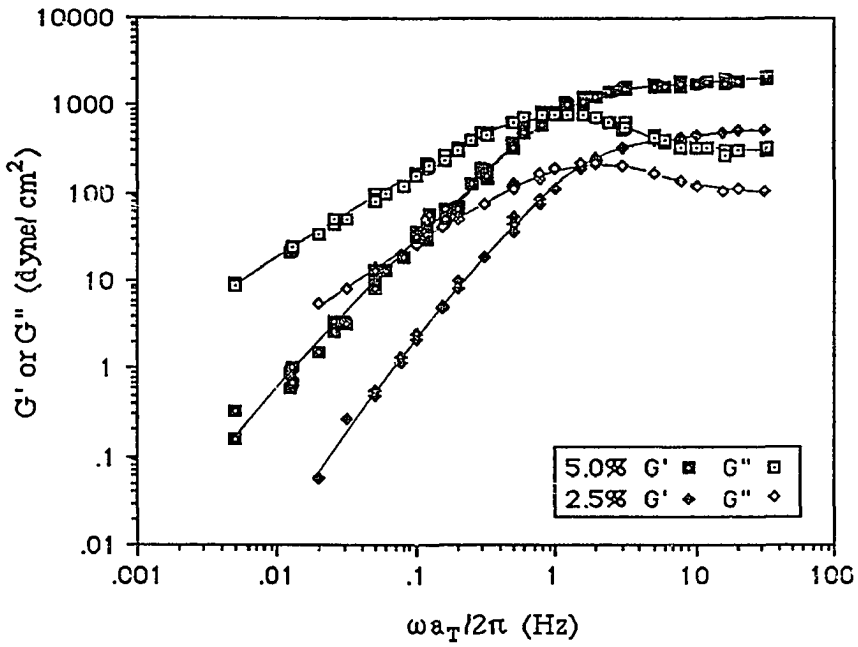

Figure 3.18: Shear moduli of aqueous solutions of a hexadecyl terminated model associative polymer with a number average molecular weight of 84,300.

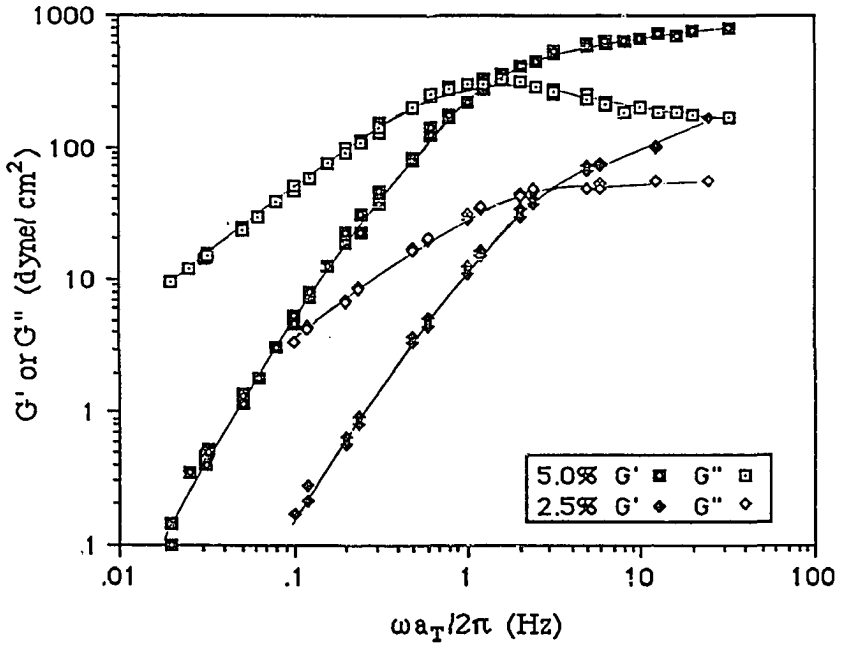

Figure 3.19: Shear moduli of aqueous solutions of a hexadecyl terminated model associative polymer with a number average molecular weight of 100,400.

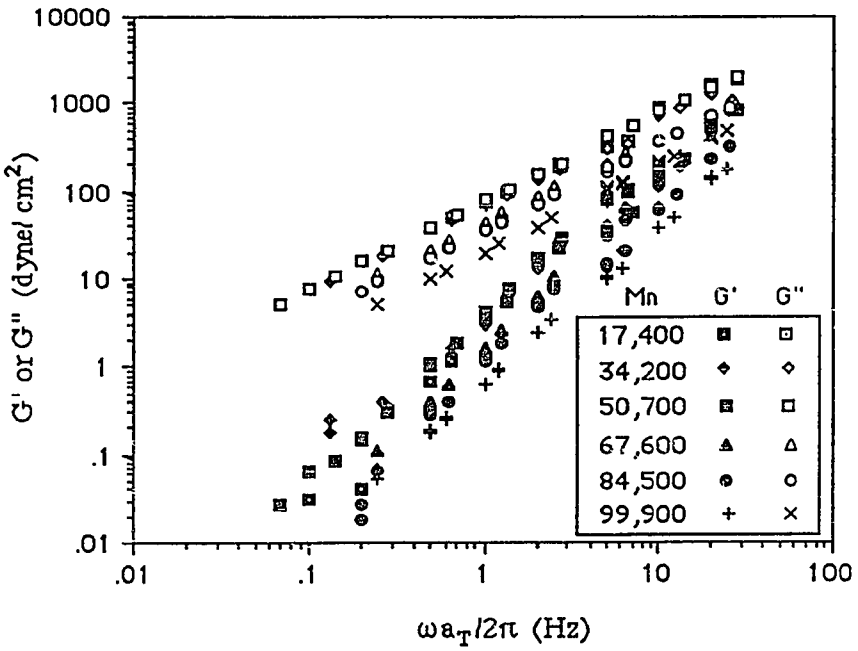

Figure 3.20: Shear moduli of 5 weight % aqueous solutions of dodecyl terminated model associative polymers of various number average molecular weights.

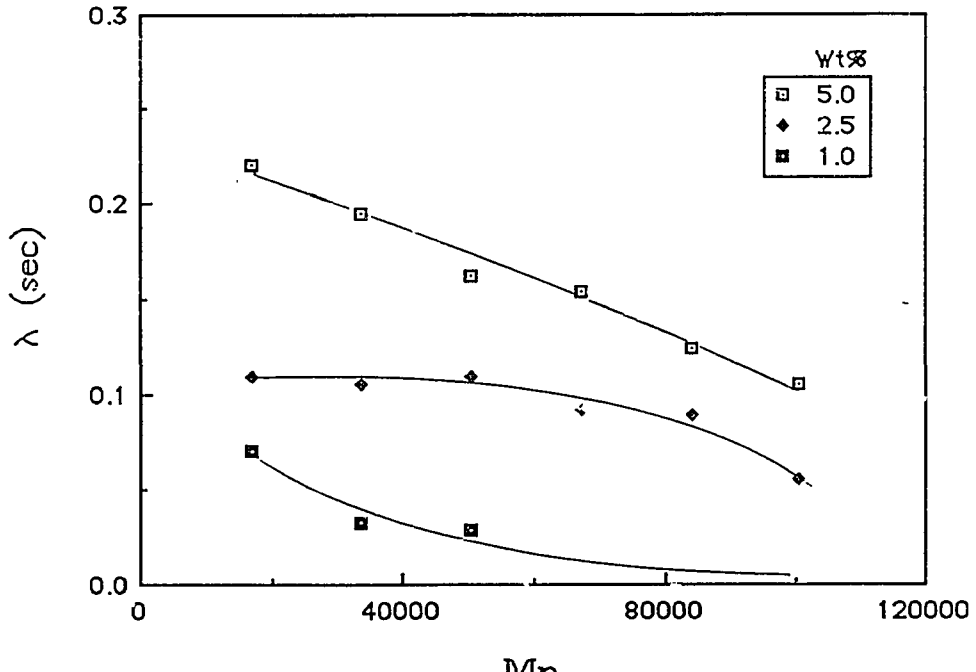

Figure 3.21: Influence of polymer concentration and molecular weight on the relaxation time constants for the hexadecyl terminated model associative polymers in water.

$$G^{o}_{en} = \nu RT = \frac{2}{\pi} \int_{-\infty}^{a'} G'' \, d\ln(\omega) \qquad (3.1)$$

where R is the gas constant, T is the temperature in Kelvin, and a', the frequency at the upper limit of integration, is chosen to include the maximum in longest times of the relaxation spectrum within the range of integration. To determine the pseudo– equilibrium modulus, we can integrate Equation (3.1) graphically from the data, or analytically by either fitting the data with an empirical function or a constitutive equation. In this work, we use the corotational Maxwell constitutive equation [77], which approximates the relaxation spectrum with its principle value as given by the relaxation time constant λ. This model predicts the following material functions:

$$\eta(\gamma) = \frac{\eta_o}{1+()\gamma)^2}; \; G'(\omega) = \frac{\eta_o \lambda \omega^2}{1+(\omega\lambda)^2}; \; G''(\omega) = \frac{\eta_o \omega}{1+(\lambda\omega)^2} \qquad (3.2)$$

$$J'(\omega) = \frac{\lambda}{\eta_o}; \; J''(\omega) = \frac{1}{\eta_o \omega}$$

where η_o is the low shear limiting viscosity that is determined independently in the steady shear experiment. As seen from Equation (3.2), we can experimentally determine λ from the point at which $G'(\omega)$ equals $G''(\omega)$, or from the high frequency plateau in $J'(\omega)$. Figure 3.21 displays how the relaxation time constant depends upon thickener molecular weight and concentration. The relaxation time constant increases with decreasing thickener molecular weight and increasing thickener concentration, which means that the relaxation

Table 3.1: Viscoelastic Properties and Model Parameter for Model Associative Polymers in Water at 24.5°C

Solution	η_o (Poise)	J' (cm^2/dyne)	λ (sec)	$\omega^\dagger$ (Hz)	ν (10^3M)	[H]* (10^3M)
5.0% C_{16-18}	2563	8.6×10^{-5}	.220	.72	.47	6.0
2.5%	435	2.5×10^{-4}	.109	1.5	.16	3.0
1.0%	23.3	3.0×10^{-3}	.070	2.3	.013	1.2
5.0% C_{16-34}	1220	1.6×10^{-4}	.195	.82	.25	3.0
2.5%	250	4.2×10^{-4}	.105	1.5	.096	1.5
1.0%	3.0	1.1×10^{-2}	.033	4.8	.0036	0.6
5.0% C_{16-51}	405	4.0×10^{-4}	.162	1.0	.101	2.0
2.5%	129	8.5×10^{-4}	.110	1.4	.048	1.0
1.0%	.951	3.1×10^{-2}	.029	5.5	.0013	0.4
5.0% C_{16-68}	386	4.0×10^{-4}	.154	1.0	.101	1.5
2.5%	70.7	1.3×10^{-3}	.092	1.7	.031	0.7
1.0%	.53	-	.027 §	-	-	.28
5.0% C_{16-84}	239	5.2×10^{-4}	.124	1.3	.077	1.2
2.5%	40.4	2.2×10^{-3}	.089	1.8	.018	0.6
1.0%	.25	-	.022 §	-	-	.24
5.0% C_{16-100}	58.6	1.8×10^{-3}	.105	1.5	.022	1.0
2.5%	4.99	1.1×10^{-2}	.055	2.9	.0037	0.5
1.0%	.065	-	.016 §	-	-	.20

* The molar concentration of associative polymer hydrophobes

† Frequency at which $G'(\omega)=G''(\omega)$

§ Extrapolated from Figures 3.22 and 3.23

time constant increases with increasing network structure. The corotational Maxwell fluid model describes the oscillatory shear response of the associative polymer solutions quite well; it is not necessary to use the model to perform the integration, but it expedites the integration without altering its physical interpretation. Substitution of Equation (3.2) into Equation (3.1) results in:

$$G^{o}_{en} = \frac{2\eta_o}{\lambda\pi}\int_{o}^{a}\frac{d(\lambda\omega)}{1+(\lambda\omega)^2} = \frac{2\eta_o}{\lambda\pi}\tan^{-1}(\lambda\omega)\Big|_{o}^{a} = \frac{2\eta_o}{\lambda\pi}\tan^{-1}(\lambda a) = \frac{\eta_o}{\lambda} = \frac{1}{J'} \qquad (3.3)$$

where a'= ln(a). The last simplification in Equation (3.3) results because the upper limit of the frequency range that encompasses the maximum in G"(ω) in the data of Figures 3.14 through 3.19 is so large that the inverse tangent is always within 6% of π/2. The physical interpretation of this result is that the plateau value of the storage modulus equals the pseudo – equilibrium modulus for these solutions. In general, both the zero shear limiting viscosity and the relaxation time constant depend upon ν. Table 3.2 compiles the molar density of network crosslinks obtained from this analysis.

Scaling Behavior

The viscoelastic response and the enhanced viscosity of solutions of polymers with hydrophobic end- groups, as compared to solutions of polymers without hydrophobic end-groups, suggest that the contribution to network junctions by chain entanglement is small relative to that by association. Hence, the pseudo–equilibrium modulus of an associative polymer solution essentially measures the molar density of network junctions formed by association. As shown in Figure 3.22, when the viscosities presented in Figure

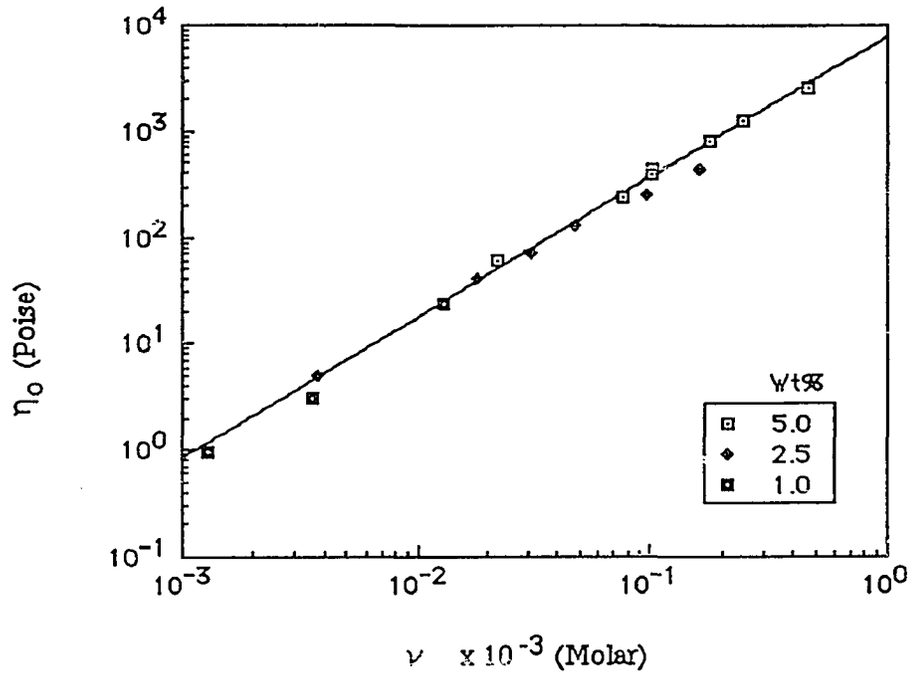

Figure 3.22: Correlation between low shear limiting viscosities (taken from Figure 3.12) for solutions of the hexadecyl terminated model associative polymers and the molar density of association.

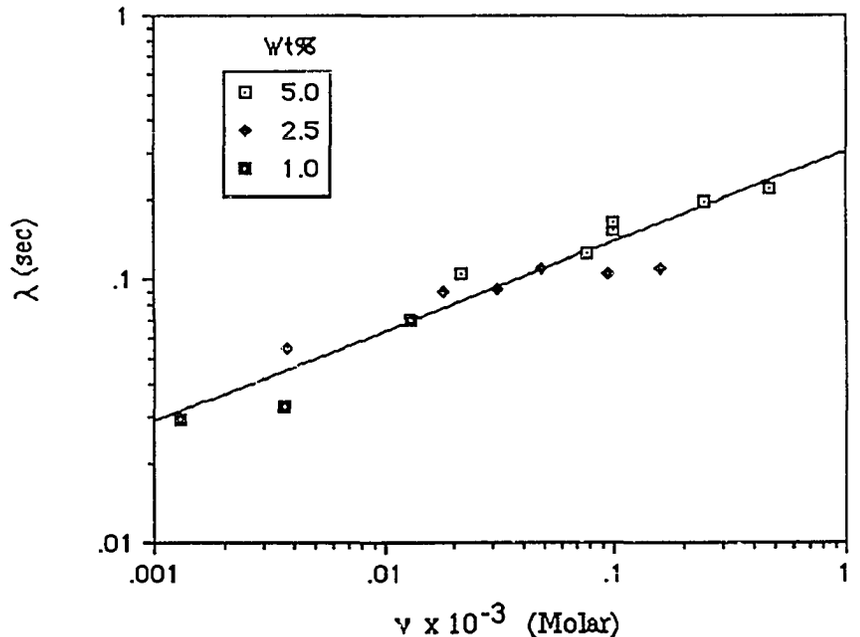

Figure 3.23: Correlation between relaxation time constants (taken from Figure 3.20) for solutions of hexadecyl terminated model associative polymers and the molar density of association.

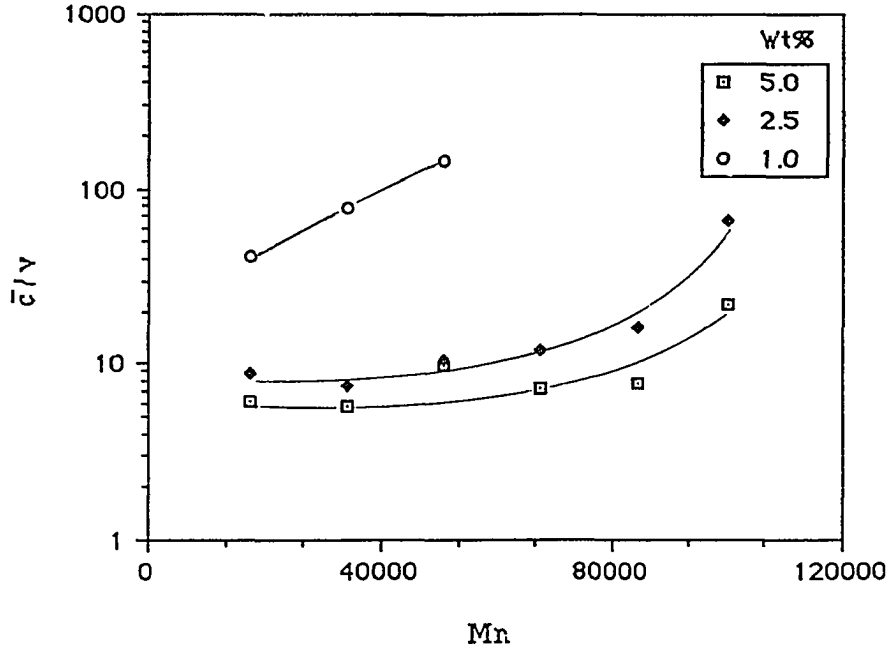

Figure 3.24: Number of model associative polymers between network junctions for aqueous solutions of the hexadecyl terminated model associative polymers.

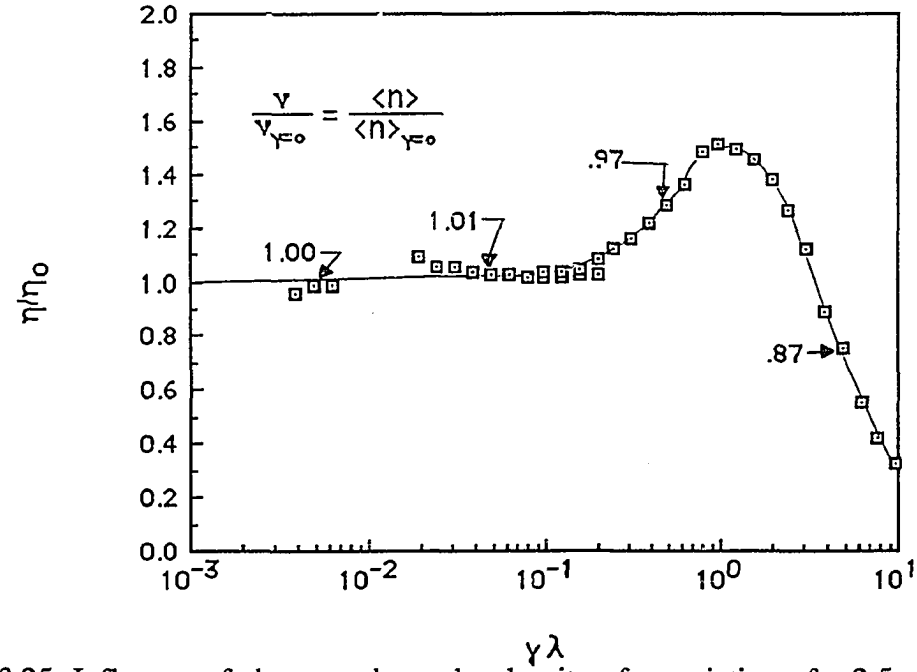

Figure 3.25: Influence of shear on the molar density of association of a 2.5 weight % solution of a hexadecyl terminated model associative polymer of number average molecular weight of 67,600.

3.12 for all six hexadecyl terminated model polymers at various concentrations are plotted against the molar density of association junctions, a single line with a slope of approximately 4/3 results. As shown in Figure 3.23, when the relaxation time constants presented in Figure 3.21 are plotted against the molar density of association junctions, a single line with a slope of approximately 1/3 results. The correlation holds irrespective of associative polymer concentration and molecular weight as long as a relaxation time (i.e. elastic response) can be measured. In principle, if we can predict the molar density of network junctions from thickener structure or solution formula, then we can predict the basic rheological properties of our model thickener solutions. Although we understand qualitatively how a cosolvent or a surfactant might influence the molar density of network junctions, we do not yet have a quantitative measurement of it. Such a determination would require additional experimental data, such as those obtained from light scattering. In the meantime, we could empirically relate with the molar concentration of thickener hydrophobes in solution (for example, $\nu \approx 9.4 \times 10^{-5}$ [H], where [H] is the molar concentration of associative polymer hydrophobic groups. These correlations between rheological parameters and the molar association density indicate that the morphology, size, and strength of the association junctions, rather than traditional volume exclusion mechanisms, determine the rheological properties of associative polymer solutions.

The pseudo–equilibrium modulus is usually interpreted in terms of an apparent molecular weight between entanglement points: $\nu = G_{en}^{o}/RT = c/M_e$, where M_e is the apparent molecular weight between entanglement points and c is the associative polymer mass concentration [78]. Hence, the ratio $\bar{c}/\nu$, where $\bar{c}$ is the molar concentration of model associative polymer, is the dimensionless ratio of the apparent molecular weight between junctions to the polymer molecular weight, M_e/M_n. Thus M_e/M_n is 1 or greater for an association network. As shown in the Figure 3.24 for solutions of model polymers

with hexadecyl hydrophobes, M_e/M_n is greater than one and decreases as concentration increases. This implies that several associative polymers must cooperate to span the distance between hydrophobic junctions.

Although the functionality of the association junction (i.e., the average number of hydrophobes in a given association cluster) is still unknown, we can calculate the upper limit of the functionality from the data in Figure 3.24. A mole balance on the associative polymers hydrophobic end- groups yields:

$$n\left(\frac{\#\text{ Hydropobes}}{\text{AP}}\right)\bar{c}\left(\begin{matrix}\text{Moles of AP}\\ \text{not in network}\end{matrix}\right)+\nu\left(\begin{matrix}\text{Moles of AP in}\\ \text{network junctions}\end{matrix}\right)f\left(\frac{\#\text{ Hydrophobes}}{\text{junction}}\right)$$

$$=\bar{c}\left(\begin{matrix}\text{Total Moles of}\\ \text{AP in solution}\end{matrix}\right)n\left(\frac{\#\text{ Hydrophobes}}{\text{AP}}\right)$$

...(3.4)

where n is the number of hydrophobic groups capable of intermolecular association in a given associative polymer backbone, f is the "functionality", the number of hydrophobes in a given association junction, and the concentration are molar concentrations of associative polymer. The mole balance says the thickener hydrophobe can be in one of two places: either in the network, or not. ν is measured from the viscoelastic characterization, and $\bar{c}$ is known because we know the total mass of associative polymer in solution. Thus, Equation (3.4) has two unknowns: the functionality of the association network junction and the molar concentration of polymers that are in solution but do not exist in the network; hence we need either another measurement or equation. Nevertheless, we can calculate the upper limit of the functionality of the association cluster by assuming that the association network is "perfect", where every hydrophobe resides in a network junction. With this

assumption, $\mathfrak{E}$ is zero. It is clear from Equation (3.4) that this assumption overestimates the functionality by counting some polymers that may not be in the network as in the network, and that the actual functionality of the association junction will be less by whatever amount of associative polymer is not in the network. It is self evident that the "perfect" network assumption applies best to the data of the 5% solutions. With the assumption of a perfect network, Equation (3.4) used in conjunction with the data in Figure 3.24 reveals that an association junction must contain twelve hydrophobes or less. From their fluorescence studies on a hydrophobically modified poly(oxyethylene) of weight average molecular weight of 50,000, Richey et al. [79] calculated that the association cluster contains about six hydrophobes. Our estimate of the functionality is similar to both the value calculated by Richey et al., and to the value of ten calculated by Flynn and Goodwin. Therefore, the number of associative polymer hydrophobes in a given association network junction is relatively small, on the order of a dozen or so.

The rheological data of many polymers often exhibit a power law dependence on concentration and molecular weight, as predicated by the de Gennes c* theorem [80]:

$$\eta \sim [\overline{c}/c^*]^X \ , \ \lambda \sim [\overline{c}/c^*]^Y \qquad (3.5)$$

where c* is the overlap concentration. Experimental evidence demonstrates that the exponent X can be as high as 4, but is usually near 3.4 for most polymers. Following Equation 3, we regressed the rheological properties of the concentrated polymer solutions to an equation of the form: $\eta,\nu,\lambda = c^a M^b$, where c is in wt%. Selecting the results with best regression statistics yielded: $\eta = c^{3.36}/M^{1.67} = (c/\sqrt{M})^{3.36}$; $\nu = c^{2.47}/M^{1.24} =$

$(c/\sqrt{M})^{2.47}$; and $\lambda = c^{0.88}/M^{0.44} = (c/\sqrt{M})^{.88}$, which are self–consistent because they satisfy $\eta = \nu^{4/3}$, and $\eta = \nu\lambda$. de Gennes showed that in a dense system of chains, such as found in a concentrated solution, the polymer chains follow a random walk where $c^* \sim M^{-1/2}$, so that $[\overline{c}/c^*] \sim (c/\sqrt{M})$. Hence, the scaling of the rheological properties of the model associative polymer solutions with $(c/\sqrt{M})$ is not surprising. In Figure 3.24, the ratio M_e/M scales as $(c/\sqrt{M})^{-.6}$, which indicates that the correlation length ξ (i.e., mesh size of the network), decreases rapidly with increasing concentration. This is comparable to de Gennes's prediction that the correlation length $\xi \sim [\overline{c}/c^*]^{-3/4}$. Therefore, the strength and completeness of the network decreases as molecular weight increases.

Influence of Shear on the Concentration of Association Junctions

Now that a technique to measure the concentration of network junctions by association from the viscoelastic properties of the solutions has been established, we can determine whether the shear - thickening observed in our model polymer solutions results from an increase in the number of intermolecular junctions during shear or from the extension of the network under shear. To monitor how shear forces disrupt the association network, we sheared an associative polymer solutions at a given shear rate for five minutes to ensure steady state and to give the shear forces a chance to disrupt the network. Then we switched instantaneously to an oscillatory shear strain and measured the frequency dependence of the storage and loss moduli. The switch-over from steady shear to dynamic shear was accomplished as fast as mechanically possible to prevent the solution from relaxing from its sheared state to its rest state. Because the number density of network junction may be calculated from the pseudo-equilibrium plateau in the storage modulus using the theory of rubber elasticity, this experiment measures how shear changes the number density of network junctions.

Figure 3.25 shows the results of the experiment.[1] In this figure, the steady shear viscosity has been normalized with respect to the low shear viscosity plateau (i.e., η/η_o), and the shear rate has been made dimensionless by multiplying it with the relaxation time constant of the solution (i.e., $\gamma\lambda$). The flow field is considered strong and capable of stretching a polymer chain if the product $\gamma\lambda$ is greater than one. In the figure, the concentration of the association junctions measured at the various shear rates have been normalized with respect to the number density of association junctions measured for an unsheared solution (i.e., $\nu/\nu_{\gamma=o}$), and superimposed upon the steady shear viscosity profile. In this way, the influence of shear on the number of association junctions can be directly compared to the shear - thickening region in the viscosity profile. The data for $\nu/\nu_{\gamma=o}$ shown on Figure 3.25 indicate that the concentration of association junctions remains constant (i.e., $\nu/\nu_{\gamma=o} = 1$) until the shear rate exceeds that required to produce shear - thinning in the viscosity profile, and only at larger shear rates does $\nu/\nu_{\gamma=o}$ decreases slightly (to $\nu/\nu_{\gamma=o} = .87$). The data do not show a dramatic increase in relaxation time constant in the shear - thickening region, or in the concentration of intermolecular associations, as would be expected if a shear induced change from intramolecular to intermolecular associations produced the shear - thickening region in the viscosity profile. Thus, a mechanism other that a shear- induced increase in the concentration of association network junctions is needed to explain the shear- thickening region in the viscosity profile. These data are consistent with those of Richey et al. [79], whose fluorescence measurements show that the number of junctions were independent of shear up to 1500 sec^{-1}. In addition, the complex viscosity does not exhibit a shear thickening region; hence, the shear-thickening results only when large strains have been applied to the model associative polymer solutions. Thus, the shear - thickening in the viscosity profiles of our

[1] These measurements are courtesy of Mehdi Durali.

model associative polymer solutions is a natural consequence of the stretching of an association network under large strains.

Conclusions

Physical interpretation of the rheological properties of aqueous model associative polymer solutions suggests the following qualitative association mechanism. At rest, Brownian processes build up a highly entangled association network, where the primary source of entanglement comes from associations among the model polymers' hydrophobic end- groups. (Figures 3.26 and 3.27) Nevertheless, intramolecular associations between hydrophobic end- groups that belong to the same polymer molecule, which do not contribute to the overall strength of the network, can exist. Because the association junctions are dynamic (i.e., continuously building and rupturing through Brownian processes), the network is not an infinite cluster that spans the entire solution, but is instead a finitely sized hydrodynamic unit whose lifetime is longer than the relaxation time of the solution. Since the association junctions are relatively strong and long-lived, small to moderate amounts of shear stress can extend the network structure before rupturing it. (Figure 3.28) This extension decreases the configurational entropy of the polymer chains that construct the network system, and provides an additional resistance to flow as manifested in the solutions' shear-thickening viscosity profiles. Intuitively, one might expect that the shear – thinning that follows the shear - thickening region in the the viscosity profile begins when shear forces disrupt the association network. Surprisingly, the data presented in Figure 3.25 suggest that the contribution of this disruption to the shear-thinning viscosity can be small, and that other mechanisms may be responsible for the shear - thinning. The statistical mechanical network model developed in Chapter IV considers the non-Gaussian free energies of finitely extendable polymer chains under large

strain. These non-Gaussian chain statistics, and the change in hydrodynamic resistance of the polymer chain as it is extends, gives rise to the non - affine deformation of the association network under shear. This non - affine deformation produces shear - thinning in the viscosity profile, even when no association junctions have been broken. In short, the number density and functionality of the association junctions primarily determine the strength of the overall network, and hence, the rheological properties of the solutions.

$$R - O - (DI - PEG)_y - DI - O - R$$

R = HYDROPHOBE

DI = DIISOCYANATE

PEG = POLY(ETHYLENE GLYCOL), $HO - (C_2H_4O)_n - H$

Figure 3.26: Schematic representation of the linear model associative polymer. The alkyl end- groups are denoted by the rectangular blocks. Figure courtesy of reference [25]

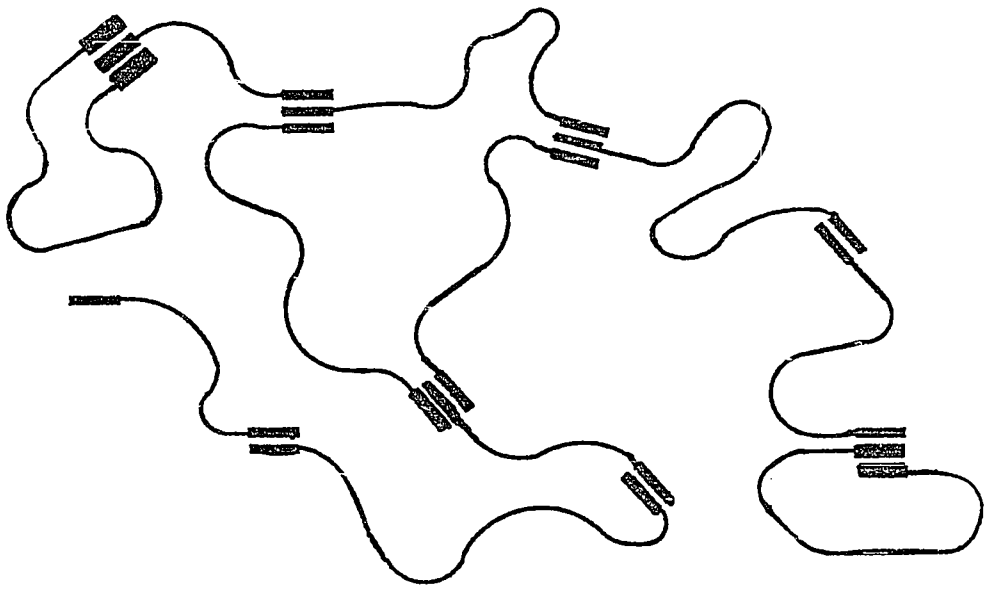

Figure 3.27: Schematic representation of the asscciation network in a concentrated solution at rest.

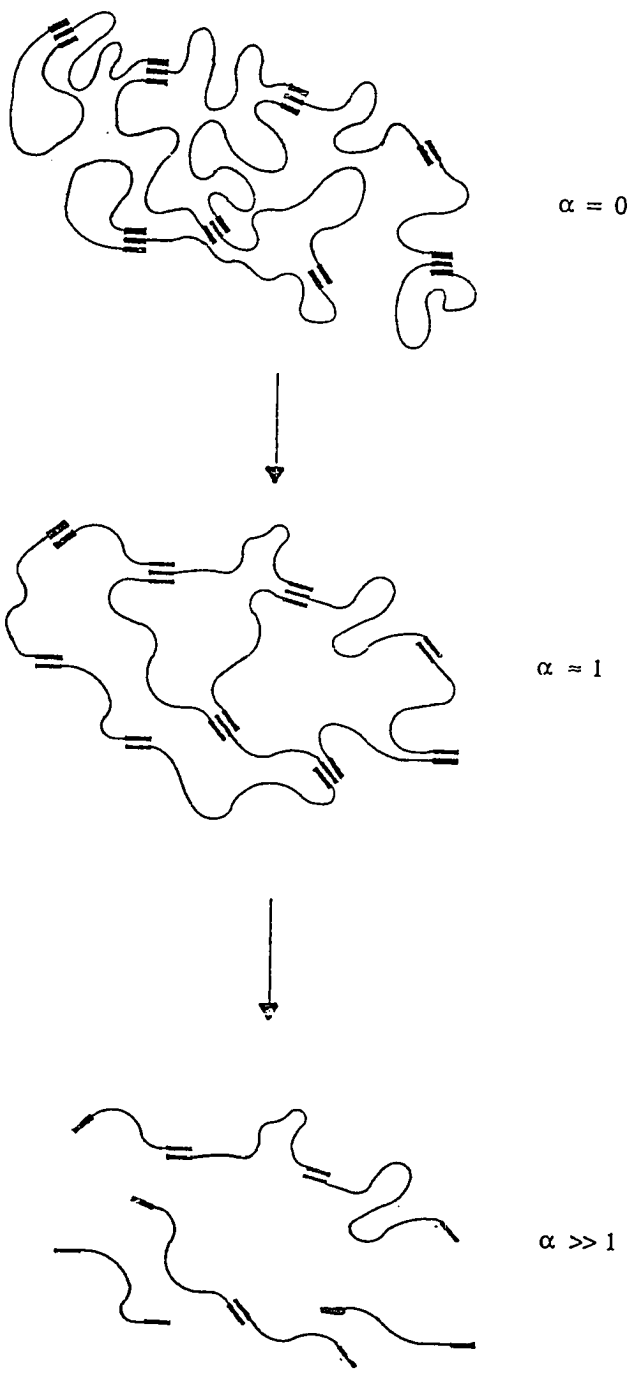

Figure 3.28: Schematic representation of the dynamics of the association network under shear.

Chapter IV

Statistical Mechanical Network Modeling of Associative Polymer Solution Rheology

Introduction

Motivation

Chapter III demonstrated that the shear-thickening viscosity profiles seen in our model associative polymer solutions revealed insight into dynamics of the associative polymer network under shear. To gain insight into the molecular reasons for the shear-thickening phenomenon, we have modelled the rheological properties of the model associative polymer solutions with a statistical mechanical network theory. Examples of the shear-thickening phenomenon are shown in Figures 4.1 and 4.2 . In these Figures, the steady shear viscosity profiles have been normalized against the low shear viscosity, and the shear rate has been made dimensionless through multiplication with the relaxation time constant of the solution ($1/\beta_0$). The magnitude of the viscosity increase that occurs in the shear-thickening region decreases as the length of the polymer chain increases, and decreases as the concentration increases. The desired product of the modeling is a constitutive equation developed from molecular considerations that quantitatively describes the rheological properties of the associative polymer solutions. Such a constitutive equation will link the formation of network junctions by the associating polymer chains to macroscopically observed rheological properties.

Yamamoto Network Models

The modeling of the rheological properties of concentrated polymer solutions from molecular considerations usually follows one of two approaches: 1) modify dilute solution kinetic theory to accommodate interactions among chains as the solution becomes more concentrated, (for example, see the work of Bird et. al. [81]) or 2) generalize the theory of rubber elasticity to polymer networks that have physical rather than chemical junctions. The latter approach is taken by Yamamoto network theory [82 - 84], which considers a modified rubber-like network of polymer chains constructed from physical entanglement junctions that continuously rupture and reform. As shown in Chapter III, the model associative polymers form a strong, shear sensitive, network in solution through dynamic association junctions that continuously break and reform; hence, Yamamoto network theory is consistent with our physical interpretation of the rheological data.

Yamamoto network theory makes the following five assumptions. First, statistical mechanical equilibrium applies at each instant in time during the rheological measurement. This first assumption does not imply that the network is static or permanent, but rather that the micro-Brownian movements of network chain segments and junction breakage and reformation processes are so fast that the junctions are essentially at equilibrium at any given shear rate. Such a dynamic network can support stress and appear to have properties that are similar to a permanent network as long as the lifetime of an association junction is nearly as long as the hydrodynamic relaxation time of the association unit [73]. Second, the free energy of a single chain in the network depends on the number of statistical elements in the chain, denoted N, and the end-to-end distance of the chain, denoted $\underline{R}$. This does not necessarily mean that the network is composed of Gaussian chains. Third, the free energy of the whole network consists of the sum of free energy of individual chains in the network, (i.e. this is a "single chain problem"). Fourth, the junctions always assume their

most probable positions. Although this assumption may have no physical basis, it is necessary to keep the mathematics of the problem within manageable limits. Fifth, the energy dissipation of the network occurs only through the breakage and reformation of junctions. The applicability of this last assumption for our model polymer solutions is supported by the fact that, for a given molecular weight and concentration, the viscosity of a solution of model polymer with hexadecyl hydrophobic end- groups is orders of magnitudes larger than that of a solution of model polymer without hydrophobic end-groups. This suggests that viscous dissipation in these solutions occurs primarily through the association process, rather than by conventional volume exclusion or chain entanglement mechanisms.

With these assumptions, the stress supported by the physical polymer network $\underline{\underline{\tau}}_p$ is the free energy change in a volume element upon deformation. Since the polymers have a distribution of end-to-end distances, and therefore free energies, the free energy of the network is the free energy change of a single polymer chain multiplied by the distribution of end-to-end distances, viz:

$$\underline{\underline{\tau}}_p = \int_{-\infty}^{\infty}\int_{-\infty}^{\infty}\int_{-\infty}^{\infty} (\underline{R}\underline{R}) \left[\frac{1}{r} \frac{\partial \Psi(r,N,T)}{\partial r} \right]_{r = |\underline{R}|} f(\underline{R},N,t)\, d\underline{R} \qquad (4.1)$$

where the distribution function $f(\underline{R},N,t)$ describes the number of polymer chains with N segments with an end-to-end distance $\underline{R}$ in range of $\underline{R}$ to $\underline{R}+d\underline{R}$ at time t, and $\Psi(r,N,T)$ describes the polymer segment free energy that depends on the number of subunits N and the extent of elongation. Thus, the product of $(\underline{R}\underline{R})/r$ and the derivative of the polymer segment free energy is the tension that contributes to the stress in the network. To account for the entropically driven finite extensibility of the polymer chain, we use a series

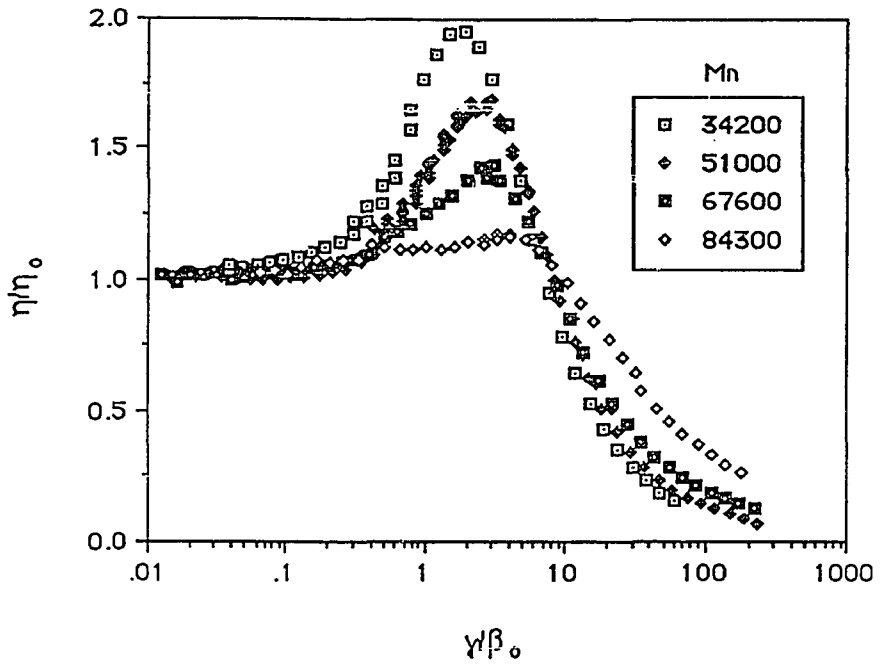

Figure 4.1: Normalized steady shear viscosity profiles of 1% solutions of model associative polymers with hexadecyl hydrophobic end- groups.

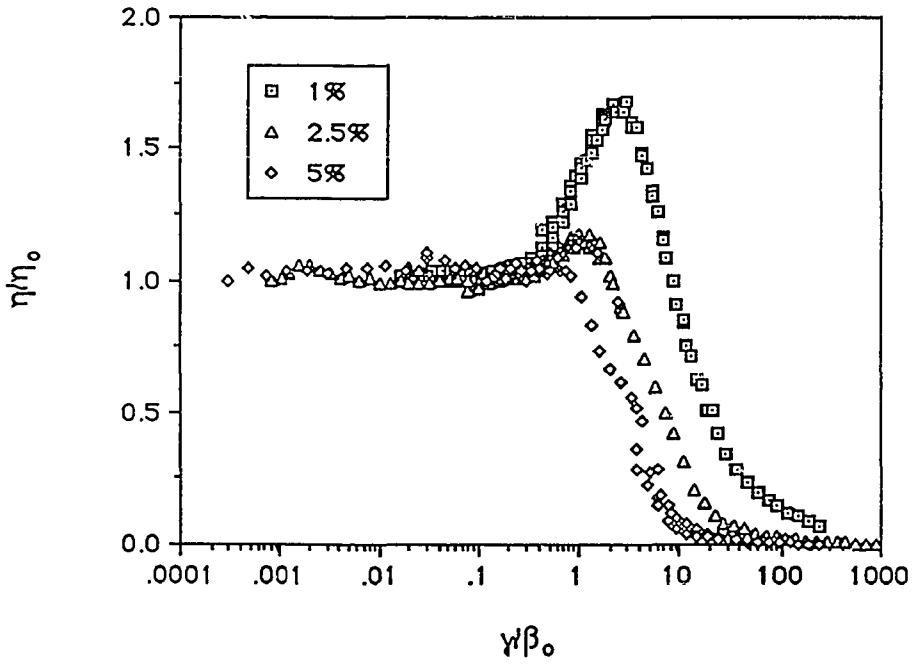

Figure 4.2: Normalized steady shear viscosity profiles of solutions of a model associative polymer of molecular weight 51000 with hexadecyl hydrophobic end- groups. Concentration is in weight percent.

expansion of the well established inverse Langevin function [85, 86] to obtain an expression for the free energy of the of the polymer chain:

$$\Psi(\underline{x},N,T) = \frac{3kTN}{2}|\underline{x}|^2\left(1 + \frac{3}{10}|\underline{x}|^2 + \frac{33}{175}|\underline{x}|^4 + \ldots\right) \tag{4.2}$$

where $\underline{x}$ is the end-to-end distance made dimensionless with respect to the maximum extension of the polymer chain, k is the Boltzmann constant, and T is the absolute temperature. This is an extension of the approach taken by Vrahopoulou and McHugh [76], who considered only the first two terms of the expansion, and of the approach taken by Fuller and Leal [87], who considered the first term of the expansion, (i.e. a Gaussian network). With the expression for the polymer chain free energy given by Equation (4.2), the stress tensor for the network now becomes:

$$\underline{\underline{\tau}}_p = 3kTN\left(\langle\underline{x}\underline{x}\rangle + \frac{3}{5}\langle(\underline{x}\underline{x})(x^2+y^2+z^2)\rangle + \frac{99}{175}\langle(\underline{x}\underline{x})(x^2+y^2+z^2)^2\rangle\right) \tag{4.3}$$

where the angular brackets denote averaging over configuration space. The calculation of the statistical averages $\langle\underline{x}\underline{x}\rangle$, $\langle(\underline{x}\underline{x})(x^2+y^2+z^2)\rangle$, and $\langle(\underline{x}\underline{x})(x^2+y^2+z^2)^2\rangle$ requires an explicit expression for the distribution function $f(\underline{x},N,t)$. This is found by solving a conservation equation for the distribution function [88]:

$$\frac{\partial f}{\partial t} + \underline{\nabla}\cdot\left[\left(\underline{\underline{\Gamma}} - \xi\,\underline{\underline{D}}\right)\cdot\underline{x}\,f\right] = G(\underline{x},N) - \beta(\underline{x},N)\,f \tag{4.4}$$

which states that the change in the distribution function with respect to time plus the change due to deformation equals the change due to junction creation processes minus the change due to junction destruction processes. In Equation (4.4), the function $G(\underline{x},N)$ governs the rate of junction creation, the function $\beta(\underline{x},N)$ describes the probability of junction breakage during the time interval and has a physical meaning as the reciprocal of the relaxation time, $\underline{\underline{\Gamma}}$ is the velocity gradient tensor, $\underline{\underline{D}}$ is the rate of deformation tensor, and non-zero values of the empirical "slip tensor" ξ describes the non-affine deformation of the network. Because the relationship between stress and strain along the network chain is not linear (i.e., it has a non-Gaussian free energy) , a deformation on one end of the network will not necessarily produce a deformation of equal magnitude at the other end of the network. Thus, the network junctions will not necessarily move affinely. The velocity gradient tensor $\underline{\underline{\Gamma}}$ for a general linear flow field is:

$$\underline{\underline{\Gamma}} = \frac{\gamma}{2}\begin{bmatrix} (1+\lambda) & (1-\lambda) & 0 \\ -(1-\lambda) & -(1+\lambda) & 0 \\ 0 & 0 & 0 \end{bmatrix} \tag{4.5}$$

where γ is the magnitude of the local velocity gradient, and the parameter λ specifies the particular type of the two dimensional flow field: λ is zero and the coordinate system is rotated clockwise 45 degrees for pure shear flow, and λ is unity for extensional flow.

Yamamoto network theory does not prescribe the junction creation and destruction potentials $G(\underline{x},N)$ and $\beta(\underline{x},N)$, and this feature makes the network model quite flexible.

Mathematically, all that is required is that these potentials possess spherical symmetry. Previous authors have used ad hoc, but physically reasonable, choices for these potentials. Fuller and Leal used the Gaussian approximation for $G(\underline{x},N)$, where the rate of junction formation is proportional to the distribution of end-to-end distances assumed by Gaussian network segments:

$$G(\underline{x},N) = L\left[\frac{3N}{2\pi}\right]^{3/2} \exp(-\Psi/kT) \qquad (4.6)$$

Ψ is given by the first term of Equation (4.2), and L is a rate coefficient. This assumes that the network segments follow random flight chain statistics, and never approach full extension. Vrahopoulou and McHugh showed that the finite extensibility of the network chain, which gives rise to non-Gaussian chain statistics, can be modeled by using the series expansion of the inverse Langevin function for Ψ in Equation (4.6). We have extended their approach to include the next term in the series expansion. Thus, for the polymer segment free energy given in Equation (4.2), the normalized rate of junction creation in our model is given by:

$$G(\underline{x},N) = L\left(\frac{3N}{2\pi}\right)^{3/2} \frac{e^{\left\{\frac{-3N}{2}(x^2+y^2+z^2)\left[1+\frac{3}{10}(x^2+y^2+z^2)+\frac{33}{175}(x^2+y^2+z^2)^2\right]\right\}}}{\frac{2}{\sqrt{\pi}}\int_0^\infty \sqrt{h}\, e^{-h[1+h/5N+44h^2/525N^2]}\, dh} \qquad ...(4.7)$$

where h is a dummy variable.

The probability of rupturing an association network junction increases as the network chains extend and support stress. Indeed, the data in Figure 3.25 show how the number density of network junctions decreases as the rate of strain increases. A number of potentials of varying degree of complexity have been proposed to model this feature. For example, Yamamoto used a square well model. In this model, the probability of breaking a network junction is constant until the chains reach complete extension, whereupon probability of breaking a junction becomes infinite. Unfortunately, it is difficult to carry out the integrations specified in Equation (4.3) analytically for this network junction breakage potential [89]. A potential which exhibits the same qualitative behavior, but is easier to work with, is a Warner - type junction breakage potential:

$$\beta(\underline{x}) = \frac{\beta_o}{1 - |\underline{x}|^2} \tag{4.8}$$

The probability of junction rupture starts from its rest state value of β_o, and increases as the network chains extend. Thus, as shown in Chapter III, the inverse of the relaxation time constant as determined from the dynamic shear moduli measures β_o, because the network is perturbed only slightly in small amplitude oscillatory flows. As the relative mean square end-to-end distance of the chain approaches its fully extended value of unity, the probability of rupturing the network junction becomes infinite. To evaluate the statistical averages prescribed by Equation (4.3) for the stress tensor, it is useful to expand Equation (4.8) into its Taylor series:

$$\beta(\underline{x}) = \beta_o \left(1 + |\underline{x}|^2 + |\underline{x}|^4 + \ldots \right) \tag{4.9}$$

Truncation after the first term produces a model with a constant network junction destruction potential, and truncation after the quadratic term yields the simplest spherically symmetric conformation dependant junction destruction potential that retains the qualitative flavor of Equation (4.8). Equation (4.9) is similar to the junction destruction potentials proposed by Fuller and Leal [87], and by Phan-Thien and Tanner [88]. Fuller and Leal used:

$$\beta(\underline{x}) = \beta_o [\, 1 + \sigma(x^2 + y^2 + z^2) \,] \tag{4.10}$$

where σ is the square of the ratio of the maximum end-to-end distance of the network chain to the length scale over which $\beta(\underline{x})$ changes. Phan-Thien and Tanner used the preaveraged version of this equation. Putting σ equal to unity shows that equation (4.10) can be considered as a special case of Equation (4.8).

As the number of segments between network junctions approaches infinity, our non-Gaussian network model should reduce to the Gaussian network model of Fuller and Leal. Therefore, we use Equation (4.10) for the conformation dependent network junction breakage potential $\beta(\underline{x},N)$; our model is the generalization of Fuller and Leal's Gaussian model with a conformation dependent destruction potential to finitely extensible networks. Subsequent calculations examine the relationship between the probability of breaking a given network junction and the relative extension of the network chains that connect the junctions by varying the parameter $\varepsilon = 2\sigma/3N$. When ε is zero, the constant junction breakage potential is obtained, our model reduces to an extended version of the non-Gaussian network model derived by Vrahopoulou and McHugh. As ε increases, the probability that shear will rupture a given junction as the network chains extend increases. We therefore label ε as the "breakage index". Additionally, the network theory reduces to

the theory of ideal rubber elasticity when the rates of junction creation and destruction are zero, to the Hookean dumbbell theory of dilute macromolecular solutions when the free energy of the polymer chains is Gaussian and the rate of junction destruction is constant, and to Lodge's non-Gaussian network theory [89] when the rate of junction destruction is constant for an affine, non-Gaussian network. Thus, we develop the non-Gaussian model for these two choices of the destruction potential.

Development of the Model

As shown by Fuller and Leal, the solution process to determine the distribution function is expedited if the coordinate system is transformed to a new frame $\underline{\rho} = (\rho,\eta,z)$ that coincides with the principle axes of strain for the flow field such that $\underline{x} = \underline{\underline{T}} \cdot \underline{\rho}$ Then the velocity gradient vector is diagonalized through $\underline{\underline{T}}^{-1} \cdot [\, \underline{\underline{\Gamma}} - \xi \underline{\underline{D}} \,] \cdot \underline{\underline{T}} = \underline{\underline{V}}$, viz:

$$\underline{\underline{V}} = \frac{\gamma}{2}\begin{bmatrix} \sqrt{\nu} & 0 & 0 \\ 0 & -\sqrt{\nu} & 0 \\ 0 & 0 & 0 \end{bmatrix} \tag{4.11}$$

where $\nu = (1-\xi)^2(1+\lambda)^2 - (1-\lambda)^2$, and $\underline{\underline{T}}$ is the tensor of eigenvectors of the velocity gradient tensor. Application of this change of variables to the equation to solve for the distribution function yields:

$$\frac{\partial f}{\partial t} + \gamma\frac{\sqrt{\nu}}{2}\rho\frac{\partial f}{\partial \rho} - \gamma\frac{\sqrt{\nu}}{2}\eta\frac{\partial f}{\partial \eta} = \hat{G}(\underline{\rho},N) - \hat{\beta}(\underline{\rho},N)f \tag{4.12}$$

Equation (4.12) is solved by the method of characteristics to yield the distribution function in closed form:

$$f(\rho,\eta,z,t) = f_o(\rho_o,\eta_o,z_o)\exp\left\{ -\int_o^t dt'\, \hat{\beta}(\rho_o e^{\gamma\sqrt{\nu}\, t'/2}, \eta_o e^{-\gamma\sqrt{\nu}\, t'/2}, z_o, N) \right\}$$

$$+ \int_o^t dt'\, \hat{G}(\rho_o e^{\gamma\sqrt{\nu}\, t'/2}, \eta_o e^{-\gamma\sqrt{\nu}\, t'/2}, z_o, N) \qquad (4.13)$$

$$\times \exp\left\{ -\int_{t'}^{t''} dt''\, \hat{\beta}(\rho_o e^{\gamma\sqrt{\nu}\, t''/2}, \eta_o e^{-\gamma\sqrt{\nu}\, t''/2}, z_o, N) \right\}$$

where the initial distribution $f_o(\rho,\eta,z)$ equals $\hat{G}(\rho,\eta,z,N)/\hat{\beta}(\rho,\eta,z,N)$. The initial distribution is simply $G(\underline{x},N)/\beta_0$ for the constant junction breakage potential model; this is also true for the conformation dependent junction breakage model as long as $\sigma << N$.

Thus, statistical average of any function $g(\rho,\eta,z)$ is calculated from:

$$\langle g(\rho,\eta,z)\rangle = \sqrt{1-\omega^2} \int_{-\infty}^{\infty}\int_{-\infty}^{\infty}\int_{-\infty}^{\infty} d\rho d\eta dz\, g(\rho,\eta,z)\, f_o(\rho e^{-\gamma\sqrt{\nu}\, t/2}, \eta e^{\gamma\sqrt{\nu}\, t/2}, z)$$

$$\times \exp\left\{ \frac{-2}{\gamma\sqrt{\nu}} \int_{\rho e^{-\gamma\sqrt{\nu}\, t/2}}^{\rho} \frac{d\rho'}{\rho'} \hat{\beta}(\rho', \frac{\eta\rho}{\rho'}, z, N) \right\} + \sqrt{1-\omega^2}\, \frac{2S}{\gamma\sqrt{\nu}}$$

$$\times \int_{-\infty}^{\infty}\int_{-\infty}^{\infty}\int_{-\infty}^{\infty} d\eta d\rho dz \int_{1}^{\infty} \frac{d\theta}{\theta}\, g\left(\theta\rho,\, \eta\,\frac{S+\theta\, e^{-\gamma\sqrt{\nu}\, t/2}}{\theta},\, z\right) \tag{4.14}$$

$$\times\, \hat{G}\left(\rho(S+\theta e^{-\gamma\sqrt{\nu}\, t/2}),\, \eta,\, z, N\right) \exp\left\{\frac{-2}{\gamma\sqrt{\nu}} \int_{S+\theta\exp(-\gamma\sqrt{\nu}\, t/2)}^{\theta} \frac{d\theta'}{\theta'}\, \hat{\beta}\left(\theta'\rho, \eta\frac{S+\theta e^{-\gamma\sqrt{\nu}\, t/2}}{\theta'},\, z, N\right)\right\}$$

where $\omega = (1-\lambda)/(1-\xi)(1+\lambda)$, and $S = 1 - \exp(-\gamma\sqrt{\nu}\, t/2)$. The averages required for calculation of the rheological properties indicated in Equation (4.3) are related to the moments in the transformed coordinate frame $\underline{\rho} = (\rho,\eta,z)$ calculated from Equation (4.14) through the relation:

$$\langle(\underline{xx})\rangle = \langle \underline{\rho}\cdot\underline{\underline{T}}^{\dagger}\cdot\underline{\underline{T}}\cdot\underline{\rho}\rangle \tag{4.15}$$

Hence, the shear viscosity η, first ψ_1 and second ψ_2 normal stress difference coefficients, and the extensional viscosity $\bar{\eta}$ of the of the network are calculated from Equation (4.3):

$$\eta = \frac{\tau_{xy}}{\dot{\gamma}} = \frac{3k\Gamma N}{2\dot{\gamma}}\left\{\langle x^2-y^2\rangle + \frac{3}{5}\langle(x^2-y^2)(x^2+y^2+z^2)\rangle + \frac{99}{175}\langle(x^2-y^2)(x^2+y^2+z^2)^2\rangle\right\}$$

...(4.16)

$$\Psi_1 = \frac{\tau_{xx}-\tau_{yy}}{\gamma^2} = \frac{-6kTN}{\gamma^2}\left\{<xy> + \frac{3}{5}<(xy)(x^2+y^2+z^2)> + \frac{99}{175}<(xy)(x^2+y^2+z^2)^2>\right\}$$

...(4.17)

$$\Psi_2 = \frac{\tau_{yy}-\tau_{zz}}{\gamma^2} = \frac{3kTN}{2\gamma^2}\left\{ <x^2+y^2-2z^2> + 2<xy> + \frac{3}{5}\left[<(x^2+y^2-2z^2)(x^2+y^2+z^2)>\right.\right.$$

$$\left.\left. + 2<(xy)(x^2+y^2+z^2)>\right] + \frac{99}{175}\left[<(x^2+y^2-2z^2)(x^2+y^2+z^2)^2 +2<(xy>(x^2+y^2+z^2)^2>\right] \right\}$$

...(4.18)

$$\overline{\eta} = \frac{\tau_{xx}-\tau_{yy}}{\gamma_\varepsilon} = \frac{3kTN}{\gamma_\varepsilon}\left\{<x^2-y^2> + \frac{3}{5}<(x^2-y^2)(x^2+y^2+z^2)> + \frac{99}{175}<(x^2-y^2)(x^2+y^2+z^2)^2>\right\}$$

...(4.19)

where γ_ε is the rate of elongation in an extensional flow field, and the required statistical averages are as given below.

Constant Junction Breakage Potential

The following statistical averages are derived using the non-Gaussian polymer segment free energy given by Equation (4.2) and a constant probability of network junction breakage $\beta(\underline{x},N) = \beta_o$.

$$<n> = \frac{L}{\beta_o} \qquad (4.20)$$

$$\langle x^2-y^2\rangle = \frac{4\alpha}{9}\frac{L}{\beta_o N}\frac{(1-\xi)(1+\lambda)}{(1-\alpha^2\nu)}\frac{\int_0^\infty h^{3/2}\exp\{-h[1+h/5N+44h^2/525N^2]\}\,dh}{\int_0^\infty \sqrt{h}\,\exp\{-h[1+h/5N+44h^2/525N^2]\}\,dh}$$

$$\times\,[1-e^{-t^*}\cosh(\alpha\sqrt{\nu}\,t^*)-\alpha\sqrt{\nu}\,e^{-t^*}\sinh(\alpha\sqrt{\nu}\,t^*)]$$

...(4.21)

$$\langle xy\rangle = \frac{2\alpha}{9}\frac{L}{\beta_o N}\frac{(1-\xi)(1+\lambda)(1-\lambda)}{(1-\alpha^2\nu)}\frac{\int_0^\infty h^{3/2}\exp\{-h[1+h/5N+44h^2/525N^2]\}\,dh}{\int_0^\infty \sqrt{h}\,\exp\{-h[1+h/5N+44h^2/525N^2]\}\,dh}$$

$$\times\,[-\alpha+e^{-t^*}\frac{\sinh(\alpha\sqrt{\nu}\,t^*)}{\sqrt{\nu}}+\alpha e^{-t^*}\cosh(\alpha\sqrt{\nu}\,t^*)]$$

...(4.22)

$$\langle x^2+y^2-2z^2\rangle = \frac{4}{9}\frac{L\,\alpha}{\beta_o N}\frac{(1-\xi)^2(1-\lambda)^2}{(1-\alpha^2\nu)}\frac{\int_0^\infty h^{3/2}\exp\{-h[1+h/5N+44h^2/525N^2]\}\,dh}{\int_0^\infty \sqrt{h}\,\exp\{-h[1+h/5N+44h^2/525N^2]\}\,dh}$$

$$\times\,[\alpha-e^{-t^*}\frac{\sinh(\alpha\sqrt{\nu}\,t^*)}{\sqrt{\nu}}-\alpha e^{-t^*}\cosh(\alpha\sqrt{\nu}\,t^*)]$$

...(4.23)

$$<(x^2-y^2)(x^2+y^2+z^2)> = \frac{8}{45}\frac{L}{\beta_o N^2(1-\xi)(1+\lambda)}\frac{\alpha\nu}{}\frac{\int_o^\infty h^{5/2}\exp\{-h[1+h/5N+44h^2/525N^2]\}\,dh}{\int_o^\infty \sqrt{h}\,\exp\{-h[1+h/5N+44h^2/525N^2]\}\,dh}$$

$$\left\{\frac{2\,[\,1-e^{-t^*}\cosh(2\alpha\sqrt{\nu}\,t^*)-2\alpha\sqrt{\nu}\,e^{-t^*}\sinh(2\alpha\sqrt{\nu}\,t^*)\,]}{(1-\omega^2)^2(1-4\alpha^2\nu)}\right.$$

$$+\frac{1-e^{-t^*}\cosh(\alpha\sqrt{\nu}\,t^*)-\alpha\sqrt{\nu}\,e^{-t^*}\sinh(\alpha\sqrt{\nu}\,t^*)}{3(1-\omega^2)(1-\alpha^2\nu)}$$

$$\left.-\frac{2\omega^2\,[\,1-e^{-t^*}\cosh(\alpha\sqrt{\nu}\,t^*)-\alpha\sqrt{\nu}\,e^{-t^*}\sinh(\alpha\sqrt{\nu}\,t^*)\,]}{(1-\omega^2)^2(1-\alpha^2\nu)}\right\}$$

...(4.24)

$$<(xy)(x^2+y^2+z^2)> = \frac{4}{45}\frac{L}{\beta_o N^2}\frac{\omega}{(1-\omega^2)^2}\frac{\int_o^\infty h^{5/2}\exp\{-h[1+h/5N+44h^2/525N^2]\}\,dh}{\int_o^\infty \sqrt{h}\,\exp\{-h[1+h/5N+44h^2/525N^2]\}\,dh}$$

$$\times\left\{-\frac{1-2\alpha\sqrt{\nu}\,e^{-t^*}\sinh(2\alpha\sqrt{\nu}\,t^*)-4\alpha^2\nu\,e^{-t^*}\cosh(2\alpha\sqrt{\nu}\,t^*)}{(1-4\alpha^2\nu)}+\frac{(1-\omega^2)}{3}\right.$$

$$\left.+\frac{(5+7\omega^2)}{3(1-\alpha^2\nu)}[\,1-\alpha\sqrt{\nu}\;e^{-t^*}\sinh(\alpha\sqrt{\nu}\,t^*)-\alpha^2\nu\,e^{-t^*}\cosh(\alpha\sqrt{\nu}\,t^*)]-(1+2\omega^2)\right\}$$

...(4.25)

$$<(x^2+y^2-2z^2)(x^2+y^2+z^2)> = \frac{8}{135}\frac{L}{\beta_o N^2}\frac{1}{(1-\omega^2)}\frac{\int_0^\infty h^{5/2}\exp\{-h[1+h/5N+44h^2/525N^2]\}\,dh}{\int_0^\infty \sqrt{h}\,\exp\{-h[1+h/5N+44h^2/525N^2]\}\,dh}$$

$$\left\{\frac{3}{(1-4\alpha^2\nu)(1-\omega^2)}[\,1-2\alpha\sqrt{\nu}\,e^{-t^*}\sinh(2\alpha\sqrt{\nu}\,t^*)-4\alpha^2\nu\,e^{-t^*}\cosh(2\alpha\sqrt{\nu}\,t^*)\,]\right.$$

$$-\frac{(1+11\omega^2)}{(1-\alpha^2\nu)(1-\omega^2)}[\,1-\alpha\sqrt{\nu}\,e^{-t^*}\sinh(\alpha\sqrt{\nu}\,t^*)-\alpha^2\nu\,e^{-t^*}\cosh(\alpha\sqrt{\nu}\,t^*)\,]$$

$$\left.+\frac{(1+2\omega^2)^2}{(1-\omega^2)}+(4\omega^2-3)\right\}$$

...(4.26)

$$<(x^2-y^2)(x^2+y^2+z^2)^2> =$$

$$\frac{16}{189}\frac{L}{\beta_o N^3}\frac{\alpha\nu}{(1-\xi)(1+\lambda)(1-\alpha^2)}\frac{\int_0^\infty h^{7/2}\exp\{-h[1+h/5N+44h^2/525N^2]\}\,dh}{\int_0^\infty \sqrt{h}\,\exp\{-h[1+h/5N+44h^2/525N^2]\}\,dh}$$

$$\{[\frac{1}{5}-\frac{4\omega^2}{5(1-\omega^2)}+\frac{(1+4\omega^2)^2}{5(1-\omega^2)^2}][\frac{1-e^{-t^*}\cosh(\alpha\sqrt{\nu}\,t^*)-\alpha\sqrt{\nu}\,e^{-t^*}\sinh(\alpha\sqrt{\nu}\,t^*)}{(1-\alpha^2\nu)}]$$

$$+[\frac{4}{5(1-\omega^2)}-\frac{8\omega^2}{(1-\omega^2)^2}][\frac{1-e^{-t^*}\cosh(2\alpha\sqrt{\nu}\,t^*)-2\alpha\sqrt{\nu}\,e^{-t^*}\sinh(2\alpha\sqrt{\nu}\,t^*)}{(1-4\alpha^2\nu)}]$$

$$+\frac{3}{(1-\omega^2)^2}[\frac{1-e^{-t^*}\cosh(3\alpha\sqrt{\nu}\,t^*)-3\alpha\sqrt{\nu}\,e^{-t^*}\sinh(3\alpha\sqrt{\nu}\,t^*)}{(1-9\alpha^2\nu)}]\}$$

...(4.27)

$$\langle(xy)(x^2+y^2+z^2)^2\rangle =$$

$$\frac{8}{189}\frac{L\,\omega}{\beta_o N^3}\frac{\int_o^\infty h^{7/2}\exp\{-h[1+h/5N+44h^2/525N^2]\}\,dh}{\int_o^\infty \sqrt{h}\,\exp\{-h[1+h/5N+44h^2/525N^2]\}\,dh}$$

$$\{-\frac{[\,1-3\alpha\sqrt{\nu}\;e^{-t^*}\sinh(3\alpha\sqrt{\nu}\,t^*)-9\alpha^2\nu\,e^{-t^*}\cosh(3\alpha\sqrt{\nu}\,t^*)\,]}{(1-9\alpha^2\nu)(1-\omega^2)^3}$$

$$+[\frac{2(1+2\omega^2)}{(1-\omega^2)^3}-\frac{2}{5(1-\omega^2)^2}][\frac{[1-2\alpha\sqrt{\nu}\;e^{-t^*}\sinh(2\alpha\sqrt{\nu}\,t^*)-4\alpha^2\nu\,e^{-t^*}\cosh(2\alpha\sqrt{\nu}\,t^*)\,]}{(1-4\alpha^2\nu)}]$$

$$- \left[\frac{(1+4\omega^2)(11+4\omega^2)}{(1-\omega^2)^3} - \frac{4(1+\omega^2)}{(1-\omega^2)^2} + \frac{1}{(1-\omega^2)} \right] \frac{1}{5(1-\alpha^2\nu)} \left[1 - \alpha\sqrt{\nu}\, e^{-t^*} \sinh(\alpha\sqrt{\nu}\, t^*) \right.$$

$$\left. - \alpha^2\nu\, e^{-t^*} \cosh(\alpha\sqrt{\nu}\, t^*) \right] + \frac{2(1+4\omega^2)(3+2\omega^2)}{5(1-\omega^2)^3} - \frac{2(1+2\omega^2)}{5(1-\omega^2)^2} + \frac{1}{5(1-\omega^2)} \Big\}$$

...(4.28)

$$\langle (x^2+y^2-2z^2)(x^2+y^2+z^2)^2 \rangle =$$

$$\frac{8}{189} \frac{L}{\beta_o N^3} \frac{1}{(1-\omega^2)^3} \frac{\int_o^\infty h^{7/2} \exp\{-h[1 + h/5N + 44h^2/525N^2]\}\, dh}{\int_o^\infty \sqrt{h}\, \exp\{-h[1 + h/5N + 44h^2/525N^2]\}\, dh}$$

$$\Big\{ \frac{2}{(1-9\alpha^2\nu)} [1 - 3\alpha\sqrt{\nu}\, e^{-t^*} \sinh(3\alpha\sqrt{\nu}\, t^*) - 9\alpha^2\nu\, e^{-t^*} \cosh(3\alpha\sqrt{\nu}\, t^*)]$$

$$- \frac{12\omega^2}{(1-4\alpha^2\nu)} [1 - 2\alpha\sqrt{\nu}\, e^{-t^*} \sinh(2\alpha\sqrt{\nu}\, t^*) - 4\alpha^2\nu\, e^{-t^*} \cosh(\alpha\sqrt{\nu}\, t^*)]$$

$$+ \frac{6[(1+4\omega^2)^2 - (1-\omega^2)^2]}{5(1-\alpha^2\nu)} [1 - \alpha\sqrt{\nu}\, e^{-t^*} \sinh(\alpha\sqrt{\nu}\, t^*) - \alpha^2\nu\, e^{-t^*} \cosh(\alpha\sqrt{\nu}\, t^*)]$$

$$- \frac{4\omega^2(3+2\omega^2)^2}{5} + \frac{6\omega^2(1-\omega^2)^2}{5} - 2(1-\omega^2)^3 \Big\}$$

...(4.29)

where $t^*=t\beta$ is a dimensionless time, and $\alpha=\gamma/\beta$ is a dimensionless shear rate. The integrals in Equations (4.21) through (4.29) are in Gauss-Laguerre form, and as such, are easy to evaluate numerically. The apparent singularity that occurs when the network is affine (i.e., when $\omega=1$) in the above equations can be removed with some algebra.

Conformation Dependent Junction Breakage Potential

Development of the statistical averages for a non-Gaussian network with a conformation dependent breakage potential given by Equation (4.10) follows along lines that are similar to that of the model with a constant breakage potential. For example, transformation of Equation (4.14) into spherical polar coordinates for the breakage potential given by Equation (10) results in the following for the first integral term:

$$\frac{\frac{L}{\beta_o} Q(t^*)\, e^{-t^*} \frac{1}{4\pi}}{\int_0^{\infty} \sqrt{h}\, e^{-h[1+h/5N + 44h^2/525N^2]}\, dh} \int_0^{\infty} \int_{-\pi/2}^{2\pi} \int_{\pi/2} f_1(h,\theta,\phi)\, \sqrt{h}\, e^{-h}\, R(h,\theta,\phi) \cos\phi\, d\phi\, d\theta \qquad ...(4.30)$$

where $f_1(h,\theta,\phi)$ is a function that depends on the exact average being evaluated, and

$$R(h,\theta,\phi) = \exp\left\{\frac{-h^2}{5N}\Xi(t^*)\left[1 + \frac{44\, h\, \Xi(t^*)}{105\, N}\right]\right\} \qquad (4.31)$$

$$\Xi(t^*) = D^+(t^*)\cos^2\theta\cos^2\phi + D^-(t^*)\sin^2\theta\cos^2\phi + \frac{\sin^2\phi}{Z(t^*)} + \frac{\cos^2\phi\cos\theta\sin\theta(K^-(t^*)-K^+(t^*))}{\sqrt{K^+(t^*)\,K^-(t^*)\,C(t^*)}}$$

...(4.32)

$$C(t^*) = 1 + \frac{2\,\varepsilon}{\alpha\sqrt{\nu}}\sinh(\alpha\sqrt{\nu}\,t^*) + \frac{2\,\varepsilon^2}{\alpha^2\nu}[\,\cosh(\alpha\sqrt{\nu}\,t^*) - 1\,] - \omega^2\,Z^2(t^*)$$

...(4.33)

$$D^{\pm}(t^*) = \{\,1 + \frac{\varepsilon}{\alpha\sqrt{\nu}}\sinh(\alpha\sqrt{\nu}\,t^*) - \omega^2\,Z(t^*)$$

$$\pm\,\omega\sqrt{C(t^*) + \omega^2\,Z^2(t^*)}\;\left[\,1 - \frac{Z(t^*)(1 + -\frac{\varepsilon}{\alpha\sqrt{\nu}}\sinh(\alpha\sqrt{\nu}\,t^*))}{C(t^*) + \omega^2\,Z^2(t^*)}\right]\,\}/C(t^*)$$

...(4.34)

$$K^{\pm}(t^*) = 1 \pm \frac{\varepsilon}{\alpha\sqrt{\nu}}\left(e^{\pm\,\alpha\sqrt{\nu}\,t^*} - 1\right) \quad Q(t^*) = \sqrt{\frac{1-\omega^2}{C(t^*)\,Z(t^*)}}$$

...(4.35)

$$Z(t^*) = 1 + \varepsilon t^* \quad \varepsilon = \frac{2\sigma}{3N} \qquad (4.36)$$

Because $D^+(t^*)$ does not in general equal $D^-(t^*)$, and because $K^+(t^*)$ does not in general equal $K^-(t^*)$, analytical integration of Equation (4.30) is not possible. Although it is possible to perform the integrations numerically, it is pedagogically useful to seek an approximate analytical solution in closed form.

Expanding the exponential in its Taylor series in the polar and azimuthal angles θ and ϕ about the center of the integration limits uncouples the angular dependence in the exponential. The Taylor expansion about the center of the integration intervals, truncating third order and higher terms, is:

$$R(h,\theta,\phi) \cong R(h,\pi,0) + \pi \frac{\partial}{\partial\theta} R(h,\theta,\phi) + \frac{\pi^2}{2}\frac{\partial^2}{\partial\theta^2} R(h,\theta,\phi) + \ldots \qquad (4.37)$$

where the derivatives are evaluated at $(h,\pi,0)$. This has, in effect, replaced the angular terms in the exponential with their mean values over the integration intervals while preserving the time dependent response. We could have expanded about the end points of the integration interval, or about the origin of the coordinate system, but many of the derivatives of $R(h,\theta,\phi)$ are zero at these points. Hence, an expansion about the midpoint of the integration interval should yield a better approximation of the integral. In the limit as the breakage index ε goes to zero, the integrals in Equation (4.30) can be evaluated analytically because $D^+(t^*)=D^-(t^*)=K^+(t^*)=K^-(t^*)=1$.

Following the spirit of the notation of Fuller and Leal, and Vrahopoulou and McHugh, the moments in (x,y,z) space are:

$$\langle n \rangle = \frac{L}{\beta}\left\{ Q(t^*)E(t^*)\, e^{-t^*} + \int_0^{t^*} Q(t'^*)E(t'^*)\, e^{-t'^*}\, dt'^* \right\} \qquad (4.38)$$

$$\langle x^2-y^2\rangle = \frac{L}{3\beta_o N}\left\{\frac{Q(t^*)H(t^*)[A^+(t^*)-A^-(t^*)]\,e^{-t^*}}{C(t^*)}+\int_o^{t^*} dt'^*\,\frac{Q(t'^*)H(t'^*)[A^+(t'^*)-A^-(t'^*)]\,e^{-t'^*}}{C(t'^*)}\right\}$$

...(4.39)

$$\langle xy\rangle = \frac{L}{3\beta_o N}\left\{\frac{Q(t^*)H(t^*)B(t^*)\,e^{-t^*}}{C(t^*)}+\int_o^{t^*}\frac{Q(t'^*)H(t'^*)B(t'^*)\,e^{-t'^*}\,dt'^*}{C(t'^*)}\right\}$$

...(4.40)

$$\langle x^2+y^2-2z^2\rangle = \frac{L}{3\beta_o N}\left\{\,Q(t^*)H(t^*)\left[\frac{A^+(t^*)+A^-(t^*)}{C(t^*)}-\frac{2}{Z(t^*)}\right]e^{-t^*}\right.$$
$$\left.+\int_o^{t^*} Q(t'^*)H(t'^*)\left[\frac{A^+(t'^*)+A^-(t'^*)}{C(t'^*)}-\frac{2}{Z(t'^*)}\right]e^{-t'^*}\,dt'^*\,\right\}$$

...(4.41)

$$\langle (x^2-y^2)(x^2+y^2+z^2)\rangle = \frac{2L}{3\beta_o N^2}\,\frac{\alpha\nu}{(1-\xi)(1+\lambda)}\left\{\,\frac{Q(t^*)\,I(t^*)\,M(t^*)\,e^{-t^*}}{C(t^*)}+\right.$$
$$\left.\int_o^{t^*}\frac{Q(t'^*)\,I(t'^*)\,M(t'^*)\,e^{-t'^*}\,dt'^*}{C(t'^*)}\,\right\}$$

...(4.42)

$$\langle (xy)(x^2+y^2+z^2) \rangle = \frac{L\omega}{3\beta_o N^2} \left\{ \frac{Q(t^*)\, I(t^*)\, P(t^*)\, e^{-t^*}}{C(t^*)} + \int_o^{t^*} \frac{Q(t'^*) I(t'^*) P(t'^*)\, e^{-t'^*}}{C(t'^*)}\, dt'^* \right\}$$

...(4.43)

$$\langle (x^2+y^2-2z^2)(x^2+y^2+z^2) \rangle = \frac{2L}{3\beta_o N^2} \left\{ \frac{Q(t^*)\, I(t^*)\, U(t^*)\, e^{-t^*}}{C(t^*)} + \int_o^{t^*} \frac{Q(t'^*) I(t'^*) U(t'^*) e^{-t'^*}}{C(t'^*)}\, dt'^* \right\}$$

...(4.44)

$$\langle (x^2-y^2)(x^2+y^2+z^2)^2 \rangle = \frac{2\,L}{9\,\beta_o\, N^3\, \alpha\, (1-\xi)(1+\lambda)} \left\{ \frac{Q(t^*)\, J(t^*)\, V(t^*)\, e^{-t^*}}{C(t^*)} + \int_o^{t^*} \frac{Q(t'^*)\, J(t'^*)\, V(t'^*)\, e^{-t'^*}}{C(t'^*)}\, dt'^* \right\}$$

...(4.45)

$$\langle (xy)(x^2+y^2+z^2)^2 \rangle = \frac{2\,\omega L}{9\,\beta_o N^3} \left\{ \frac{Q(t^*) J(t^*) W(t^*)\, e^{-t^*}}{C(t^*)} + \int_o^{t^*} \frac{Q(t'^*) J(t'^*) W(t'^*)\, e^{-t'^*}}{C(t'^*)}\, dt'^* \right\}$$

...(4.46)

$$<(x^2+y^2-2z^2)(x^2+y^2+z^2)^2> = \frac{2\,L}{9\beta_o N^3}\left\{ \frac{Q(t^*)J(t^*)Y(t^*)\,e^{-t^*}}{C(t^*)} + \int_o^{t^*} \frac{Q(t'^*)J(t'^*)Y(t'^*)\,e^{-t'^*}}{C(t'^*)}\,dt'^* \right\}$$

...(4.47)

where

$$A^{\pm}(t^*) = \left\{ \left[(1-\xi)(1+\lambda) \pm \frac{\varepsilon}{\alpha}\right]\cosh(\alpha\sqrt{\nu}\,t^*) + \left[\frac{(1-\xi)(1+\lambda)\varepsilon}{\alpha} \pm \nu\right]\frac{\sinh(\alpha\sqrt{\nu}\,t^*)}{\sqrt{\nu}} \right.$$

$$\left. \mp \frac{\varepsilon}{\alpha} - \omega(1-\lambda)Z(t^*) \right\} / (1-\xi)(1+\lambda)$$

...(4.48)

$$B(t^*) = \left\{(1-\xi)(1+\lambda)\omega Z(t^*) - (1-\lambda)\left[\cosh(\alpha\sqrt{\nu}\,t^*) + \frac{\varepsilon}{\alpha\sqrt{\nu}}\sinh(\alpha\sqrt{\nu}\,t^*)\right]\right\}/(1-\xi)(1+\lambda)$$

...(4.49)

$$E(t^*) = \int_o^{\infty} h^{1/2}\, e^{-h}\, \Lambda(h,t^*)\, dh \qquad (4.50)$$

$$H(t^*) = \frac{2}{3}\int_o^{\infty} h^{3/2}\, e^{-h}\, \Lambda(h,t^*)\, dh \qquad (4.51)$$

$$I(t^*) = \frac{4}{15}\int_o^{\infty} h^{5/2}\, e^{-h}\, \Lambda(h,t^*)\, dh \qquad (4.52)$$

$$J(t^*) = \frac{8}{105}\int_o^{\infty} h^{7/2}\, e^{-h}\, \Lambda(h,t^*)\, dh \qquad (4.53)$$

$$\Lambda(t^*) = \frac{e^{\frac{-h^2 D^{+2}(t^*)}{5N}\left(1+\frac{44\,h\,D^{+}(t^*)}{105N}\right)}}{\int_0^{\infty}\sqrt{h}\; e^{-h[1+h/5N+44h^2/525N^2]}dh}\left\{\,1-\frac{\pi h^2}{5N}\left[\frac{2\,D^{+}(t^*)(K^{-}(t^*)-K^{+}(t^*))}{\sqrt{K^{-}(t^*)\,K^{+}(t^*)\,C(t^*)}}\right.\right.$$

$$\left.\frac{\pi\,(K^{-}(t^*)-K^{+}(t^*))^2}{K^{+}(t^*)\,K^{-}(t^*)\,C(t^*)}+2\pi\,D^{+}(t^*)\,(D^{-}(t^*)-D^{-}(t^*))\right]-\frac{22\pi\,h^3\,D^{+}(t^*)}{175N^2}\left[\frac{2D^{+}(t^*)(K^{-}(t^*)-K^{+}(t^*)}{\sqrt{K^{-}(t^*)K^{+}(t^*)C(t^*)}}\right.$$

$$\left.+\frac{2\pi(K^{-}(t^*)-K^{+}(t^*))^2}{K^{+}(t^*)K^{-}(t^*)C(t^*)}+2\pi D^{+}(t^*)(D^{-}(t^*)-D^{+}(t^*))\right]+\frac{2\pi^2\,h^4\,D^{+2}(t^*)\,(K^{-}(t^*)-K^{+}(t^*))^2}{25N^2K^{-}(t^*)K^{+}(t^*)C(t^*)}$$

$$+\frac{88\pi^2\,h^5\,D^{+3}(t^*)(K^{-}(t^*)-K^{+}(t^*))^2}{875N^3\,K^{+}(t^*)K^{-}(t^*)\,C(t^*)}+\frac{968\,\pi^2\,h^6\,D^{+4}(t^*)(K^{-}(t^*)-K^{+}(t^*))^2}{30625N^4\,K^{+}(t^*)K^{-}(t^*)\,C(t^*)}\Big\}$$

...(4.54)

$$M(t^*)=\Big\{\,(1+\frac{\varepsilon^2}{\alpha^2\nu})\frac{\sinh(2\alpha\sqrt{\nu}\,t^*)}{\alpha\sqrt{\nu}\;C(t^*)}+\frac{2\,\varepsilon}{\alpha^2\nu}\frac{\cosh(2\alpha\sqrt{\nu}\,t^*)}{C(t^*)}$$

$$+\Big(\frac{C(t^*)}{3Z(t^*)}-2\omega^2Z(t^*)-\frac{2\,\varepsilon^2}{\alpha^2\nu}\Big)\frac{\sinh(\alpha\sqrt{\nu}\,t^*)}{\alpha\sqrt{\nu}\;C(t^*)}+\Big(\frac{C(t^*)}{3Z(t^*)}-2\omega^2Z(t^*)-2\Big)\frac{\varepsilon\cosh(\alpha\sqrt{\nu}\,t^*)}{\alpha^2\nu\,C(t^*)}$$

$$-\frac{\varepsilon}{\alpha^2\nu}\Big(\frac{1}{3Z(t^*)}-\frac{2\omega^2\,Z(t^*)}{C(t^*)}\Big)\Big\}$$

...(4.55)

$$P(t^*) = \frac{-2\,\varepsilon}{\alpha\sqrt{\nu}}\frac{\sinh(2\alpha\sqrt{\nu}\,t^*)}{C(t^*)} - \left(1+\frac{\varepsilon^2}{\alpha^2\nu}\right)\frac{\cosh(2\alpha\sqrt{\nu}\,t^*)}{C(t^*)}$$

$$+\left[\frac{2(1+\omega^2)Z(t^*)}{C(t^*)} - \frac{1}{3Z(t^*)} + \frac{2}{C(t^*)}\right]\frac{\varepsilon\sinh(\alpha\sqrt{\nu}\,t^*)}{\alpha\sqrt{\nu}} +$$

$$\left[\frac{2(1+\omega^2)Z(t^*)}{C(t^*)} - \frac{1}{3Z(t^*)} + \frac{2\,\varepsilon^2}{\alpha^2\nu\,C(t^*)}\right]\cosh(\alpha\sqrt{\nu}\,t^*) - \frac{3\omega^2Z^2(t^*)}{C(t^*)} - \frac{\varepsilon^2}{\alpha^2\nu\,C(t^*)} - \frac{2}{3}$$

...(4.56)

$$U(t^*) = \left[1+\frac{\varepsilon^2}{\alpha^2\nu}\right]\frac{\cosh(2\alpha\sqrt{\nu}\,t^*)}{C(t^*)} + \frac{2\,\varepsilon\sinh(2\alpha\sqrt{\nu}\,t^*)}{\alpha\sqrt{\nu}\;C(t^*)}$$
$$-\left[\frac{2\,\varepsilon^2}{\alpha^2\nu\,C(t^*)} + \frac{4\omega^2\,Z(t^*)}{C(t^*)} + \frac{1}{3Z(t^*)}\right]\cosh(\alpha\sqrt{\nu}\,t^*)$$
$$-\left[\frac{2}{C(t^*)} + \frac{4\omega^2\,Z(t^*)}{C(t^*)} + \frac{1}{3Z(t^*)}\right]\frac{\varepsilon\sinh(\alpha\sqrt{\nu}\,t^*)}{\alpha\sqrt{\nu}}$$
$$+\frac{\varepsilon^2}{\alpha^2\nu\,C(t^*)} + \frac{\omega^2}{3} + \frac{(1+2\omega^2)}{3C(t^*)}[C(t^*)+3\omega^2Z^2(t^*)] - \frac{C(t^*)}{Z^2(t^*)} \qquad ...(4.57)$$

$$V(t^*) = \left\{5(\alpha^2\nu+3\varepsilon^2)\frac{\sinh(3\alpha\sqrt{\nu}\,t^*)}{\alpha\sqrt{\nu}} + 5\varepsilon\left(3+\frac{\varepsilon^2}{\alpha^2\nu}\right)\cosh(3\alpha\sqrt{\nu}\,t^*)\right.$$
$$+\left[-30\varepsilon^2 + 2\left(\frac{C(t^*)}{Z(t^*)} - 10\omega^2Z(t^*)\right)(\alpha^2\nu+\varepsilon^2)\right]\frac{\sinh(2\alpha\sqrt{\nu}\,t^*)}{\alpha\sqrt{\nu}}$$
$$\left.+\left[-15\varepsilon\left(1+\frac{\varepsilon^2}{\alpha^2\nu}\right) + 4\varepsilon\left(\frac{C(t^*)}{Z(t^*)} - 10\omega^2Z(t^*)\right)\right]\cosh(2\alpha\sqrt{\nu}\,t^*)\right.$$

$$\left[15\varepsilon^2 - 4\varepsilon^2\left(\frac{C(t^*)}{Z(t^*)} - 10\omega^2 Z(t^*)\right) + \left(\frac{C^2(t^*)}{Z^2(t^*)} - 4\omega^2 C(t^*) + (1+4\omega^2)(C(t^*)+5\omega^2 Z^2(t^*))\alpha^2\nu\right]\frac{\sinh(\alpha\sqrt{\nu}\, t^*)}{\alpha\sqrt{\nu}}\right.$$

$$\left[\frac{15\,\varepsilon^3}{\alpha^2\nu} - 4\varepsilon\left(\frac{C(t^*)}{Z(t^*)} - 10\omega^2 Z(t^*)\right) + \varepsilon\left(\frac{C^2(t^*)}{Z^2(t^*)} - 4\omega^2 C(t^*) + (1+4\omega^2)(C(t^*)+5\omega^2 Z^2(t^*))\right]\cosh(\alpha\sqrt{\nu}\, t^*)\right.$$

$$\left. - \frac{5\,\varepsilon^3}{\alpha^2\nu} - \varepsilon\left[\frac{C^2(t^*)}{Z^2(t^*)} - 4\omega^2 C(t^*) + (1+4\omega^2)(C(t^*)+5\omega^2 Z^2(t^*))\right]\right\} / C^2(t^*)$$

...(4.58)

$$W(t^*) = \left\{ \frac{-5}{2}\left(1 + \frac{3\,\varepsilon^2}{\alpha^2\nu}\right)\cosh(3\alpha\sqrt{\nu}\, t^*) - \frac{5}{2}\left(3 + \frac{\varepsilon^2}{\alpha^2\nu}\right)\frac{\varepsilon \sinh(3\alpha\sqrt{\nu}\, t^*)}{\alpha\sqrt{\nu}}\right.$$

$$+ \left[\frac{15\varepsilon^2}{\alpha^2\nu} + \left(1 + \frac{\varepsilon^2}{\alpha^2\nu}\right)\left(5(1+2\omega^2)Z(t^*) - \frac{C(t^*)}{Z(t^*)}\right)\right]\cosh(2\alpha\sqrt{\nu}\, t^*)$$

$$+ \left[\frac{15}{2}\left(1 + \frac{\varepsilon^2}{\alpha^2\nu}\right) + 2\left(5(1+2\omega^2)Z(t^*) - \frac{C(t^*)}{Z(t^*)}\right)\right]\frac{\varepsilon \sinh(2\alpha\sqrt{\nu}\, t^*)}{\alpha\sqrt{\nu}}$$

$$+ \left[\frac{-15\varepsilon^2}{2\alpha^2\nu} - \frac{2\varepsilon^2}{\alpha^2\nu}\left(5(1+2\omega^2)Z(t^*) - \frac{C(t^*)}{Z(t^*)}\right) + 2(1+\omega^2)C(t^*) - \frac{C^2(t^*)}{2Z^2(t^*)}\right.$$

$$\left. - \frac{(11+4\omega^2)}{2}[C(t^*)+5\omega^2 Z^2(t^*)]\right]\cosh(\alpha\sqrt{\nu}\, t^*) + \left[\frac{-15\,\varepsilon^2}{2\alpha^2\nu} - 2\left(5(1+2\omega^2)Z(t^*) - \frac{C(t^*)}{Z(t^*)}\right)\right.$$

$$\left. + 2(1+\omega^2)C(t^*) - \frac{C^2(t^*)}{2Z^2(t^*)} - \frac{(11+4\omega^2)}{2}[C(t^*)+5\omega^2 Z^2(t^*)]\right]\frac{\varepsilon \sinh(\alpha\sqrt{\nu}\, t^*)}{\alpha\sqrt{\nu}}$$

$$+ (1+4\omega^2)Z(t^*)[3C(t^*) + 5\omega^2 Z^2(t^*)] - \frac{C(t^*)[C(t^*) + 6\omega^2 Z^2(t^*)]}{2\,Z(t^*)}$$

$$\left. \frac{\varepsilon^2}{\alpha^2\nu}\left[5(1+2\omega^2)Z(t^*) - \frac{C(t^*)}{Z(t^*)}\right]\right\} / C^2(t^*) \qquad \text{...(4.59)}$$

$$Y(t^*) = \{ (1 + \frac{3\varepsilon^2}{\alpha^2\nu})\cosh(3\alpha\sqrt{\nu}\, t^*) + (3 + \frac{\varepsilon^2}{\alpha^2\nu})\frac{\varepsilon \sinh(3\alpha\sqrt{\nu}\, t^*)}{\alpha\sqrt{\nu}} - 6[\frac{\varepsilon^2}{\alpha^2\nu} +$$

$$(1 + \frac{\varepsilon^2}{\alpha^2\nu})\omega^2 Z(t^*)]\cosh(2\alpha\sqrt{\nu}\, t^*) - 3[(1 + \frac{\varepsilon^2}{\alpha^2\nu}) + 4\omega^2 Z(t^*)]\frac{\varepsilon \sinh(2\alpha\sqrt{\nu}\, t^*)}{\alpha\sqrt{\nu}}$$

$$+ 3\left[\frac{\varepsilon^2}{\alpha^2\nu} + \frac{4\varepsilon^2\omega^2 Z(t^*)}{\alpha^2\nu} + \frac{1}{5}\left((1+4\omega^2)[C(t^*) + 5\omega^2 Z^2(t^*)] - \frac{C^2(t^*)}{Z^2(t^*)}\right)\right]\cosh(\alpha\sqrt{\nu}\, t^*)$$

$$+ 3\left[\frac{\varepsilon^2}{\alpha^2\nu} + 4\omega^2 Z(t^*) + \frac{1}{5}\left((1+4\omega^2)[C(t^*) + 5\omega^2 Z^2(t^*)] - \frac{C^2(t^*)}{Z^2(t^*)}\right)\right]\frac{\varepsilon \sinh(\alpha\sqrt{\nu}\, t^*)}{\alpha\sqrt{\nu}}$$

$$+ \frac{3\omega^2}{5}\frac{C(t^*)}{Z(t^*)} - \frac{C^3(t^*)}{Z^3(t^*)} - \frac{2\omega^2(2\omega^2+3)Z(t^*)[3C(t^*) + 5\omega^2 Z^2(t^*)]}{5} - \frac{6\varepsilon^2\omega^2 Z(t^*)}{\alpha^2\nu}\Big\}\frac{5}{C^2(t^*)}$$

...(4.60)

It is not difficult to show when the breakage index is zero, Equations (4.38) to (4.60) reduce to Equations (4.20) to (4.29), and that in the Gaussian limit (i.e.as N goes to infinity) for non-zero values of the breakage index, Equations (4.38) through (4.60) reduce to Equations (30) and (31) of Fuller and Leal's paper [87].

Results and Discussion

Calculations

As shown in Figure 4.3, the non-affine deformation of a polymer network composed of polymer chains possessing non-Gaussian polymer segment free energies exhibits a maximum in the steady shear viscosity profile. The inclusion of additional terms in polymer segment free energy expansion increases magnitude of the viscosity

enhancement, and the inclusion of all three terms in the polymer segment free energy expansion produces a model that reaches a maximum in the shear viscosity of over 2, just as in the data of Figure 4.1. When only the first term of the expansion is used for the polymer segment free energy, and when the network chains are Gaussian, the network model does not exhibit shear-thickening. Therefore, all subsequent calculations use all three terms in the expansion for the polymer segment free energy given by equation (4.2).

The calculations in Figure 4.3 were made with the constant junction breakage potential, where the normalized concentration of network junctions is constant and equal to L/β_o. Since the number of junctions remain constant, and since the shear thickening occurs only for networks that have segments with non-Gaussian free energies, the shear-thickening phenomenon results from the finite extensibility of the network chains under shear. Hence, the increase in the resistance of the chain to further extension under shear as it reaches its limit of extensibility provides an additional energy dissipation mechanism. As shown in Figure 4.4 for a network composed of non-Gaussian chains with a constant junction breakage potential, the effect of the length of the network chain mimics that observed in data shown in Figure 4.1: the magnitude of the viscosity enhancement decreases as chain length increases, and vanishes in the Gaussian limit ($N=\infty$). This dependence on the number of statistical sub-units in the network chain is expected because, at a given rate of elongation, shorter chains reach their finite limit of extensibility before longer chains.

Nevertheless, our data show that the number density of network junctions in the associative polymer solutions depends on shear rate, which is a feature that can be modelled through the conformation dependent junction breakage potential. As we now discuss, including this feature in the model influences the absolute magnitude of the

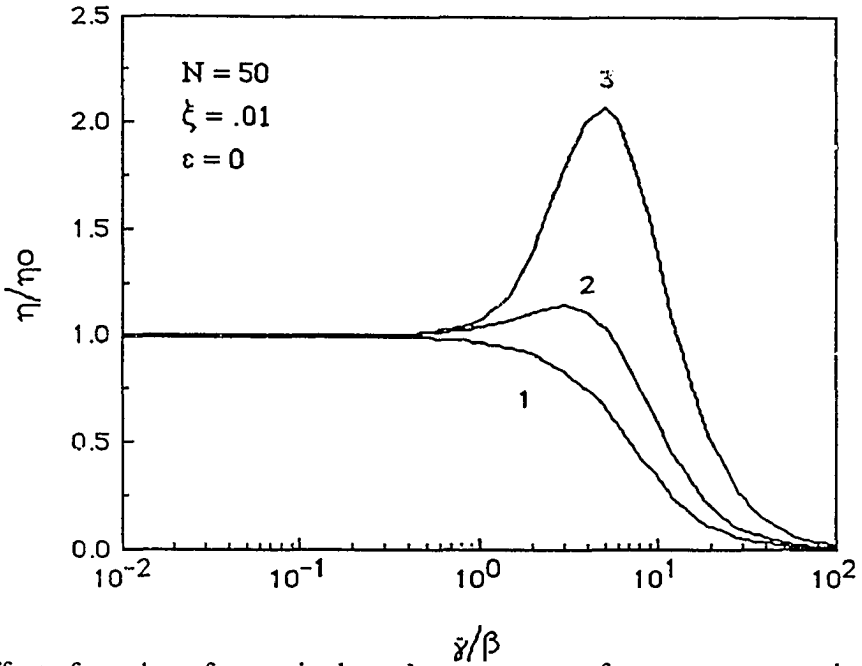

Figure 4.3: Effect of number of terms in the polymer segment free energy expansion given by Equation (4.2) on the normalized steady shear viscosity profile. The number of terms included in the free energy expansion are indicated on the figure.

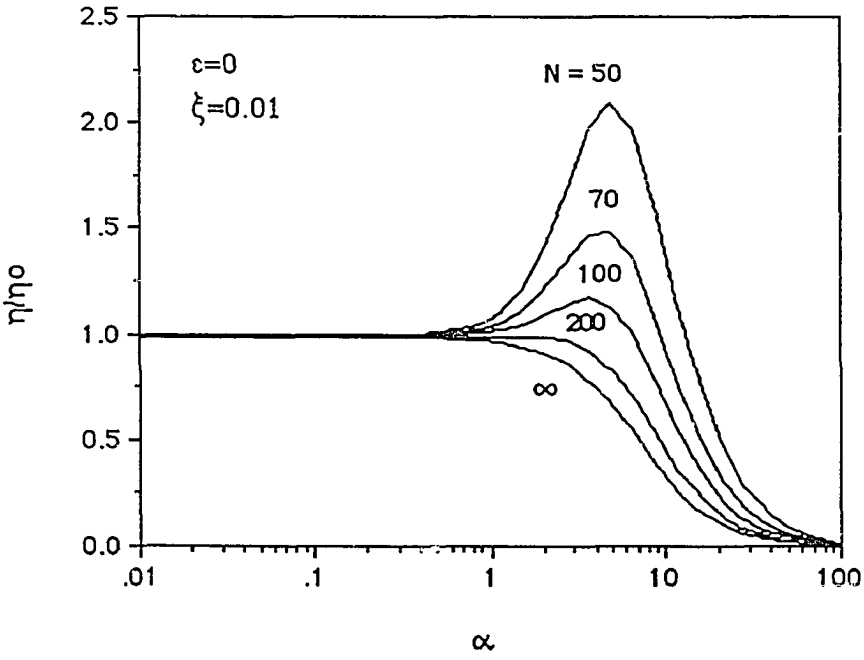

Figure 4.4: Normalized steady shear viscosity of non-affine, non-Gaussian networks with a constant breakage potential for different values of the number of statistical subunits in the polymer chain N.

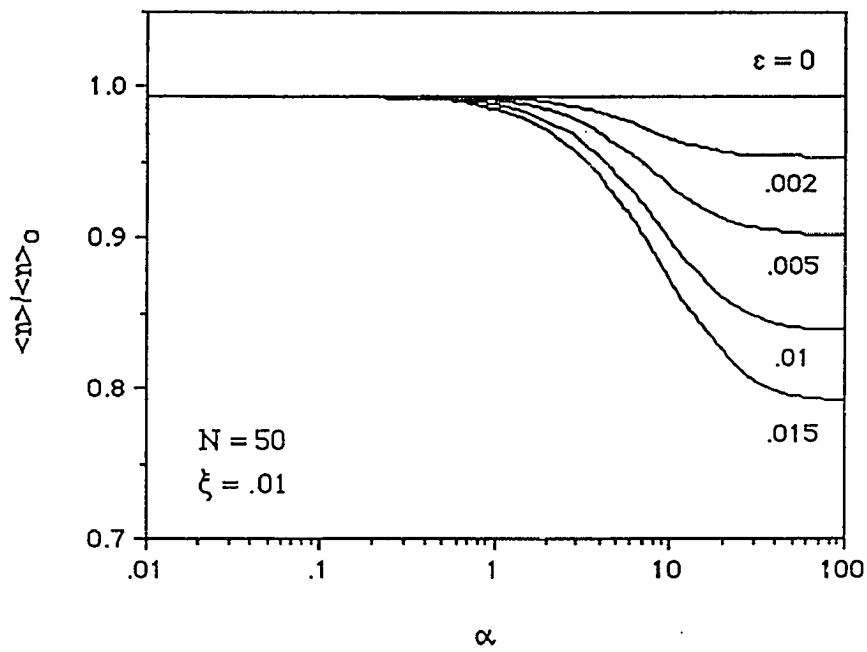

Figure 4.5 Effect of the breakage index on the network junction concentration in steady shear of a non-affine, non-Gaussian network with a conformation dependent junction breakage potential.

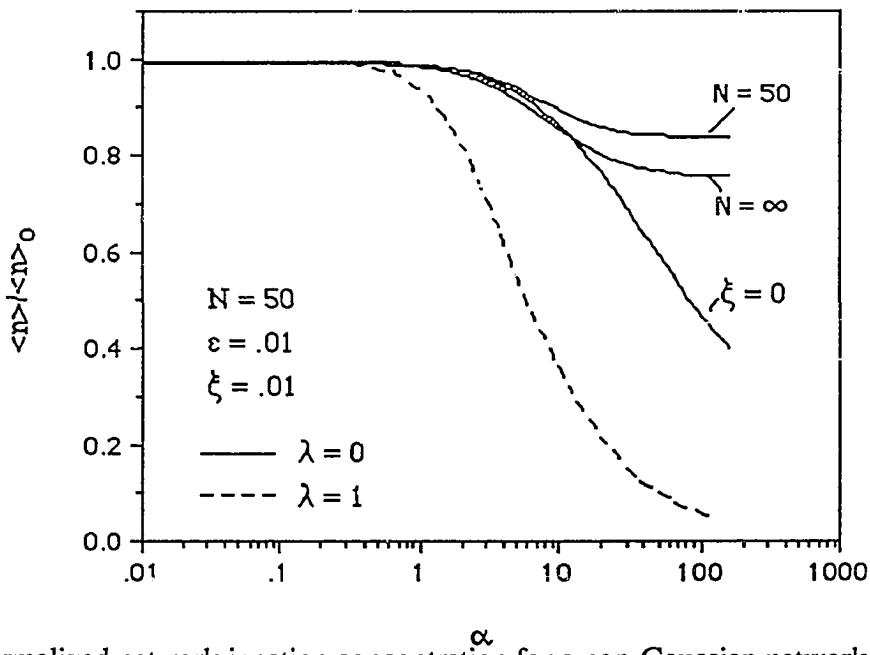

Figure 4.6 Normalized network junction concentration for a non-Gaussian network with a conformation dependent junction breakage potential.

increase in viscosity in the shear-thickening region, but does not change the qualitative interpretation of the shear-thickening viscosity profile given in the previous paragraph.

For a Gaussian network at rest and at equilibrium, we can integrate Equation (4.38) analytically, with the result that:

$$\left.\frac{\langle n\rangle \beta_o}{L}\right|_{\alpha=0,t=\infty} = \frac{2}{\varepsilon}\left[1 - \frac{\sqrt{\pi}\, e^{1/\varepsilon}}{\sqrt{\varepsilon}}\,\mathrm{erfc}(1/\sqrt{\varepsilon})\right] \qquad (4.61)$$

where erfc(x) is the complimentary error function. For small values of the breakage index ε, the complimentary error function may be expanded into its Taylor series, which yields:

$$\left.\frac{\langle n\rangle \beta_o}{L}\right|_{\alpha=0,t=\infty} \cong 1 - \frac{3\varepsilon}{2} + \frac{15\,\varepsilon^2}{4} + \ldots \qquad (4.62)$$

For values of the breakage index of less than 0.1, the approximation given by Equation (4.62) is accurate to within 1%. Thus, we used the following definitions for the proper normalization of the rheological properties predicted by our model:

$$\langle n\rangle_o = \langle n\rangle \Big|_{\substack{\alpha = 0 \\ t = \infty \\ N = \infty}}$$

$$\eta_o = \frac{kT\,(1-\xi)(1+\lambda)\,\langle n\rangle_o}{\beta_o} \quad ; \quad \Psi_{1,0} = \frac{2kT\,(1-\xi)(1+\lambda)\,\langle n\rangle_o}{\beta_o^2} \qquad \ldots(4.63)$$

$$\Psi_{2,0} = \frac{kT\,(1-\xi)(1+\lambda)\,\langle n\rangle_o}{\beta_o^2}; \quad \bar{\eta}_o = \frac{2kT\,(1-\xi)(1+\lambda)\,\langle n\rangle_o}{\beta_o}$$

When the breakage index is zero, these equations reduce to the definitions used by Fuller and Leal, and by Vrahopoulou and McHugh. It is obvious from these equations that the conformation dependent probability of junction breakage causes the number of network junctions to decrease as the breakage index increases from zero, even when the network is at rest.

Equation (4.63) is nothing more than the theory of rubber elasticity. For a small amplitude oscillatory shear strain, and if the slip parameter is small , then:

$$\frac{\eta_o\,\beta_o}{RT} = \frac{\langle n\rangle_o}{N_a} = \frac{G_\infty}{RT} = \nu_e \tag{4.64}$$

where R is the gas constant, N_a is Avogadro's number, G_∞ is the pseudo-equilibrium modulus, and ν_e is the molar density of association. Thus, it is not surprising that the rheological data of the networking model associative polymers given in Chapter III scaled with the molar density of association. Because $\eta_o \sim (C/\sqrt{M})^{3.4}$, and $1/\beta_o \sim (C/\sqrt{M})^{0.9}$, this implies that the rate coefficient for the formation of association junctions for our model associative polymer solutions scales a $L \sim (C/\sqrt{M})^{1.6}$.

Figures 4.5 and 4.6 present the dependence of the network junction concentration on the following: shear rate, slip parameter, breakage index, number of statistical segments between junctions, and flow field vorticity. Figure 4.5 shows that, in simple shear, the concentration of network junctions in a non-affine, non-Gaussian network with a non-zero

breakage index remains near its rest state value until the rate of strain approaches the relaxation time constant of the solution. At larger shear rates, the junction concentration decreases rapidly, and the slope on the figure depends on the breakage index. At high shear rates, the junction concentration approaches a limiting value that depends on the value of the breakage index. Comparison of the curves for N=50 and N=∞ for simple shear flow in Figure 4.6 reveals that the non-Gaussian chain statistics that govern the behavior of finitely extensible chains slightly suppress the break up of network junctions. The influence of the type of flow field on the junction concentration of a non-affine, non-Gaussian network is also depicted in Figure 4.6 : the solid lines are for a simple shear flow field, and the dashed line is for an extensional flow field. The extensional flow field is more efficient in breaking network junctions that the simple shear flow field, and almost an order of magnitude difference between the junction concentrations results at large shear rates. The slip parameter measures the degree that the network deviates from affine deformation in simple shear flow. As the slip parameter increases, the flow field becomes less efficient in destroying network junctions, which is obvious because the function Q(t*) approaches unity in the limit as the slip parameter approaches unity. In an extensional flow field, Equation (4.11) shows that the effect of the slip parameter ξ is simply to scale the velocity gradient by a factor of $(1-\xi)$. Thus, the degree to which the network deviates from affine deformation, as modelled by the slip parameter, and the relative strength of the network junctions, as modelled by the breakage index, will strongly influence the rheological properties of the network.

Figures 4.7 through 4.12 present the effect of the slip coefficient on the normalized shear viscosities of networks composed of both Gaussian and non-Gaussian chains. Consistent with the decrease in junction concentration shown in Figure 4.5, Figure 4.7 shows that the breakage index strongly influences the magnitude of the viscosity maximum

in the shear-thickening viscosity profiles of a non-affine, non-Gaussian network. The effect is intuitive: for strong network junctions, the viscosity maximum is quite large because the network chains can extend to their full length before the network junctions rupture; for weaker junctions, the junctions rupture before the polymer chains between junctions fully extend, and the viscosity maximum decreases. Thus, the network junctions formed by our model associative polymers are strong enough that the chains in the network stretch and uncoil during shear flow before shear forces tear the association network apart. Figure 4.8 shows that the degree of shear-thickening decreases with increasing slip coefficient for a non-Gaussian network. For both Gaussian and non-Gaussian networks, the shear rate at which shear-thinning begins decreases as the slip parameter increases. The effect of the slip parameter on the non-Gaussian network is analogous to the behavior seen in the data of Figure 4.2 when the associative polymer concentration is increased. When the slip parameter is zero, and the deformation is affine, the Gaussian network with a constant junction breakage potential is independent of shear rate. (Figure 4.9) However, when a conformation dependent breakage potential is used, even an affine Gaussian network exhibits shear-thinning. (Figure 4.10) The shear-thinning starts at smaller shear rates than for the constant breakage potential, and the slope of the shear-thinning region increases as the slip parameter increases, and is less than that for the constant breakage potential. Additionally, the level of the viscosity for the model with the conformation dependent breakage potential is smaller than that of the model with the constant breakage potential. In contrast, when a non-Gaussian network with a constant breakage potential deforms affinely, the steady shear viscosity increases with increasing dimensionless shear rate, and the viscosity profiles in Figure 4.11 diverge as the square of the shear rate. Nevertheless, the magnitude of shear-thickening behavior again decreases to reach the Gaussian limit at long chain lengths. When the junctions are allowed to rupture under

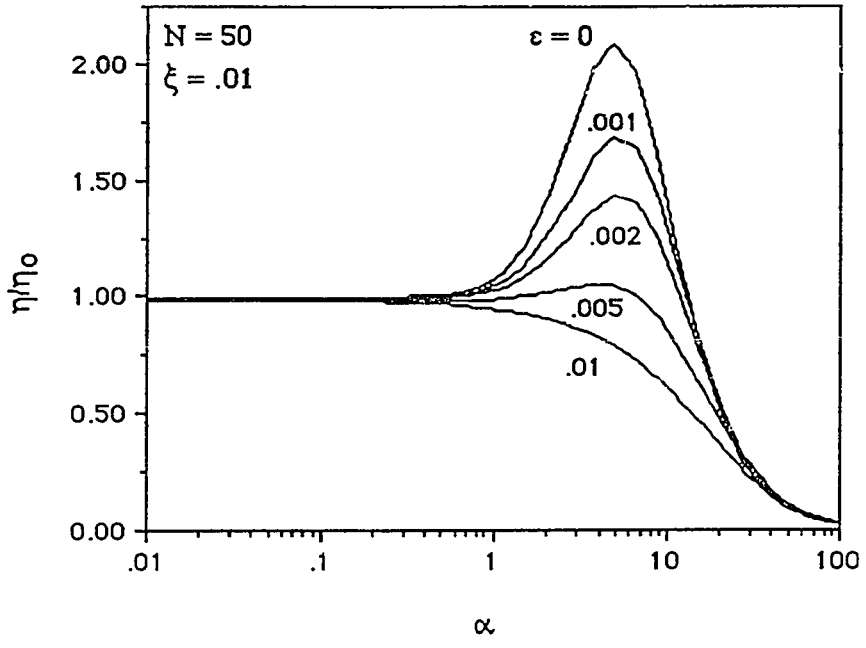

Figure 4.7: Influence of the breakage index on the normalized steady shear profiles of a non-affine, non-Gaussian network with a conformation dependent breakage potential.

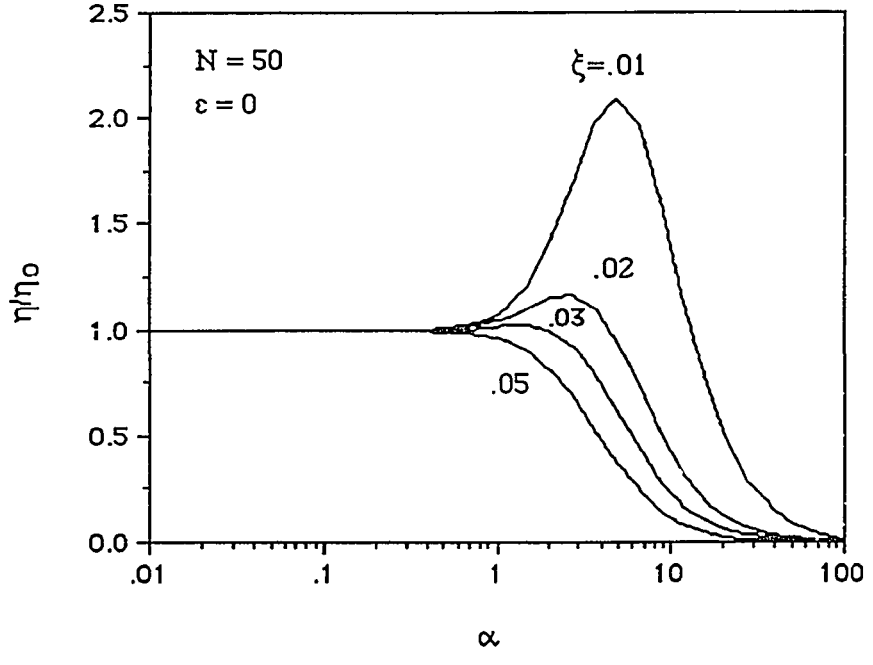

Figure 4.8: Influence of the slip coefficient on the normalized steady shear profiles of a non-Gaussian network with a constant junction breakage potential.

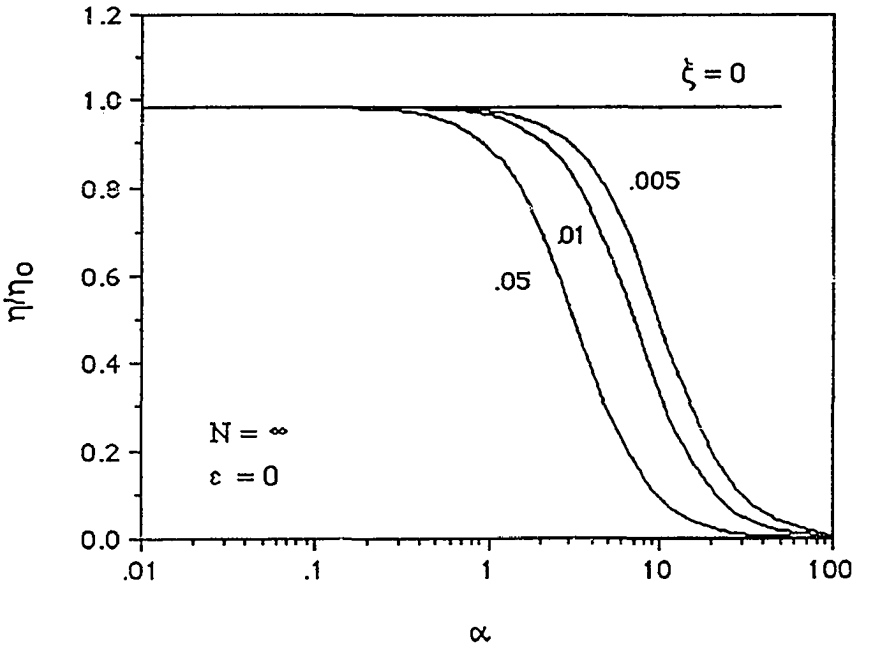

Figure 4.9: Influence of the slip parameter on the normalized shear viscosity of affine and non-affine Gaussian networks with a constant breakage potential.

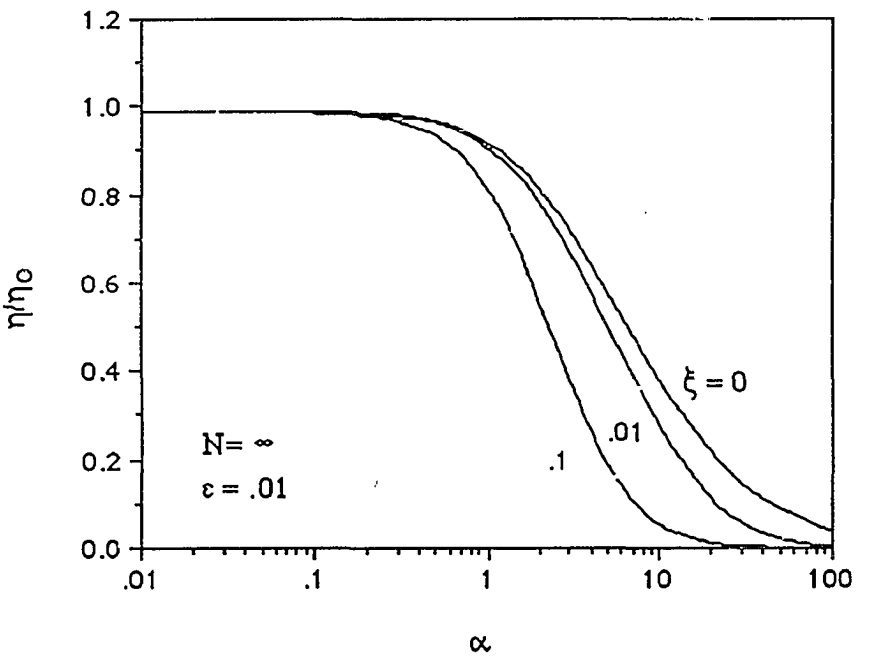

Figure 4.10: Influence of the slip parameter on the normalized shear viscosity of affine and non-affine Gaussian networks with a conformation dependent breakage potential.

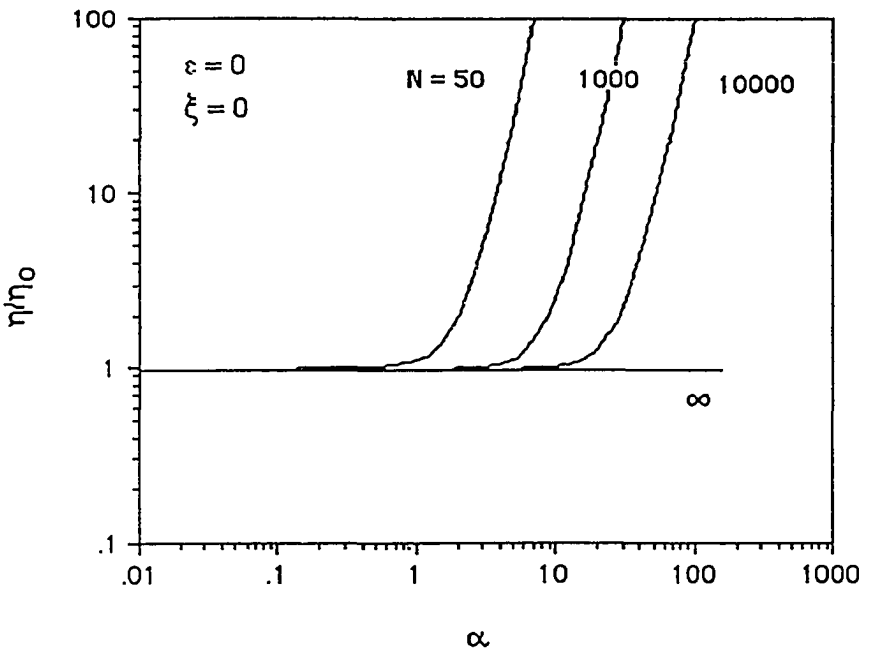

Figure 4.11: Normalized steady shear viscosity profiles on affine non-Gaussian networks with a constant breakage potential for various values of the number of statistical subunits between network junctions N.

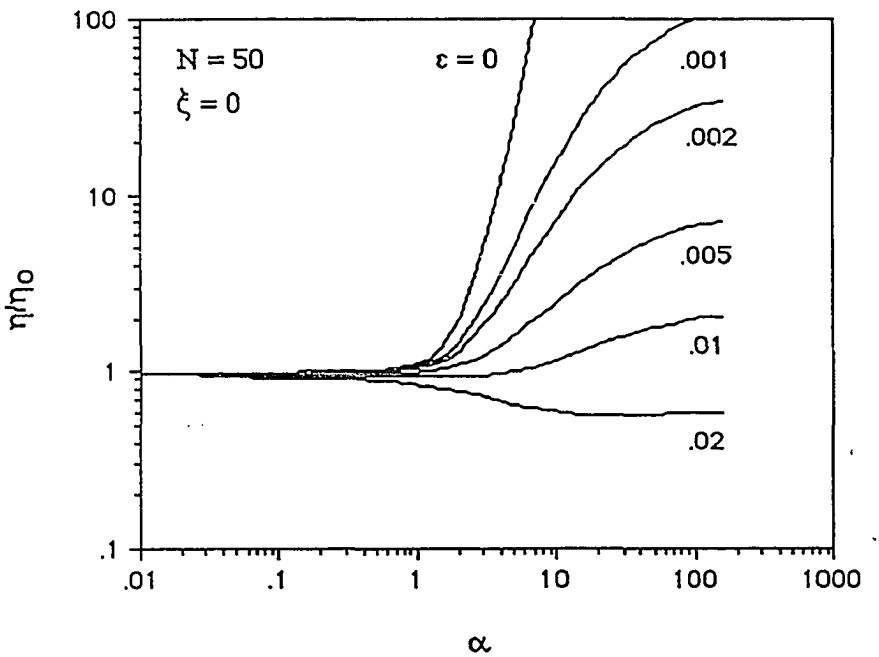

Figure 4.12: Influence of the breakage parameter on the normalized steady shear viscosity profiles of affine non-Gaussian networks.

shear, as modelled with the conformation dependent breakage potential, the divergent behavior seen with the affine deformation in Figure 4.11 decreases as the breakage index increases, and the curves approach a high shear limiting viscosity. (Figure 4.12) Indeed, when the breakage index is greater than 0.02, shear-thinning is seen in the viscosity profile. Thus, the network model produces a surprisingly large variety of rheological properties.

Figures 4.13 through 4.20 present the influence of chain length, breakage index, and slip coefficient on the steady first and second normal stress coefficients of networks containing either Gaussian or non-Gaussian segments. In general, the effect of these parameters parallel their effects on the steady shear viscosity. As indicated in Chapter III, some of the highly elastic model associative polymer solutions were expelled from the testing chamber at moderate shear rates during measurement, which is consistent with the large increase in the first normal stress coefficient shown in Figure 4.13. The steady first normal stress coefficient for a Gaussian network does not exhibit shear-thickening, and shows shear-thinning only in non-affine deformation (Figure 4.16). As shown in Figure 4.17, the network model with the constant breakage potential predicts either a positive or a negative second normal stress coefficient for networks containing non-Gaussian segments, depending on the length of the chain, the value of the slip coefficient, and the dimensionless shear rate. However, when the conformation dependent breakage potential is used in the model, the second normal stress difference changes sign from positive to negative as the breakage index increases past 0.002 (Figure 4.17). This is in contrast to networks that are composed of Gaussian chains, where the negative second normal stress coefficient is always negative or zero because $-\psi_2/\psi_1 = \xi$ for both breakage potentials (Figure 4.20). Other molecular models, such as Bird's rigid-rod model [90], predicts positive second normal stress coefficients for short chains, and negative second normal

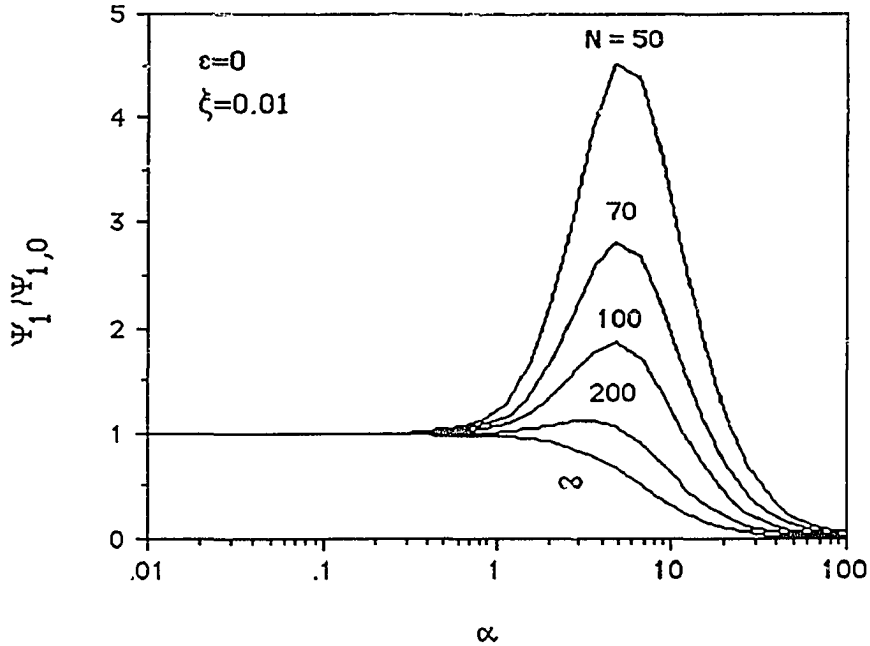

Figure 4.13: Normalized steady first normal stress coefficient of a non-affine, non-Gaussian network with a constant breakage potential for different values of the number of statistical subunits in the polymer chain N.

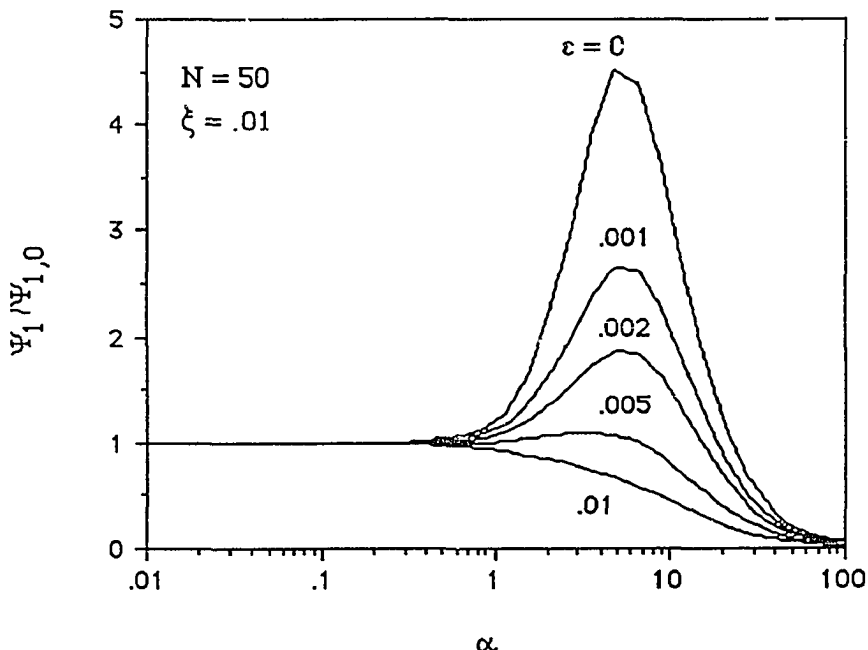

Figure 4.14: Influence of the breakage index on the normalized first normal stress coefficient of a non-affine, non-Gaussian network with a conformation dependent breakage potential.

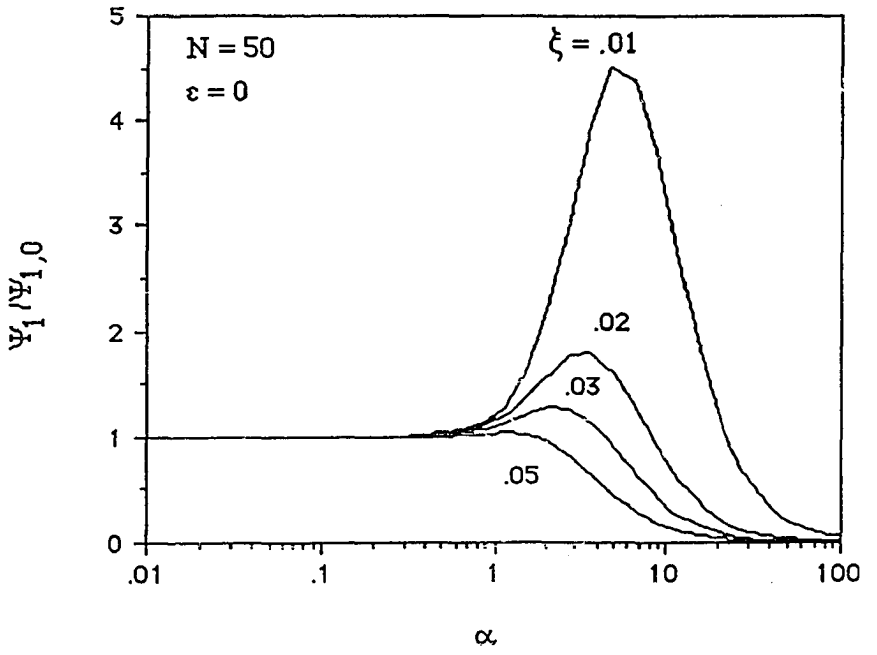

Figure 4.15: Influence of the slip parameter on the normalized first normal stress coefficient of non-Gaussian networks with a constant breakage potential.

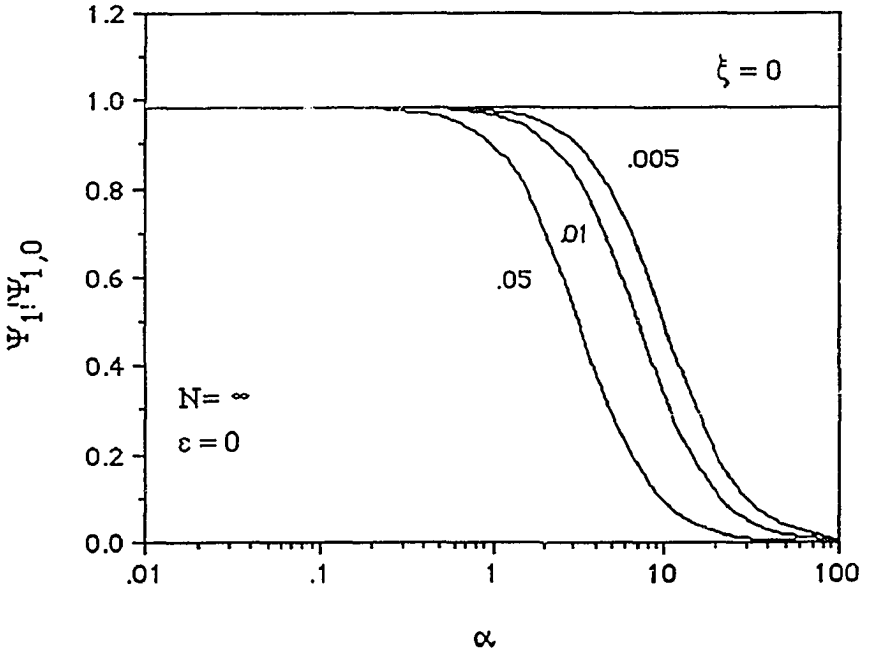

Figure 4.16: Influence of the slip parameter on the normalized first normal stress coefficient of Gaussian networks with a constant breakage potential.

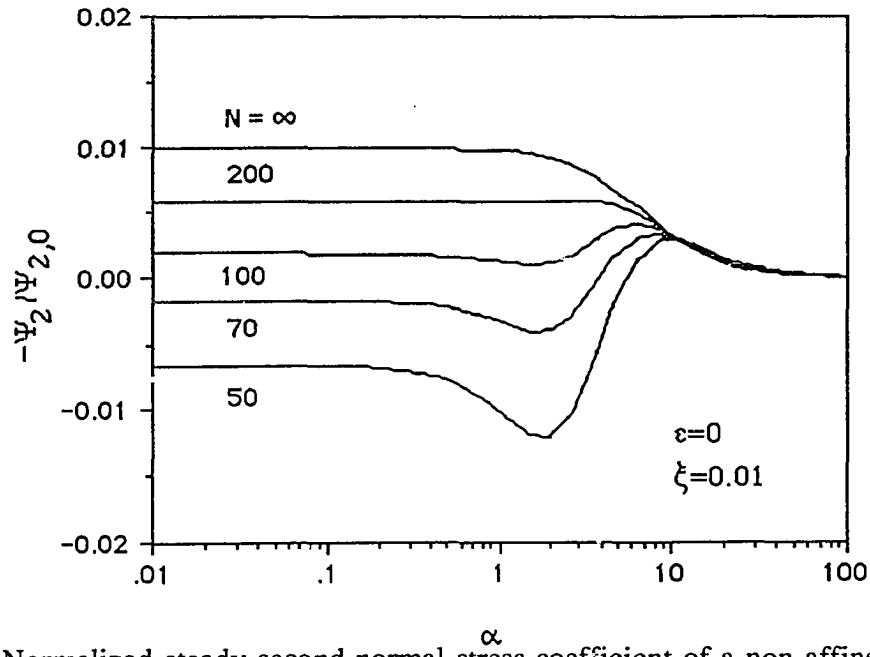

Figure 4.17: Normalized steady second normal stress coefficient of a non-affine, non-Gaussian networks with a constant breakage potential for different values of the number of statistical subunits in the polymer chain N.

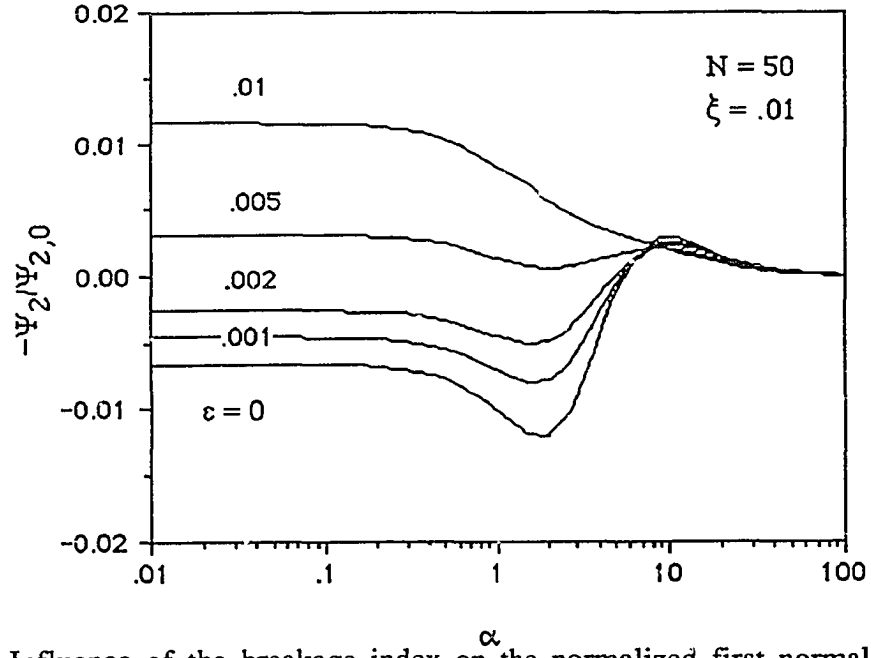

Figure 4.18: Influence of the breakage index on the normalized first normal stress coefficient of a non-affine, non-Gaussian network with a conformation dependent breakage potential.

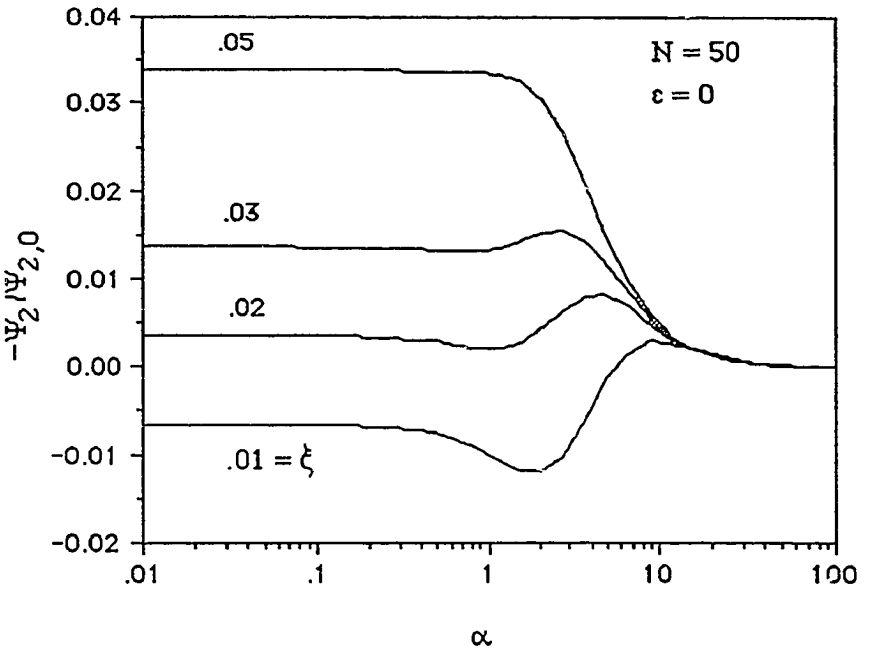

Figure 4.19 Influence of the slip parameter on the normalized first normal stress coefficient of non-Gaussian networks with a constant breakage potential.

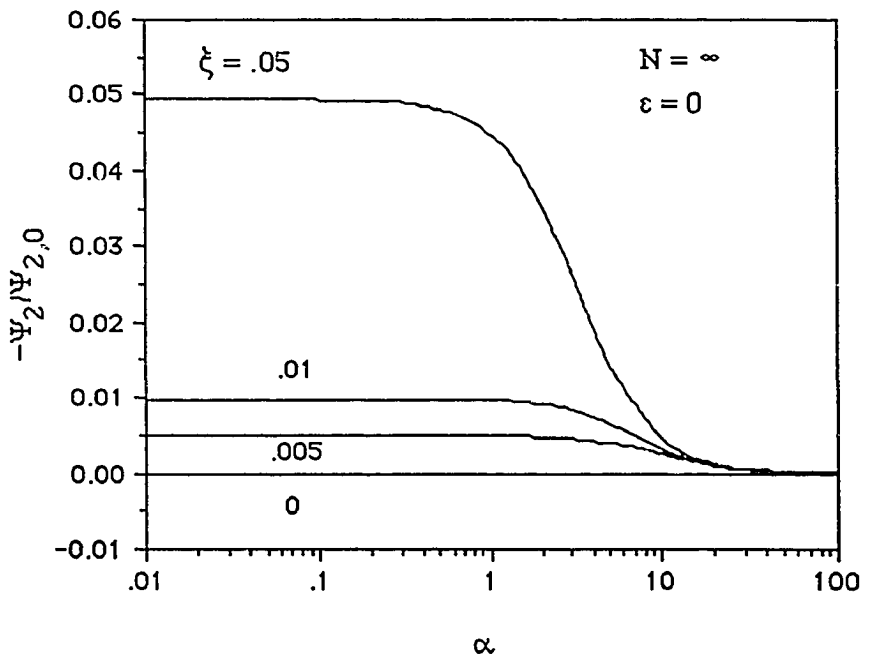

Figure 4.20. Influence of the slip parameter on the normalized first normal stress coefficient of Gaussian networks with a constant breakage potential.

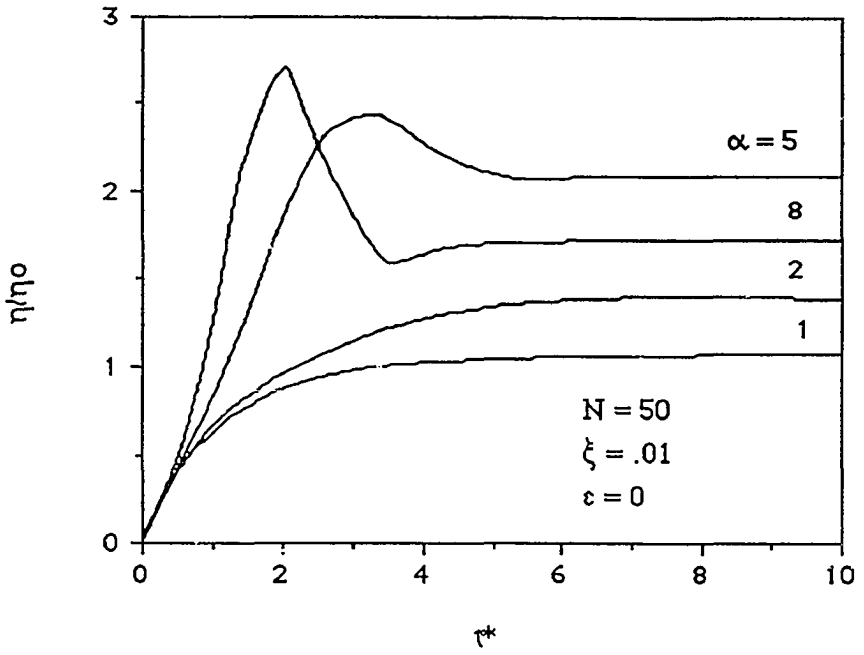

Figure 4.21: Transient normalized shear viscosity of a non-affine network with a constant junction breakage potential composed of chains with non-Gaussian free energy at various dimensionless shear rates.

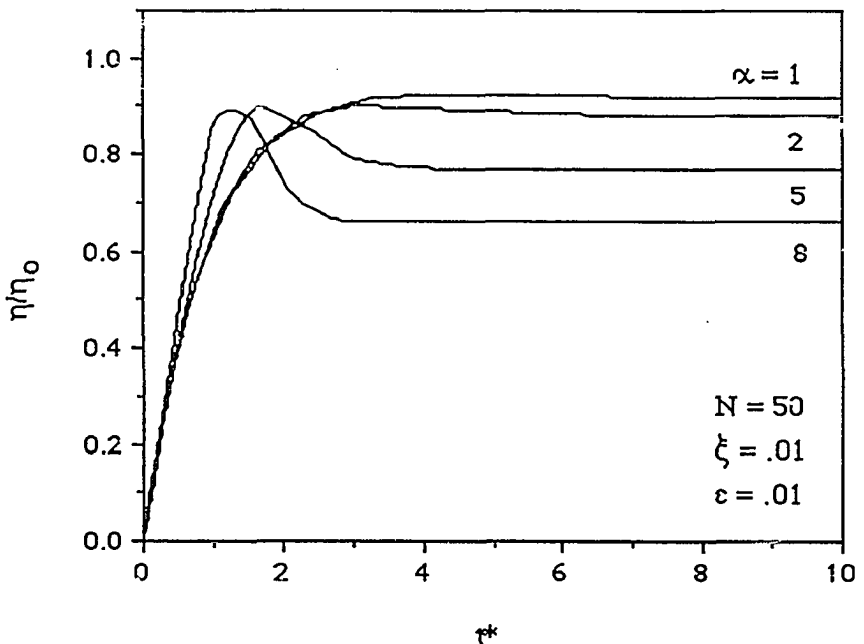

Figure 4.22: Transient normalized shear viscosity of a non-affine network with a conformation dependent junction breakage potential composed of chains with non-Gaussian free energy at various dimensionless shear rates.

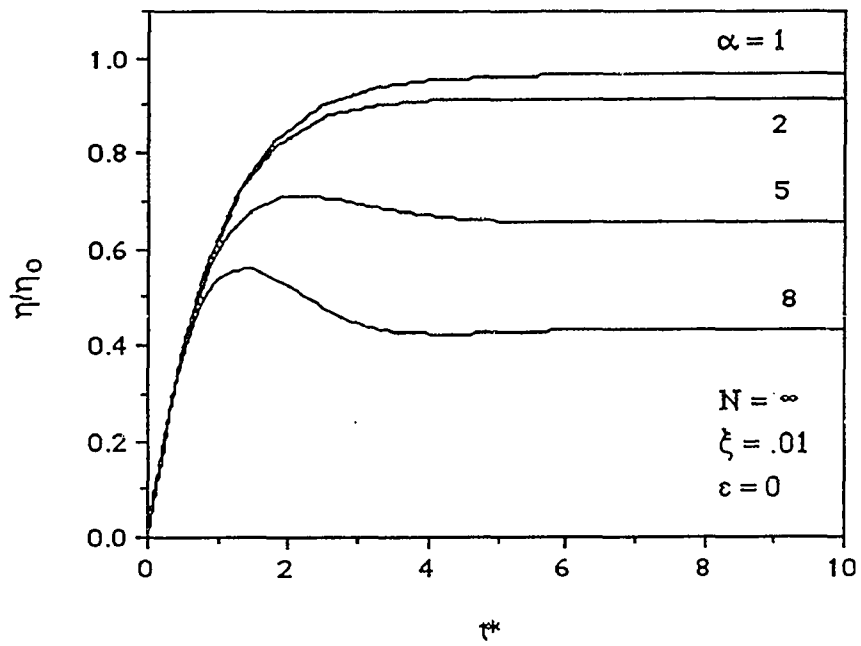

Figure 4.23: Transient normalized shear viscosity of a non-affine network with a constant junction breakage potential composed of chains with Gaussian free energy at various dimensionless shear rates.

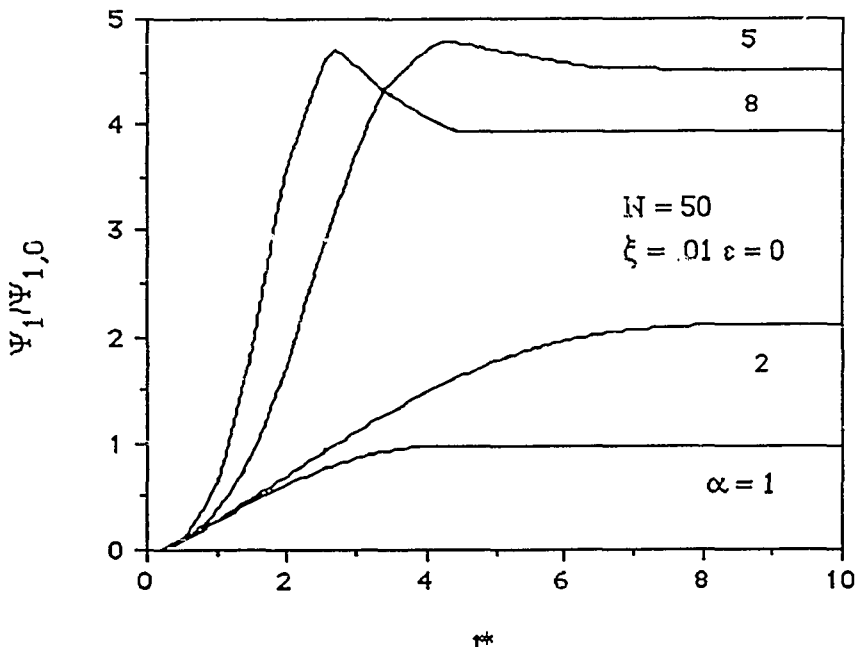

Figure 4.24: Transient normalized first normal stress coefficient of a non-affine network with a constant junction breakage potential composed of chains with non-Gaussian free energy at various dimensionless shear rates.

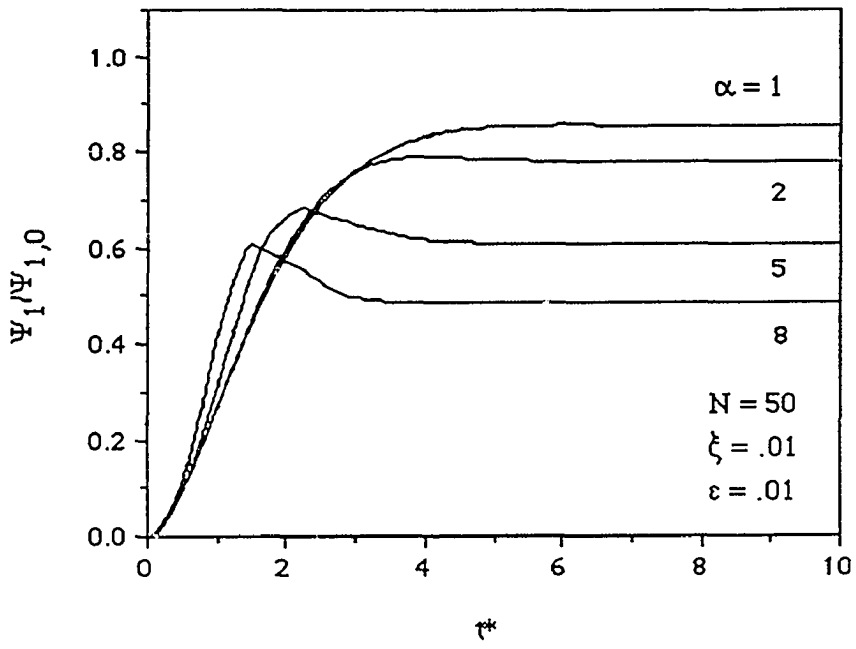

Figure 4.25: Transient normalized first normal stress coefficient of a non-affine network with a conformation dependent junction breakage potential composed of chains with non-Gaussian free energy at various dimensionless shear rates.

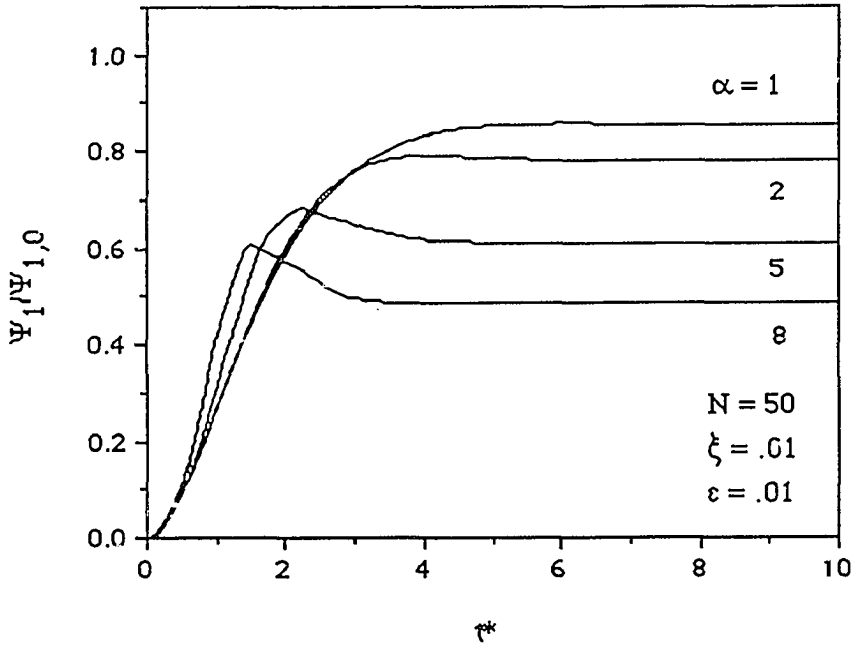

Figure 4.26: Transient normalized first normal stress coefficient of a non-affine network with a constant junction breakage potential composed of chains with Gaussian free energy at various dimensionless shear rates.

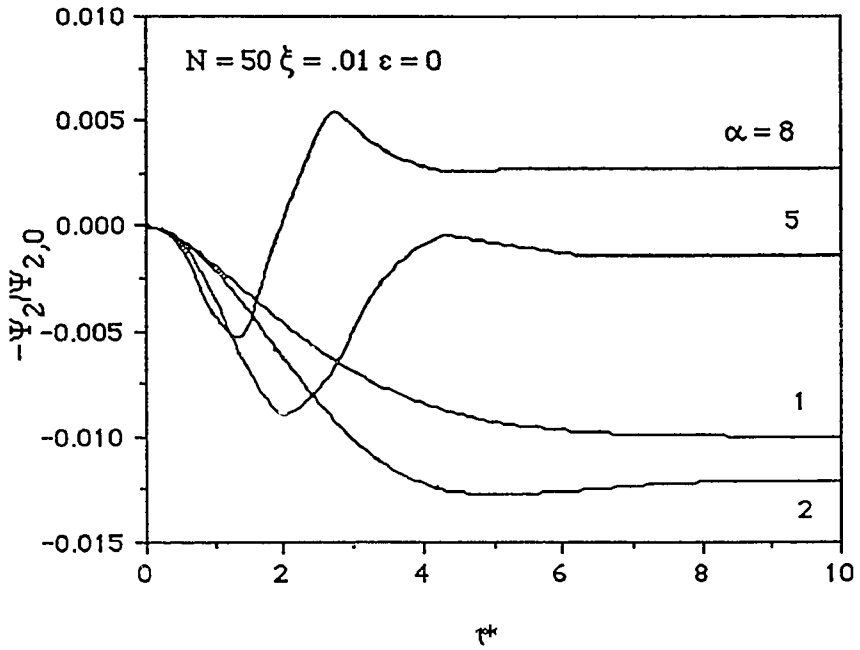

Figure 4.27: Transient normalized second normal stress coefficient of a non-affine network with a constant junction breakage potential composed of chains with non-Gaussian free energy at various dimensionless shear rates.

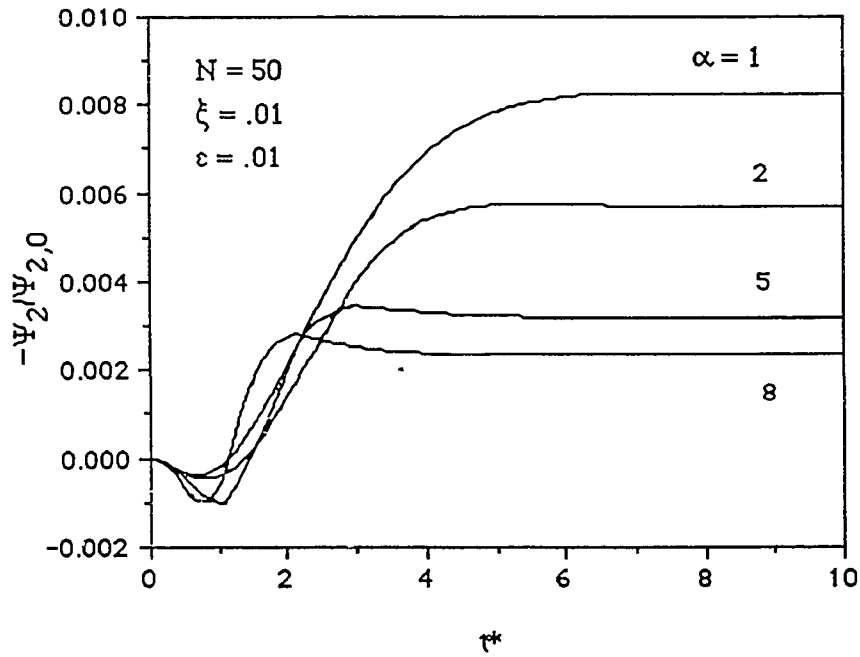

Figure 4.28: Transient normalized second normal stress coefficient of a non-affine network with a conformation dependent junction breakage potential composed of chains with Gaussian free energy at various dimensionless shear rates.

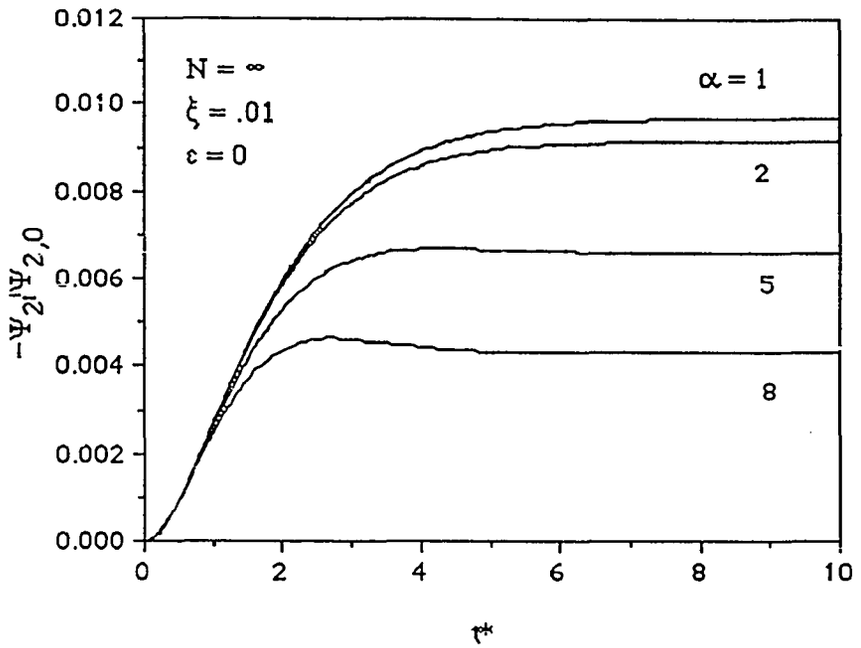

Figure 4.29: Transient normalized second normal stress coefficient of a non-affine network with a constant junction breakage potential composed of chains with Gaussian free energy at various dimensionless shear rates.

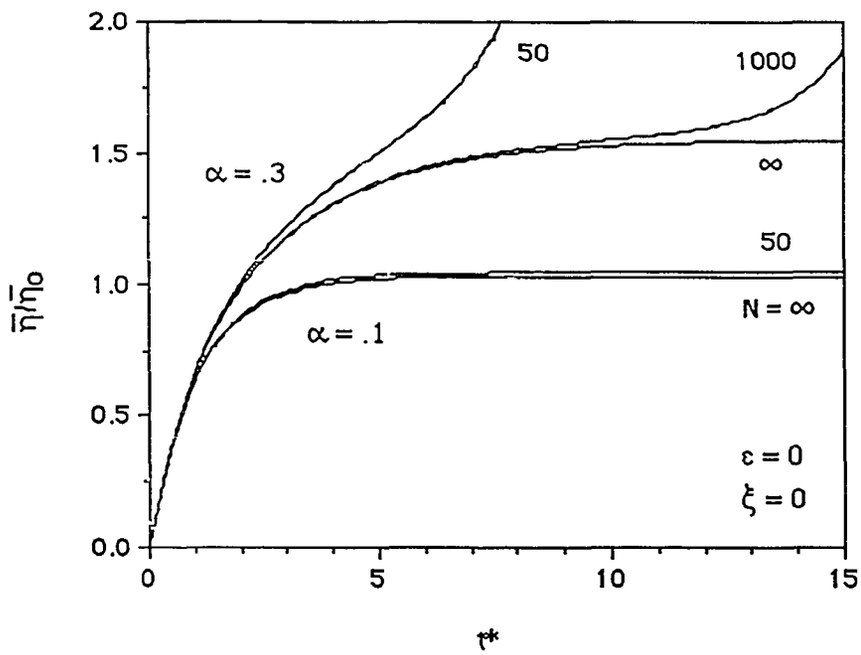

Figure 4.30: Transient normalized extensional viscosity of networks with constant junction breakage potentials composed of chains with Gaussian and non-Gaussian free energies at various dimensionless elongation rates.

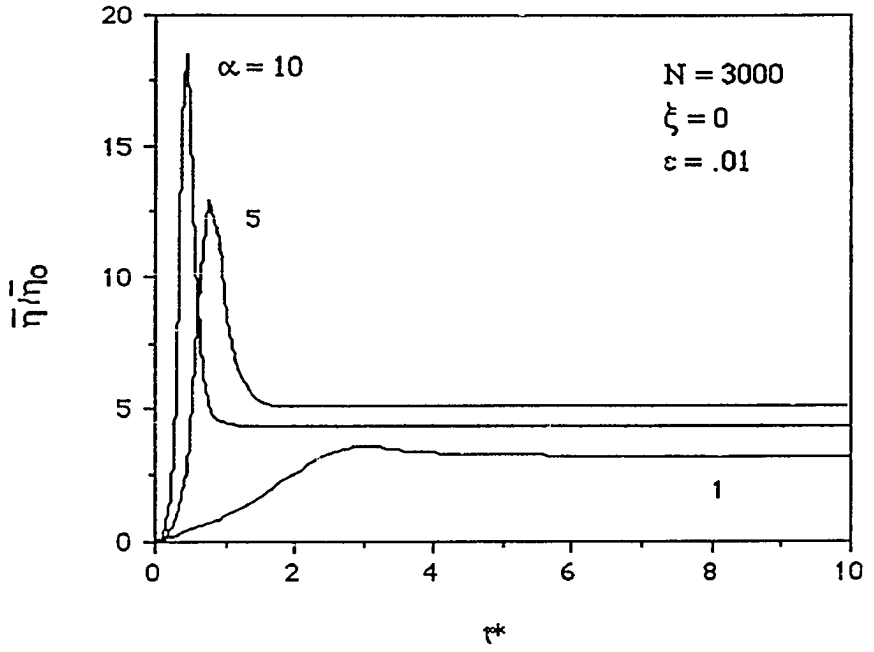

Figure 4.31: Transient normalized extensional viscosity of a network with a conformation dependent junction breakage potential composed of chains with Gaussian and non-Gaussian free energies at various dimensionless elongational rates.

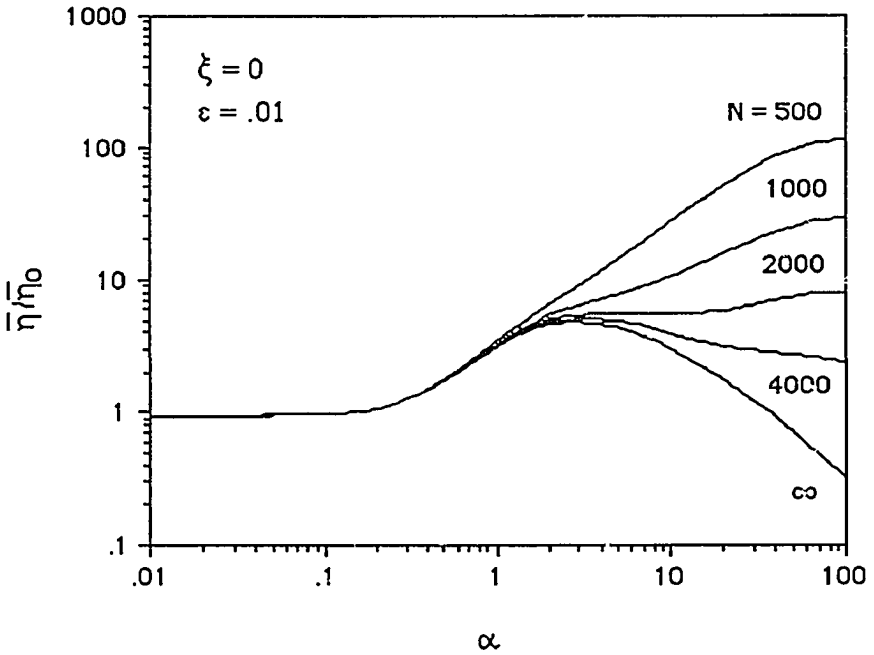

Figure 4.32: Steady normalized extensional viscosity of networks with constant junction breakage potentials composed of chains Gaussian and non-Gaussian for various values of the number of statistical subunits in the polymer chain N.

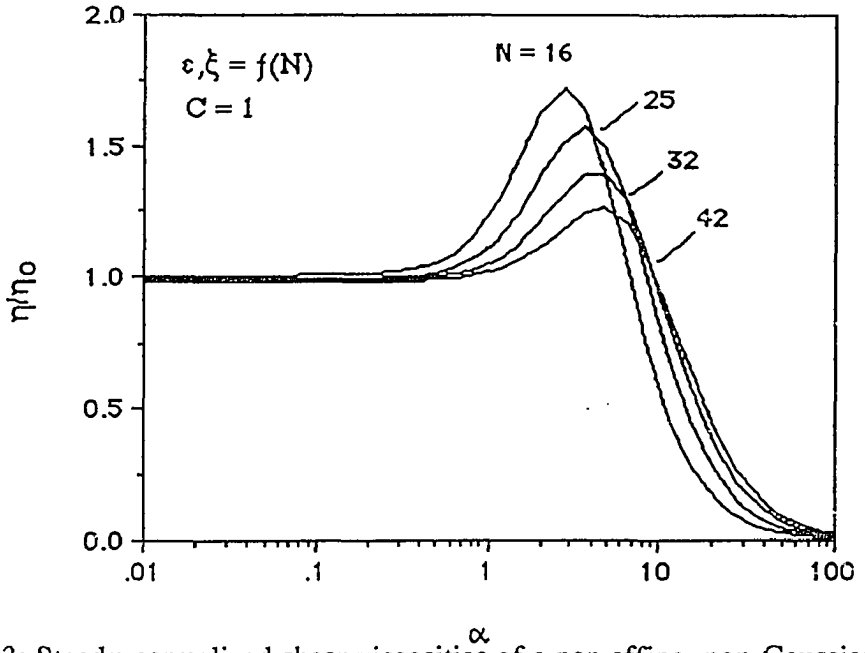

Figure 4.33: Steady normalized shear viscosities of a non-affine, non-Gaussian network with conformation dependent junction breakage potential for various values of the number of statistical subunits in the polymer chain N. The breakage index and the slip parameter are given by Equations (4.67) and (4.70), respectively.

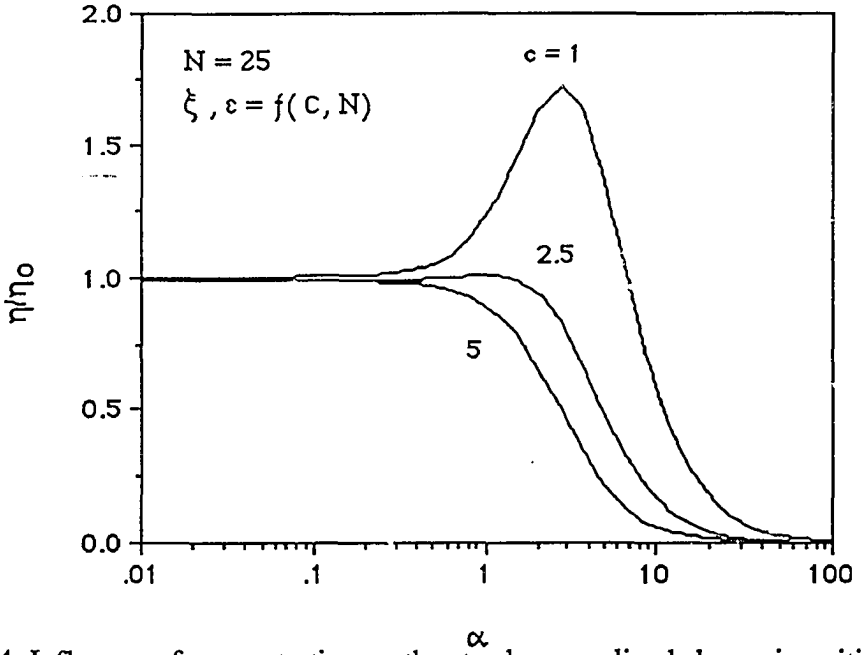

Figure 4.34: Influence of concentration on the steady normalized shear viscosities of non-affine, non-Gaussian networks with conformation dependent junction breakage potentials. The breakage index and the slip parameter are given by Equations (4.67) and (4.70), respectively.

stress coefficients for long chains too. Although, it is generally accepted that the second normal stress coefficient should be negative, it is still a matter of debate, and experimental evidence exists to support both positions. Ultimately, experimentation must resolve whether or not the second normal stress coefficients of our model associative polymer solutions can become positive under the appropriate conditions.

Figures 4.21 through 4.29 present the transient start-up response of the viscometric functions of networks containing either Gaussian or non-Gaussian segments in non-affine simple shear. At large values of the dimensionless shear rate, all three viscometric functions exhibit stress overshoot with oscillations that dampen to steady state at dimensionless times $t^* = t\beta_0$ of 10. The overshoot results when the time scale of deformation is short as compared to the time scale of junction rupture, and the network responds by deforming rather than by rupturing. At longer times after the imposition of the shear field, the network relaxes, some junctions rupture, and the oscillations in the viscometric functions dampen. This behavior is more severe for the networks with non-Gaussian segments as compared to networks containing Gaussian segments. The breakage index dramatically suppresses the stress overshoot in the model, and the functions approach steady state much more rapidly than for those of the model with the constant breakage potential. This is perhaps seen most dramatically in the second normal stress coefficient in Figure 4.28. The measurement of the steady shear viscosity profiles reported in this chapter, and in previous chapters, were made at values of the dimensionless time exceeding 10; hence they are true steady state measurements.

Figures 4.30 through 4.32 present the extensional viscosities of non-Gaussian networks for both the constant breakage potential and the conformation dependent breakage potential. Figure 4.30 shows the transient normalized extensional viscosity for networks

with Gaussian chains, and for networks with non-Gaussian segments with 50 and 1000 statistical subunits, with a constant breakage potential. For the constant breakage potential, the statistical averages presented in Equations (4.21) through (4.29) have singularities at $\alpha=1/\sqrt{\nu}$, $1/2\sqrt{\nu}$, and $1/3\sqrt{\nu}$ because the hyperbolic functions in the non-Gaussian terms diverge when the dimensionless shear rate is greater than $1/3\sqrt{\nu}$ and the hyperbolic functions in the Gaussian terms diverge when the dimensionless shear rate exceeds $1/\sqrt{\nu}$. Thus, in Figure 4.30, the extensional viscosity reaches steady state for $\alpha = 0.1$, since this value of the dimensionless shear rate is less than that required to make the hyperbolic functions diverge. However, the flow is so weak that the effect of the finite extensibility of the chain is barely detectable, and the curves for the Gaussian network ($N=\infty$) and the non-Gaussian network ($N=50$) superimpose. For $\alpha = 0.3$, the hyperbolic functions diverge, and the non-Gaussian network model cannot achieve steady state. As shown by Figure 4.31, these singularities are removed by allowing the chain breakage probability to depend on polymer conformation. The transient extensional viscosity of the non-Gaussian network model shows a large, abrupt overshoot that subsides quickly to steady state, for the same reasons discussed previously for the viscometric functions in shear flow. In Figure 4.32, the normalized steady extensional viscosity of a non-Gaussian network shows a dramatic increase after the critical elongational rate of $\alpha=0.3$ is surpassed. In the limit as the breakage index goes to zero, the conformational dependent breakage potential degenerates to the constant breakage potential, and this abrupt increase becomes infinite. Networks with Gaussian chains show a maximum in the steady extensional viscosity, which results because the junction concentration decreases rapidly with increasing elongational rate. Because the non-Gaussian statistics of finitely extendible chains, this decrease in junctions is suppressed for shorter network chains, and the extensional viscosity looses the extremum as the number of segments in the network decreases. For networks with a small

number of statistical subunits between junctions, the shape of the extensional viscosity profiles is qualitatively similar to those derived for FENE dumbbells [81].

Comparison of the Model to Data

The slip parameter and the breakage index should be more than just curve fitting parameters; these parameters should depend on molecular structure in some reasonable and non-random way. Thus, we now derive some semi-theoretical expressions to relate these model parameters to associative polymer structure.

The breakage index is $\varepsilon = 2\sigma/3N$, where σ is the square of the ratio of the maximum end-to-end distance of the network segment to the length scale in which the breakage potential changes. Since the maximum end-to-end distance scales as N, σ scales as:

$$\sigma \sim \sigma_o \left[\frac{N^2}{N^\delta} \right] \tag{4.65}$$

where σ_o is a constant that includes the length of the individual network chain subunit, and δ is the power by which the length scale $\beta(\underline{x},N)$ changes depends on the number of subunits in the network chain. Rather than introduce another parameter, we assume that the length scale in which $\beta(\underline{x},N)$ changes does not depend on N, (i.e. $\delta = 0$). We could use δ to better fit the experimental data, but here we are primarily interested in determining how the breakage index should depend on N. Thus,

$$\varepsilon \sim 2\sigma_o N/3. \tag{4.66}$$

for finite N. In the Gaussian limit, our model should reduce to that of Fuller and Leal. Although Fuller and Leal did not disclose what value of the breakage index they used in their calculations, we have deduced from their figures that they used $\varepsilon = 0.01$. Thus, the breakage index should approach 0.01 as N goes to infinity. Since no theory exists to describe how the breakage index should depend on the number of network segments between network junctions, we choose a simple function that will smoothly connect the two limiting asymptotes:

$$\varepsilon(N) = \frac{(\frac{2\sigma_o}{3})\, N\, \varepsilon_\infty}{1 + (\frac{2\sigma_o}{3})\, N} \tag{4.67}$$

Equation (4.67) scales with N like Equation (4.66) for small values of N, and Equation (4.67) approaches the breakage index ε_∞ used by Fuller and Leal for large values of N. Equation (4.67) implies that the strength of the association junctions, which resist the breakup of the junction by shear forces, decreases and approaches a limiting value as N increases . Note because we match the results of Fuller and Leal, σ is always less than N, and the initial distribution $f_o(\rho,\eta,z)$ may be approximated with $\hat{G}(\rho,\eta,z,N)/\hat{\beta}(\rho,\eta,z,N)$. The parameter σ_0 governs the critical segment chain length N_c above which the network behaves as a Gaussian network, i.e. when $N > N_c = 3/2\sigma_0$. A value of σ_0 of 0.015 seems to fit the data in Figures 4.1 and 4.2.

To qualitatively account for coil-stretch transition exhibited by a polymer coil in a flow field, many authors have incorporated into the kinetic dumbbell theory a conformation friction factor for the dumbbell beads (i.e., a conformation dependent diffusion coefficient), and an internal viscosity for the polymer chains [91 - 94]. Phan-Thien et al. [93] showed that the inclusion of these effects into the kinetic theory leads to a non-affine

transformation into the coordinate system, and concluded that the the velocity gradient may be replaced with an effective velocity gradient $\underline{\underline{\Gamma}}^* = \underline{\underline{\Gamma}} - \xi \underline{\underline{D}}$, where ξ is zero for affine deformation and ξ is non-zero for non-affine deformation. They generalized this idea to polymer networks [88], and this was used in our network theory, and in the network theories of Fuller and Leal, and of Vrahopoulou and McHugh.

To simulate the effect of the coil-stretch transition on the hydrodynamics of the polymer chain in the kinetic theory of polymer solutions, the polymer coil is often viewed as a deformable and orientable "particle", where the frictional interaction between polymer coil and the fluid at low Reynolds number depends on the shape of the particle. Hinch [95] showed that the rotation of a non-spherical particle in straining flow is exactly represented by an effective velocity gradient in the equations of motion for a particle. This motivated Phan-Thien et al. [96] to use

$$\xi = \frac{\xi_o N a^2}{3N a^2 + (\underline{RR})} = \frac{\frac{\xi_o}{3}}{1 + \frac{N}{3}(\underline{xx})} \tag{4.68}$$

where ξ_o is a constant on the order of unity, and 'a' is the length of the statistical subunit. Thus, the degree of non-affine deformation depends on the relative extension of the polymer chain.

Including a conformation dependent slip parameter into our model would produce eigenvectors that would likewise depend on the relative extension of the network chain. However, in the development of our model, we simplified the mathematics by transforming the coordinate system with $\underline{x} = \underline{\underline{T}} \cdot \underline{\rho}$, where the tensor of eigenvectors $\underline{\underline{T}}$ was assumed to be independent of $\underline{\rho}$. Thus, the inclusion of a conformation dependent ξ will force us to re-derive the general expression for the distribution function. To avoid such

mathematical complications, we could preaverage the (xx) in Equation (4.68). Inclusion of this factor would influence the degree of shear-thinning in the model. However, even this degree of sophistication is not needed here because all that is required is a semi-theoretical expression that describes how the slip parameter should depend on associative polymer molecular weight.

Because (xx) varies from its small equilibrium value to 1 at full extension, Equation (4.68) can be approximated by:

$$\xi = \frac{\xi_o}{N} \tag{4.69}$$

for large N. This gives us the approximate qualitative dependence of the degree of non-affine deformation on the number of statistical subunits between network junctions without unnecessarily complicating the mathematics. Additionally, the size of the associative polymer network will increase with concentration. The degree of non-affine deformation, which arises from internal viscosity and diffusional effects, should increase as the size of the network increases because the local viscosity for the network segments increases. The exact relationships between network cluster size and associative polymer concentration have yet to be worked out for our model polymers, so we approximate the concentration dependence in the concentration region of our data ($1 < c(wt\%) < 5$) as linear. Thus we take:

$$\xi = \frac{\xi_o\, c}{N} \tag{4.70}$$

where a value of ξ_o of 0.5 seems to fit the data in Figures 4.1 and 4.2.

Chapter III showed that the number of associative polymers between network junctions depended on both associative polymer concentration and on associative polymer molecular weight. Here, we simply take $N = M_n/M_o$, where M_o is the molecular weight of a single statistical subunit, and we ignore the effect of concentration. A value of M_o of 2000 seems to fit the data in Figures 4.1 and 4.2.

Figures 4.33 and 4.34 show that with these simplistic, semi-theoretical equations, the model reproduces the concentration and molecular weight dependence of the steady shear viscosity profiles shown in Figures 4.1 and 4.2 quite well. The model with the conformation dependent breakage potential, where the breakage index is given by Equation (4.67) and the slip parameter is given by Equation (4.70), has a maximum in the viscosity profile at the correct shear rate, and the shear rate at which the maximum occurs depends on molecular weight in the same way as the data. In addition, the relative magnitude of the viscosity maximum is correct, and correctly decreases with increasing associative polymer molecular weight. In both the data and in the model, the viscosity profiles cross one another at a large shear rate so that larger molecular weight polymers have higher high shear viscosities than lower molecular weight polymers. Thus with only three parameters, the network model represents entire families of viscosity profiles and the dependence of these profiles on molecular weight and concentration.

Conclusions

In summary, we have generalized Yamamoto's network model for concentrated solutions to include simultaneously a non-Gaussian polymer segment free energy and conformation dependent junction breakage potential. In the Gaussian limit, our model reduces to the network model of Fuller and Leal, and in the limit of a zero breakage index, our model reduces to an extended version of the non-Gaussian network model of

Vrahopoulou and McHugh. Our model accurately portrays the steady shear viscosity data of our model associative polymer solutions, and fits well with our intuitive physical picture of the association network.

This network model has aided our interpretation of the shear-thickening viscosity profile in terms of network dynamics. Apparently, network junctions that are created by association are strong enough to support stress so that the chains to extend during shear before the the junctions break. Thus, the observed shear-thickening behavior results from the finite extensibility of network chains, and the magnitude of the viscosity enhancement decreases as the length of the network chain between junction increases. A change in the hydrodynamics of the polymer coil during extension (i.e., the coil-stretch transition) causes the network to deform non-affinely. This non-affine deformation, which suppresses shear-thickening behavior of the network, becomes more severe as polymer concentration, and hence network size, increases. Thus, the shear-thinning observed in the viscosity profile of associative polymer solutions results from both the rupture of network junctions under shear and the non-affine deformation of the association network.

Chapter V

Adsorption of Model Associative Polymers on Monodisperse Polystyrene Latex

Introduction

Motivation

Now that the first four chapters of this dissertation have examined the aqueous phase networking behavior of associative polymers, we can begin to probe the association mechanism in more complicated model systems made from various combinations of associative polymer, latex particles, surfactants, and cosolvents. The first step toward understanding the influence of the associative mechanism on latex rheology is to uncouple the influence due to the interaction between associative polymers and the latex particle interface from that due to aqueous phase networking. This means investigating the intimate connections among adsorption, colloidal stability, and latex rheology.

Adsorption

A long standing controversy has surrounded the adsorption behavior of associative polymer: is adsorption necessary in the rheological control of latex dispersions? Two divergent views on this subject have given rise to the particle bridging theory, and the associative cluster bridging theory [11]. The particle bridging theory claims that associative polymers thicken latex dispersions by the simultaneous adsorption of hydrophobes from a given associative polymer to two or more latex particles. Thus, the thixotropic and shear-thinning rheology that is necessary for good flow and levelling results from the desorption of the associative polymer under shear, and the diffusion controlled readsorption of the

associative polymer after the shear has been removed. This theory implies that the structures and chemical natures of the associative polymer's backbone and hydrophobes must be carefully optimized to enhance adsorption. However, the particle bridging theory alone cannot account for the high viscosities of associative polymer solutions that lack latex. The associative cluster bridging theory claims that when the concentration of associative polymer exceeds the critical concentration that is required to saturate the solution, a phase transition at the molecular level occurs, and association among thickener hydrophobes builds up a shear-sensitive, pseudo-high molecular weight species in solution. The association junctions in this network are dynamic micelle-like clusters, the lifetime of which is related to a chemical potential difference between hydrophobes and solution environment, and to steric factors. Thus, this theory states that the thickening action of the associative polymer in latex dispersions does not require the adsorption of the associative polymer to latex particles, and the desired hysteresis in the rheological properties of the latex dispersion results from the diffusion controlled rebuilding of aqueous phase network after it has been sheared. This implies that placement of hydrophobes is critical to thickening ability of the associative polymer, and that the structure of the associative polymer backbone is unimportant as long as it provides the entire polymer with solubility in water. However, the associative cluster bridging theory cannot explain either the influence of associative polymers on the colloidal stability of latexes, nor the influence of particle size on the rheological properties of latexes that contain associative polymer. Although neither theory is all inclusive, they guide us to study whether or not our model associative polymers adsorb to latex, and if so, to deduce the mechanism of adsorption and how it affects rheological properties.

Glancy and Bassett [97], Thibeault et. al. [15], and Karunasena et. al. [52] have provided experimental evidence for the interaction between associative polymer and latex. Glancy and Bassett examined how associative polymer molecular weight and hydrophobe

content influenced the low and high shear viscosities of acrylic and styrene acrylic latexes of various particle sizes. They noted that the thickeners interacted more with small sized latex particles to substantially increase the high shear viscosity of small particle size latexes, as compared to large particle size latexes. Thibeault et. al. measured the adsorption isotherms and viscosity profiles of the following model polymers in monodisperse acrylic latex dispersions: a low molecular weight ethylene oxide based copolymer model associative polymer with large hydrophobe content, an ammonium salt of an anionic acrylic copolymer of high molecular weight with low hydrophobe content, and a (hydroxyethyl)cellulose non–associative polymer. They studied the effect of latex particle size, surfactant concentration, and cosolvent concentration, and observed that the degree of interaction of associative polymer increased as particle size decreased, and that the desorption of the model polymer from the latex particle through the addition of surfactants and cosolvents coincided with a decrease in dispersion viscosity. They concluded that the associative polymer interacted with latex particles to physically cross–link the dispersion, and that the shear–thinning viscosity profiles of the dispersion resulted from the disruption of the physical cross–links by shear forces. Karunasena et. al. also saw how the degree of interaction between associative polymer and latex increased as particle size decreased, as reflected in an increase in the low shear viscosity of coatings that contained styrene or methyl methacrylate latexes and titanium dioxide particles that had been stabilized with oligomeric methyl methacrylate and excess nonionic surfactant. Such behavior is expected from electroviscous effects. They speculated from the influence that oligomeric methacrylic surface acids exerted on the low shear viscosities of their coatings that the poly(oxyethylene) backbone of the associative polymer, and not the alkyl end-group, adsorbed to the latex surface via an ion-dipole mechanism. They concluded that a synergistic interaction occurs between the associative polymer and the latex because the viscosity of the total coating was greater than the sum of the viscosities of its components.

Stability

In addition to influencing rheological properties, the adsorption of associative polymer on latex surfaces also influences the colloidal stability of dispersions. Since associative polymers have multiple hydrophobes, one can adsorb to the particle surface while the remaining hydrophobes network in solution; or, both hydrophobes can adsorb to different particles to flocculate the latex by bridging; or if the hydrophobes do not adsorb to the particle, the polymer can flocculate the latex through volume restriction. In their experiments, Sperry et al. [19] and Santore [98, 99] observed the bridging flocculation of latexes by associative polymers that had molecular structures that were similar to our model associative polymers. The degree of adsorption depends on the following: the particle size and size distribution of the latex particles, the hydrophobicity of the latex particle due to particle composition and surfactants used in particle synthesis, the strength of interaction between the associative polymers' hydrophobes and particle surface, the position of hydrophobe on polymer backbone, the flexibility of the associative polymer backbone, and the concentration and type of surfactants and cosolvents in the latex serum. Santore's statistical mechanical calculations showed that moving the hydrophobe away from the ends of a flexible, non-adsorbing polymer chain to a position deeper inside the polymer coil decreases the degree of adsorption of polymer to the particle surface. Her pseudo-one component model predicts that associative polymers that have hydrophobes that interact strongly with the particle surface flocculate the latex by bridging when the concentration of associative polymer in the serum is on the order of 0.01 weight percent, and restabilizes the latex when the concentration of associative polymer in the serum is on the order of 1 weight percent. This was verified with experiments with 240 nm and 68 nm acrylic latices that contained QR708, a commercially available associative polymer made by Rohm and Haas that is a hydrophobically modified urethane-ethoxylate polymer that has a molecular

weight between 30,000-40,000. Sperry et al. also examined the effect of surfactant on phase behavior of associative polymer in acrylic latex. Electron microscopy detected flocculation by bridging at low polymer concentrations in latex, but failed to detect microscopic domains at polymer concentrations that were large enough to restabilize the latex. They concluded that a "floc of infinite extent" (i.e., a homogeneous network of associative polymer and latex particles) had formed when the dispersions restabilized. Santore compared her one-component model to the data of Sperry et. al, and concluded that adding surfactant to the dispersion had the same effect on dispersion stability as decreasing the strength of interaction between the polymer hydrophobe and the surface.

The previous discussion underscores the complex, and sometimes system dependent, nature of the latex particle-associative polymer interaction. Our motivation for studying the adsorption behavior of model associative polymer is derived from the experiments depicted in the first two figures of this chapter; they show that colloidal stability and rheology are closely connected to adsorption behavior. In a simple bench-top experiment that was designed to gain some insight into the effect of associative polymer on colloidal stability, we added various amounts of previously solvated model associative polymer to four centimeter test tubes that contained previously cleaned 190 nm monodisperse polystyrene latex. Each test tube was capped and shaken until the mixture appeared homogeneous to the unaided eye, and then the test tube was stored in the dark. The height of sediment in the test tube, which indicated the degree of flocculation, was measured periodically. In all of the experiments, the rate of change of the sediment cake height with respect to time (i.e., dh_{cake}/dt) tapered off after a couple of weeks, which suggested that the flocculated systems approached an equilibrium. In total, we examined the effect of associative polymer molecular weight, hydrophobic end-group length, and added sodium chloride concentration.

Figure 5.1[1] shows typical results for these experiments: a minimum degree of networking is required to flocculate the latex, whereupon the cake height increases to a maximum at about 1% associative polymer by weight, and then decreases to zero. Both the concentration of associative polymer required to flocculate, and then to restabilize the latex, decreases with increasing molecular weight. We realize that sometimes a latex can be too viscous to separate into colloid- rich and colloid- poor phases within the time scale of an experiment, even though microscopy would have revealed that the particles are flocculated, and that this behavior is sometimes misinterpreted as restabilization. Although we do not have microscopic evidence, we believe that the restabilization observed in Figure 5.1 is genuine. We make this inference based on the work of Sperry et al. [19], and on the similarity of their model associative polymers to ours.

The degree of flocculation for a given concentration and molecular weight increases as the hydrophobe length increases in the order C16>C12>H. A very slight amount of flocculation occurs with the polymer without hydrophobic end-groups, but the hydrophobic end-groups significantly enhance the degree of flocculation. The degree of flocculation depends on molecular weight, and passes through a maximum at a molecular weight near 50,000-80,000. This behavior seems quite natural because the driving force for networking decreases, and the length of associative polymer backbone increases, as the molecular weight increases. These competing effects should produce an optimum associative molecular weight that will flocculate the latex.

These experiments indicate that the ability of the associative polymer to flocculate a latex depends on the ability of the associative particle to cooperatively network to span the distance between particles. The average interparticle distance of a 9.3% solids content latex is about the same as the particle size of the latex, and the average end-to-end distance of the associative polymers, as estimated from the intrinsic viscosity experiments in Chapter II, is

[1] Measurements courtesy of Mehdi Durali.

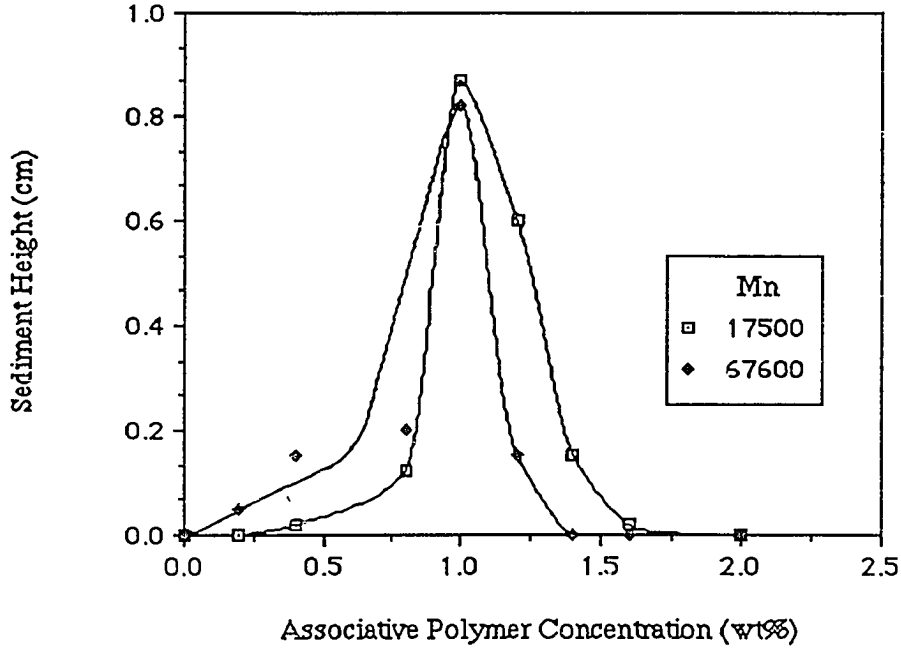

Figure 5.1: Flocculation and restabilization of a 10% solids content 190 nm polystyrene latex by model associative polymer of various molecular weights with hexadecyl hydrophobic end-groups. The sediment height is the thickness (in centimeters) of the flocculated cake in a 4 centimeter test tube.

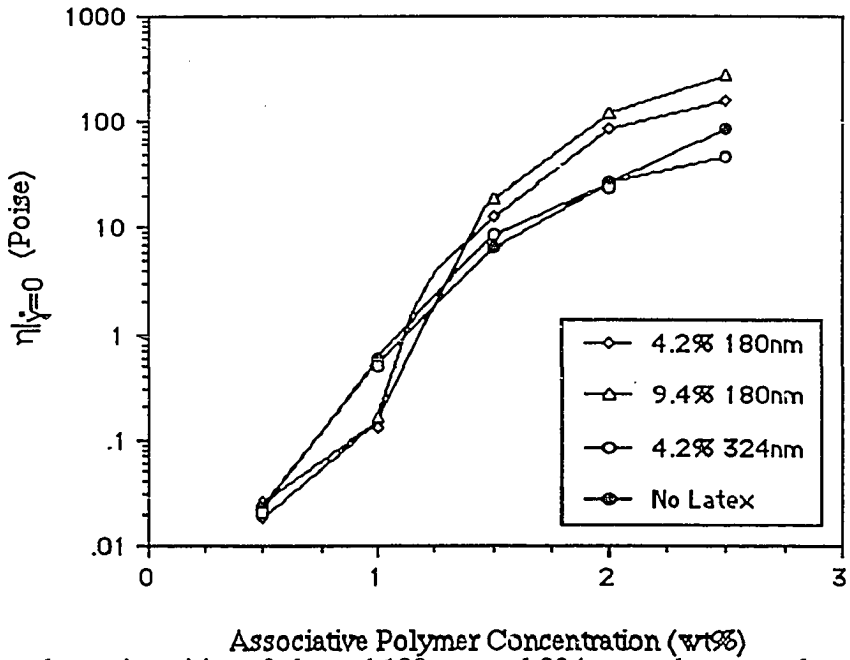

Figure 5.2: Low shear viscosities of cleaned 180 nm and 324 nm polystyrene latexes that contain model associative polymer of 51,000 molecular weight with hexadecyl end-groups.

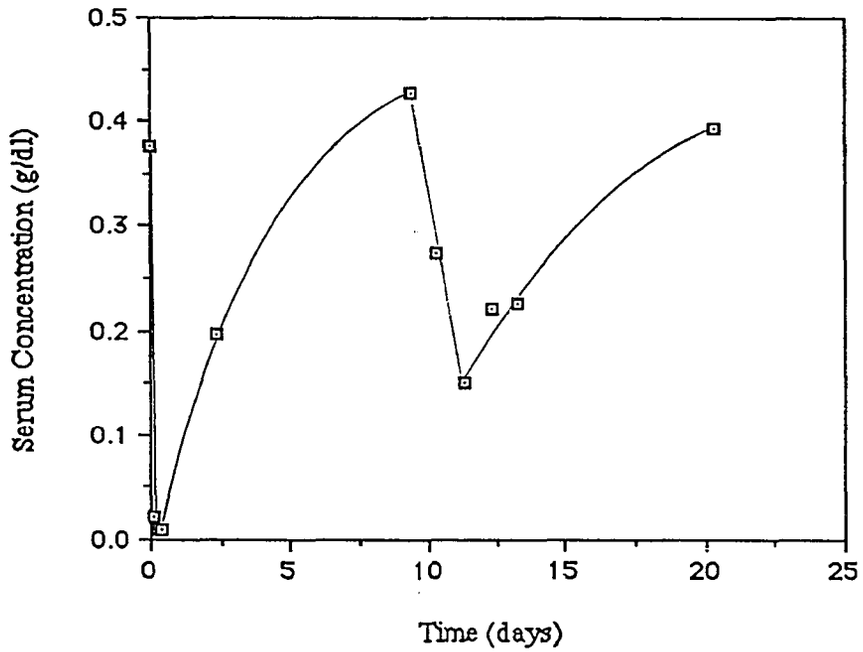

Figure 5.3 Variation of serum concentration with adsorption time for a model associative polymer of molecular weight 51,000 with hexadecyl hydrophobic end-groups. The 400 ml serum replacement cell was charged with 2.477 grams of the associative polymer and 0.277 grams of clean 324 nm monodisperse polystyrene latex. See text for a description of the flow history of the cell.

between 10-30 nm. On the average, it therefore takes the cooperative networking of six to twelve associative polymers to bridge two latex particles. Thus particle size and concentration, which dictate the average interparticle spacing, and associative polymer concentration, molecular weight, and hydrophobe size and placement, which control both the ability of the associative polymers to network in the aqueous phase and to adsorb to a latex particle, control the stability of latexes that contain associative polymer. The ability of the model associative polymer to flocculate latexes by bridging would not occur if the polymers did not adsorb to the latex particles.

Figure 5.2 shows how the viscosity of dispersions that contain associative polymer depend on associative polymer concentration, and on latex concentration and particle size. The filled symbols represent viscosity data for solutions of associative polymer only, and

the open symbols represent latex systems that contain identical amounts of associative polymer. For the 180 nm particles, the associative polymers flocculate the latex by particle bridging at associative polymer concentrations between 0.5% and 1.5% by weight to lower the viscosities of the latexes to below those of associative polymer solutions that contain identical amounts of thickener. The latex dispersions are stable at larger associative polymer concentrations, and the viscosities of these dispersions are larger than those of the associative polymer solutions sans latex, which indicates a synergistic interaction exists between the associative polymer and latex particles. The restabilization indicates the formation of a homogeneous network of associative polymer and latex particles. Chapter VI, which covers the shear dependence of the rheological properties of such systems, describes the rheological implications of this behavior in more detail. The dependence of the dispersion viscosity of the 324 nm latex on associative polymer concentration in Figure 5.2 is different from that of the 180 nm latex: the viscosities of 324 nm latexes that contain associative polymer follows those of the associative polymer solutions. For a given solids content, the total surface area of a latex decreases as particle size increases. This suggests that the 324 nm latex has already been fully covered at associative polymers concentrations of associative polymer that exceed 0.5%. (This fact is supported by the adsorption data presented later in this chapter.) To conclude, the rheological properties and phase behavior of latexes containing associative polymer depend upon the partitioning of associative polymer between the particle surface and the dispersion medium, and to understand this interaction from more fundamental principles, we have measured the adsorption isotherms of our model associative polymers on monodisperse latex particles.

Adsorption Isotherms Via Serum Replacement

The classical method of measuring the adsorption isotherm is to add various amounts of the polymer to a known amount of the latex, allow the system to equilibrate,

separate the serum from the latex either by filtration or centrifugation, and analyze for the amount of polymer remaining in the serum. The amount of polymer adsorbed to the latex is then determined from a mass balance. Obviously, the filtration method will work only if the hydrodynamic radius of the polymer is smaller than the pore size of the membrane, and if the diameter of the latex particles are larger than the pore size of the membrane. This is not always true with associative polymers, because they can build networks that approach the colloidal size range, and usually we have no way of knowing a priori at what concentration the associative polymer network will become too large to pass through the membrane. In addition, the time scale of desorption of a flexible polymeric species is often quite large compared to its time scale of adsorption, even if the polymer is reversibly adsorbed. If each contact point between the colloid and the associative polymer is of order kT, then the probability that all of the contact points are simultaneously desorbed is small because of the large number of points of contact between the adsorbed polymer and the colloid.

We have measured the time scale of desorption of our model associative polymers from polystyrene latex. (Figure 5.3) In this desorption experiment, we have charged a serum replacement cell with the following: 2.477 grams of a model associative polymer of molecular weight 51,000 with hexadecyl hydrophobic end- groups, 0.277 grams of 324 nm polystyrene latex particles, and DDI water. The concentration of associative polymer residing in the serum was monitored during the complicated flow history of the cell, which is described as follows. The cell was left undisturbed for one week, then flushed with DDI water at the flow rate of 13 mls/hr, and then allowed to equilibrate over another 10 days. Then the cell was subjected to an even slower flushing with DDI water at a flow rate of 20 ml in two days, and again allowed to equilibrate. Figure 5.3 shows that the time period required for the thickener to desorb from the particle is quite large, on the order of days. This time dependence for desorption is well known for polymers with hydrophobic

segments, and it results from diffusion of the polymer to, and reorientation of the polymer at, the particle surface [100]. The high viscosity of the serum due to the presence of the associative polymer slows down the diffusion of the polymer, and hence, retards the approach to equilibrium. Integration of the effluent stream concentration profile to determine the mass of polymer removed prior to the achievement of equilibrium, coupled with a mass balance, determined that 2.5 grams of polymer adsorbed to the latex at both equilibrium points. This is much larger than the amount that the same molecular weight model associative polymer without the hydrophobic end-groups adsorbs under identical conditions; hence, the hydrophobes enhance the adsorption of the polymer to the latex surface.

Since the filtration technique is difficult to apply to latexes that contain the model associative polymers, we could have tried to separate the serum from the latex by centrifugation. However, this technique assumes that the centrifugation does not influence the adsorption-desorption equilibrium, and that any polymer that becomes trapped in the serum within the cake is in equilibrium with the polymer on the particle surface. Rather than use these assumptions, we have modified the serum replacement technique to determine the adsorption isotherms of the model associative polymers.

The serum replacement technique [101, 102], which has been used to determine the adsorption isotherms of anionic and nonionic surfactants, consists of charging a serum replacement cell with cleaned latex that has been equilibrated with a known amount of surfactant, and then washing the latex with distilled water. The concentration of surfactant in the effluent stream is measured, and the mass of surfactant adsorbed to the latex surface is determined through a mass balance. Alternately, the cell can be charged with cleaned latex, then washed with a surfactant solution, and the isotherm is again determined through a mass balance. Experiments in our laboratory show that the time scale of adsorption is very fast as compared to the desorption data presented in Figure 5.3. As explained in the

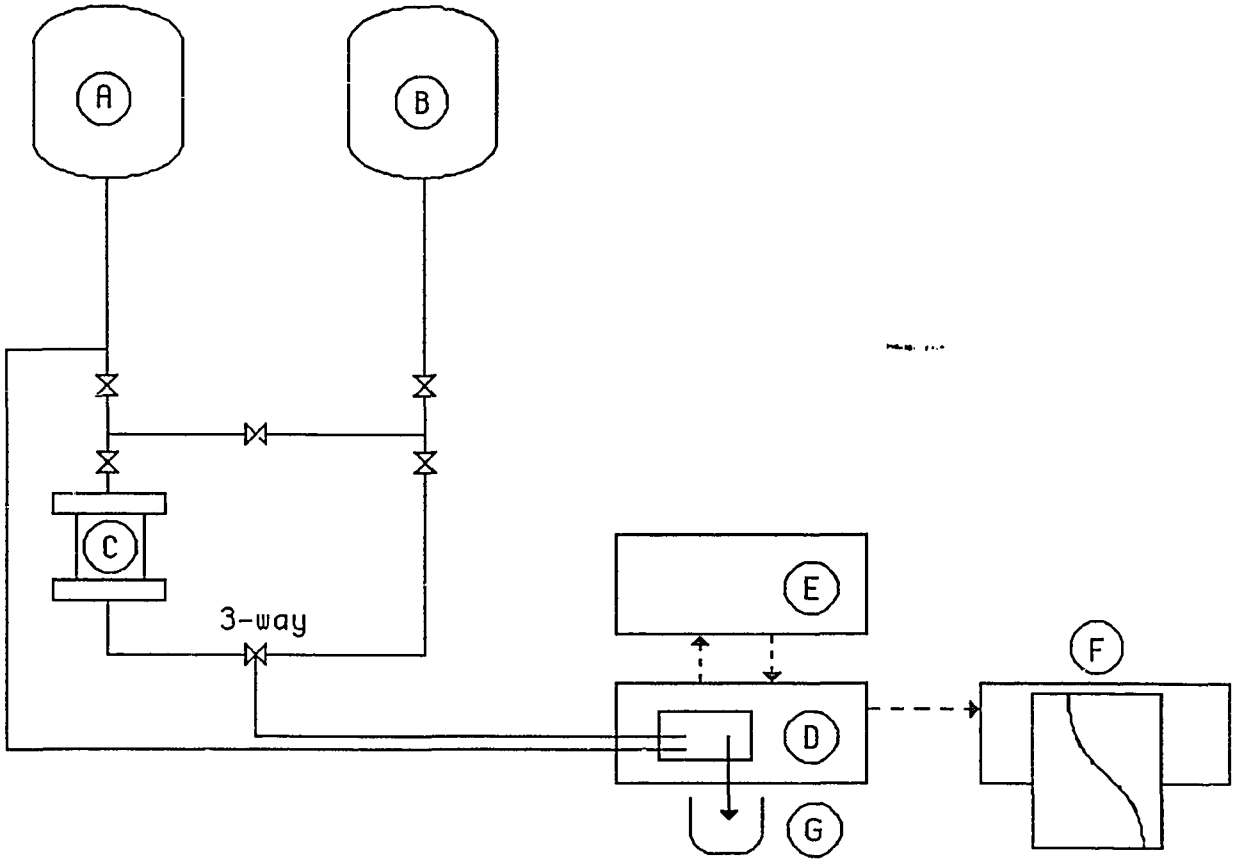

Figure 5.4: Schematic diagram of the adsorption apparatus. Key: (A) distilled deionized water reservoir ; (B) associative polymer solution reservoir ; (C) serum replacement cell ; (D) differential refractometer ; (E) constant temperature bath ; (F) chart recorder ; (G) weighed efflux. The bows represent valves.

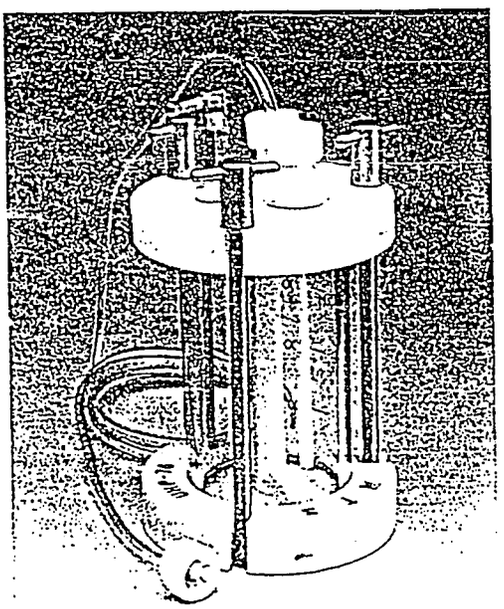

UHP 76

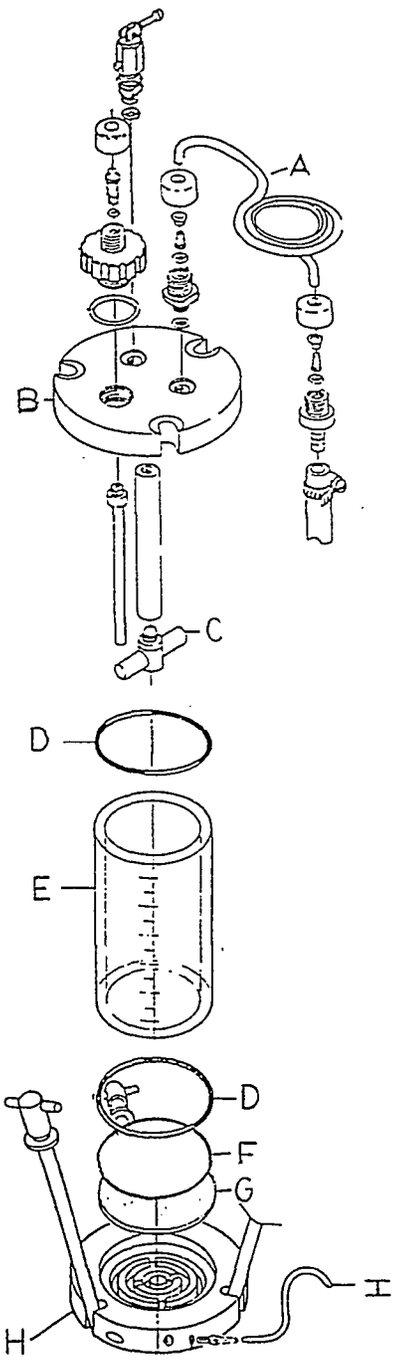

Figure 5.5: Exploded view of the serum replacement cell. Key: (A) feed stream inlet ; (B) polyacetal top plate ; (C) Teflon coated stirring bar ; (D) ethylene-propylene copolymer O - ring ; (E) polycarbonate reservoir ; (F) Nucleopore membrane; (G) polyethylene porous disk ; (H) polyacetal bottom plate ; (I) filtrate outlet.

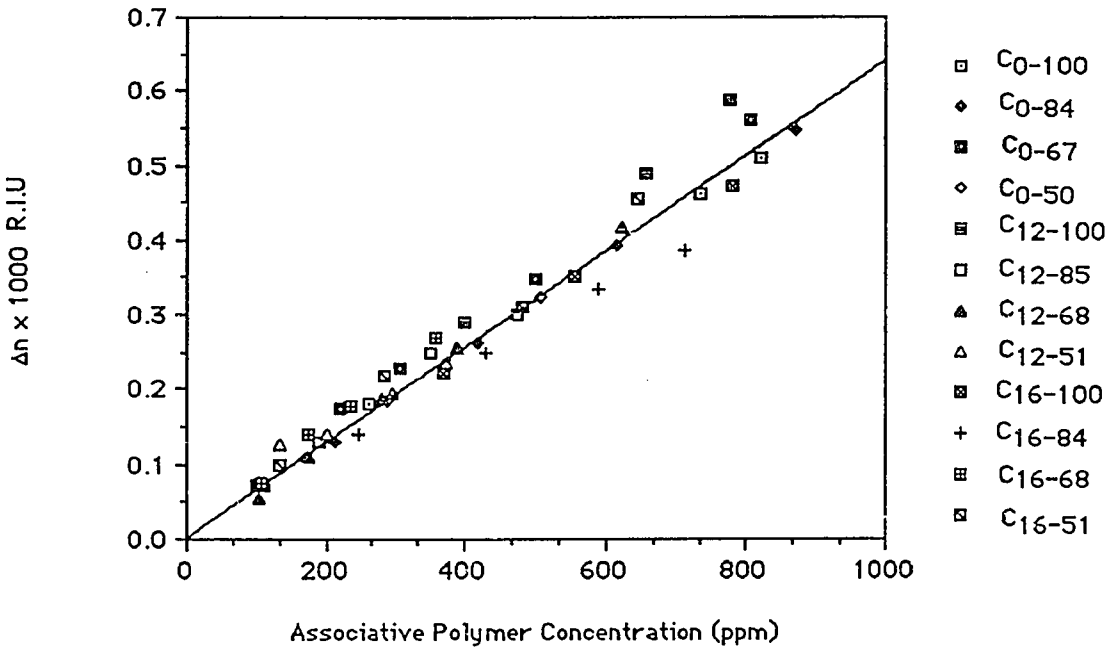

Figure 5.6: The refractive index increment of model associative polymers in water at 28°C.

experimental details that follow, we start with the naked colloid, and wash it with an associative polymer solution to determine the adsorption isotherm.

Experimental Detail

Figures 5.4 and 5.5 present schematic diagrams of the adsorption apparatus and of the serum replacement cell (model UHP-76 from Micro Filtration Systems). This section begins with a brief description of the anatomy of the adsorption apparatus, then develops the analysis to calculate both the adsorption and desorption isotherms, and concludes with some pertinent notes on the operation of the adsorption apparatus.

Apparatus

In Figure 5.4, reservoirs A and B hold distilled deionized (DDI) water and nominally 300 parts per million by weight (ppm) associative polymer solution, respectively. The polymer feed solutions were made by diluting the five weight percent stock solutions described in Chapter III, stirring the diluted solutions gingerly, and then allowing them to stand overnight to achieve a homogeneous solution. By opening or closing the appropriate valves, either water or associative polymer solution flows by gravity either to a differential refractometer (D) via a bypass line, or to a serum replacement cell that contains a 0.5 - 1% solids suspension of latex that had been previously cleaned by serum replacement to remove adsorbed emulsifier and free electrolyte from the dispersion medium (C). (The reasons for choosing these associative polymer and latex concentrations will be described shortly.) The efflux is collected and weighed to determine the cumulative associative polymer mass flux through the serum replacement cell. The mass flow rate is typically between 1 - 1.5 g/min. Weighing the cumulative mass of the exit stream directly with an electronic top loading scale with digital readout affords more precision than the conventional method of measuring the volumetric flow rate in a graduated cylinder and then using density to calculate the cumulative mass efflux. The serum replacement cell holds 419 grams of water, so that the average residence time in the cell is 4 - 7 hours. The differential refractometer (Refractomonitor III, LDC Analytical), using distilled deionized water as a reference, continuously monitored the concentration of associative polymer in the exit stream of the cell. So that the concentration measured by the refractometer is indeed the actual concentration of associative polymer in the latex serum, the dead volume in tubing between cell and detector and axial dispersion are minimized by using the smallest possible length and diameter of tubing. Calibration of the refractometer with solutions of model associative polymer of known concentration facilitated measurement of the absolute concentration of polymer in the efflux stream. As shown in Figure 5.6, the range of

associative polymer concentrations used in these experiments is dilute enough to provide a master refractive index increment curve that is seemingly independent of associative polymer molecular weight and hydrophobic end-group length. From the line on Figure 5.6 (and neglecting the small intercept that results from the regression analysis), the refractive index increment is $\Delta n = 0.664 \times 10^{-7}$ [AP], where [AP] is the concentration of associative polymer in parts per million by weight. As shown in the following data analysis section, the amount of associative polymer adsorbed onto the latex can be deduced from the differences in associative polymer mass flux into and out of the serum replacement cell.

The model colloids used in the adsorption study in this chapter and the rheological studies of Chapter VI are monodisperse polystyrene latexes LS-1101A, LS-1102A, LS-1121B, and LS-1166B prepared by the Dow Chemical Company. The particle sizes were verified by a Nicomp® particle size analyzer, and were near the particle sizes provided by Dow. The latexes were cleaned by serum replacement until the conductance of the effluent stream was nearly that of DDI water. Conductametric titration with 0.02N sodium hydroxide standard solution determined the surface charge density of the latex particles [103]. To place the surface acids on the particle surface in their strong acid form before the conductametric titration, the latexes were cleaned by serum replacement until the conductance of the effluent stream was nearly that of DDI water, then acidified by washing with 5×10^{-4} N hydrochloric acid, and subsequently washed with DDI water again. Table 5.1 summarizes the properties of the model colloids used in the adsorption and rheological studies.

Table 5.1: Number Average Particle Size and Surface Charge Density of Model Colloids used in Adsorption and Rheological Studies

Reference	Dow (nm)	Nicomp (nm)	Surface Charge Density ($\mu C/cm^2$)
LS-1101A	170	180	1.69
LS-1102A	190	188	1.35†
LS-1121B	310	324	6.56
LS-1166B	1100	1151	5.95†

† from reference [104]

Data Analysis

A mass balance on the serum replacement cell simply states that the rate of accumulation of associative polymer in the serum replacement cell is the rate of associative polymer flux into the cell minus the rate of associative polymer efflux from the cell. The associative polymer can accumulate in either of two places: in the latex serum, a quantity that is measured, or on the latex particle surface, the quantity of which is desired. The accumulation of associative polymer in the latex serum can be either in the form of single associative polymer chains, or in associated units. As described in the following text, the conditions of the experiment minimized the latter contribution. The ordinary first order differential equation that results from the mass balance is:

$$\frac{d(A\Gamma)}{dt} + V_{cell}\frac{dC_{out}}{dt} = \frac{dq_{in}}{dt}C_{in} - \frac{dq_{out}}{dt}C_{out} \qquad (5.1)$$

where C_i is the associative concentration in the i^{th} stream, dq_i/dt is the mass flow rate of the ith stream, V_{cell} is the mass of fluid in the serum replacement cell, A is the total latex surface area, and Γ is the mass of associative polymer adsorbed to the latex surface in a

given unit area. The mass flow rates in and out of the cell do not have to be constant, but they are equal provided that the serum replacement cell does not leak. In fact, the flow rate decreases slightly as the experiment progresses due to an accumulation of polymer in the cell, which increases serum viscosity, and due to a decrease in the head available for flow as the reservoirs become depleted. When written in dimensionless variables, Equation (5.1) becomes:

$$\frac{d\,\Gamma^*}{d\,q^*} + \frac{d\,C^*_{out}}{d\,q^*} = C^*_{in} - C^*_{out} \qquad (5.2)$$

where $C_i^* = C_i/C_{Feed}$, $\Gamma^* = (A\,\Gamma)/(V_{cell}\,C_{Feed})$, and $q^* = q/V_{cell}$ is the ratio of the cumulative mass flux through the serum replacement cell to the mass of fluid in the cell, which is a dimensionless residence volume.

To aid in the comprehension of the proposed adsorption/desorption experiment, Figure 5.7 diagrams the responses of the concentration of associative polymer in the exit stream of the serum replacement cell to a step disturbance in the feed stream concentration. At time zero (i.e. when the cumulative flow is zero) the serum replacement cell experiences a step change in the serum replacement cell inlet stream concentration of associative polymer from zero to some value: $C_{in}/C_{Feed} = 1$. If the serum replace cell does not contain latex, and if other means of retaining the association polymer, such as, dead volume, adsorption of associative polymer to the serum replacement cell itself, or aqueous phase networking are absent, then the concentration of associative polymer in the exit stream grows exponentially (curve A). This is seen readily by solving Equation (5.2) with the initial condition that only water is in the cell at the beginning of the experiment: $C_{out}\,(t=0) = 0$, and $\Gamma^* = 0$. The solution is:

$$C^*_{out} = 1 - e^{-q^*} \tag{5.3}$$

Thus for this "blank" experiment, the serum replacement cell behaves as a continuously stirred tank reactor (CSTR), as shown by the curve labelled as "blank" in Figure 5.8. When the serum replacement cell contains latex, the concentration of associative polymer in the exit stream is somewhat less than for that of the blank experiment. (See curve B in Figure 5.7, and the data in Figure 5.8). Indeed, it is this deviation from CSTR behavior that measures the adsorption isotherm: the amount of associative polymer that adsorbs to the latex particle surface for a given concentration of associative polymer in the serum. Solving Equation (5.2) for this situation yields:

$$\Gamma(q^*) = q^* - C^*_{out}(q^*) - \int_0^{q^*} C^*_{out}(q^*)\, dq^* \tag{5.4}$$

Because $C^*_{out}(q^*)$ is measured, Equation (5.4) may be used to calculate the adsorption isotherm $\Gamma^*(C^*_{out})$ (i.e., curve C), where the amount of polymer adsorbed is plotted against the concentration of polymer in the serum.

After the associative polymer saturates the latex surface, at a cumulative mass efflux of q^*_1, the associative polymer feed stream is switched off, and DDI water is fed to the cell. This marks the beginning of the desorption experiment. For the blank experiment, the concentration of associative polymer in the exit stream immediately decreases exponentially (curve D) because the serum replacement cell behaves as a continuously stirred tank reactor. This follows from the solution of Equation (5.2) with the initial condition $C^*_{out}(q^*_1) = (1 - e^{-q^*_1})$:

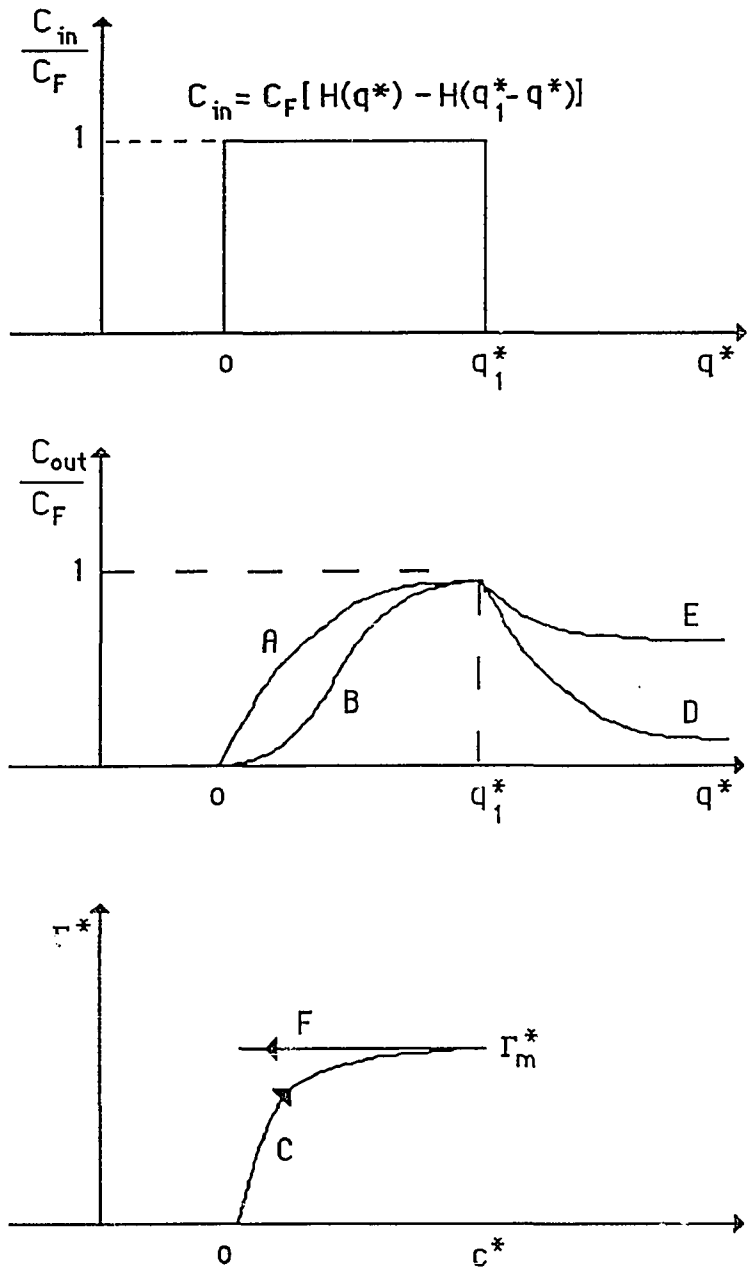

Figure 5.7: Schematic representation of the response of the associative polymer concentration in the exit stream to a pulse disturbance in the feed stream concentration, and the adsorption/desorption isotherms calculated from this response. See text for a description of the various curves. H(x) is Heaviside's unit step function.

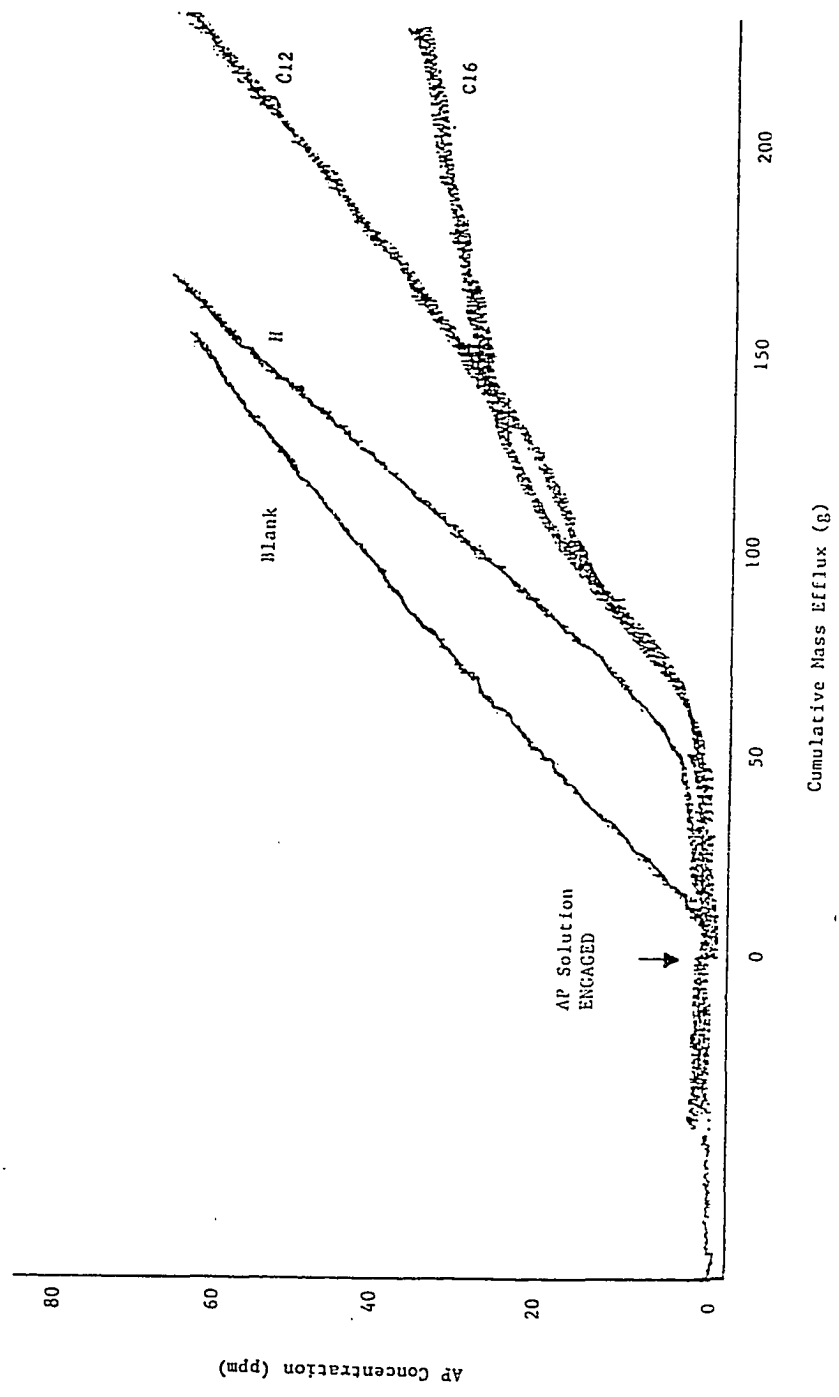

Figure 5.8: Actual concentration traces from the adsorption experiment for associative polymers with various end-groups. The associative polymer molecular weight is 67000, and the latex particle size is 190 nm. See Table 5.2 for the operating conditions. The blank curve is for a cell without latex.

$$C^*_{out}(q^*) = (1 - e^{-q^*_1})\, e^{-(q^* - q^*_1)} \qquad (5.5)$$

When the serum replacement cell contains latex, the dependence of the concentration of associative polymer in the efflux stream depends on the nature of the desorption (see, for example, curve E). The solution of Equation (5.2) that describes this desorption is:

$$\Gamma^*(q^*) = \Gamma^*(q^*_1) + C^*_{out}(q^*_1) - C^*_{out}(q^*) - \int_{q^*_1}^{q^*} C^*_{out}(q^*)\, dq^* \qquad (5.6)$$

where $\Gamma^*(q^*_1)$ is Equation (5.4) evaluated at q^*_1 .

The shape of the desorption isotherm depends both on the free energy gain of the associative polymer on adsorption, and on the time scale of desorption relative to the time scale of the flow washing the polymer from the latex surface. This is highlighted by considering two limiting extremes for the desorption kinetics. If the time scale of the flow is very fast as compared to the time scale of desorption, and if the polymers are strongly adsorbed to the particle surface, then none of the adsorbed polymers will be desorbed by the washing process (curve F), and the concentration of associative polymer in the exit stream will vary exponentially with the cumulative mass of water washed through the cell. In the other extreme, if the adsorption is quite weak, or if the time scale of the exchange of associative polymers on the surface with the associative polymers in the serum is quite fast as compared to the time scale of the washing flow, then the process occurs at steady state, and the desorption isotherm should retrace the adsorption isotherm. Thus, the degree of hysteresis depends both on the strength or free energy of adsorption, and on the relative

time scales of desorption relative to desorption, and hence provides a qualitative measure of the strength of adsorption and kinetics of desorption.

Thus, a cumulative mass balance on the associative polymer in the serum replacement cell determines the complete adsorption/ desorption isotherm:

$$\Gamma^*(q^*) = \Gamma^*_A(q^*)\, H(q^*_1 - q^*) + \Gamma^*_D(q^*)\, H(q^* - q^*_1) \qquad (5.7)$$

where $\Gamma^*_A(q^*)$ is Equation (5.4), $\Gamma^*_D(q^*)$ is Equation (5.6), and H(x) is Heaviside's unit step function.

An important benefit arises from monitoring the instantaneous concentration of the associative polymer in the exit stream on-line: the integral terms in Equations (5.4) and (5.6) can be rigorously evaluated to within an arbitrary degree of precision. On-line measurement of the associative polymer concentration avoids the conventional approximations that are used for the integral terms when an average concentration in a discrete volume element is measured. Because the rate of change of concentration of the associative polymer in the exit stream is large at the beginning of the experiment and decreases as the concentration in the exit stream asymptotically approaches the feed stream concentration, we can numerically integrate the data using the trapezoidal rule with a variable step size without sacrificing precision. To minimize computation time, a small step size for the integration is used for data obtained at the beginning of the experiment, and progressively larger step sizes are used for data obtained later in the experiment. It would be worthwhile to interface the adsorption apparatus with a computer, which could make the calculations for the adsorption isotherm on-line and display the results in real time.

The integral terms in Equations (5.4) and (5.6) sum up the cumulative area between the concentration response and the baseline on the chart recorder on Figure 5.8. Physically, this area represents the cumulative amount of associative polymer that has

exited the cell. Thus, to maintain the accuracy of the experiment, it is mandatory to minimize any drift in baseline. To protect the refractometer from changes in the ambient temperature, a water circulator held the temperature of the refractometer's fluid-optical cell at 28°C, which was approximately five degrees above room temperature. Since degassed solutions absorb air to produce baseline drift, air-saturated solutions were used. A split stream from the DDI water reservoir to the refractometer fluid-optical reference cell, with the same mass flow rate as the sample stream, also improved baseline stability. In addition, air bubbles that have become trapped in the refractometer's fluid-optical cell produce much short term noise and baseline drift, and air bubbles that pass through the optical cell produce a momentary and undesirable spike in the measured concentration response. These effects are avoided by thoroughly cleaning the refractometer's fluid-optical cell after each experiment with acetone, by applying a small amount of back pressure on refractometer, and by elevating the DDI water and associative polymer solution reservoirs to 10 feet above the refractometer to keep pressure on the refractometer's fluid-optical cell. By stopping the flow of fluid to the serum replacement cell, and then bypassing some of the associative polymer solution or water to the differential refractometer before, during and after the experiment, the stability of the baseline can be monitored.

The previous mathematical analysis depends on the assumption of perfect mixing in the serum replacement cell, so that the concentration of associative polymer that elutes from the cell is the same as the concentration in the latex serum. Use of the magnetic stirrer helps to eliminate concentration gradients in the cell and, and brings the associative polymer close to the latex particle surface by convection to promote adsorption equilibrium. Dye visualization experiments verified that the mixing in the serum replacement cell is quite good. The flow from the serum replacement cell may also be started and stopped

periodically to verify steady state: no change should occur in the concentration of associative polymer in the serum over time for a cell at steady state.

So that the correct molecular areas of adsorption are calculated from the adsorption isotherms, the amount of latex surface area must remain constant during the adsorption experiment; it must not change by particle flocculation, or by swelling of the latex particles by a water miscible cosolvent. (If a water miscible cosolvent is used in the adsorption experiment, the latex should be pre-swollen with the cosolvent). Particle size distributions of the latex, as measured by a Nicomp® particle size analyzer before and after the adsorption experiment, showed no evidence of flocculation of the latex by associative polymer. This was expected because the associative polymer and latex concentrations used in the experiment were extremely dilute and well below those used in the colloidal stability experiment shown in Figure 5.1. The dilute conditions minimize amount of networking among associative polymers, and makes the average distance between particles quite large.

Blank experiments, conducted under conditions that were identical to those used in the adsorption experiments except that the serum replacement cell contained no latex, verified that the cell did not retain associative polymers either by adsorption of associative polymers to the cell itself, or by aqueous phase networking of associative polymers. Indeed, Bisio et al. measured the adsorption of a nonionic surfactant to a polycarbonate membrane [105]. By networking in the aqueous phase, the associative polymers can build a network structure that becomes too large to pass through the pores of the membrane. When the concentration of associative polymer in the feed stream is too large (say 1/3 wt%), this networking can increase viscosity of the serum enough to dramatically decrease the efflux from the cell, and to cause the concentration of associative polymer measured in the efflux stream to actually drop as associative polymer is fed to the cell. This practical upper limit on the feed stream concentration limit depends on membrane pore size and on associative polymer molecular weight and hydrophobe length; all adsorption experiments

Table 5.2: Operating Conditions and Molecular Areas of Adsorption of Model Associative Polymers on 190 nm Monodisperse Polystyrene Latex†

M_n	End-group	C_{Feed} (ppm)	Latex Area x 10^{-5} (cm^2)	Adsorption Area ($Å^2$/molecule)
100400	H	336	2.251	10,700
84000	H	342	2.246	7,800
67000	H	300	2.214	6560
50200	H	336	2.212	4380
99900	C12	329	2.283	4690
84500	C12	335	2.244	4020
67700	C12	316	2.202	3750
50700	C12	316	2.339	2710
100400	C16	320	2.205	3820
84300	C16	322	2.234	3230
67600	C16	332	2.233	2590
51000	C16	342	2.233	2570
		163	2.300	2750
		400	2.214	2400

† Membrane nominal pore size is 200 nm.

Table 5.3: Operating Conditions and Molecular Areas of Adsorption of Model Associative Polymers on 1100 nm Monodisperse Polystyrene Latex†

M_n	End-group	C_{Feed} (ppm)	Latex Area x 10^{-5}(cm^2)	Adsorption Area ($Å^2$/molecule)
100400	H	310	1.527	25,500
84000	H	284	5.560	21,800
67000	H	240	2.313	18,300
50200	H	357	1.709	10,700
99900	C12	348	2.333	15,800
84500	C12	226	2.422	12,800
67700	C12	179	2.660	11,100
50700	C12	278	1.456	4220
100400	C16	155	.982	11,000
84300	C16	213	2.566	8240
67600	C16	368	1.851	6440
51000	C16	161	1.309	3570

† Membrane nominal pore size is 600 nm.

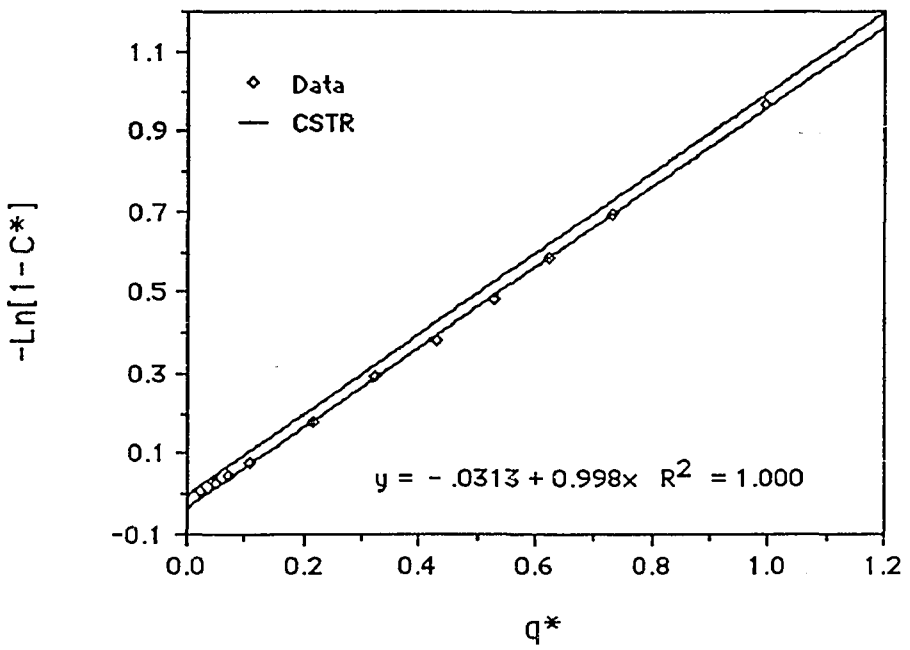

Figure 5.9: Variation of exit stream concentration with cumulative mass efflux for a blank experiment. The model associative polymer has a molecular weight of 85000 and is hydroxyl terminated. The cell contains no latex, and the membrane has 600 nm pores. The top line is the predicted response for a CSTR. The bottom line is the predicted response for a CSTR in series with transportation lag.

were conducted with a polymer feed stream concentration that was less than this upper limit. (See Tables 5.2 and 5.3).

The selection of latex concentration in the serum replacement cell during the adsorption experiment is also important: if too little colloid is present, then the latex surface saturates too rapidly to afford a precise measurement; if too much colloid is present, then the time scale required to fully cover the particle surface becomes so long that other aspects of the experiment, such as baseline stability and convenient operation, foil the experiment. In the adsorption experiments reported in this chapter, the latex concentration was varied to achieve nominally 2.2 x 10^{+5} cm^2 for all particle sizes. (Consult Tables 5.2 and 5.3).

Even though the nominal pore size of the membrane used in the experiments listed in Table 5.2 is about 5% larger than the nominal particle diameter, our experience has been that no latex escapes from the cell. Thus, to properly perform the adsorption experiment, the particle size and concentration of the latex, the pore size of the membrane, and the concentration of associative polymer fed to the serum replacement cell, must be carefully optimized.

When all of the caveats in the experimental technique described in the previous paragraphs are met, and when the serum replacement does not contain latex, the exit concentration of the polymer from the cell should follow Equations (5.3) and (5.5). Thus, a plot of $Ln\{1 - C^*_{out}\}$ versus cumulative flow volume q* should produce a line with a slope of unity and an intercept of zero for the adsorption phase of the experiment. Figure 5.9 shows data that are typical of a blank experiment. The data do indeed have a slope of one, but they also have a small negative intercept. This indicates that a short delay exists in the measured concentration of associative polymer in the exit stream, as demonstrated in the actual polymer concentration traces presented in Figure 5.8. This delay, or transportation lag, is due to the chamber under the membrane support in the serum replacement cell, which is clearly visible in component (H) in Figure 5.7. Even though in actuality the flow field in this chamber is complicated and has a large degree mixing, we can model the serum replacement cell as a CSTR in series with a plug flow pipe of volume V_{dead}. A mass balance around the CSTR and pipe yields:

$$-Ln\{1 - C^*_{out}\} = q^* - \frac{V_{dead}}{V_{cell}} \qquad (5.8)$$

This model predicts a slope of one and a small negative intercept equal to the ratio of the dead volume to the entire volume of the serum replacement cell. This model agrees well with the data presented in Figure 5.9, and the dead volume measured in this way by the blank experiment agrees well with the dead volume measured by weighing the difference of the cell before and after enough water had been added to just fill the chamber under the membrane support. Thus, we can correct the adsorption data for dead volume inherent in the construction of the serum replacement cell by simply subtracting the volume of the chamber from the total measured cumulative mass efflux. Ignoring this dead volume would result in a slight overestimation of the true amount of associative polymer adsorbed, as this hold-up would be mistaken as adsorption.

Results and Discussion

Adsorption Isotherms

Figures 5.10 through 5.13 present adsorption and desorption isotherms for model associative polymers of molecular weight 51,000 through 100,000 on 190 nm monodisperse polystyrene latexes. The filled symbols indicate adsorption data, and are read from left to right on the figures; the open symbols represent desorption data, and are read from right to left in the figures. Figure 5.14 shows the effect of feed stream concentration on the adsorption isotherms. Figures 5.16 through 5.19 show the adsorption isotherms on 1100 nm polystyrene latex to examine the effect of the curvature of the latex particle surface. In Figures 5.10 through 5.13, and in Figures 5.16 through 5.19, the square symbols are data for the hydroxyl terminated model polymer, the diamond shaped symbols are data for the dodecyl terminated polymers, and the triangular symbols are data

for the hexadecyl terminated polymers. Figures 5.15 and 5.20 display the molecular areas of adsorption as calculated from the adsorption isotherms.

The adsorption isotherms are plotted in terms of a dimensionless adsorption number, N_{Γ^*}, against a dimensionless concentration number, N_{C^*}. These dimensionless groups are defined as:

$$N_{\Gamma^*} = \frac{A\Gamma}{V_{cell} C_{Feed}} \frac{C_{Feed}}{C_{Ref}} \frac{A_{Ref}}{A} \quad ; \quad N_{C^*} = C^* \frac{C_{Feed}}{C_{Ref}} \tag{5.9}$$

where C_{Ref} is 340 ppm, and A_{Ref} is 2.2 x 10^{+5} cm^2. These dimensionless groups result from making the mass balance on the associative polymer in the serum replacement cell dimensionless, as was done in the derivation of Equation (5.2). By normalizing the data with respect to a standard state, the adsorption isotherms plotted in Figures 5.10 through 5.19 can be compared directly, even if either the concentration of associative polymer in the feed stream or the surface areas of latex in the serum replacement cell vary from experiment to experiment. As discussed later in this section, this allows the superposition of data that were obtained with different feed stream concentrations to form a master adsorption isotherm.

Two features about the adsorption isotherms in Figures 5.10 through 5.13 are worth noting. First, hydrophobic end-groups substantially enhance the amount of associative polymers adsorbed to the latex, and the backbone of the model polymer adsorbs slightly as well. This is expected since poly(oxyethylene) does adsorb to polystyrene [106], and the isophorone diisocyantes that connect the poly(oxyethylene) blocks in the backbones of the model polymers are also slightly hydrophobic. Second, the adsorption isotherms for the hydroxyl terminated polymers follow a Langmuir type L2 equation, where the amount of polymer adsorbed increases rapidly with serum concentration and

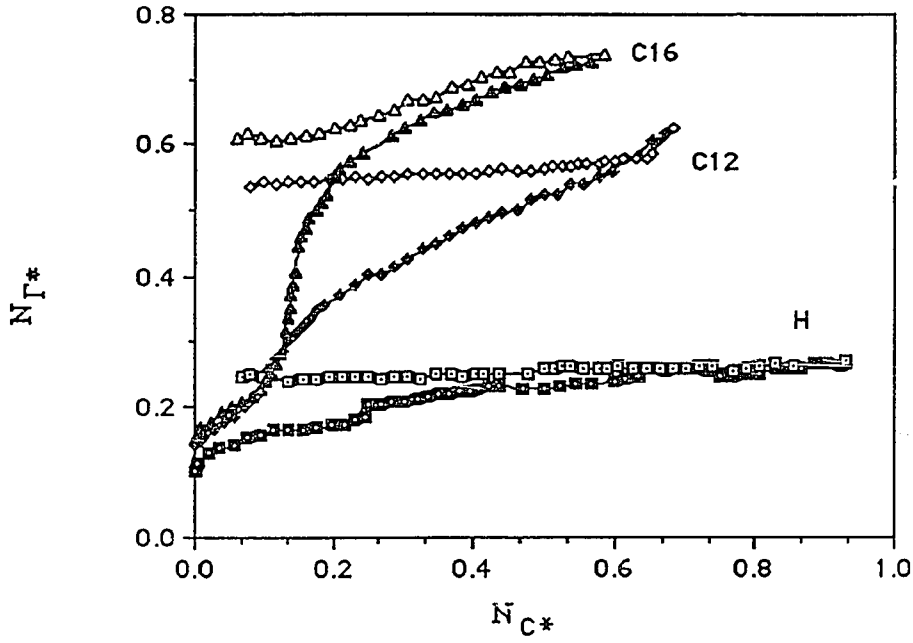

Figure 5.10: Adsorption (filled symbols) and desorption (open symbols) isotherms of model associative polymers of molecular weight 100,000 for various hydrophobic end-groups on 190 nm polystyrene latex. See Table 5.2 for operating conditions.

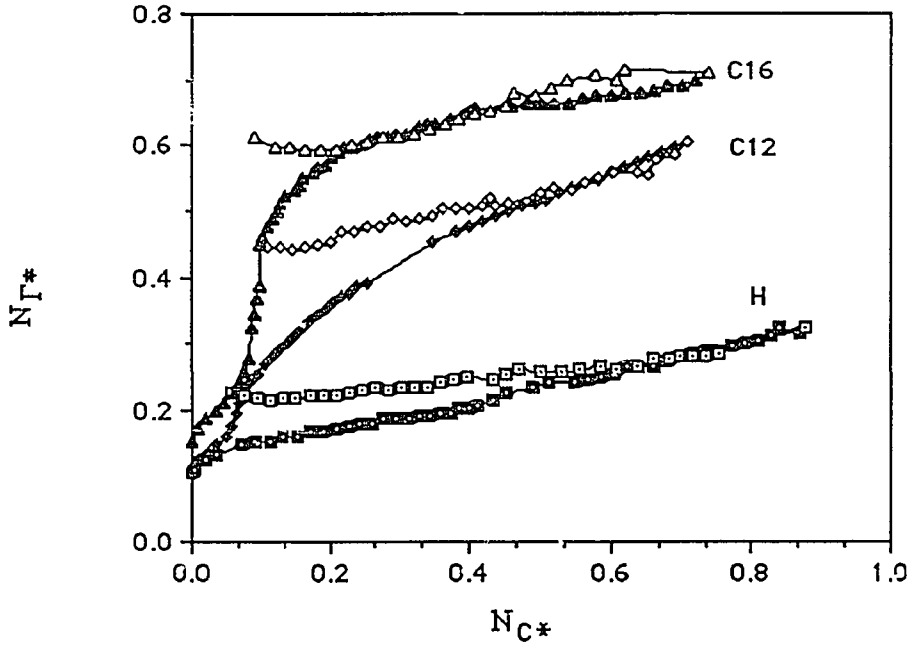

Figure 5.11: Adsorption (filled symbols) and desorption (open symbols) isotherms of model associative polymers of molecular weight 84,500 for various hydrophobic end-groups on 190 nm polystyrene latex. See Table 5.2 for operating conditions.

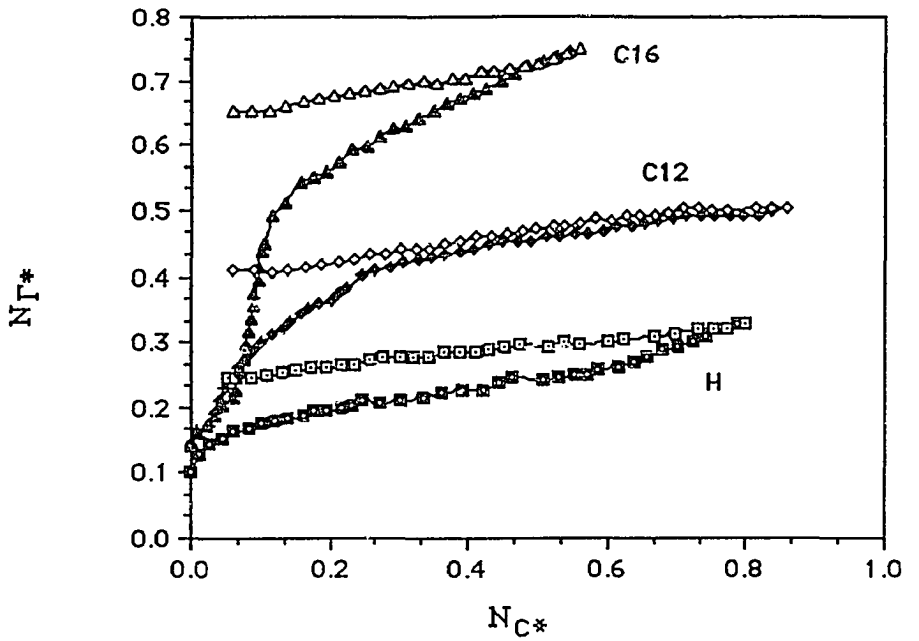

Figure 5.12: Adsorption (filled symbols) and desorption (open symbols) isotherms of model associative polymers of molecular weight 67,000 for various hydrophobic end-groups on 190 nm polystyrene latex. See Table 5.2 for operating conditions.

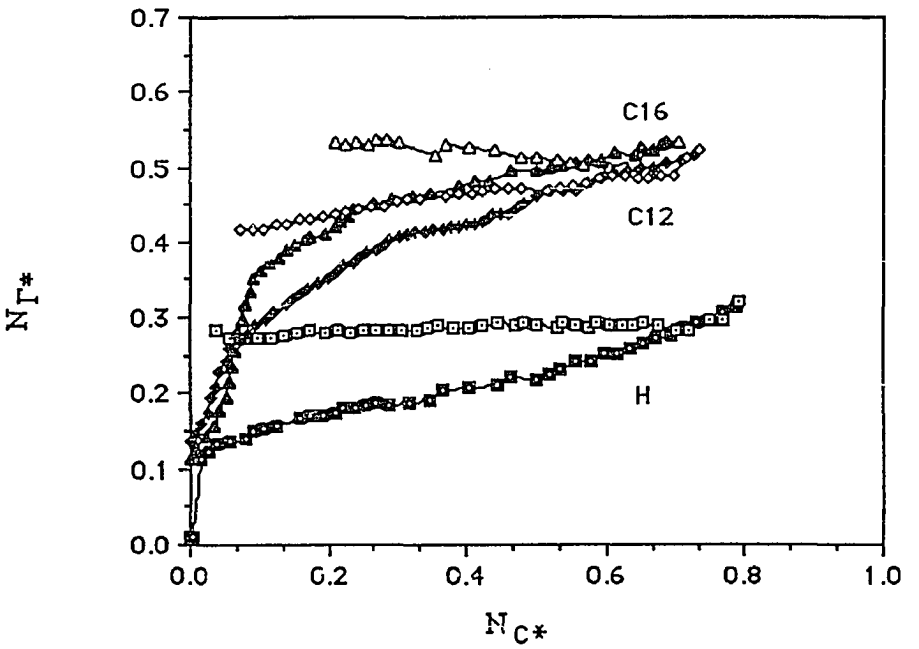

Figure 5.13: Adsorption (filled symbols) and desorption (open symbols) isotherms of model associative polymers of molecular weight 51,000 for various hydrophobic end-groups on 190 nm polystyrene latex. See Table 5.2 for operating conditions.

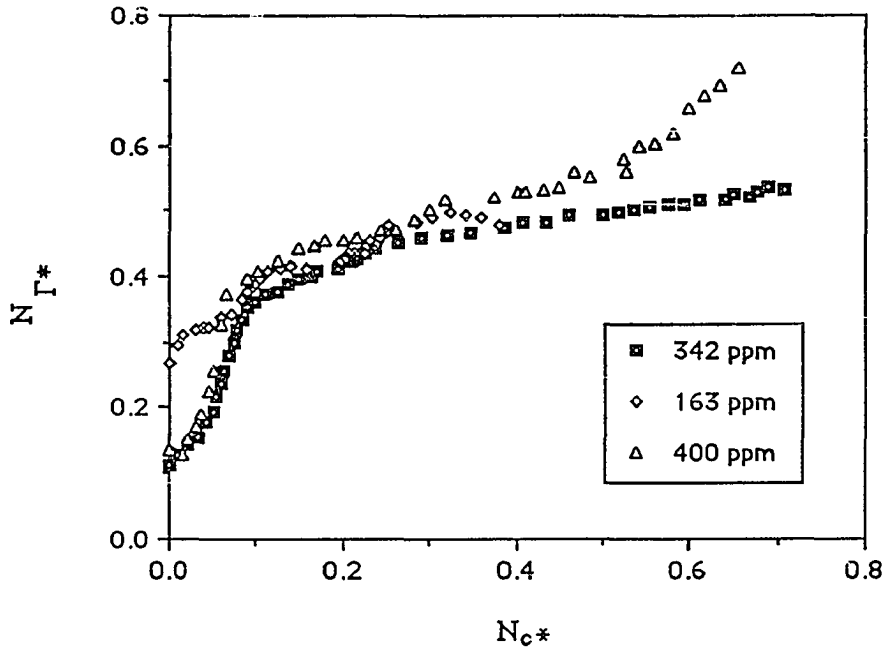

Figure 5.14: Master adsorption isotherm of model associative polymers of molecular weight 51,000 with hexadecyl end-groups on 190 nm polystyrene latex for various feed concentrations. See Table 5.2 for operating conditions, and text for a description of the reduced variables.

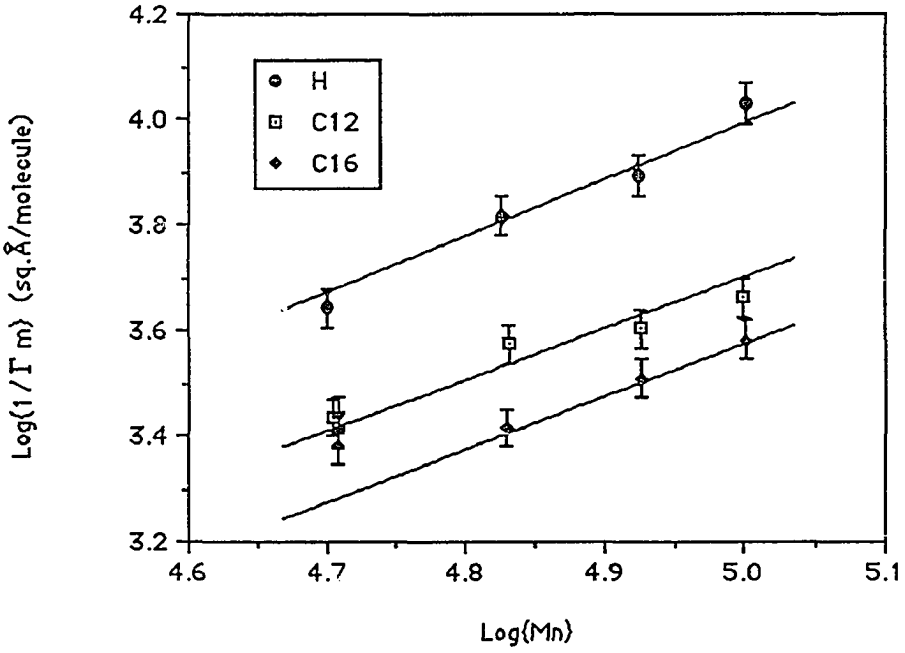

Figure 5.15: Molecular Areas of adsorption of model associative polymers of various molecular weights and hydrophobic end-groups on 190 nm polystyrene latex.

then levels off to a plateau. In contrast, the adsorption isotherms for hexadecyl terminated polymers have a sigmoidal shape, which sometimes called the Langmuir type L4 equilibrium adsorption isotherm. As the concentration of the hexadecyl terminated associative polymer in the latex serum increases, the amount of the adsorbed associative polymer increases rapidly to a plateau region, which is followed by another region in the adsorption isotherm where the adsorbed amount increases rapidly to a second plateau. The adsorption isotherms for the dodecyl terminated polymers exhibit a behavior that is intermediate between that of the hydroxyl terminated and hexadecyl terminated associative polymers.

Conformation of the Adsorbed Layer

Our model associative polymers and typical nonionic surfactants have markedly similar chemical compositions: both species have poly(oxyethylene) hydrophilic portions that are linked to an alkyl or alkylphenol hydrocarbon chain. Thus, even though the model associative polymers have molecular weights that are an order of magnitude larger than those of typical nonionic surfactants, and have two hydrophobic moieties instead of one, it is not surprising that the adsorption isotherms of the model associative polymers are qualitatively similar to those of nonionic surfactants [107]. Further, surface tension measurements [25] show that the model associative polymers have surface active properties, and may therefore be considered as a polymeric nonionic surfactant. Therefore, we can use the classical theory of the adsorption of nonionic surfactants [107] to deduce the conformation of the adsorbed layer of the model associative polymers with alkyl end- groups from their adsorption isotherms.

When the concentration of associative polymer in the latex serum is less than 30 ppm, nearly the same amount of associative polymer adsorbs irrespective of the size of the

hydrophobic end-group for a given molecular weight of the associative polymer. This is expected because the concentration of associative polymer in serum is dilute enough that polymer-polymer interactions are negligible, and individual associative polymers interact with individual latex particles. Poly(oxyethylene) adsorbs to polystyrene as loops and trains, and since the model associative polymers are composed mostly of poly(oxyethylene), they must adsorb with a similar conformation. Both hydrophobic end-groups adsorb to the same particle surface because no other hydrophobic surface or associative polymer hydrophobe is nearby due to the extremely dilute conditions. Hemker et al. [108] measured the adsorption of pyrene end-tagged poly(oxyethylene) of molecular weight 4250 and 8650 on polystyrene using excimer fluorescence. The complete disappearance of the excimer emission upon the addition of latex to the polymer solution indicated that the hydrophobic pyrene groups strongly attached themselves to the polystyrene surface. From a red shift in fluorescence emission spectra, they concluded that the tagged polymer assumed a ring-like conformation with both pyrene tags adsorbed to the latex particle surface. Apparently the gain in free energy from the adsorption of the associative polymers' alkyl end-groups compensates for the loss in configurational energy experienced by the high molecular weight backbone when both hydrophobes are pinned to the same particle surface.

As the concentration of associative polymer approaches that required to saturate the particle surface with a monolayer of polymer, the slope in the adsorption isotherm gradually decreases and the isotherm approaches the first plateau. Because the hydrophilic backbone is only weakly adsorbed, adsorption at larger associative polymer concentrations occurs by the displacement of associative polymer backbone segments from the particle surface by the alkyl hydrophobic end-groups of adjacent polymers. In addition, the driving force for networking among the associative polymer increases as the concentration of associative polymer in the latex serum increases. Both effects vertically orient an adsorbed

polymer that has hydrophobic end- groups to enhance the packing of hydrophobic groups on the particle surface, and hence, to increase the amount of adsorbed polymer. Dynamic light scattering has also measured a sudden transition in the thickness of the adsorbed layer due to a change in conformation of the adsorbed polymers at a critical associative polymer concentration [51], and Richey et al. [79] concluded from their fluorescence measurements that the associative polymer backbones stretched to facilitate tighter packing of the associative polymer hydrophobes on a latex particle surface. Even though the adsorbed polymer loses some configurational entropy upon stretching, the whole system (i.e., particles and adsorbed polymers) apparently gains more than enough free energy to compensate for this loss when the hydrophobic end- group adsorbs. Thus, the isotherm shows a sharp increase in the amount of associative polymer adsorbed to the latex as the adsorbed polymer changes from a flat conformation to a bristle-like conformation.

In hindsight, this change in the conformation of the adsorbed polymers could have been perceived from the results of the colloidal stability experiments presented in Figure 5.1; the flocculation and restabilization behavior that occur at certain minimum associative polymer concentrations can only occur if the adsorbed polymer associates with polymers in the aqueous phase. In addition, the rheology of a latex system where both hydrophobic groups are adsorbed onto the same particle surface would be Newtonian, and the viscosity of the dispersion could be calculated by considering the effect of the adsorbed layer on the effective volume fraction of the colloidal species. As shown with the rheological data presented in Chapter VI, this is definitely not the case.

Desorption Isotherms

The adsorption of multiple layers of associative polymer is one possible alternate explanation for the sudden increase in the amount of adsorbed polymer and the sigmoidal shape in the adsorption isotherm. By "multiple layers", we mean either polymers that are

retained near the particle surface, but are not actually adsorbed to it, through entanglement with polymers that are truly adsorbed [109], or the adsorption of associative polymer aggregates [104]. Because the adsorption experiment only measures the hold-up of polymer on the latex surface, and not how it is partitioned on it, the adsorption experiment cannot distinguish between polymers that are actually adsorbed from those that are simply entrapped in the adsorbed layer. Intuitively, we expect that at some large associative polymer concentration in the latex serum both entrapment of associative polymer in the adsorbed layer and the adsorption of aggregates will occur. Of course, the hydrodynamic diameter of these aggregates must be less than the pore size of the membrane because the blank experiments showed that the serum replacement cell itself did not retain associative polymer under identical experimental conditions.

The desorption experiment is an attempt to uncouple the amount of polymer that is really adsorbed to the surface from that which is trapped in the adsorbed layer. The solution rheology presented in Chapter III demonstrated that the lifetime of the dynamic association junction in the aqueous phase is on the order of fractions of seconds, and the desorption data in Figure 5.3, demonstrated that the time scale of desorption is at least an order of magnitude larger. Thus by rapidly purging the cell with distilled water, it is possible to flush out the entrapped polymer while leaving behind the truly adsorbed polymer. Here "rapidly" means that the residence time of the cleansing water is much smaller than the time scale of desorption. Because nearly half of all of the associative polymer that was introduced into the serum replacement cell has adsorbed, as calculated from the adsorption isotherm, the amount of entrapped polymer could be significant.

In practice, the desorption experiment is difficult. The adsorption phase of the experiment takes ten to twelve hours, and the desorption experiment that takes place immediately afterwards requires another twelve hours. The length of the experiment taxes the stability of the baseline, especially at night when the temperature in laboratory can drop

precipitously. Therefore, the precision of the desorption data is somewhat less than the adsorption data because the adsorption and desorption experiments are performed in series, and because any systematic errors in the the adsorption experiment propagate into the desorption experiment.

Nonetheless, the desorption experiment provides some useful results. In Figures 5.10 through 5.13, the desorption isotherms consist of two regions: a region where the desorption curve briefly follows adsorption isotherm, and a region where it approaches a plateau. The fact that the desorption isotherms partly retrace the adsorption isotherms suggests that the associative polymer that was removed from the cell during the initial part of the desorption experiment had either been entrapped in the adsorbed layer or adsorbed to the latex surface. Indeed, hydrodynamic forces during flow increase the rate of desorption of polymer from surfaces as compared to no-flow conditions [110]. However, both amounts are very small because each of the desorption isotherms approaches a plateau value, the level of which indicates nearly all of the adsorbed polymer is truly bound to the latex surface.

The hysteresis between the adsorption and desorption isotherms does not imply that the adsorption was irreversible, but only that the time scale was too small to allow desorption to take place. Cohen Stuart et al. [111] showed that the hysteresis in the adsorption/desorption isotherm is a necessary, but not sufficient, proof of irreversibility. In any event, these results show that the amount of entrapped polymer is small in the adsorption experiments described in this chapter. Thus, the adsorption isotherms have truly measured the amount of associative polymer that has adsorbed to the latex surface, and the sigmoidal shape in the adsorption isotherms for the hexadecyl terminated polymers results from a rearrangement in the conformation of the adsorbed polymer layer and not from multilayer adsorption.

Effect of Feed Stream Concentration

Another way to determine whether or not associative polymer aggregates are present in the feed stream to the serum replacement cell is to vary the concentration of associative polymer in the reservoir. Intuitively we expect that aggregates will form in the feed stream at some large associative polymer feed stream concentration. The area occupied by such on the particle surface is larger than the area occupied by a molecularly dispersed associative polymer chain; aggregates do not pack as well because of steric effects. Thus, we varied the concentration of associative polymer in the reservoir from 162 to 400 ppm while holding all other variables constant to examine the effect of the feed stream concentration of the adsorption isotherm. The resulting isotherms presented in Figure 5.14 are plotted using the dimensionless groups presented in Equation (5.9). The results fall on a master curve, which indicates that the conformation of the adsorbed polymer did not depend on the feed concentration over the range of concentration that we studied. This verifies that the adsorption number and concentration number are the appropriate dimensionless group to reduce data taken at various particle concentrations and feed stream concentration, provided that aggregates are not present. Blank experiments have shown that the data presented in this chapter meet this criterion. The isotherm that corresponds to 400 ppm reservoir concentration shows a slight increase in the amount adsorbed at larger concentrations as compared to the more dilute reservoir concentrations. This possibly indicates the beginning of interaction between polymers in the aqueous phase and those adsorbed at the particle surface. Nonetheless, the plateaus in the adsorption isotherms overlap, which means that the molecular areas of adsorption that are calculated from these three curves are the same. The existence of the master curve suggests that it is possible to combine results from several experiments to obtain a complete adsorption isotherm. For example, an experiment that uses a dilute feed stream concentration to focus on the dilute part of the isotherm may be combined with an experiment that uses more

concentrated solution to focus on the behavior of isotherm at larger concentrations. If we wish to examine the adsorption behavior of associative polymer aggregates, we would need to use very large sized particles so that the pore size of the membrane could be large. Then the experiment may be conducted under conditions where large aggregates are present in the latex serum, and can pass through the pores of the membrane.

Molecular Areas of Adsorption

The free energy of adsorption, which measures the strength of interaction between the adsorbed polymer and the latex particle, and the area occupied by a single polymer chain on a latex particle's surface, are two key parameters that are calculated from an adsorption isotherm. Figure 5.15 presents the molecular areas of adsorption that are calculated from the plateaus in the adsorption isotherms presented in Figures 5.10 through 5.13. The molecular areas of adsorption are large, between 2000-11,000 $Å^2$/molecule, and increase as the length of the thickener backbone increases; these results indicate that the polymer conformation on the surface probably consists of loops and trains with many points of contact between the adsorbed associative polymer and the latex particle surface. The molecular areas of adsorption decrease as the length of the alkyl end- group increases, which indicates that the adsorption of the alkyl end- group promotes tighter packing of the entire associative polymer on the latex particle. This is due to the gain in free energy experienced by the total latex system when the aqueous phase excludes the alkyl end- group to the latex particle surface. The zeroth order approximation for the conformation of the adsorbed associative polymer assumes that the adsorbed polymer chain occupies a cylinder that has a cross sectional area that equals the molecular area of adsorption and a height that equals the hydrodynamic thickness of the adsorbed layer. As calculated from the intrinsic viscosity measurements of Chapter II, the hydrodynamic volume of the associative polymer in dilute solution scales with molecular weight as $V_{hydro} = M[\eta] \sim M^{1.6}$. In Figure 5.15,

the molecular areas of adsorption scale roughly as molecular weight to the first power. Thus, the hydrodynamic thickness of the adsorbed layer should depend on molecular weight to the 0.6 power, which has been confirmed with dynamic light scattering measurements [51]. From the molecular area of adsorption of the hexadecyl terminated model associative polymer with a molecular weight of 67,700 presented in Figure 5.15, we calculate that an associative polymer concentration of 1.4 weight percent in the latex serum is required to fully cover a 190 nm polystyrene latex of 10% solids content. This coincides with the concentration of associative polymer in Figure 5.1 that restabilizes the latex. A similar calculation for an associative polymer with a molecular weight of 51,000 and with hexadecyl hydrophobes shows that a concentration of 1.2 weight percent of the associative polymer is required to fully cover a 180 nm polystyrene latex of 9.4% solids content. This concentration coincides with the critical concentration of associative polymer in Figure 5.2 that restabilizes the latex.

The free energy of adsorption is usually calculated by fitting experimentally measured adsorption data to a model. The classical analysis for nonionic surfactants uses the Langmuir model, where the initial slope of the adsorption isotherm measures an equilibrium constant K that governs the partitioning of the solute between the surface phase and the bulk phase [112]. The standard molar free energy of adsorption $\Delta\mu^o$ is related to this equilibrium constant through:

$$\Delta\mu^o = -RT\,Ln(K) \qquad (5.10)$$

where R is the gas constant and T is the absolute temperature in degrees Kelvin. As deduced from the large molecular areas of adsorption in Figure 5.15, the model associative polymers adsorb to latex particles through many contact points with the surface. The strength of the individual contact point must be on the order of a few kT because the

polymers adsorb reversibly, even if the desorption takes many days (Figure 5.3). Because the adsorption isotherms for associative polymers with the alkyl end-groups do not follow the simple Langmuir model, it is not possible to uncouple the relative contributions of the polymer backbone and alkyl end-groups to the free energy of adsorption from the initial slope of the adsorption isotherm. This calculation will require a more sophisticated theory that considers the entire adsorption isotherm. Having not yet developed such a theory, we are limited to an order of magnitude estimate of the free energy of adsorption via the classical analysis as applied to the adsorption isotherms of the hydroxyl terminated polymers. Because the initial slopes of the adsorption isotherms of model polymers with alkyl end-groups are slightly larger than for those of the hydroxyl terminated polymer, the free energy of adsorption for the polymers with alkyl end-groups is slightly larger than for the hydroxyl terminated polymer, and therefore, the hydrophobic alkyl end-groups must contribute to the overall free energy of adsorption. The standard molar free energy of adsorption of the hydroxyl terminated polymers as measured by this analysis is 30 to 40 KJ/mole, which is similar in magnitude to those of conventional poly(oxyethylene) based surfactants.

To examine the influence that the curvature of the latex particle's surface exerts on adsorption, we measured the adsorption isotherms of associative polymer on a 1100 nm latex. Direct comparison of isotherms obtained with the 1100 nm latex (Figures 5.16 through 5.19) to isotherms obtained with the 190 nm latex (Figures 5.10 through 5.13) reveals that the mass of adsorbed associative polymer decreases as particle size increases, and that the isotherms depend on associative polymer molecular weight and alkyl end-group length in the same way for both particle sizes. Increasing the size of the latex particle suppresses the transition in the adsorption isotherms of the hexadecyl terminated polymers that corresponds to the change in the conformation of the adsorbed layer. This is expected because flat latex surfaces promote the adsorption of trains [106]. This precludes the

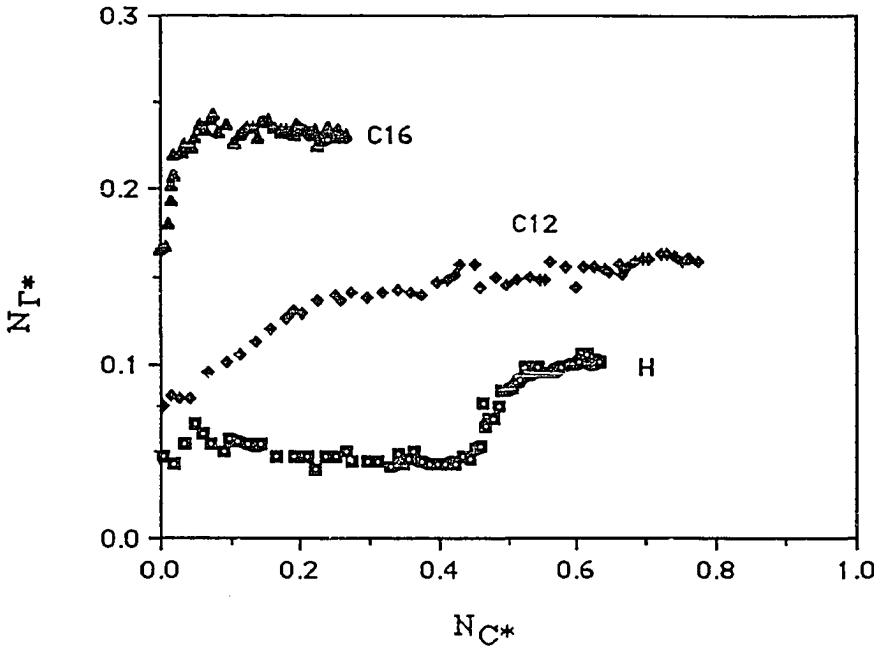

Figure 5.16: Adsorption isotherms of model associative polymers of molecular weight 100,000 for various hydrophobic end-groups on 1100 nm polystyrene latex. See Table 5.3 for operating conditions.

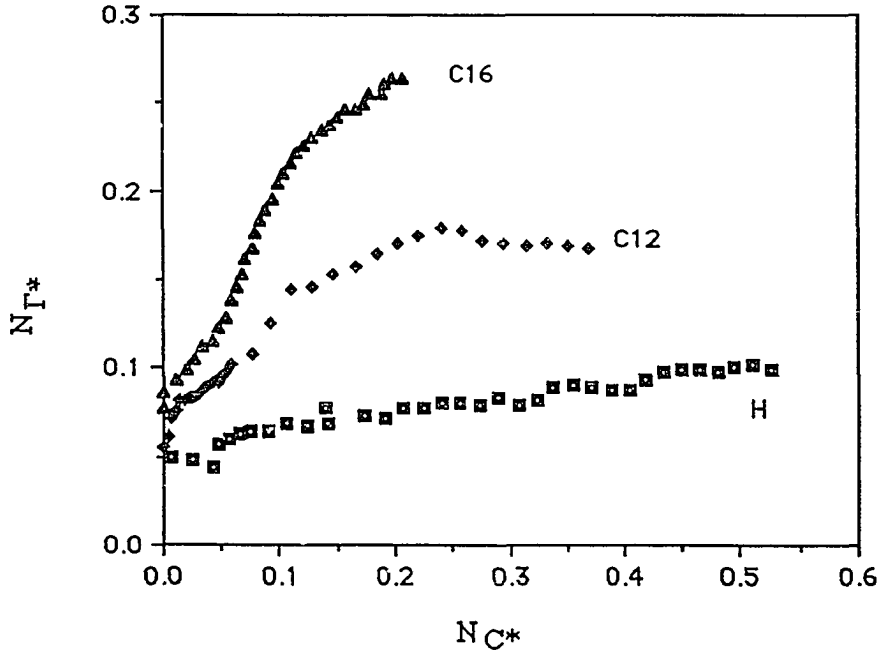

Figure 5.17: Adsorption isotherms of model associative polymers of molecular weight 84,500 for various hydrophobic end-groups on 1100 nm polystyrene latex. See Table 5.3 for operating conditions.

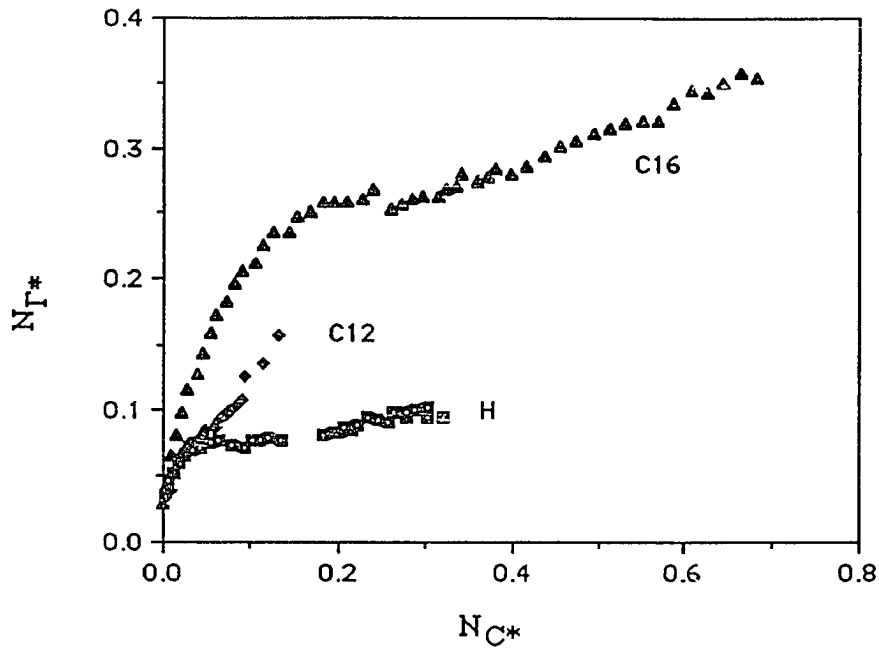

Figure 5.18: Adsorption isotherms of model associative polymers of molecular weight 67,000 for various hydrophobic end-groups on 1100 nm polystyrene latex. See Table 5.3 for operating conditions.

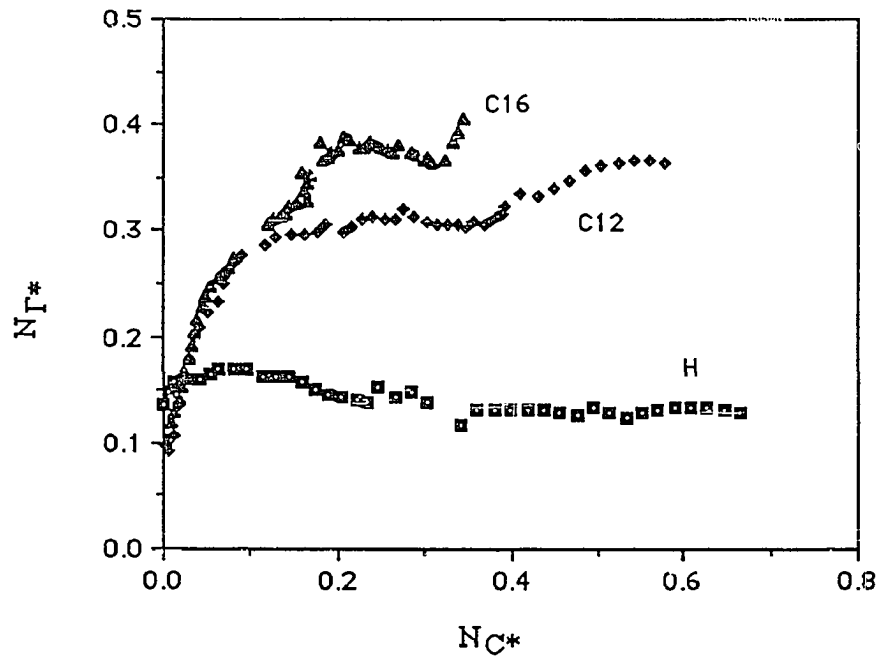

Figure 5.19: Adsorption isotherms of model associative polymers of molecular weight 51,000 for various hydrophobic end-groups on 1100 nm polystyrene latex. See Table 5.3 for operating conditions.

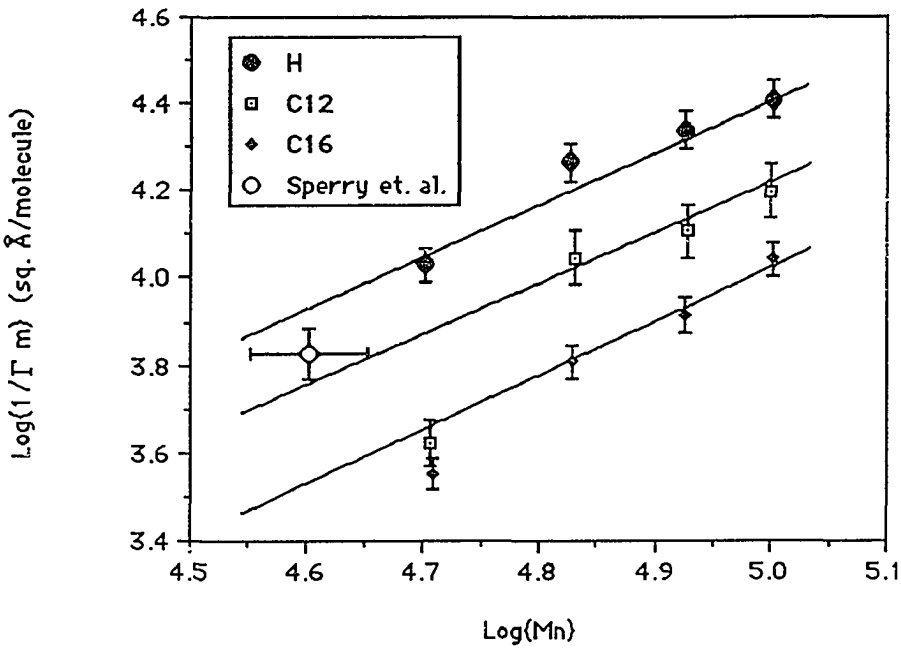

Figure 5.20: Molecular Areas of adsorption of model associative polymers of various molecular weights and hydrophobic end-groups on 1100 nm polystyrene latex.

adsorption of "tail" segments to aid the associative polymer backbone in its competition against alkyl end-groups for the latex surface. Also, the associative polymer backbone must bend more to adsorb onto a small diameter latex particle. This loss in configurational entropy should favor the adsorption of the alkyl end- groups over the backbone on smaller sized particles. These effects are reflected in the molecular areas of adsorption of the model associative polymers on the 1100 nm latex: they are roughly two and one half times larger than on the 190 nm latex. These results are consistent with the molecular area of adsorption calculated from the data by Sperry et al. [19], which is plotted on Figure 20 for comparison. Thus, the adsorbed layer flattens and does not extend as far out into solution when on a large diameter latex particle. This has been confirmed from preliminary dynamic light scattering measurements of the thickness of the adsorbed layer [51]. In agreement with the data of Sperry et al.[19], the initial slopes of the isotherms obtained with the 1100

nm latex are slightly smaller than those obtained with the 190 nm latex, which indicates that the strength of adsorption decreases as particle size increases. The effect of latex particle size on the adsorption behavior of the model associative polymers is consistent with the generally accepted conclusion that the interaction between latex particles and associative polymers increases as latex particle size decreases.

Conclusions

In this chapter, we have examined the adsorption of model associative polymers to well characterized and cleaned polystyrene latex surfaces. A cynic, who might not realize the value of these experiments, might point out that other factors will influence the adsorption of associative polymers when it takes place in the presence of surfactants and cosolvents. For example, a strongly adsorbed surfactant could convert a hydrophobic surface into a hydrophilic surface if the surfactant is bound more strongly to the surface. This, and competitive adsorption with the surfactant, will most certainly influence the adsorption of the associative polymer. Likewise, decreasing the polarity of the solvent by the addition of a water miscible cosolvent would favor displacement of the alkyl chains or adsorption of the hydrophilic portion of the associative polymer. Such effects were studied by Sperry et al. [19]. Karunasena et al. [52] concluded that there are so many variables in a coatings formulation that no mechanism of adsorption of the associative polymer may be universal. We heartily agree, and this very fact mandates that control experiments, where the adsorption of associative polymer takes place unencumbered by the presence of a surfactant or cosolvent, must be performed. In this way, the effect of surfactants and cosolvents can then be studied in a systematic and truly scientific manner.

Figures 5.21 through 5.24 summarize what the data in this chapter reveal about the mechanism of interaction between polystyrene latex particles and associative polymers.

Figure 5.21 depicts how the conformation of the adsorbed polymers depends on concentration. At low concentrations, where the associative polymers do not network in the latex serum, the single associative polymer chain approaches and adsorbs to a latex particle. (first panel) If the associative polymer has alkyl end-groups, both of these end-groups adsorb to the latex particle surface. The associative polymer backbone adsorbs as loops and trains on surface with many points of contact between the associative polymer backbone and the particle surface. As more polymers are added to the system, adsorption continues in this manner (second panel) until the surface begins to saturate. (third panel) Because the entire polymer/latex system gains more energetically when the alkyl hydrophobe is adsorbed than when than the poly(oxyethylene) backbone is adsorbed, a competition between the previously adsorbed backbone segments and the alkyl end-groups of the newly added associative polymer results. The alkyl end-groups win, (fourth panel) and hydrophobes adsorb at the expense of backbone segments. Expulsion of hydrophobes from the latex serum drives both the adsorption and aqueous phase networking. Thus, the associative polymers in solution tend to interact with the free hydrophobes on an adsorbed associative polymer. These effects cause the adsorbed polymer to orient such that it is more stretched to extend out into solution. (Fifth panel.) This permits greater packing of the associative polymers, which decreases the molecular area of adsorption as the length of the alkyl end-group increases, and causes an increase in the thickness of the adsorbed layer, as measured from dynamic light scattering. (Figure 5.22)

At larger concentrations, the associative polymer networks in the aqueous phase to produce a homogeneous network of associative polymer and latex particles. (Figure 5.23) In this figure, the associative polymer concentration exceeds that required to fully saturate the particle surface. Primarily through the hydrophobic junctions, the latex particles are connected to the dynamic associative polymer network in the aqueous phase, which was described in detail in Chapter III. The rheological data of Chapter VI, and the colloidal

stability data of this chapter, indicate that loops of associative polymer that have both hydrophobes adsorbed to the same surface are not favored when the associative polymer concentrations in the latex serum is large. A decrease in particle size favors the adsorption of the alkyl end-groups hydrophobes, and they compete more effectively with previously adsorbed associative polymer backbones. This intensifies the interaction between the latex particles and the associative polymer so that more associative polymer adsorbs, and the molecular area of adsorption decreases. (Figure 5.24) This increase in the intensity of interaction between associative polymers and latex particles as the particle size decreases has been known for some time.

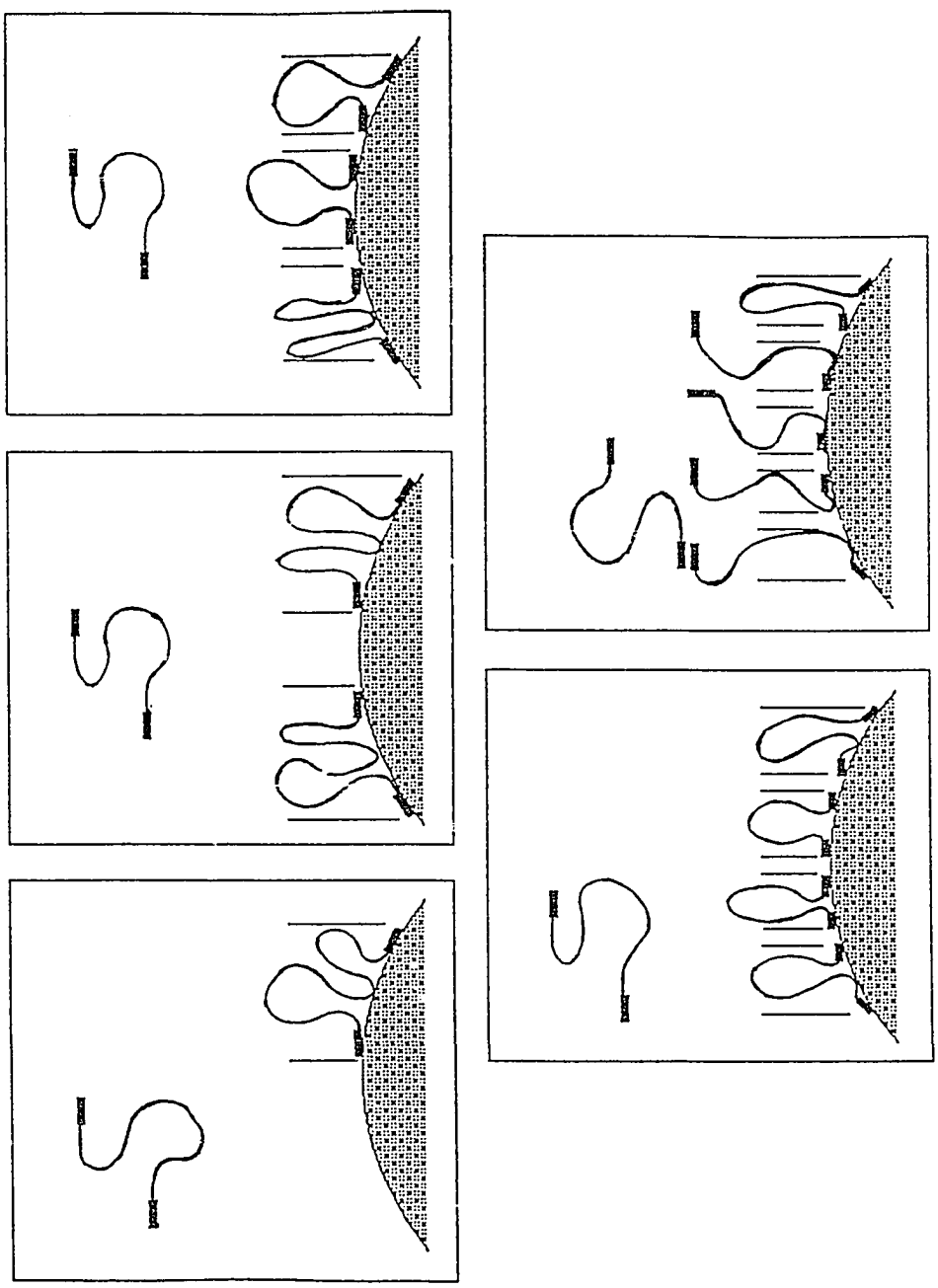

Figure 5.21: Schematic diagram of the dependence of the conformation of adsorption on associative polymer concentration in the latex serum.

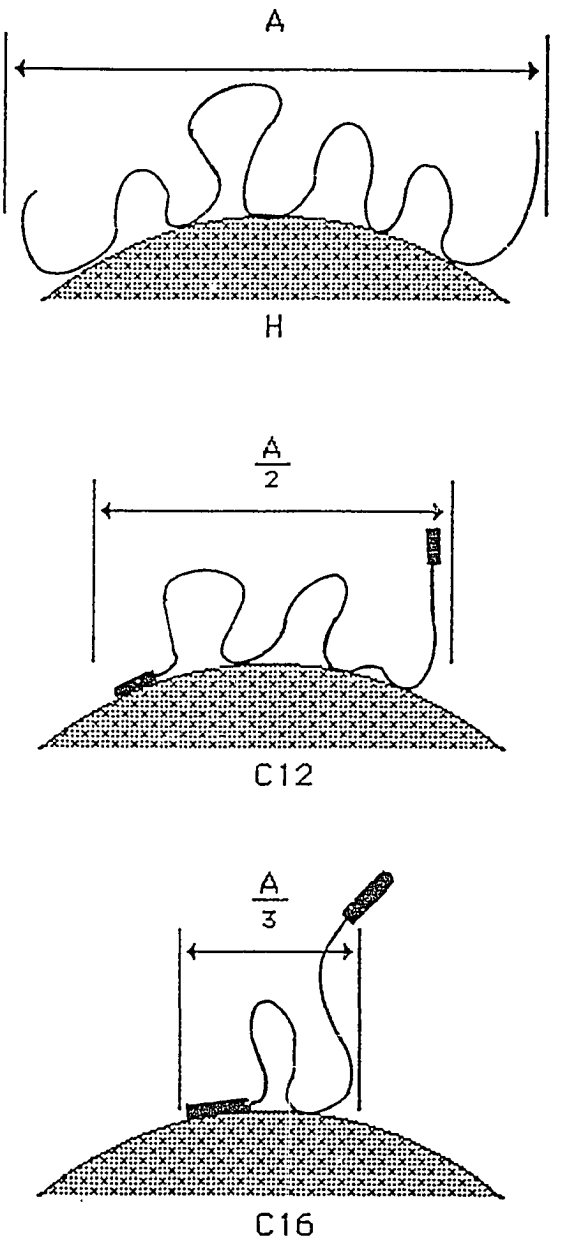

Figure 5.22: Schematic diagram depicting the influence of hydrophobic end-group length on the conformation of the adsorbed layer.

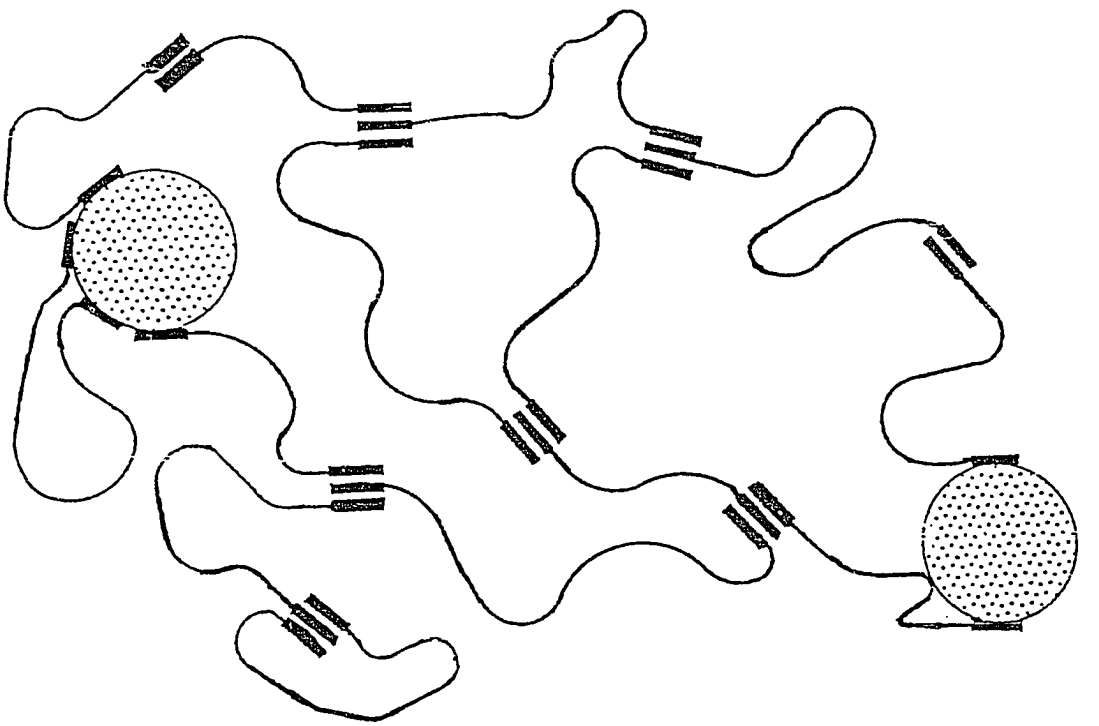

Figure 5.23: Schematic diagram depicting the homogeneous network formed by associative polymer and latex particles once the associative polymer concentration is large enough to saturate the latex surface.

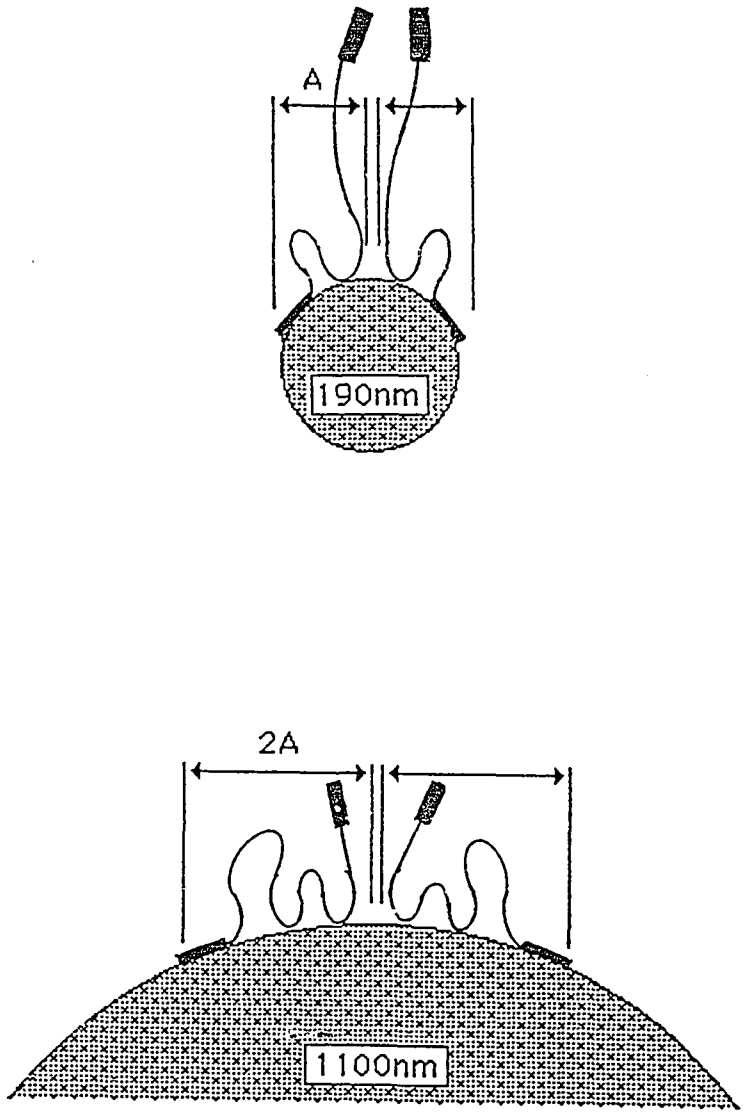

Figure 5.24: Schematic diagram depicting the influence of latex particle size on the conformation of the adsorbed layer.

Chapter VI

Rheology of Latex Dispersions That Contain Model Associative Polymers, Surfactants, and Cosolvents

Introduction

Motivation

Commercial latex paints contain a befuddling number of formulation ingredients, and they all interact simultaneously to make the prediction of coatings rheology based on formulation extremely difficult. Our goal has been to gain insight into some of the more fundamental aspects of the association mechanism in latex dispersions; something that previous studies have shown is difficult to do with fully formulated coatings (see Chapter I). So we have examined "stripped- down" systems that contain some of the more essential ingredients found in a latex paint, such as latex particles, associative polymers, surfactants, and coalescing aids. We realize that we have not yet addressed all of the perturbations that are possible in latex paint formulation; that is not our intent. We hope that these studies will help reveal some fundamental features of the association mechanism, and establish a level of understanding that will pave the way for future studies in our research group on much more complicated systems.

Thus, our model latex systems use monodisperse polystyrene latexes, even though commercial paint formulations use vinyl acrylic, acrylate, or styrene- butadiene based latexes. Our reason for using the polystyrene surfaces is that they are so well characterized they have become recognized as "standard" surfaces. And although many kinds of anionic and nonionic surfactants are used in paint formulations, we use sodium dodecyl sulfate as a model surfactant to highlight interactions among associative polymers, latex and surfactant. The interaction of sodium dodecyl sulfate with the polystyrene latexes has also been well

characterized [101], and we have studied the adsorption of the model associative polymer on these surfaces in Chapter V. Along the same lines of reasoning, we use Butyl Carbitol, a diethylene glycol monobutyl ether, as a model coalescing aid and formulation cosolvent. As indicated in a later section of this chapter, Butyl Carbitol is one of the most effective cosolvents in altering the viscosity of an associative polymer solution.

Previous Research

An intimate connection exists between the adsorption of associative polymers and the rheology and stability of latex systems that contain associative polymer. Sperry et al. [9, 15, 19] examined the strong influence that surfactants and cosolvents exert on the interrelations among these properties. They used laboratory thickeners that modelled commercialized associative polymers: an anionic acrylate copolymer of molecular weight of 400,000, and a nonionic polyurethane based on ethylene oxide of molecular weight of 40,000 with dodecyl end-groups. They related the effect that surfactants and cosolvents had on adsorption of the model thickeners on butyl acrylate/ methyl methacrylate latexes of particle diameters ranging from 50 to 600 nm to changes that these agents produced in low shear viscosities of latexes containing associative polymer. We take special note of the results from their nonionic associative polymer because its molecular structure is much like the structure of one of our own model thickeners.

They measured the adsorption isotherms of the model thickeners on latexes of 25% solids by volume by centrifugation, followed by colorimetric titration of the serum for free thickener. They found that their nonionic polyurethane thickener adsorbed more strongly than any of the other thickeners, and that the amount of thickener adsorbed increased rapidly as particle diameter decreased (like the data presented in Chapter V). Sodium dodecyl sulfate does desorb the nonionic associative polymer, but complete desorption of the associative polymer does not occur until the concentration of sodium dodecyl sulfate

that was added to the latexes exceeds the surfactants' critical micellar concentration (CMC). In addition, the amount of sodium dodecyl sulfate required to desorb the nonionic associative polymer increased as the particle size decreased [15]. These results indicate the nonionic associative polymer can compete effectively with the surfactant for the particle surface, and that the strength of the binding between the associative polymer and the latex surface increases as the particle size of the latex decreases. Likewise, Butyl Carbitol causes the desorption of the associative polymer from the latex. However, the concentration of Butyl Carbitol in the dispersion medium required to desorb one weight percent of the nonionic thickener from a latex of twenty five percent solids, based on volume, exceeds 10 weight percent.

Sperry et al. [19] used microscopy to determine the influence of sodium dodecyl sulfate on the flocculation phase diagrams of latexes that contained nonionic associative polymer. The microscopy revealed that low levels of surfactant or associative polymer in the latex (less than about 0.5% thickener and less than 1 CMC of sodium dodecyl sulfate in a 25 volume % solids 300 nm latex) gave rise to bridging flocculation. Larger amounts of either surfactant or associative polymer restabilized the latex, and produced an "infinite floc" (i.e., a homogeneous network of associative polymer, surfactant and latex particles). For sodium dodecyl sulfate concentrations that exceeded 2 CMCs of the surfactant, the latexes flocculated via a volume restriction mechanism, which Sperry et al. attributed to desorption of the associative polymer from the latex surface by the surfactant. Likewise, a small amount of sodium dodecyl sulfate produced yields stresses in the viscosity profiles of latexes thickened with associative polymers. Sperry et al. attributed this to depletion flocculation, and concluded that the latex - thickener interaction dominated the rheological behavior of latexes thickened with associative polymers.

Nonetheless, surfactants can interact with associative polymer in the dispersion medium (in addition to the interaction at the latex particle surface) to influence the

rheological properties of the dispersion, and this is sometimes manifested as a change in the viscosity of associative polymer solutions upon the addition of a surfactant. The associative polymer can participate in micelle - like associations because the monomeric free surfactant helps the associative polymer to approach its CMC in solution, and the viscosity of the associative polymer can increase or decrease, depending on the structure of the associative polymer and surfactant, and on their concentrations [11].

It is not yet clear whether or not surfactant micelles are needed to produce this increase in solution viscosity. Some investigators have found that viscosity of an associative polymer solution increases to a maximum at a surfactant concentration near the CMC of the neat surfactant, and then decreases as the concentration of surfactant increases. For example, Sau and Landoll [12] examined the solution properties of a hydrophobically modified hydroxyethylcellulose in aqueous and anionic and nonionic surfactant systems. They attributed a maximum in solution viscosity at a sodium dodecyl sulfate concentration of just below the CMC of the sodium dodecyl sulfate to the participation of the hydrophobe of the modified cellulose surfactant micelles. Similarly, Glass and his co- workers also observed a maximum in the viscosity of acrylate and acrylic latexes thickened with commercial associative polymers [113, 114], and they likewise attributed the maximum in the viscosity of the latex to the participation of the associative polymer in surfactant micelles. Lundberg et al. [67] studied the effect of an anionic surfactant and a nonionic surfactant on viscosity and viscoelastic properties of solutions and methylmethacrylate / methacrylic acid latexes that contained one of the following four hydrophobically modified urethane-ethoxylate model associative polymers: a linear polymer of molecular weight between 8700 to 24000 with either octyl, dodecyl, or nonylphenol hydrophobic end-groups, or a trimer with a molecular weight of 10500 and with nonylphenol hydrophobic end-groups. They observed that the concentration of either an anionic or nonionic surfactant that was required to produce the maximum in solution

viscosity could be near the CMC of the neat surfactant, or much greater, depending on the particular surfactant being studied. So, even though the exact nature of the interaction between surfactants and associative polymers in solution is not yet completely understood, it can influence the rheology of solutions and dispersions that contain associative polymer. Some aspects of these effects both agree with and contradict our data, as we discuss more fully later in this chapter.

The previous paragraph suggests that the aqueous phase network can have a larger influence on the rheological properties of latexes than was previously thought. Sperry et al. [9, 15, 19] interpreted the viscosity profiles of their latexes, which contained enough surfactant and associative polymer to provide a homogeneous network, in terms of the desorption of associative polymer from the latex, and the break up of the network , under shear. This is a reasonable conclusion as drawn from the rheological data. However, Richey et al. [79] later showed with their fluorescence technique that the shear - thinning region of the viscosity profiles of latexes that contained their pyrene terminated poly(oxyethylene) began before shear forces changed the aggregation number of the network junctions. This suggests that the shear - thinning results from some other kind of mechanism than the desorption of associative polymer from the latex under shear. As we showed with our statistical mechanical network model in Chapter IV, it is possible to have shear - thinning in the viscosity profile while holding the number of network junctions constant. The shear - thinning results from a change in the hydrodynamic resistance of the polymer chains in the network as it extended under shear, and is a natural consequence of the non - Gaussian statistics obeyed by extended chains in the network. In other words, the non- Gaussian chain statistics lead to the non - affine deformation of the network, which we called "slipping" in Chapter IV, and this produces shear - thinning in the viscosity profile.

In this chapter, we provide ample evidence that a homogeneous network of latex and associative polymer has a rheology that is analogous to that of an associative polymer solution, including the shear- thickening and shear- thinning regions in the steady shear viscosity profiles. (In fact, shear- thickening can also be observed in the viscosity profiles presented by Sperry et al. for latexes that contained their nonionic thickener, although they did not comment on this feature of the viscosity profile.) Thus, both the shear - thickening and the independence of the state of aggregation of the network junction in latex systems under moderate shear are not surprising to us, and reinforce the utility of our statistical mechanical network model.

Experimental Detail

This chapter examines the rheological properties of latex systems that contain associative polymer, surfactant, and cosolvents. Table 2.1 summarized the structure of the model associative polymers, and Chapter III described the rheological properties of concentrated associative polymer solutions. Five weight percent stock solutions of the model associative polymer were made by the procedure outlined in Appendix B, and hydroquinone was added to the stock solutions to prevent chemical degradation of the poly(oxyethylene) backbone of the model polymers. All latex and associative polymer concentrations reported in this chapter are by weight. The monodisperse polystyrene latexes (LS-1101A and LS–1121B; Dow Chemical Company) have particle diameters of 180 nm and 324 nm, and Table 5.1 lists the surface charge densities of these latexes. Sodium dodecyl sulfate anionic surfactant (Texapon L-100®; Henkel Corporation), and a diethylene glycol monobutyl ether water miscible cosolvent (Butyl Carbitol® ; Union Carbide Corporation) were used as supplied. Because sodium dodecyl sulfate hydrolyzes in aqueous solution to form dodecyl alcohol [115], only fresh solutions of sodium dodecyl

sulfate were used. Samples that contained both associative polymer and latex were made by mixing the associative polymer stock solution with latex and other ingredients simultaneously, and allowing the mixture to equilibrate for at least a two week period before measurement. The mixture was gently stirred frequently during this period to ensure that a homogeneous mixture formed; the stirring was not strong enough to flocculate the dispersion.

We cleaned the latexes for use in the rheological experiments by dialysis because the preparation of latex systems that contain model associative polymer in concentrations of 1 to 2.5% from stock solutions of 5% requires latex stock dispersions of at least 35% solids content or higher. The latexes were dialyzed for at least six weeks against a water medium that was changed daily. The dialysis procedure cleaned the latexes fairly well, as evidenced by the diffraction patterns produced by the cleaned latex, and by the rheological properties of the cleaned latex (see below). Admittedly, some surfactant or electrolyte may have remained bound to the particle surfaces after the dialysis procedure, but the alternative of cleaning the latexes by serum replacement or ion exchange, which involves diluting the latexes to 2% solids content and reconcentrating the latexes to 35% solids content, would have required more work than the resulting improvement in sample purity warranted.

Rheological measurements made on the model latex systems described in this chapter follow the procedure outlined in Chapter III. Unless otherwise noted, all measurements were made at 24.5°C. The viscoelastic characterizations of the latex systems were made in the linear regime; surfactants and cosolvents did not affect the linearity of the strain sweep.

Results and Discussion

Rheological Properties of Cleaned Latexes

Figures 6.1 through 6.3 show the shear - thinning viscosity profiles and the strain dependent viscoelastic properties that are typical of the cleaned latexes. As expected, the viscosity of the latex increases as the fraction of latex particles in the dispersion increases, and a transition from a Newtonian rheology to a shear - thinning rheology is observed. The dependence in the viscosity on latex concentration is greater than that predicted by Einstein's equation due to electroviscous effects. The apparent shear thickening observed in the viscosity profile of the 4.2% solids content latex shown in Figure 6.1 is an experimental artifact that results from the formation of Taylor instabilities under the cone in the Mooney-Couette shear geometry on the Bohlin VOR rheometer. This phenomenon severally limits the range of shear rates available to the Bohlin VOR rheometer for viscosity

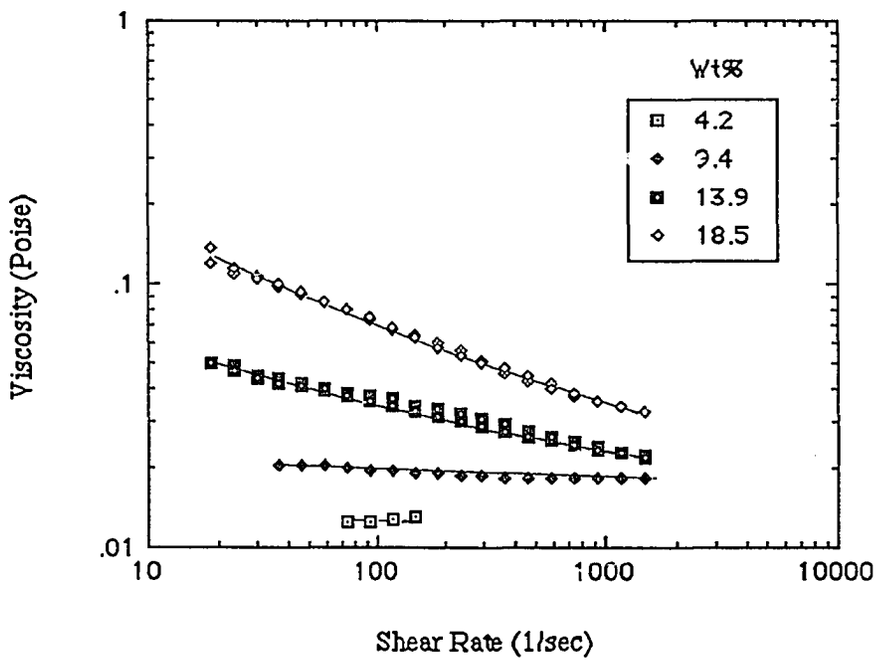

Figure 6.1: Steady shear viscosity profiles of cleaned 180 nm diameter particle size monodisperse polystyrene latexes of various solids content.

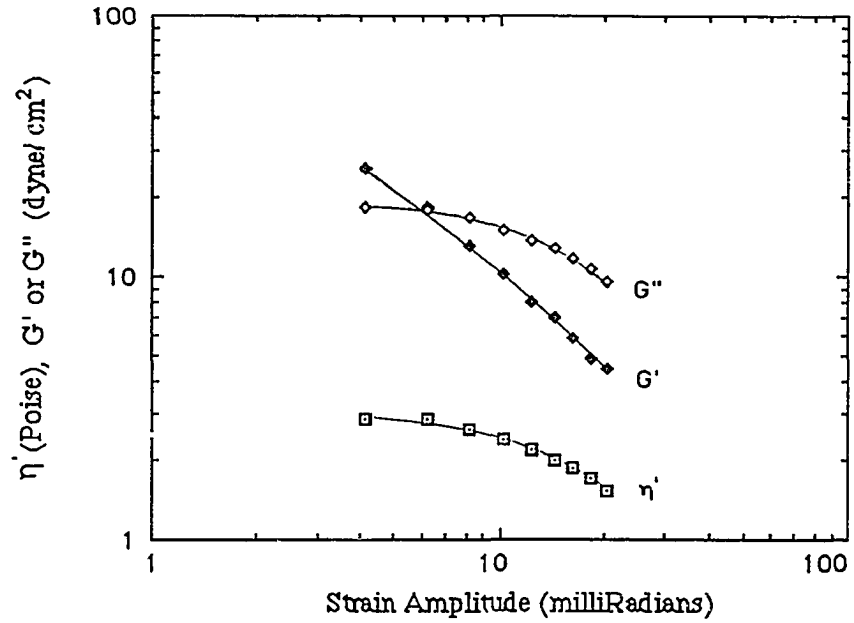

Figure 6.2: Strain sweep at 1 Hertz of a cleaned monodisperse 180 nm particle diameter polystyrene latex of 18.5% solids content.

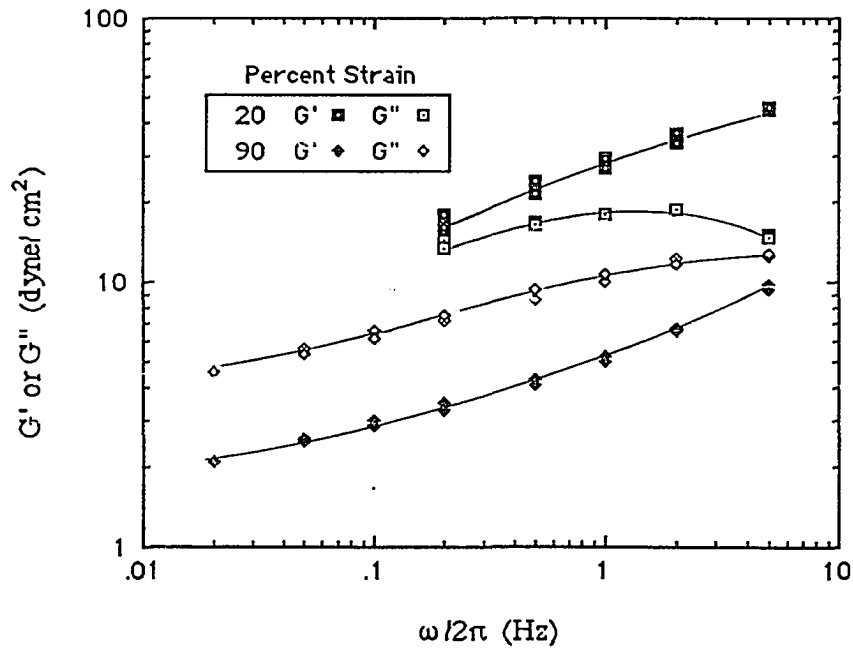

Figure 6.3: Strain dependent shear moduli of a cleaned monodisperse 180 nm particle diameter polystyrene latex of 18.5% solids content.

measurements of dilute latexes, or any other fluid with a very low kinematic viscosity, and should not be interpreted as shear induced coagulation of the latexes. Figures 6.2 and 6.3 show the strain and frequency dependencies of the linear viscoelastic properties of a cleaned latex, respectively. At small strains, a weak structure exists in the latex, and the storage modulus (G') of the latex is larger than its loss modulus (G"). This viscoelasticity is reflected in the frequency dependence of the complex shear moduli (Figure 6.3), where the moduli obtained at 20% strain exhibit a characteristic relaxation time. (100% strain equals an oscillation amplitude of twenty milliradians.) The storage modulus (G') decreases as strain increases because large strains disrupt the weak structure. The frequency dependence of the shear moduli obtained at larger strains (for example, 90%) are typical of a viscous dispersion. This rheological behavior indicated that dialysis had cleaned the latexes enough so that electrostatic repulsive forces between the particles could produce a weakly viscoelastic structure.

Interactions Between Associative Polymer and Latex

Influence of Hydrophobe Type

Figure 6.4 displays viscosity profiles that are typical of 4.2% and 9.4% solids content latexes that contain the hydroxyl terminated model associative polymer. The thickened latexes exhibit Newtonian flow, which is expected because of the Newtonian flow behavior of the individual components. The ratio of the viscosity of a dispersion that contains model polymer to the viscosity of dispersion that does not measures the relative enhancement of the viscosity of the dispersion by the polymer. Although adding the model polymer increases the viscosity of aqueous dispersion medium, the relative enhancement of the dispersion viscosity is nearly the same for both latex concentrations, and nearly equals

the relative viscosity of the polymer solution (4.0 for the solution, 3.7 for 4.2% latex, and 3.9 for 9.4% latex). As shown in Chapter V, polymers without hydrophobes do adsorb to latex particles, but the influence of this adsorption on the dispersion viscosity is small. Such effects might have included an increase in viscosity through an increase in the effective particle volume fraction; or a decrease in viscosity by a depletion of the polymer in the dispersion medium; or a decrease in viscosity due to a change in the size of the electrical double layer. Thus, polymer – polymer or polymer – particle interactions for the hydroxyl terminated polymers have little effect on rheology, and the thickened latexes behave as a suspension of particles in a viscous Newtonian medium. The rheological

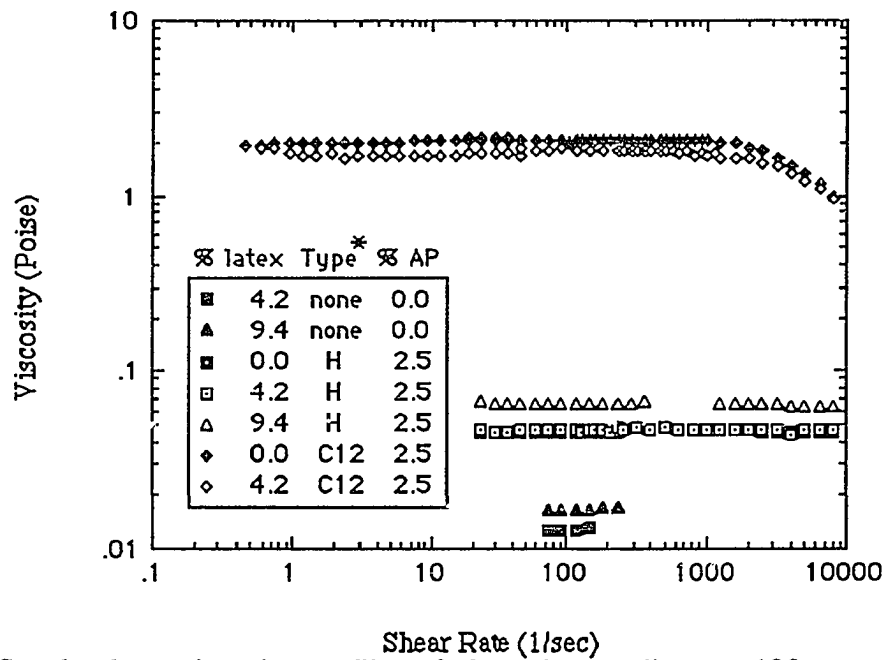

Figure 6.4: Steady shear viscosity profiles of cleaned monodisperse 180 nm particle diameter polystyrene latex of various solids content that contain model associative polymers of 51,000 number average molecular weight. * Type denotes associative polymer end-group.

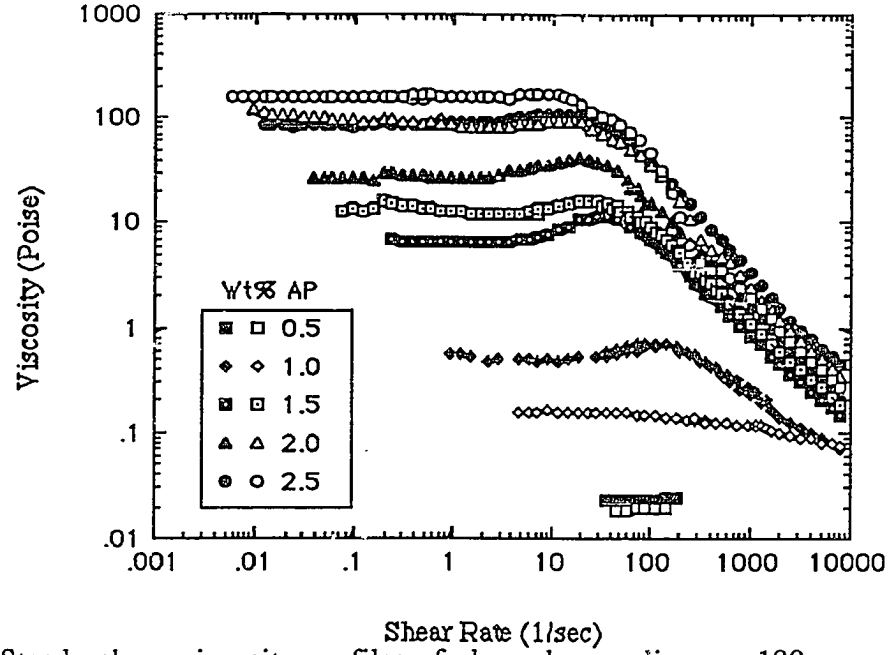

Figure 6.5: Steady shear viscosity profiles of cleaned monodisperse 180 nm particle diameter polystyrene latexes of 4.2% solids content that contain hexadecyl terminated model associative polymers of 51,000 number average molecular weight. Closed and open symbols denote solutions and latexes that contain associative polymer, respectively.

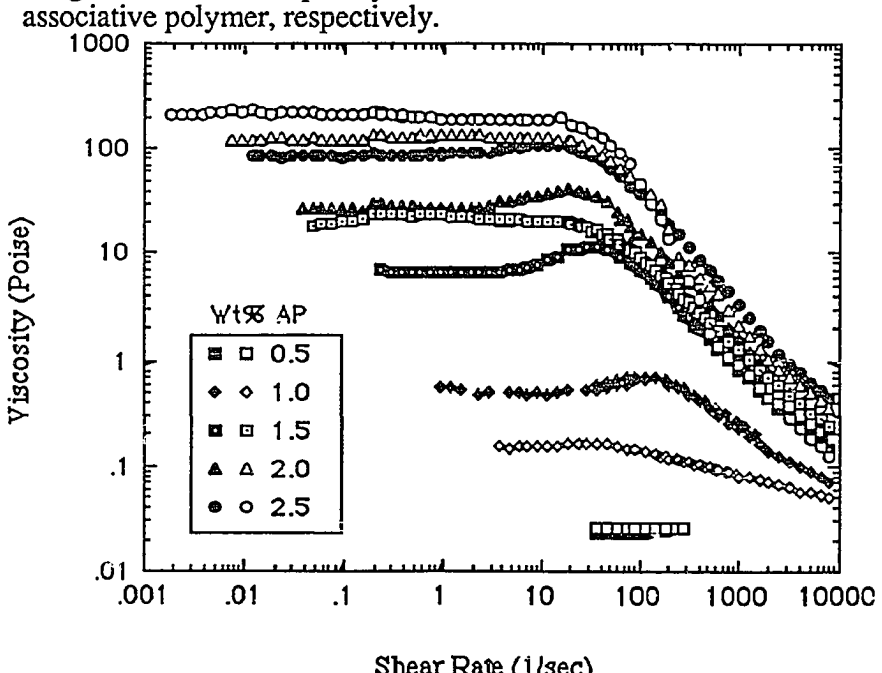

Figure 6.6: Steady shear viscosity profiles of cleaned monodisperse 180 nm particle diameter polystyrene latexes of 9.4% solids content that contain hexadecyl terminated model associative polymers of 51,000 number average molecular weight. Closed and open symbols denote solutions and latexes that contain associative polymer, respectively.

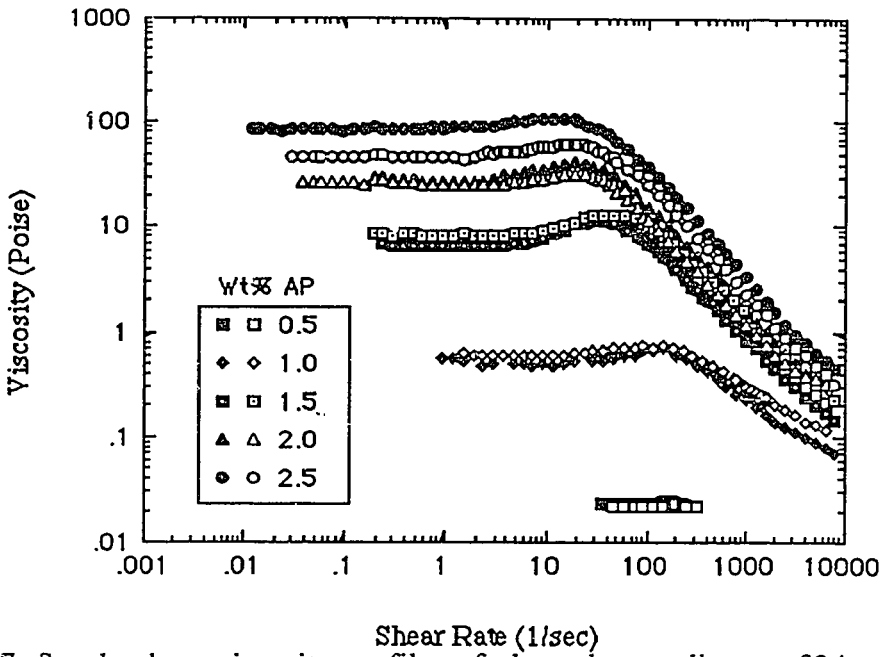

Figure 6.7: Steady shear viscosity profiles of cleaned monodisperse 324 nm particle diameter polystyrene latexes of 4.2% solids content that contain hexadecyl terminated model associative polymers of 51,000 number average molecular weight. Closed and open symbols denote solutions and latexes that contain associative polymer, respectively.

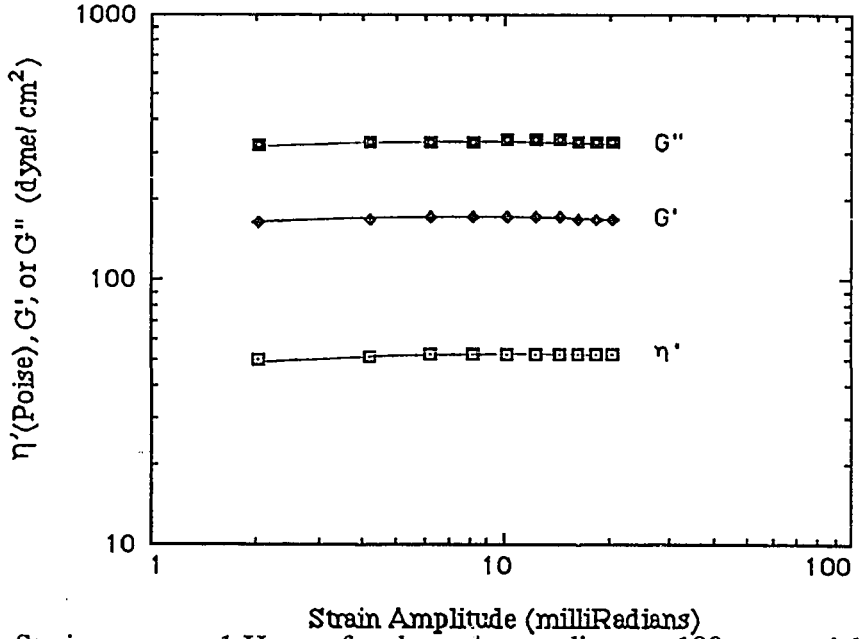

Figure 6.8: Strain sweep at 1 Hertz of a cleaned monodisperse 180 nm particle diameter polystyrene latex of 9.4% solids content that contains 2.5% hexadecyl terminated model associative polymer of number average molecular weight 67,600.

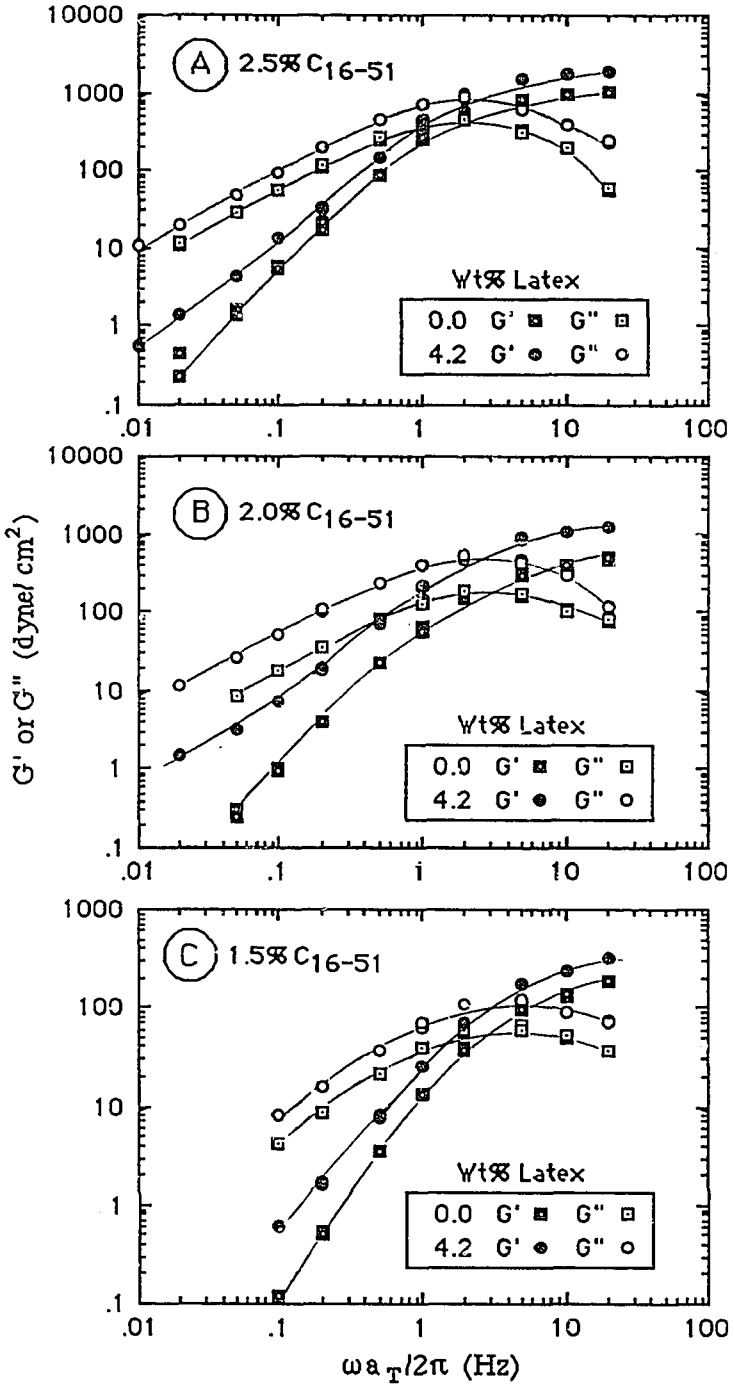

Figure 6.9: Dynamic shear moduli of cleaned 4.2% solids content 180 nm monodisperse polystyrene latexes that contain (A) 2.5%, (B) 2.0%, and (C) 1.5% hexadecyl terminated model associative polymer of 51,000 number average molecular weight, respectively. The squares denote data for associative polymer solutions, and the circles denote data for latexes that contain associative polymer.

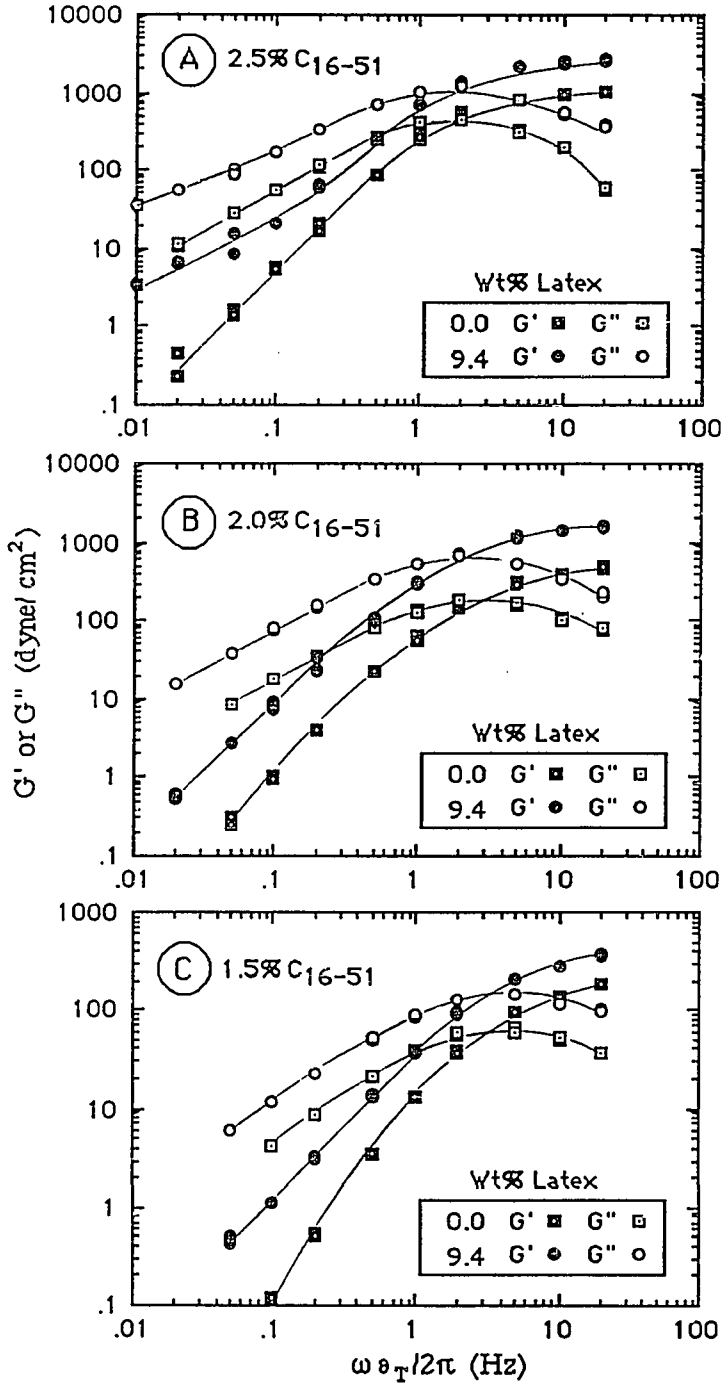

Figure 6.10: Dynamic shear moduli of cleaned 9.4% solids content 180 nm monodisperse polystyrene latexes that contain (A) 2.5%, (B) 2.0%, and (C) 1.5% hexadecyl terminated model associative polymer of 51,000 number average molecular weight, respectively. The squares denote data for associative polymer solutions, and the circles denote data for latexes that contain associative polymer.

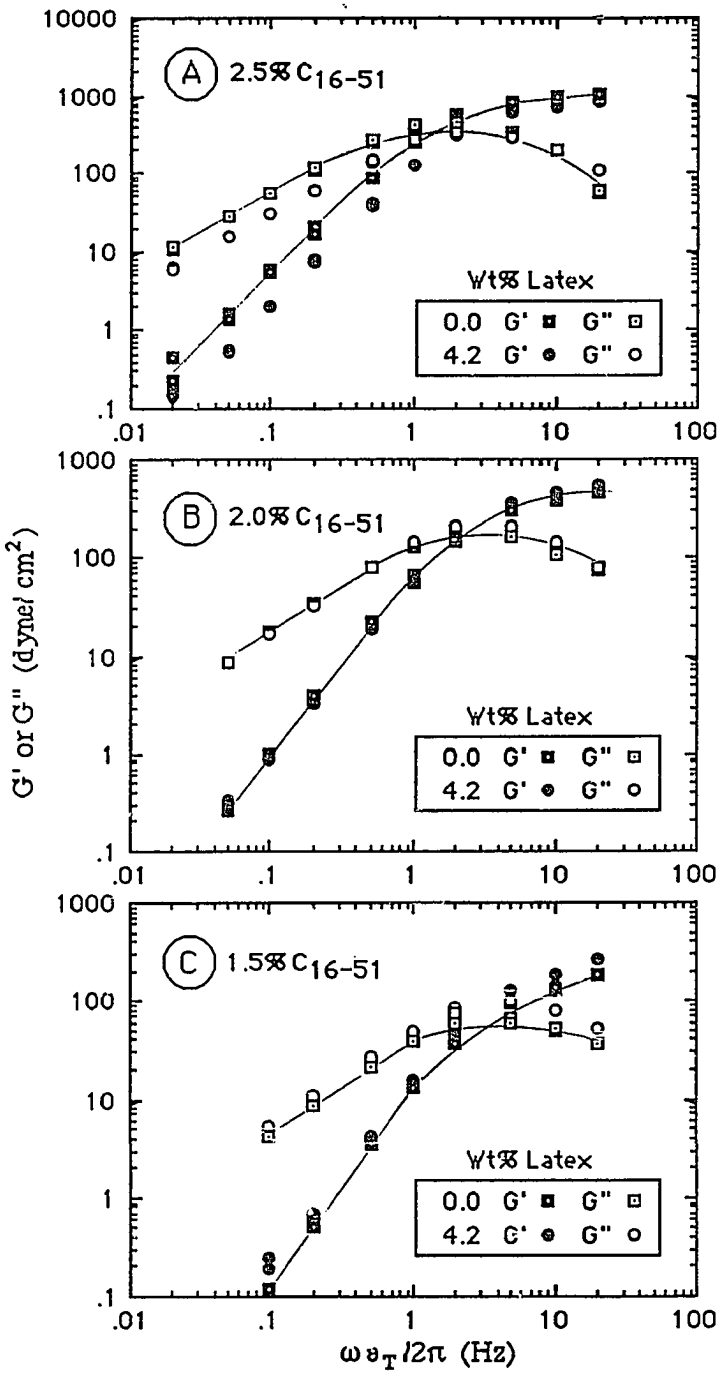

Figure 6.11: Dynamic shear moduli of cleaned 4.2% solids content 324 nm monodisperse polystyrene latexes that contain (A) 2.5%, (B) 2.0%, and (C) 1.5% hexadecyl terminated model associative polymer of 51,000 number average molecular weight, respectively. The squares denote data for associative polymer solutions, and the circles denote data for latexes that contain associative polymer.

behavior of latexes that contain hydroxyl terminated polymer serves as a control to which we can compare the effects of hydrophobic interactions on dispersion rheology.

Figure 6.4 also presents the viscosity profiles of a dodecyl terminated model associative polymer of similar molecular weight measured under identical conditions to the experiment described in the previous paragraph. The viscosity of the latex thickened with the dodecyl terminated model polymer is less than a solution with an identical concentration of associative polymer without latex particles. This is not surprising because the molecular area of adsorption of the dodecyl terminated associative polymer is smaller than that of the hydroxyl terminated polymer, and thus, relatively more of the dodecyl terminated polymer adsorbs. This adsorption depletes the aqueous phase of the dodecyl terminated associative polymer, and the viscosity of the dispersion decreases because the interactions among latex particles, adsorbed polymer, and associative polymer remaining in the aqueous phase are not strong enough to compensate for this loss. If the associative polymer did not adsorb to the latex, then the particles would have enhanced the viscosity of the polymer solution by volume exclusion. The influence of adsorption and aqueous phase networking on dispersion rheology by the hexadecyl terminated polymers are even more dramatic than for the dodecyl terminated polymers; hence, the remaining portion of this chapter focuses on the hexadecyl terminated polymers.

Influence of Associative Polymer Concentration

Figures 6.5 through 6.11 present the influence of associative polymer concentration on the steady shear viscosity profiles and viscoelastic properties of 4.2% and 9.4% 180 nm and 4.2% 324 nm polystyrene latexes that contain the hexadecyl terminated model associative polymer. As demonstrated in Chapter V, the hexadecyl terminated model associative polymers flocculate a latex by bridging at low polymer concentrations; this is not volume restriction flocculation because the hexadecyl terminated associative polymers

adsorb strongly to the latex particle surface. This flocculation lowers the viscosity of the latex to below that of a polymer solution that contains an identical amount of polymer, as demonstrated by the viscosity profile for the latexes that contain 1% associative polymer presented in Figures 6.4 and 6.5. At larger polymer concentrations (above those required for full coverage), a latex that contains model associative polymer is stable, has a smooth consistency, lacks a yield stress in its steady shear viscosity profile, and is linearly viscoelastic (Figure 6.8). The rheological properties of these stable latexes emulate those of polymer solutions, both in steady and dynamic shear. This is demonstrated by similarity of viscosity profiles of the latex that contain greater than 1.5% associative polymer in Figures 6.5 and 6.6, and by all of the viscosity profiles in Figure 6.7, where the viscosity profiles for the 324 nm latex (open symbols) so closely match the viscosity profiles of the solutions (closed symbols) that much of the data for the solutions are hidden beneath the viscosity profiles of the latexes. The viscosities of the 180 nm latexes are also much larger than those of the solutions; the enhancement is larger than can be explained by a volume filling effect by the latex particles in a network. Additional proof for this synergistic interaction comes from the dynamic shear moduli of the latexes that contain associative polymer (Figures 6.9 through 6.11). The viscoelastic properties of these dispersions resemble those of the associative polymer solutions, where they exhibit a larger characteristic relaxation time constant and a larger entanglement plateau than the solutions. Hence, the aqueous phase association network in a latex dispersion determines the rheological properties of the dispersion to a great extent.

Thus it seems that the latex particles incorporate themselves into the aqueous phase network and can reinforce it. The influence of particle size and solids content on the rheological properties of the latex is more than just a volume filling mechanism: such an argument would predict that the low shear viscosity of a 180 nm latex of 4.2% and 9.4% solids content would increase 11% and 23%, respectively. In fact, Figures 6.5 through

6.7 show that the low shear viscosity of the dispersion can be larger than, smaller than, or the same as the low shear viscosity of a solution that contains an identical amount of associative polymer. The fact that the low shear viscosities of the 180 nm latexes can be larger than the solutions indicates that some kind of interaction offsets the loss in the strength of the aqueous phase network due to adsorption. The shear - thickening in viscosity profiles, and the solution - like viscoelastic properties of the latex dispersions, indicate that enough associative polymer can exist in the aqueous phase to provide a coherent association network. These effects must result from the interactions among the latex particles, the adsorbed associative polymers, and the associative polymers that are networked in the aqueous dispersion medium. One explanation for the synergistic interaction is that the particles behave as a network junction site. Chapter V showed that the hydrophobic alkyl end-groups of the associative polymer adsorb, and that the amount of thickener adsorbed per unit is increased as particle size decreases. Also, the relatively sharper curvature of a small diameter latex enhances the adsorption of "tail" segments over the "loops and trains" of the polymer backbones, which enhances the strength of the particle - associative polymer interaction. The strength of these particle junctions can be larger than network junctions that consist solely of associative polymer hydrophobes because the particles can offer increased functionality, that is a larger number of hydrophobes per network node, and a stronger junction as compared to a junction mode of only associative polymer hydrophobes. In this way, the latex particles adsorb associative polymer and can yet reinforce the aqueous phase association network under the appropriate conditions.

Influence of Associative Polymer Molecular Weight

One way to vary the strength of interaction of the associative polymer at the particle interface relative to the strength of the interaction between associative polymers in the

dispersion medium is to vary the molecular weight of the associative polymer. Figures 6.12 through 6.24 present, by molecular weight, the effect of latex particle size and solids content on the steady shear and linear viscoelastic properties of solutions that contain 2.5% of the hexadecyl terminated polymers. In general, the rheological properties of the latexes that contain the model polymer emulate the rheological properties of the associative polymer solutions. There are some small differences, which we elaborate on in the following discussion.

The latexes that contain the lower molecular weight polymer (51,000 number average molecular weight and below), have viscosity profiles that follow the associative polymer solution viscosity profiles quite closely. Because of their smaller scale, the figures in this chapter reveal the shear - thickening regions of the steady shear viscosity profiles of the solutions more dramatically than the figures in Chapter III. The viscosity profiles of the 324 nm latexes that contain the lower molecular weight model associative polymer practically retrace the viscosity profiles of the solutions. The viscosity profiles of the 180 nm latexes that contain model associative polymer have larger low shear viscosities than the solutions, but the shear - thinning regions of the latexes and those of the associative polymer solutions superimpose. The viscosity profiles for the 180 nm latex also show that the magnitude of the shear-thickening region in the viscosity profile decreases as the solids content of the latex increases. These trends persist in the viscoelastic properties of latexes that contain the model associative polymer. As with the viscosity profiles, the viscoelastic properties of the 324 nm latexes replicate the associative polymer solutions' shear moduli, and the shear moduli of the 180 nm latexes have the same frequency dependence, although they are slightly larger in magnitude. As discussed previously, this results from the heightened interaction between small sized latexes and associative polymers.

As the number average molecular weight of the associative polymer in the latex exceeds 51,000 , the level of the low shear viscosity and the shear rate that marks the onset

of shear - thinning in the viscosity profile both decrease as compared to an equivalent system that does not contain latex for a given thickener molecular weight. This is most dramatically manifested in the data for the 324 nm latex systems, where the low shear viscosities and the viscoelastic properties of the latexes actually decrease to below those polymer solutions that contain an identical amount of associative polymer. The smaller moduli and relaxation time constants for the 324 nm latexes indicate the amount of network structure has decreased. Based on the adsorption data given in Chapter V, the amount of associative polymer needed to saturate the 324 nm latexes is less than the amount required to saturate a 180 nm latex of equivalent solids content. Thus, even though the 324 nm latexes have relatively more associative polymer in solution for a given associative polymer concentration, the rheological properties of the 324 nm latexes are smaller than those of 180 nm latexes. These differences indicate that the strength of the thickener - latex interaction decreases as particle size increases for a given thickener molecular weight.

Even though the low shear viscosities of 180 nm latexes that contain model associative polymer do not show the same degree of sensitivity to the molecular weight of the model polymer as do the 324 nm latexes (Figure 6.24), the depletion of associative polymer from the aqueous phase network by adsorption manifests itself in the steady shear viscosity profiles of the 180 nm latexes. The onset of shear - thinning begins at smaller shear rates, and the power law index is larger, as compared to the viscosity profiles of an equivalent associative polymer solution sans latex. This effect becomes more exaggerated as the molecular weight of the thickener increases. For example, the viscosity profiles in Figure 6.12 for latexes that contains a 17,500 number average molecular weight model polymer are nearly identical to the viscosity profile of the solution, while the viscosity profiles in Figure 6.22 of latexes that contains a 100,400 number average molecular weight model polymer exhibit stronger shear- thinning that begins at a smaller shear rate than the viscosity profile of the solution that does not contain latex. This extra measure of shear-

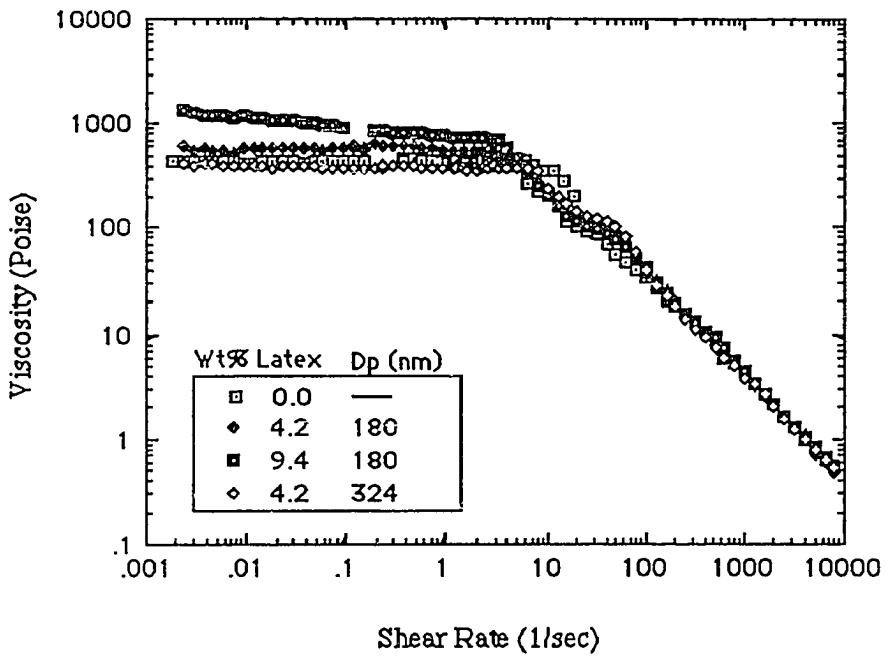

Figure 6.12: Steady shear viscosity profiles of cleaned monodisperse polystyrene latexes of various particle sizes and solids content that contain 2.5% hexadecyl terminated model associative polymer of 17,500 number average molecular weight.

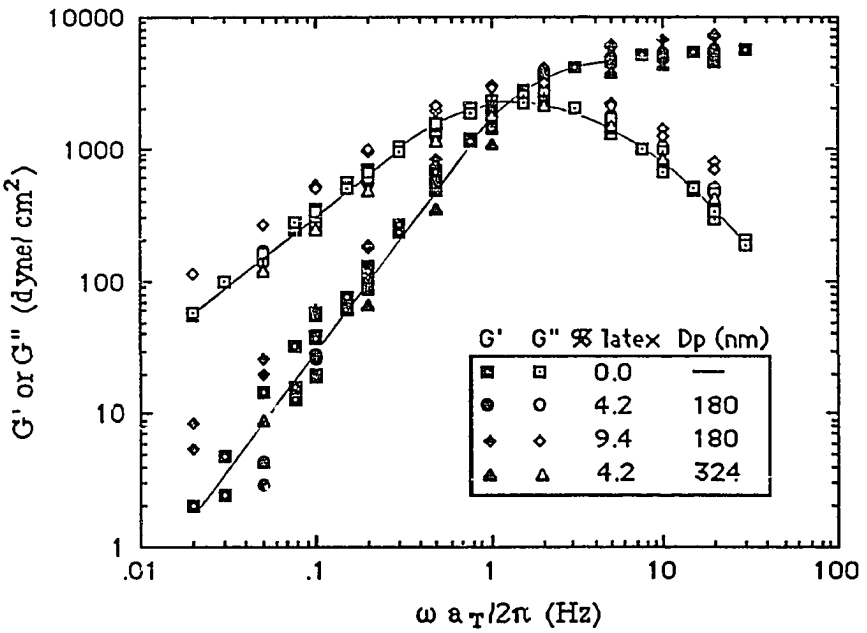

Figure 6.13: Dynamic shear moduli of cleaned monodisperse polystyrene latexes of various particle sizes and solids content that contain 2.5% hexadecyl terminated model associative polymer of 17,500 number average molecular weight.

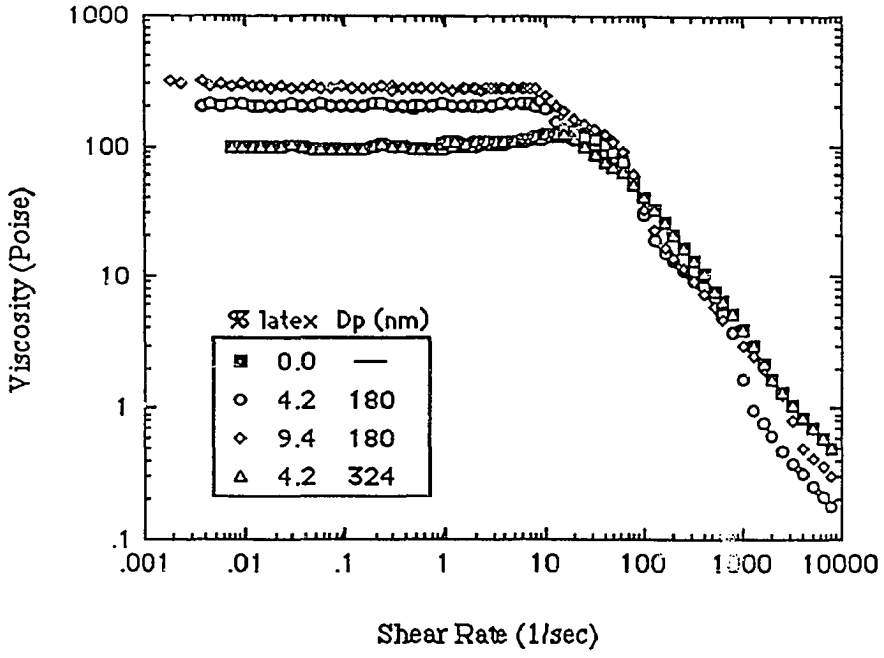

Figure 6.14: Steady shear viscosity profiles of cleaned monodisperse polystyrene latexes of various particle sizes and solids content that contain 2.5% hexadecyl terminated model associative polymer of 34,200 number average molecular weight.

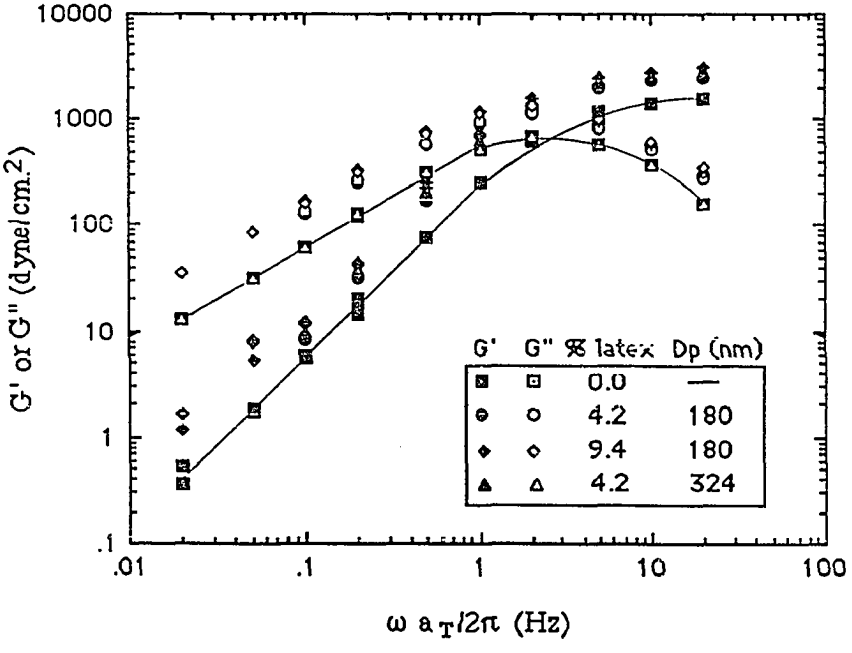

Figure 6.15: Dynamic shear moduli of cleaned monodisperse polystyrene latexes of various particle sizes and solids content that contain 2.5% hexadecyl terminated model associative polymer of 34,200 number average molecular weight.

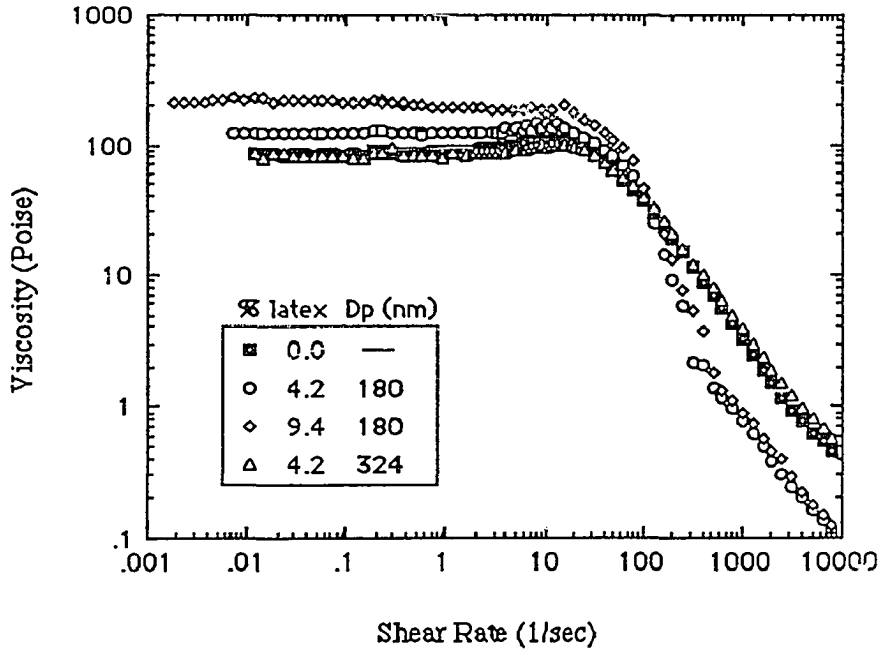

Figure 6.16: Steady shear viscosity profiles of cleaned monodisperse polystyrene latexes of various particle sizes and solids content that contain 2.5% hexadecyl terminated model associative polymer of 51,000 number average molecular weight.

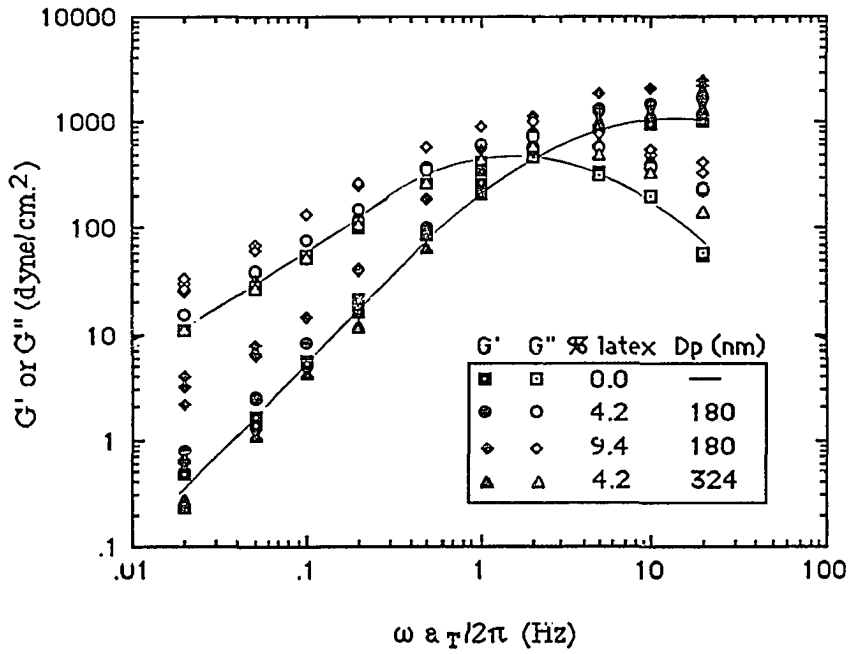

Figure 6.17: Dynamic shear moduli of cleaned monodisperse polystyrene latexes of various particle sizes and solids content that contain 2.5% hexadecyl terminated model associative polymer of 51,000 number average molecular weight.

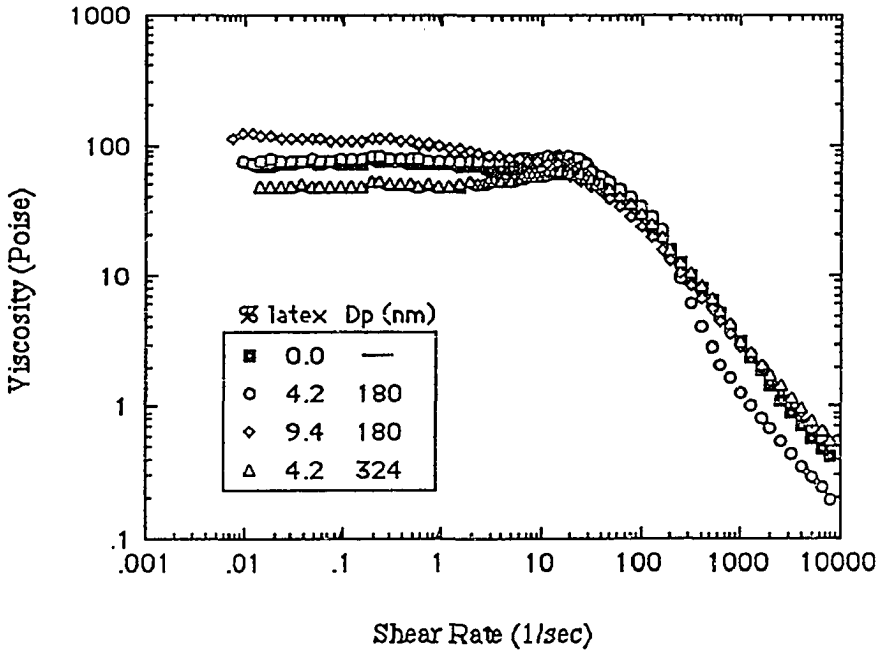

Figure 6.18: Steady shear viscosity profiles of cleaned monodisperse polystyrene latexes of various particle sizes and solids content that contain 2.5% hexadecyl terminated model associative polymer of 67,600 number average molecular weight.

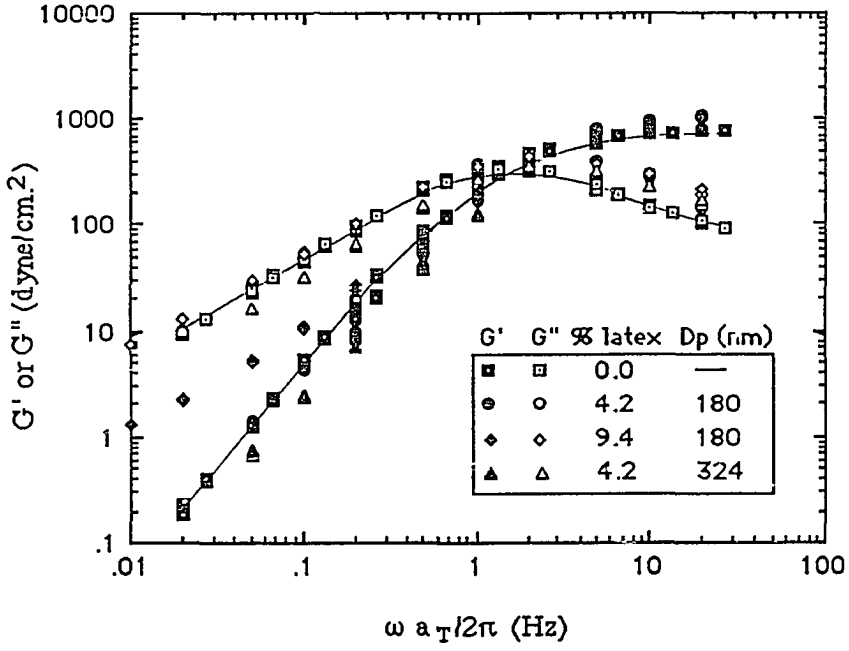

Figure 6.19: Dynamic shear moduli of cleaned monodisperse polystyrene latexes of various particle sizes and solids content that contain 2.5% hexadecyl terminated model associative polymer of 67,600 number average molecular weight.

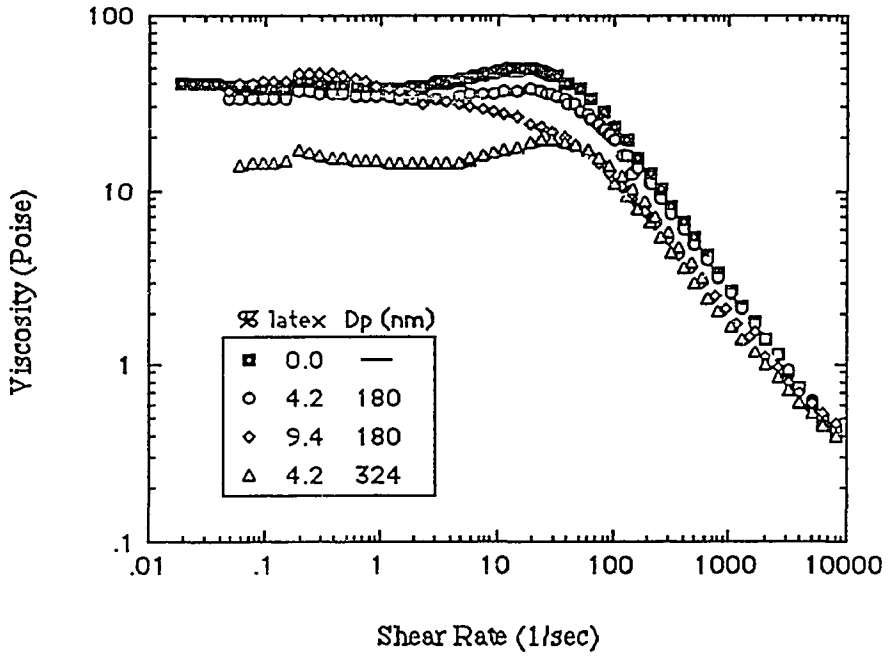

Figure 6.20: Steady shear viscosity profiles of cleaned monodisperse polystyrene latexes of various particle sizes and solids content that contain 2.5% hexadecyl terminated model associative polymer of 84,300 number average molecular weight.

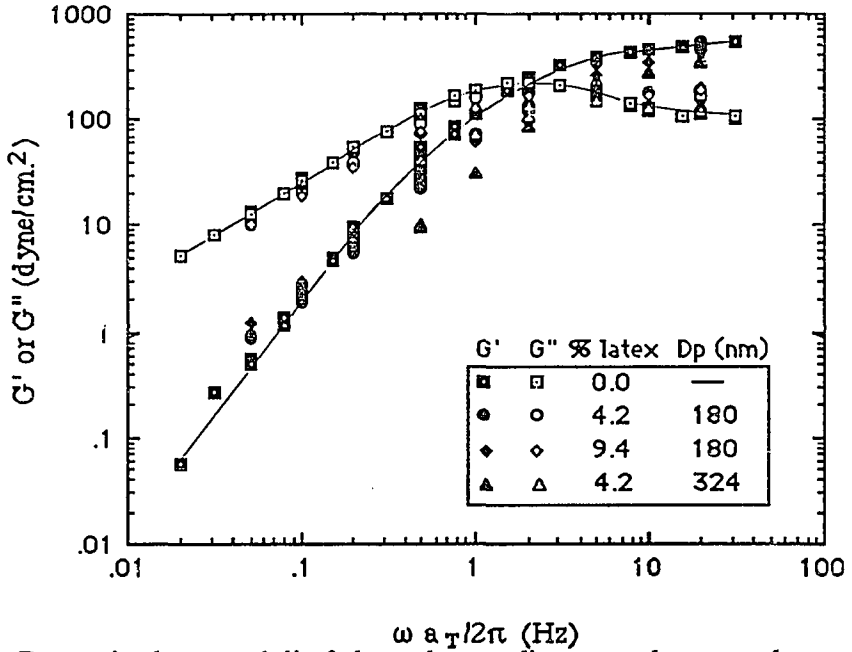

Figure 6.21: Dynamic shear moduli of cleaned monodisperse polystyrene latexes of various particle sizes and solids content that contain 2.5% hexadecyl terminated model associative polymer of 84,300 number average molecular weight.

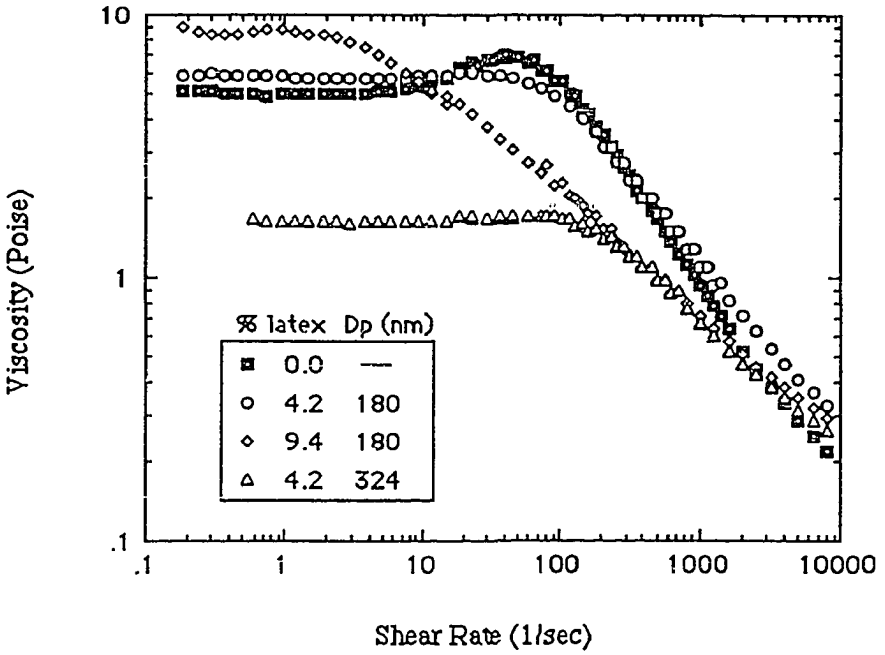

Figure 6.22: Steady shear viscosity profiles of cleaned monodisperse polystyrene latexes of various particle sizes and solids contents that contain 2.5% hexadecyl terminated model associative polymer of 100,400 number average molecular weight.

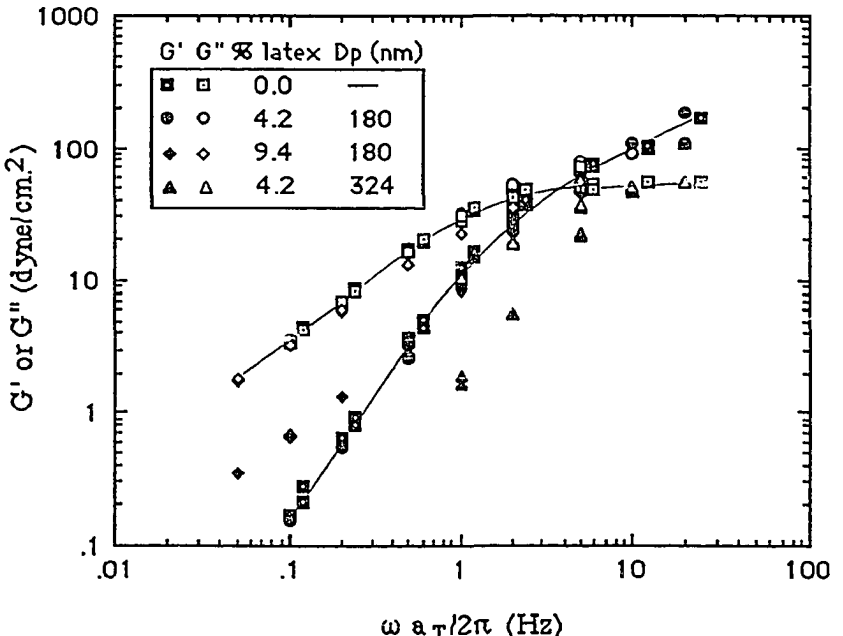

Figure 6.23: Dynamic shear moduli of cleaned monodisperse polystyrene latexes of various particle sizes and solids content that contain 2.5% hexadecyl terminated model associative polymer of 100,400 number average molecular weight.

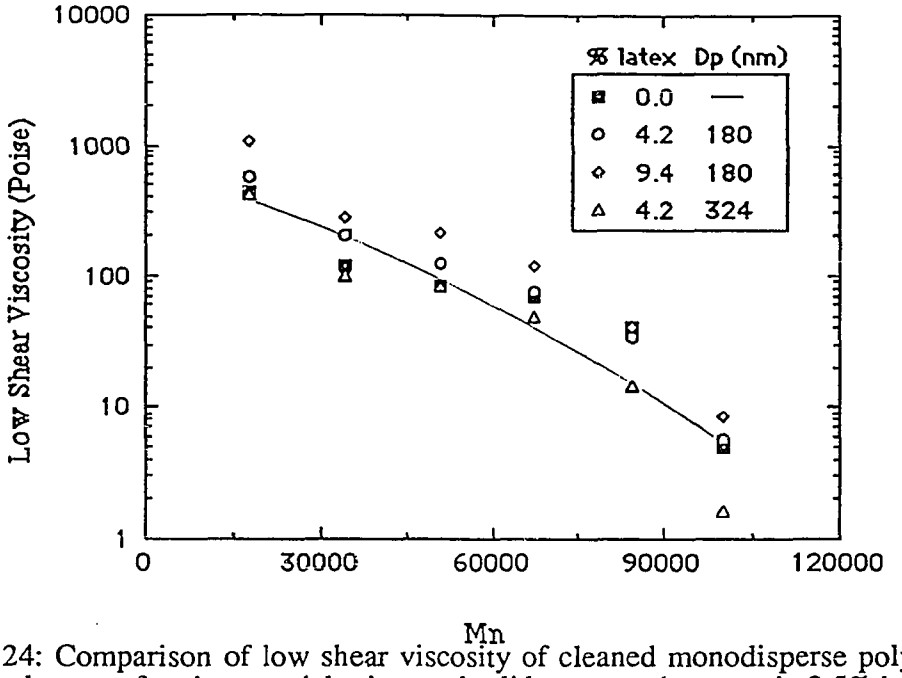

Figure 6.24: Comparison of low shear viscosity of cleaned monodisperse polystyrene latexes of various particle sizes and solids content that contain 2.5% hexadecyl terminated model associative polymer of various number average molecular weights.

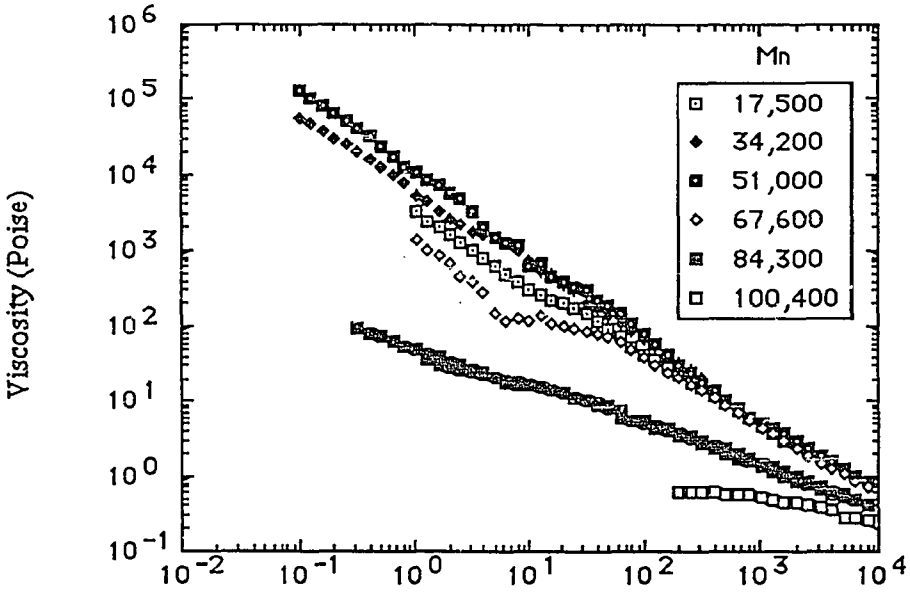

Figure 6.25: Steady shear viscosity profiles of cleaned monodisperse 180 nm particle diameter polystyrene latexes of 18.5% solids content that contain 2.5% hexadecyl terminated model associative polymer of various number average molecular weights.

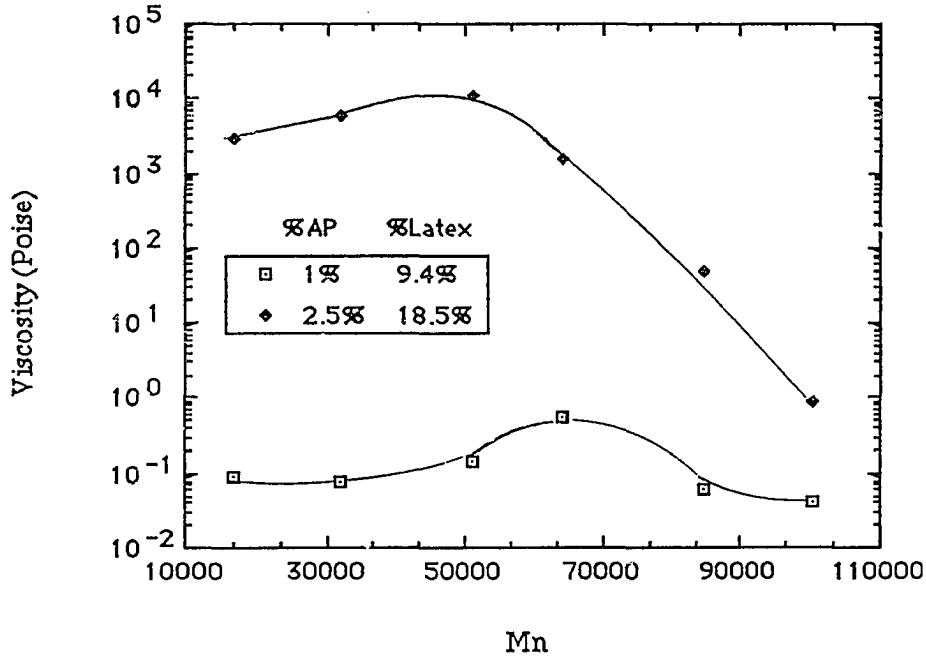

Figure 6.26: Viscosities at 1 sec^{-1} of flocculated cleaned monodisperse 180 nm particle diameter polystyrene latexes of various solids content that contain hexadecyl terminated model associative polymers of various number average molecular weights.

thinning observed with the latex systems is not an artifact due to the Weissenberg effect, because the latexes and the solutions have the same degree of viscoelasticity, and such an artifact would influence the solution and latex data in the same way. Additionally, the shear - thinning in the latex systems begins at relatively low shear rates where the Weissenberg effect is not observed. Thibeault has advanced the hypothesis that this extra measure of shear - thinning results from the rotation of the particle in the shear field, which would increase the local effective shear rate [116].

The results presented in the previous paragraphs show that the strength of interaction between the latex particle, adsorbed polymer, and aqueous phase network

depends on the molecular weight of the associative polymer, through both the strength of the association of hydrophobes in the dispersion medium and at the particle interface. This behavior is expected, based on the results of Chapter III, which showed that the number density of hydrophobes in solution is a key factor in determining the strength of the aqueous phase network, and from the results of Chapter V, which showed that the adsorption of the associative polymer depends on its molecular weight. The rheological experiments presented in this chapter were made at constant weight fraction of associative polymer, so that latexes containing the lower molecular weight polymers had a much larger number of associative polymers (and hydrophobes) in solution than latexes containing the higher molecular weight solutions. Then it is not surprising that the rheological properties of latexes containing the higher molecular weight were more burdened by the loss of a few thickeners by adsorption as compared to latexes containing the lower molecular weight polymers. Based on the results from Chapter V, it is also not surprising that the strength of the network in the latex dispersion, and therefore the viscoelastic behavior of the dispersion, depends on the particle size of the latex. Even though the amount of associative polymer that is depleted from the dispersion medium increases as the particle size of the latex decreases, the strength of the adsorption increases. Also, the conformation of the adsorbed polymer is more extended from the surface of a smaller particle, and therefore, the adsorbed polymer can interact more efficiently with the aqueous phase network. These effects apparently offset the loss in strength of the aqueous phase network from adsorption in the 180 nm latexes, but do not quite do so with the 324 nm latexes.

The work presented in the previous paragraphs considered 4.2% and 9.4% solids content latexes, where the concentration of associative polymer in the dispersion was larger than that required to fully cover the particles. If the concentration of associative polymer is held constant at 2.5%, and the solids content of the latex is increased, the associative polymer no longer saturates the particle surfaces, and a paste - like dispersion results. This

is shown in the viscosity profiles given in Figure 6.25 for 18.5% solids content 180 nm latexes. Based on the adsorption data given in Chapter V, the associative polymers cannot fully cover the particles until the concentration of associative polymer exceeds 2.6% by weight. The strongly shear - thinning viscosity profiles that result are expected for a flocculated latex.

The most important feature of Figure 6.25 is the maximum in dispersion viscosity with respect to molecular weight. This is shown more clearly in Figure 6.26, which also shows the molecular weight that maximizes dispersion viscosity depends on the concentrations of associative polymer and latex. From the flocculation experiments that were discussed in Chapter V, the maximum results from two competing effects: first, the driving force for networking decreases as associative polymer molecular weight increases; and second, the number of associative polymers needed to span the distance between particles decreases as the length of the polymer backbone increases.

Interactions Between Associative Polymer and Sodium Dodecyl Sulfate

Homopolymers of poly(oxyethylene), and block copolymers that contain poly(oxyethylene), form complexes with surfactants; the surfactant adsorbs to the polymer because the adsorbed state of the surfactant on the polymer is energetically more favorable than in regular micelles. In his excellent review article, Goddard [117] presents many polymer/surfactant systems where the viscosity of polymer solution increases with the addition of surfactant, and he also presents a variety of experimental techniques that are used to probe the nature of polymer / surfactant complexes. Polymer / surfactant systems generally show two critical concentrations: the first occurs at the concentration where the surfactant first interacts with, and adsorbs to, the polymer, and the second occurs at the concentration where the adsorption sites on polymer are saturated [118]. The concentration of surfactant at the first transition is usually less than critical micellar concentration (CMC)

of the pure surfactant, above which ordinary micelles form, and the second transition coincides with the CMC of the surfactant. For surfactant concentrations that are between the two transitions, the interaction between polymer and surfactant is stoichiometric [118, 119] .

In general, the topology assumed by a polymer / surfactant complex in solution depends on the strength of interactions among polymer, surfactant and the solvent. [120] Block copolymers with hydrophobic and hydrophilic segments, such as our model associative polymers, form segregated hydrophobic and hydrophilic regions in solution. Surfactant molecules interact with this interface: ion-dipole interactions between dipole of the ether oxygen of the poly(oxyethylene) group and the ionic headgroup of surfactant; and binding between the hydrophobic block of polymer and the hydrophobic portion of the surfactant (i.e., Nagarajan's "Type 5" topology). The clustering of surfactant molecules along the associative polymer forms a pseudo-micellar structure that shields the hydrophobic groups of the associative polymer from contact with water. This effect increases the size of, and effective number of intermolecular crosslinks in, the association network in solution to increase the viscosity of the solution.

Model associative polymers interact with sodium dodecyl sulfate (SDS) in a similar manner, as reflected in the influence of sodium dodecyl sulfate on the steady shear viscosity profiles and the viscoelastic properties of model associative polymer solutions. As shown in Figure 6.27, the low shear viscosity of a 2.5% solution of associative polymer with hexadecyl end-groups increases to a maximum, and then subsequently decreases as the concentration of sodium dodecyl sulfate increases. This maximum decreases as the molecular weight of the associative polymer increases, and disappears altogether for the largest two molecular weight polymers shown in the figure. (Table 6.2 lists the numerical values for the viscosity data given in Figure 6.27). The dependence of the concentration of surfactant required to produce the maximum in viscosity is consistent

with the conclusion presented in Chapter III that the degree of network formation by association is inversely proportional to the molecular weight of the associative polymer. Bassett [121] and Lundberg et al. [67, 74] have also observed a maximum in the viscosity of a solution of model associative polymers with respect to the concentration of anionic and nonionic surfactants. Their model polymers were of a similar chemical composition to our own, but differed in the type, length, and placement of hydrophobic groups, and in the molecular weight and architecture of the hydrophilic backbone of the associative polymer. In contrast to the data of Lundberg et al. [67], where the maximum in solution viscosity coincided with CMC of sodium dodecyl sulfate, the maximum in Figure 6.27 occurs at sodium dodecyl sulfate concentrations that are less than the CMC of sodium dodecyl sulfate (which we assume is 0.0081 Molar [122]), and the concentration of sodium dodecyl sulfate that corresponds to the maximum in solution viscosity decreases as thickener molecular weight increases. In our data, the maximum in the viscosity does not occur at the CMC of the neat surfactant, but rather when the concentration of hydrophobes in the associative polymer is stoichiometrically equivalent to the concentration of sodium dodecyl sulfate hydrophobes in solution. This is consistent with the law of mass action that usually governs the equilibrium process of adsorption of the surfactant to the polymer. Blank experiments in which sodium chloride was added to model associative polymer solutions showed that at concentrations where sodium dodecyl sulfate maximizes the viscosity of the associative polymer solution, sodium chloride actually decreases the viscosity of the solution [123]. These results indicate that the influence of sodium dodecyl sulfate on the viscosity of associative polymer solutions results from an interaction between the alkane chain of sodium dodecyl sulfate and the associative polymer.

In addition to altering the level of the low shear viscosity of associative polymer solutions, sodium dodecyl sulfate also influences their steady shear viscosity profiles (Figure 6.28). As shown in Table 6.1, the magnitude of the viscosity enhancement in the

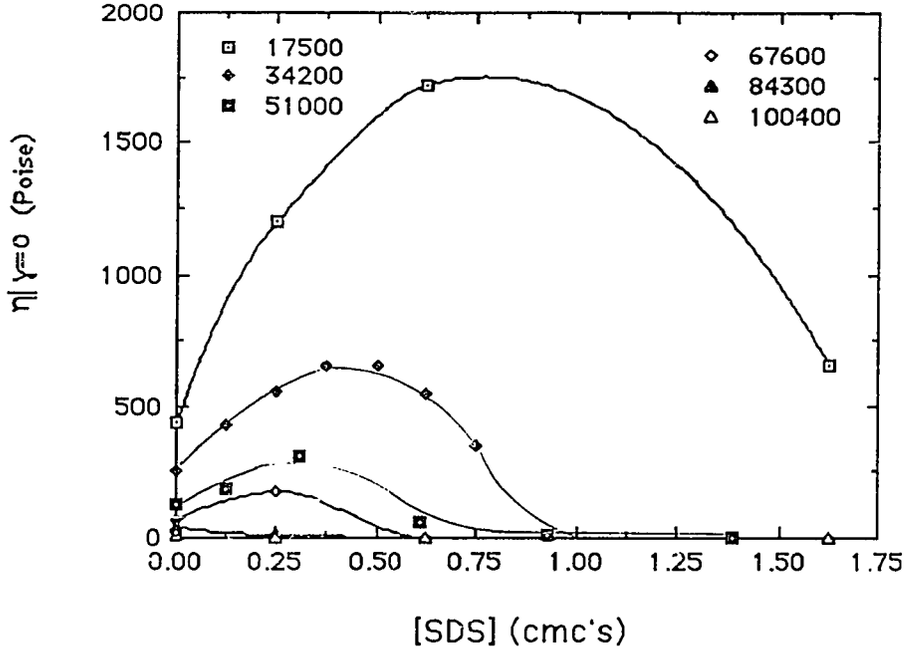

Figure 6.27: Influence of sodium dodecyl sulfate on the low shear viscosities of aqueous solutions of hexadecyl terminated model associative polymers of various number average molecular weights.

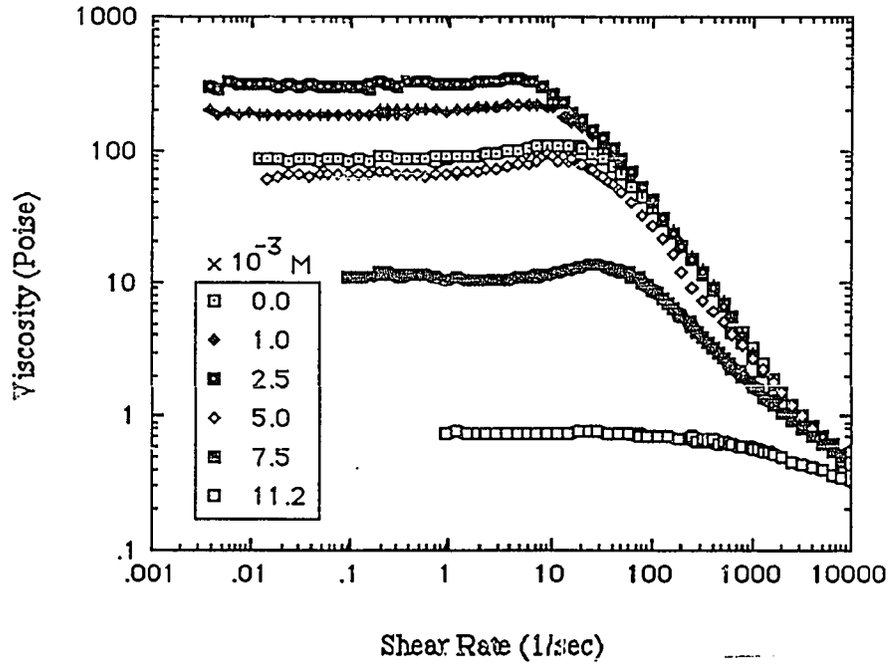

Figure 6.28: Influence of sodium dodecyl sulfate (in Molar concentration) on the steady shear viscosity profiles of aqueous solutions of a hexadecyl terminated model associative polymer of number average molecular weight 51,000.

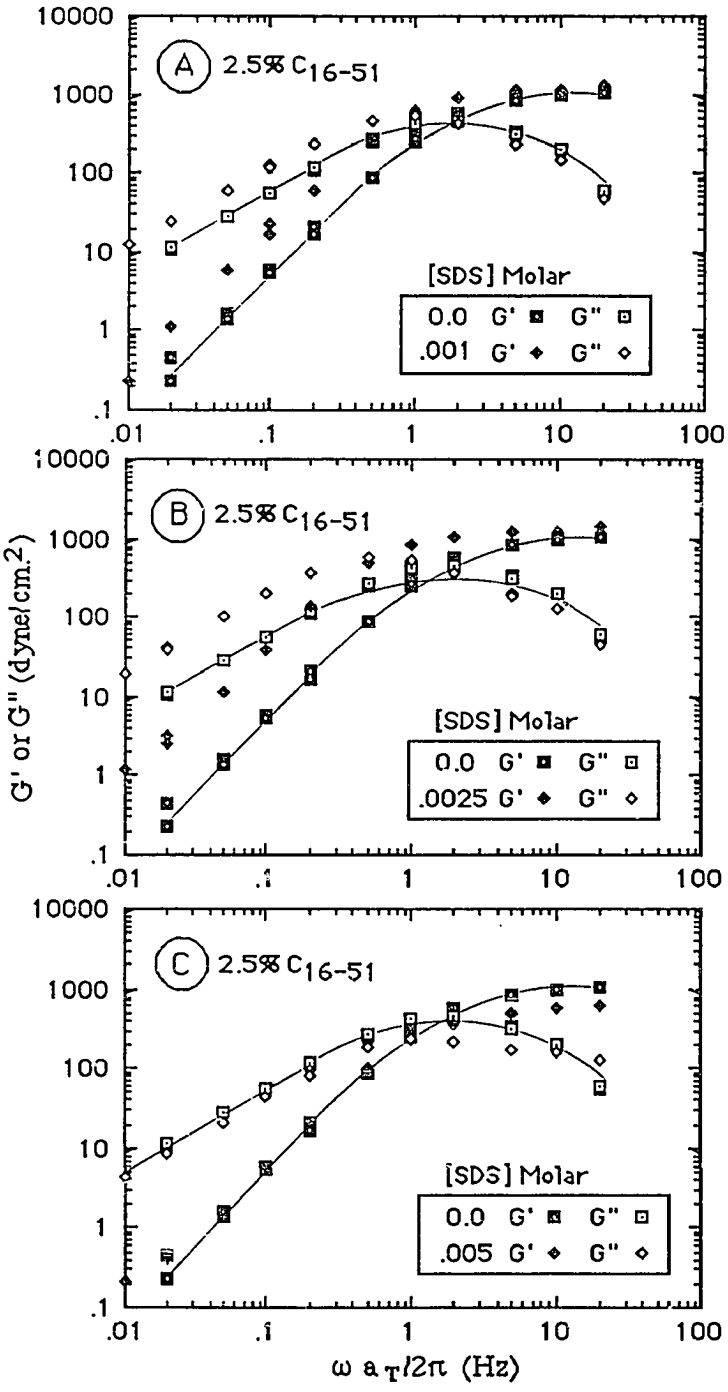

Figure 6.29: Dynamic shear moduli of 2.5% aqueous solutions of a hexadecyl terminated model associative polymer of number average molecular weight 51,000 that contain (A) 0.001 , (B) 0.0025 , (C) 0.0050, (D) 0.0075, and (E) 0.0112 Molar sodium dodecyl sulfate.

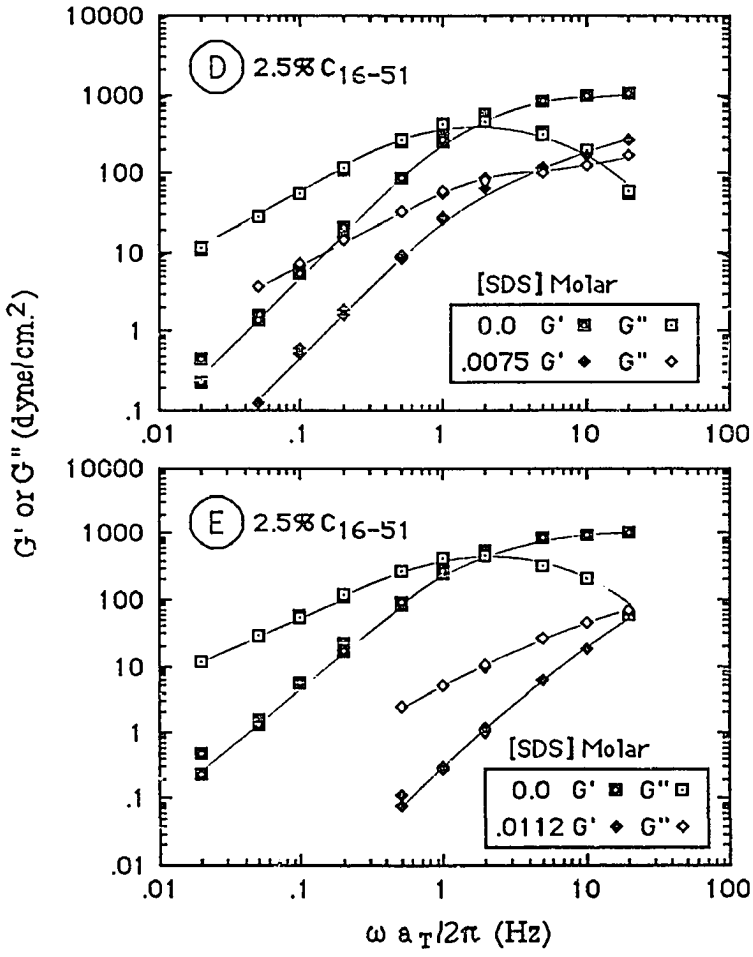

shear - thickening region in the steady shear viscosity profile, η_{max}/η_o, increases slightly and then decreases as the concentration of sodium dodecyl sulfate increases.

Table 6.1: Influence of sodium dodecyl sulfate on the magnitude of the viscosity enhancement in the shear - thickening region of the steady shear viscosity profiles given in Figure 6.28

[SDS] x 10^3 Molar	η_{max}/η_o
0.0	1.25
1.0	1.20
2.5	1.23
5.0	1.50
7.5	1.25
11.2	1.00

The maximum enhancement in the magnitude of the shear - thickening region of the viscosity profile occurs at 5.0 milliMolar of sodium dodecyl sulfate, which is larger than the concentration of 2.5 milliMolar sodium dodecyl sulfate that maximizes the low shear viscosity of the associative polymer solution. (Consult Table 6.2). Lundberg et al. [74] observed a similar response with purified samples of SCT 270, a commercial associative polymer manufactured by Union Carbide Corporation. By the law of mass action, a concentration of 5.0 milliMolar sodium dodecyl sulfate is large enough to screen interactions among the model associative polymer hydrophobes, and thus decrease the amount of network structure in solution. In other words, the effect of large quantities of sodium dodecyl sulfate is to reduce the effective concentration of the associative polymer. By the explanations developed in Chapters III and IV, we expect to see an increase and then a decrease in magnitude of the viscosity enhancement in the shear - thickening region of the viscosity profile.

The viscoelastic properties of the model associative polymer solutions monitor the influence of sodium dodecyl sulfate on the degree of network formation (Figure 6.29). Sodium dodecyl sulfate exerts the same influence on the shear moduli as it did on the low shear viscosity: the 1.0 and 2.5 milliMolar solutions are more elastic than the surfactant free solutions, and 5.0 and larger concentration of sodium dodecyl sulfate are less elastic. In Figure 6.29, the relaxation time constant increases from a value of 0.110 seconds for a solution of $C_{16\text{-}51}$ without added SDS to a maximum value of 0.243 seconds at 2.5 milliMolar SDS, (which is the same concentration that maximizes the low shear viscosity), and then decreases to essentially zero at 13.0 milliMolar SDS. (Consult Table 6.2). This indicates that the increase in the shear moduli results from an increase in the elasticity of the network, and not just from the enhancement of the low shear viscosity of the solution. Thus, the addition of the surfactant increases the number of network junctions, as measured by the molar density of association junctions; but as shown later in Figure 6.45, the viscosity of all of the solutions that contain sodium dodecyl sulfate are slightly larger than those for an aqueous solution with equivalent densities of association junctions. This indicates that the interaction between sodium dodecyl sulfate not only increases the number of network junctions, but also strengthens them, perhaps by either increasing the functionality of the network junctions or by increasing the magnitude of the free energy of association.

Interactions Among Associative Polymer, Sodium Dodecyl Sulfate, and Latex

The previous section has considered only a few of the many possible interactions that can take place between the hydrophobic and hydrophilic segments of the associative polymer and sodium dodecyl sulfate; nevertheless, the solutions serve as a control by which the effect of sodium dodecyl sulfate on the rheology of latexes containing associative polymer may be compared. Figures 6.30 through 6.33 present the influence of sodium

dodecyl sulfate on the steady shear viscosity profiles of 180 nm latexes that contain 2.5% of the hexadecyl terminated model associative polymer of 51,000 number average molecular weight. Most of the profiles in Figures 6.30 through 6.33 are similar to the profiles of the surfactant free latex systems that contain model associative polymer shown before. The low shear viscosities of the latex systems that contain both associative polymer and sodium dodecyl sulfate are slightly larger than those of solutions that contain sodium dodecyl sulfate, because of the reinforcement afforded to the association network by the 180 nm latex particles and by the surfactant. Increasing the concentration of sodium dodecyl sulfate has the same effect on the viscosity of a latex system as it did on the viscosity of an associative polymer solution (Figure 6.34): the viscosity of the latex shows a maximum at a similar concentration of sodium dodecyl sulfate seen in Figure 6.27 for a polymer solution. The surfactant exerts a similar influence on the viscoelastic properties of the latexes. Figure 6.35 through 6.38 show that the frequency dependence of shear moduli for most of the latexes that contain both associative polymer and latex are qualitatively similar to those of associative polymer solutions that contain surfactant, and as expected, the entanglement plateau and relaxation time constants shift to larger values as solids content increases. Although Sperry et al. [9, 15, 19] have shown that sodium dodecyl sulfate does desorb the associative polymer from the latex, the influence of sodium dodecyl sulfate on the rheology of the latex systems shown here suggests that in some cases the binding of the surfactant with the network in the aqueous phase can have a larger influence on rheology.

Nonetheless, desorption of the associative polymer can be important, as suggested by the apparent yield stress in the viscosity profile of the 9.4% latex presented in Figure 6.30. The frequency of dependence of the storage modulus at low frequencies also reflects the solid - like behavior of the latex: the storage modulus does not approach terminal

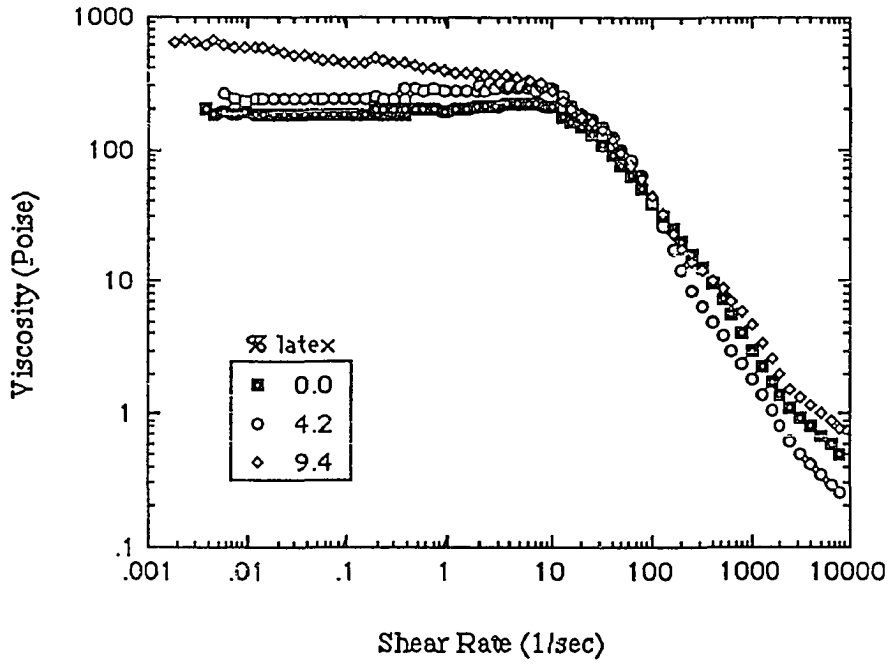

Figure 6.30: Steady shear viscosity profiles of cleaned monodisperse 180 nm particle diameter polystyrene latexes of various solids content that contain 0.001 Molar sodium dodecyl sulfate and 2.5% hexadecyl terminated model associative polymer of number average molecular weight 51,000.

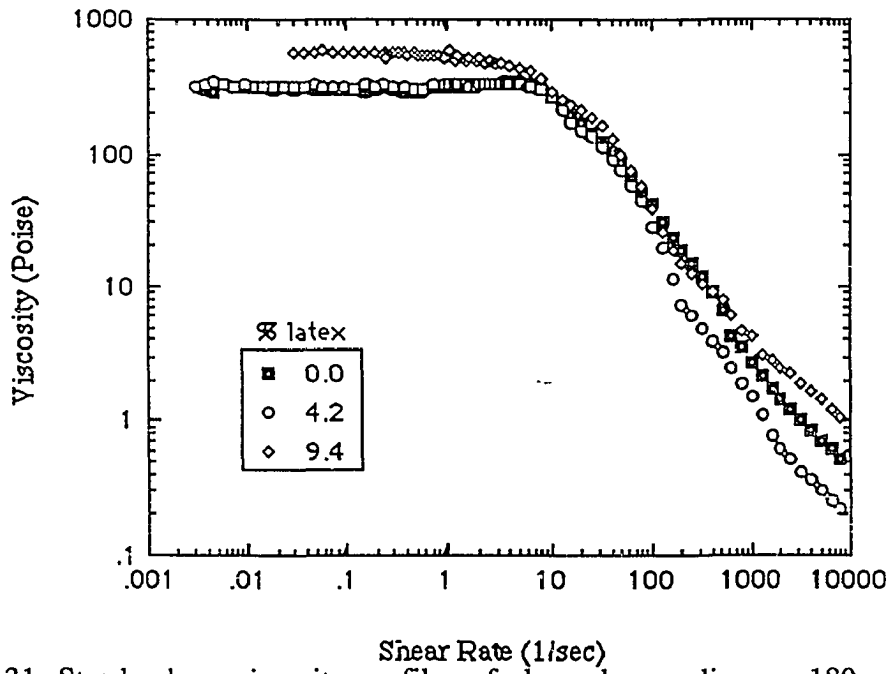

Figure 6.31: Steady shear viscosity profiles of cleaned monodisperse 180 nm particle diameter polystyrene latexes of various solids content that contain 0.0025 Molar sodium dodecyl sulfate and 2.5% hexadecyl terminated model associative polymer of number average molecular weight 51,000.

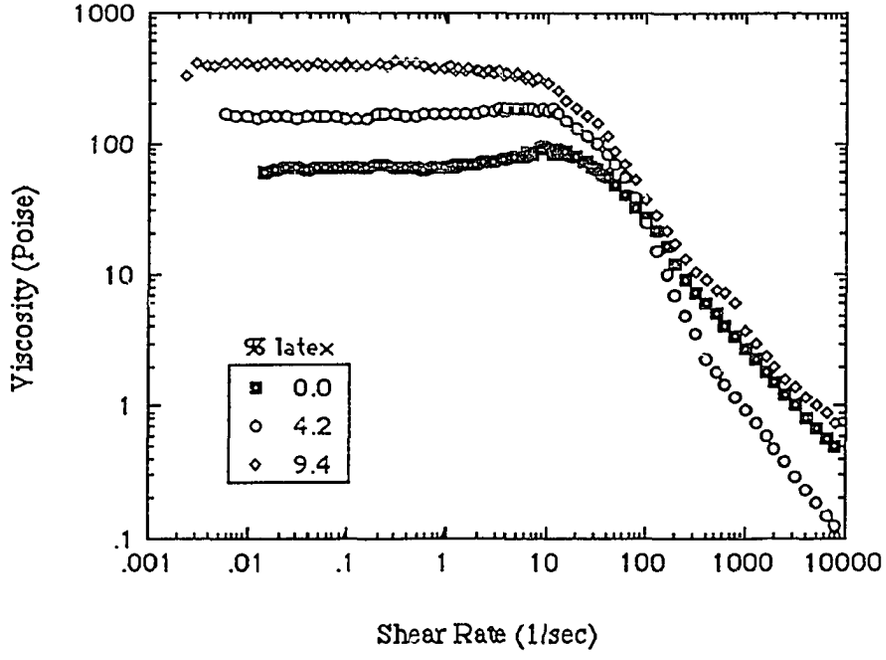

Figure 6.32: Steady shear viscosity profiles of cleaned monodisperse 180 nm particle diameter polystyrene latexes of various solids content that contain 0.005 Molar sodium dodecyl sulfate and 2.5% hexadecyl terminated model associative polymer of number average molecular weight 51,000.

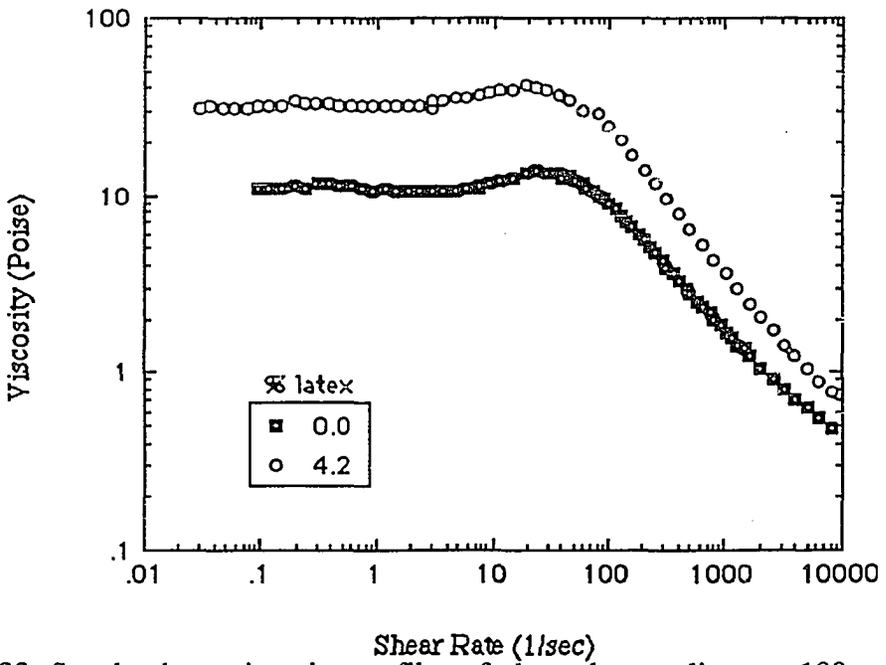

Figure 6.33: Steady shear viscosity profiles of cleaned monodisperse 180 nm particle diameter 4.2% solids content polystyrene latex that contains 0.0075 Molar sodium dodecyl sulfate and 2.5% hexadecyl terminated model associative polymer of number average molecular weight 51,000.

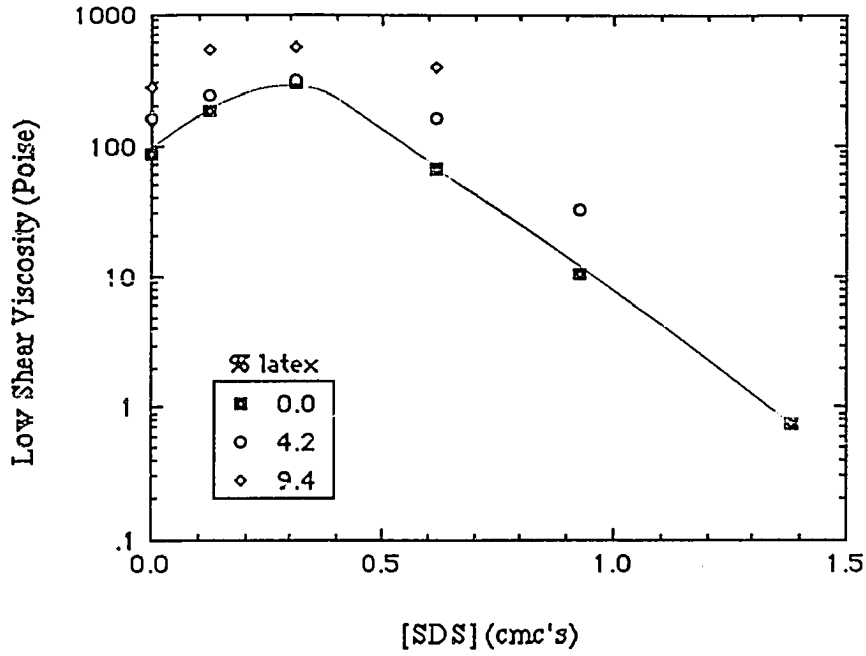

Figure 6.34: Influence of sodium dodecyl sulfate on the low shear viscosities of cleaned monodisperse 180 nm particle diameter polystyrene latexes of various solids content that contain 2.5% hexadecyl terminated model associative polymer of number average molecular weight 51,000.

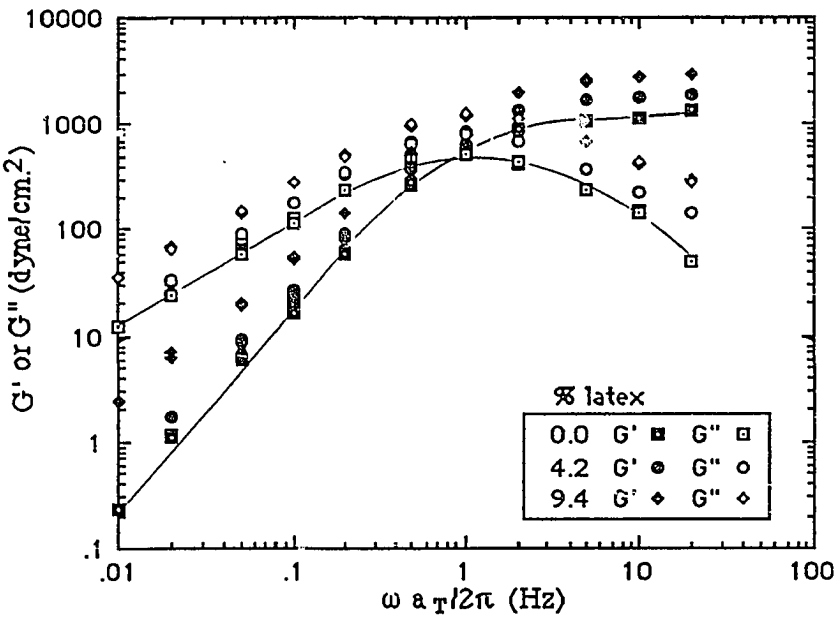

Figure 6.35: Dynamic shear moduli of cleaned monodisperse 180 nm particle diameter polystyrene latexes of various solids content that contain 0.001 Molar sodium dodecyl sulfate and 2.5% hexadecyl terminated model associative polymer of molecular weight 51,000.

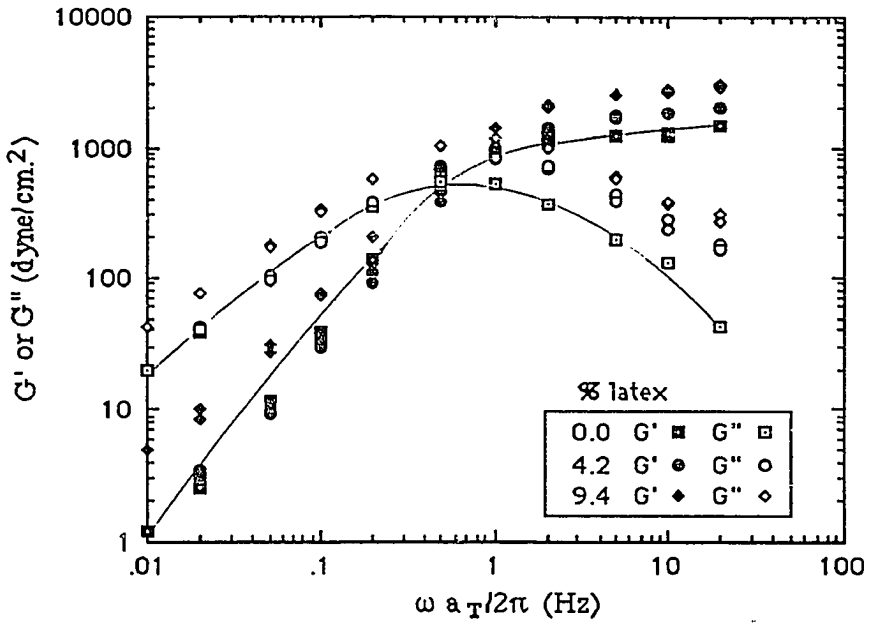

Figure 6.36: Dynamic shear moduli of cleaned monodisperse 180 nm particle diameter polystyrene latexes of various solids content that contain 0.0025 Molar sodium dodecyl sulfate and 2.5% hexadecyl terminated model associative polymer of molecular weight 51,000.

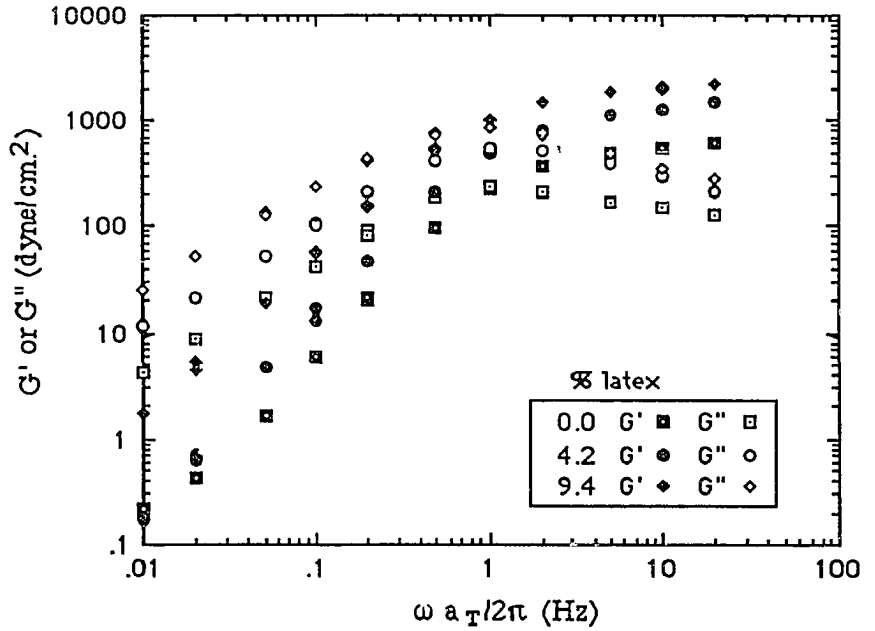

Figure 6.37: Dynamic shear moduli of cleaned monodisperse 180 nm particle diameter polystyrene latexes of various solids content that contain 0.005 Molar sodium dodecyl sulfate and 2.5% hexadecyl terminated model associative polymer of molecular weight 51,000.

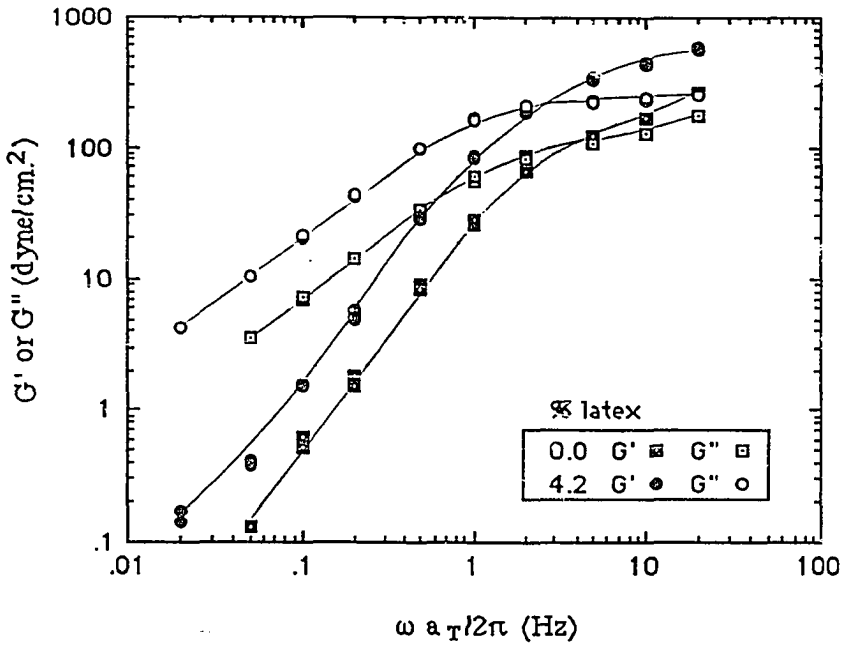

Figure 6.38: Dynamic shear moduli of cleaned monodisperse 180 nm particle diameter polystyrene latexes of various solids content that contain 0.0075 Molar sodium dodecyl sulfate and 2.5% hexadecyl terminated model associative polymer of molecular weight 51,000.

behavior (i.e., the slope on the plot is less than two on the doubly logarithmic plot). As shown in Figures 6.36 and 6.37, the storage modulus of a 9.4% solids content latex exhibits this solid- like behavior when the latex contains larger concentrations of sodium dodecyl sulfate, even though its viscosity profile does not have a yield stress. Sperry et al. showed that sodium dodecyl sulfate can desorb the associative polymer from latex, and that this can lead to volume restriction flocculation of the latex by the large associative polymer network in the dispersion medium. Based on their flocculation diagrams, this could suggest that the solid - like behavior of our latex systems that contain surfactant results from volume restriction flocculation. It seems reasonable that desorption of associative polymer by a surfactant influences the stability of the higher solids content more than a lower solids content latex that contains an equivalent concentration of

associative polymer. Likewise, it is expected that this instability would be most apparent with small amounts of surfactant, where the concentration of sodium dodecyl sulfate does not exceed that required to maximize the low shear viscosity. Competitive adsorption studies of associative polymer and sodium dodecyl sulfate are needed to uncouple the influence of desorption from the influence on binding with the aqueous phase network on the rheological properties and phase behavior of theses latexes.

Interaction Between Associative Polymer and Butyl Carbitol

Water miscible cosolvents reduce network formation, and hence both the viscosity and viscoelasticity of associative polymer solutions, by decreasing the driving force that expels the hydrophobic portions of the associative polymer from the aqueous phase. Schaller [124] studied the effect of the following water-miscible organic solvents on the viscosity of an acrylic latex thickened with a hydrophobically modified urethane-ethoxylate polymer: ethylene glycol, propylene glycol, diethylene glycol methyl ether, isopropanol, and diethylene glycol monobutyl ether (i.e., Butyl Carbitol®). Butyl Carbitol was the most effective in reducing the viscosity of latexes containing associative polymer, which is why we chose to focus on it in our investigations.

Consistent with the data that Schaller presents, the specific viscosity of associative polymer solutions decreases with increasing Butyl Carbitol concentration, and reaches a plateau at 20 weight percent cosolvent, which suggests that association effects have reached a minimum (Figure 6.39). To eliminate the variation in the viscosity of the solvent mixtures from our comparisons, the viscosity profiles in Figure 6.39 are plotted in terms of the specific viscosity of the associative polymer in solution: η/μ-1, where η is the viscosity of the solution and μ is the viscosity of the solvent mixture. (The viscosity of neat Butyl Carbitol is six times larger than the viscosity of water). The superposition of the relative viscosities of poly(oxyethylene) standards and all eighteen of our model associative

polymers in Figure 2.6 in Chapter II indicates that a 40%/60% mixture of Butyl Carbitol and water by weight has eliminated the intermolecular association. We took advantage of this effect in Chapter II and in the Appendix to verify the molecular weights of the model associative polymers.

Consistent with the disruption of network structure, Figure 6.40 shows that the addition of Butyl Carbitol to the associative polymer solution decreases their elasticity. The Butyl Carbitol suppresses the entanglement plateau in the storage modulus (G'), and shifts of relaxation time constant to higher frequencies (i.e., $\lambda \sim 1/\omega$); both effects indicate a decrease in network structure. Associative polymer solutions that contain solvent mixtures of 10% Butyl Carbitol or larger respond to the forced oscillations as purely viscous solutions. Because Butyl Carbitol is more viscous than water, we might expect that the shear moduli measured in a cosolvent mixture would be larger than that measured in pure water, and that the relaxation time constant of the associative polymer in the cosolvent mixture might shift to lower frequencies relative to that measured in pure water due to the hindered diffusion of the polymer chains in the network. Instead, the shift of the relaxation time constant of the associative polymer solutions to smaller values by the Butyl Carbitol cosolvent reflects a fundamental change in the network . For example, the relaxation time constant for the 2.5% associative polymer in 5% Butyl Carbitol (0.023 seconds) is about the same as a one percent solution of the same polymer in water (0.029 seconds), but its viscosity (30.3 Poise) is an order of magnitude larger than that of the 1% aqueous solution (0.951 Poise). So, Butyl Carbitol has affected dramatic change in elastic response of the solution, much more than can be explained from simply reducing the number of association junctions in solution. As a result, the data for model systems that contain Butyl Carbitol fall well beneath the other data in scaling correlation presented in Figures 6.44 and 6.45. This indicates that Butyl Carbitol not only disrupts the network structure, but also weakens the strength of interaction between hydrophobes.

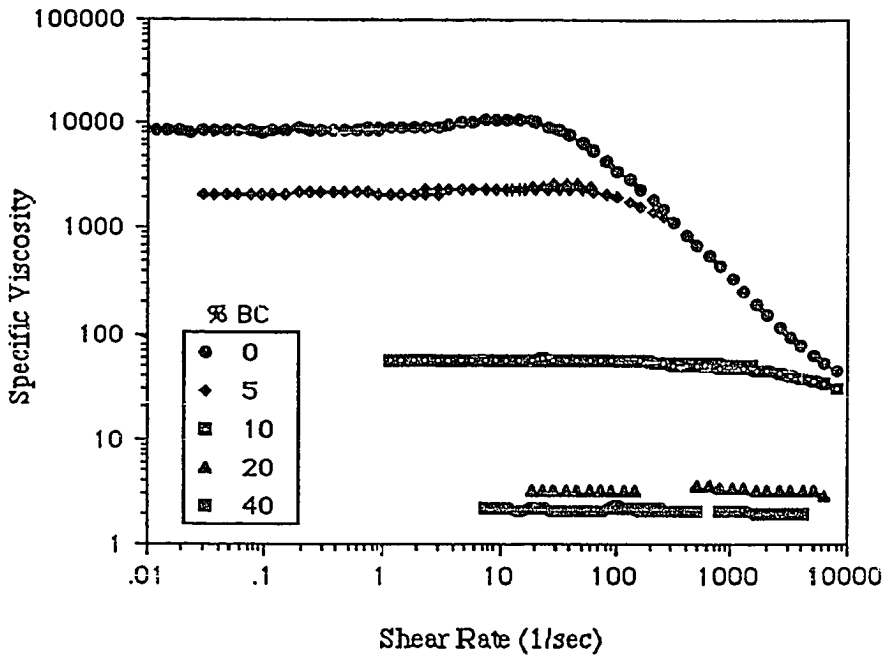

Figure 6.39: Steady specific viscosity profiles of 2.5% aqueous solutions of a hexadecyl terminated model associative polymer of number average molecular weight 51,000 that contain various weight fraction of Butyl Carbitol.

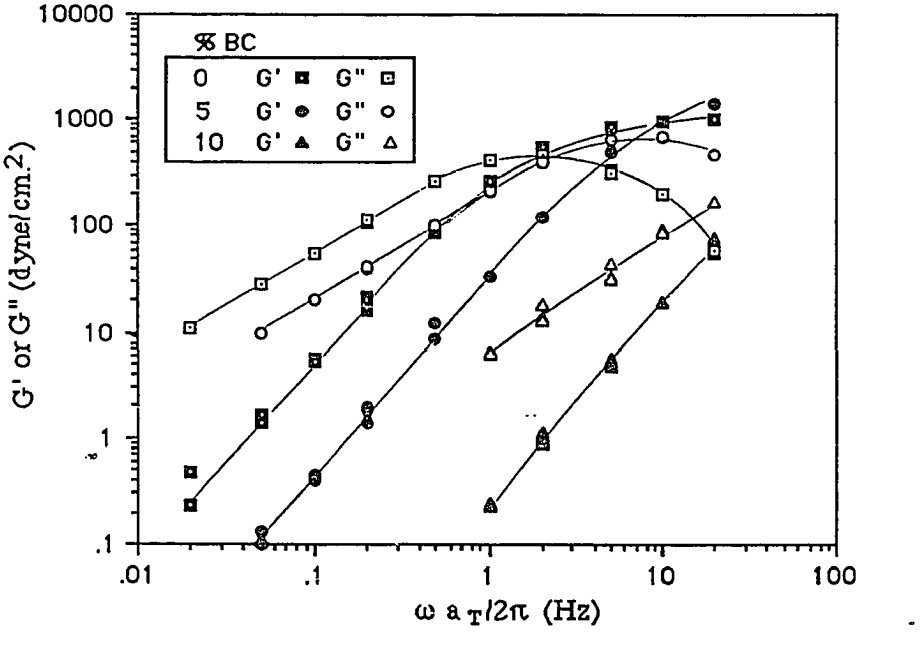

Figure 6.40: Dynamic shear moduli of 2.5% aqueous solutions of a hexadecyl terminated model associative polymer of number average molecular weight 51,000 that contain various weight fraction of Butyl Carbitol.

This could result either from a decrease in the functionality of the network junction or from a decrease in the free energy of association, as predicted by Equation (2.19) of Chapter II.

Interactions Among Associative Polymer, Butyl Carbitol, and Latex

Butyl Carbitol influences the rheological properties of latexes that contain associative polymer in exactly the same way that it influences the rheological properties of associative polymer solutions. The shear rate dependence of the specific viscosity of associative polymer in the latex systems is so close to that of associative polymer in solution, that the profiles of the latex systems overlap the viscosity profiles of the associative polymer solutions (Figures 6.41 and 6.42). This also carries over into the viscoelastic properties of latexes containing both associative polymer and Butyi Carbitol cosolvent (Figures 6.43 and 6.44). The storage and loss moduli of the latex systems are identical to those of an associative polymer solution. We might have expected that the cosolvent would swell the latex particles [125]. However, the viscosities of the latexes, as measured with a Bohlin Rheometer, were not different from the viscosities predicted by the Einstein equation when the nominal particle size of the latex and the viscosity of the cosolvent mixture are used. Sperry et al. showed that Butyl Carbitol desorbs associative polymer from latex, either by surface active displacement or by increasing the solubility of the polymer in the dispersion medium. Without adsorption isotherms made in the presence of Butyl Carbitol, it is difficult to uncouple the effect from desorption of the associative polymer from the effect of reducing the aqueous phase network on the rheology of the latex dispersions. Nonetheless, the composite effect of both effects on the specific viscosity of the associative polymer in the latex is identical to the effect of Butyl Carbitol on associative polymer solutions.

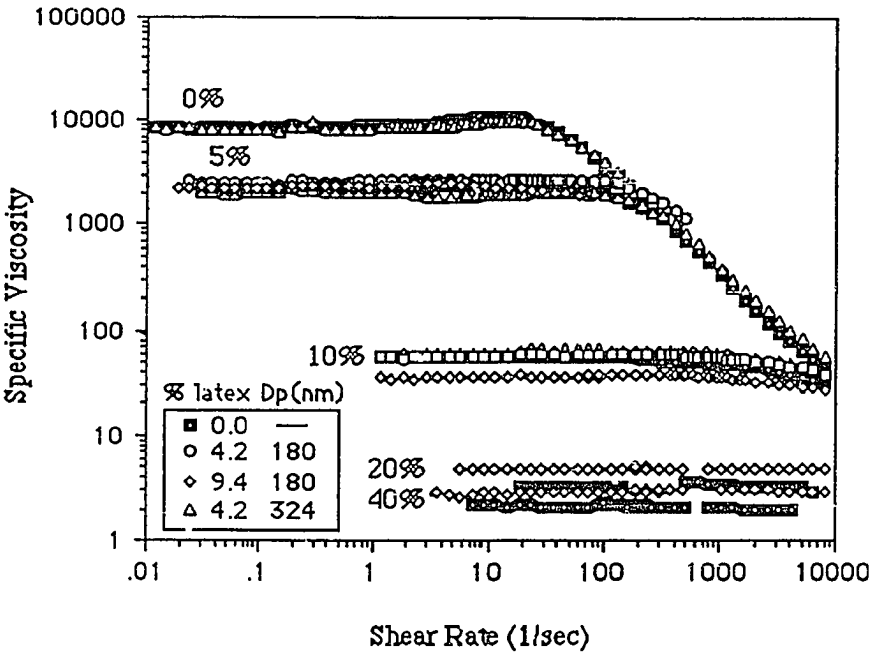

Figure 6.41:Steady specific viscosity profiles of cleaned monodisperse polystyrene latexes of various particle sizes and solids contents that contain various weight fractions of Butyl Carbitol and 2.5% hexadecyl terminated model associative polymer of 51,000 number average molecular weight.

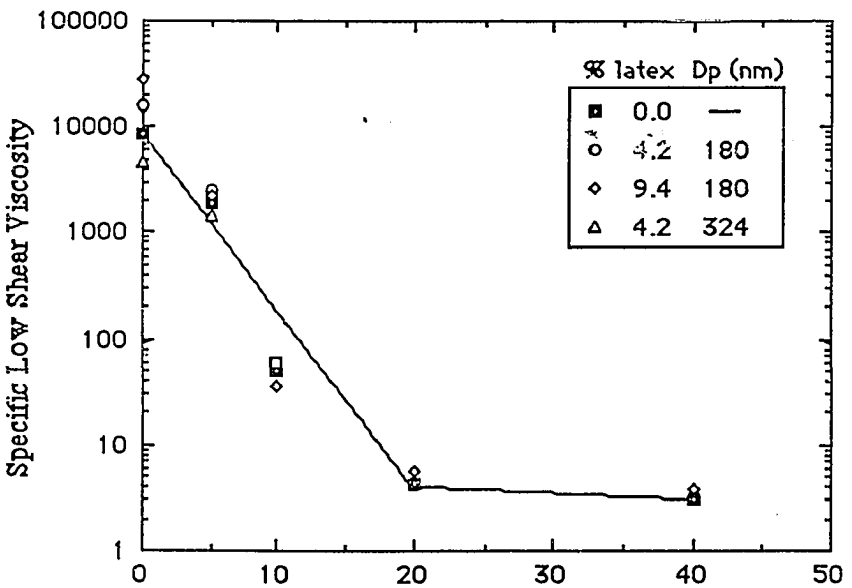

Figure 6.42: Influence of Butyl Carbitol on the specific low shear viscosities of cleaned monodisperse polystyrene latexes of various solids contents and particle diameters that contain 2.5% hexadecyl terminated model associative polymer of number average molecular weight 51,000.

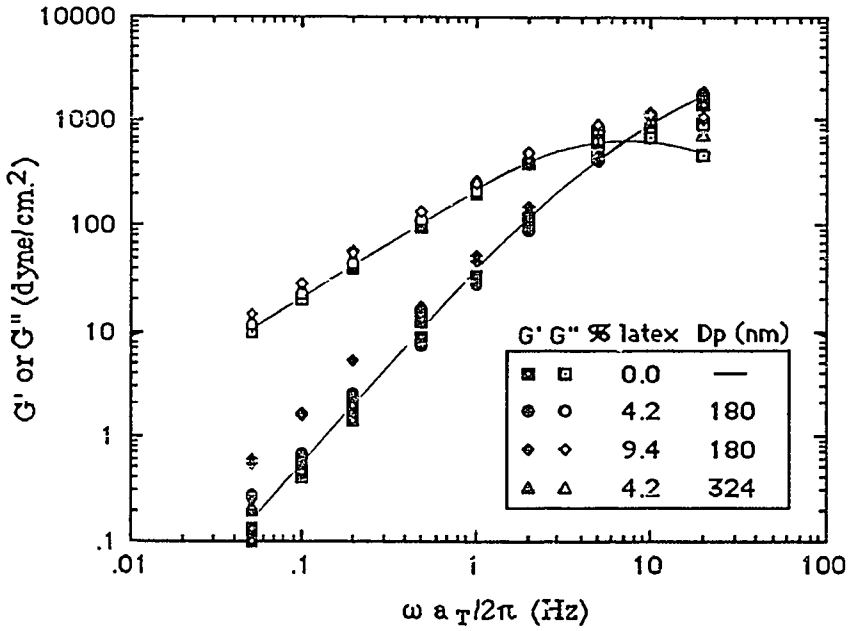

Figure 6.43: Dynamic shear moduli of cleaned monodisperse polystyrene latexes of various solids contents and particle diameters that contain 5% Butyl Carbitol cosolvent and 2.5% hexadecyl terminated model associative polymer of number average molecular weight 51,000.

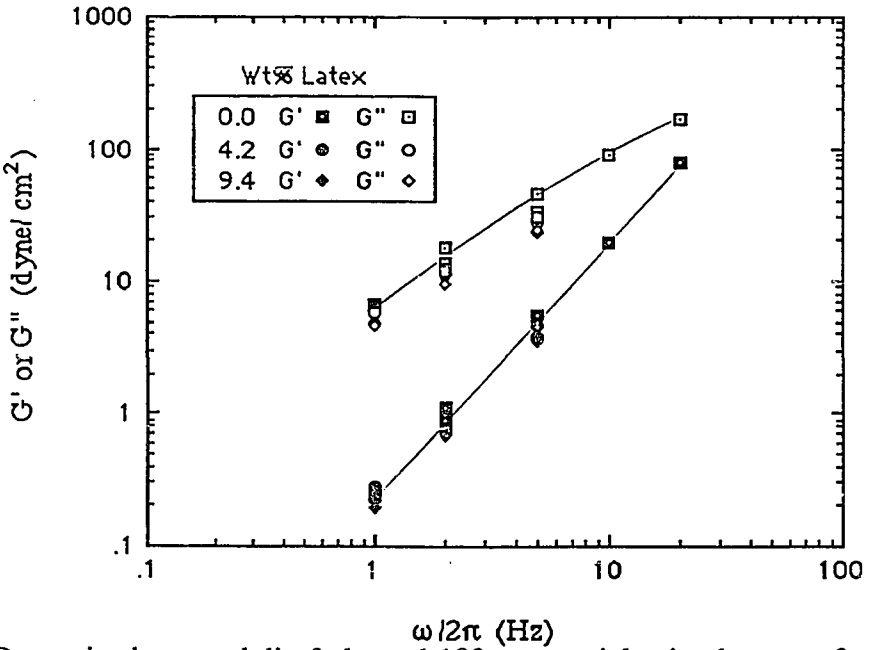

Figure 6.44: Dynamic shear moduli of cleaned 180 nm particle size latexes of various solids contents that contain 10% Butyl Carbitol cosolvent and 2.5% hexadecyl terminated model associative polymer of number average molecular weight of 51,000.

Scaling Concepts

Numerous interactions are possible in a ternary system of associative polymer, latex particles, and anionic surfactant: adsorption of the associative polymer to the particle surface, where the hydrophobic groups firmly anchor the polymer to the particle surface and the polymer backbone can adsorb in a loop and train conformation; competitive adsorption between the surfactant and the polymer at the particle surface; interaction between the hydrophobic groups of the surfactant and the hydrophobes of the polymer; ion-dipole interactions between the hydrophilic backbone and the ionic headgroup of the surfactant; and interaction between the counter-ion and the backbone of the associative polymer (e.g. the formation of a "crown ether" conformation by poly(oxyethylene) in solution). The literature usually assumes that the interaction between the associative polymer at the particle interface dominates all of the possible interactions to control the rheological properties of the latex dispersion. Furthermore, the viscosity profile of a dispersion that contains associative polymer is often interpreted in terms of desorption of thickener from the particle surface under shear, and the changes in viscosity of the dispersion upon the addition of a surfactant or a cosolvent is usually attributed to desorption of the associative polymer from the particle surface.

Despite the large number of possible interactions among associative polymers and other paint formulation components, our data indicate that the net result of the interactions is that, for dispersions that contain enough associative polymer to protect the latex against bridging flocculation, the network in the aqueous phase controls the rheological properties dispersion. For associative polymer solutions, we developed a correlation between the low shear viscosity of solution and the molar density of crosslinking by association in solution, which is calculated from the pseudo – equilibrium modulus of the solution as measured

Table 6.2: Viscoelastic Properties of Model Associative Polymer Solutions That Contain Sodium Dodecyl Sulfate

Concentration of: AP	[SDS] ($x10^3$M)	η_o (Poise)	λ (sec)	$\omega^\dagger$ (Hz)	ν ($x10^3$M)
2.5% C_{16-18}	2.0	1200	.192	.83	.253
	5.0	1720	.248	.66	.289
	13.0	655	.219	.72	.121
2.5% C_{16-34}	1.0	431	.158	1.0	.110
	2.0	552	.188	.85	.120
	3.0	658	.270	.59	.099
	4.0	652	.254	.63	.104
	5.0	551	.237	.67	.094
	6.0	356	.203	.78	.071
	13.0	4.66	-	-	-
2.5% C_{16-51}	1.0	185	.173	.92	.043
	2.5	303	.243	.65	.051
	5.0	64.9	.140	1.1	.019
	7.5	10.5	.049	3.2	.0086
	11.2	.750	.008	18	.0034
	13.0	.610	-	-	-
2.5% C_{16-68}	2.0	175	.193	.83	.037
	5.0	2.11	.032	5.0	.0027
	13.0	.022	-	-	-
2.5% C16-85	2.0	10.44	.087	1.8	.0051
	5.0	.503	-	-	-
	13.0	.116	-	-	-
2.5% C16-100	2.0	3.00	.053	2.9	.0023
	5.0	.225	-	-	-
	13.0	.114	-	-	-

† Frequency at which $G'(\omega)=G''(\omega)$

Table 6.3: Viscoelastic Properties of Latexes That Contain Model Associative Polymer

Concentration of: AP	Latex (wt%)	D_p (nm)	η_o (Poise)	λ (sec)	$\omega^\dagger$ (Hz)	ν ($\times 10^3$M)
2.5% C_{16-18}	4.2	324	411	.097	1.6	.170
2.5% C_{16-34}	4.2	324	98.9	.072	2.2	.056
2.5% C_{16-51}	4.2	324	83.2	.071	2.2	.047
2.5% C_{16-68}	4.2	324	48.6	.069	2.3	.029
2.5% C_{16-85}	4.2	324	14.4	.047	3.4	.013
2.5% C_{16-100}	4.2	324	1.65	.021	7.4	.0031
2.5% C_{16-18}	4.2	180	565	.119	1.3	.193
2.5% C_{16-32}	4.2	180	205	.095	1.7	.088
2.5% C_{16-51}	4.2	180	160	.099	1.6	.065
2.0%	4.2	180	84.5	.082	1.9	.042
1.5%	4.2	180	13.1	.051	3.1	.010
2.5% C_{16-68}	4.2	180	76.4	.086	1.8	.036
2.5% C_{16-85}	4.2	180	34.5	.079	2.0	.018
2.5% C_{16-100}	4.2	180	5.80	.046	3.5	.0051
2.5% C_{16-18}	9.4	180	430	.153	1.0	.114
2.5% C_{16-32}	9.4	180	280	.112	1.4	.101
2.5% C_{16-51}	9.4	180	278	.096	1.7	.051
2.0%	9.4	180	121	.082	1.9	.042
1.5%	9.4	180	19.1	.067	2.4	.012
2.5% C_{16-68}	9.4	180	78.0	.087	1.8	.036
2.5% C_{16-85}	9.4	180	41.0	.107	1.5	.016
2.5% C_{16-100}	9.4	180	8.54	-	-	-

† Frequency at which $G'(\omega)=G''(\omega)$

Table 6.4: Viscoelastic Properties of 180 nm Particle Diameter Latexes That Contain Model Associative Polymer and Sodium Dodecyl Sulfate

Concentration of: AP	Latex (wt%)	[SDS] (x 10^3M)	η_o (Poise)	λ (sec)	$\omega^\dagger$ (Hz)	ν (x 10^3M)
2.5% C_{16-51}	4.2	1.0	236	.142	1.1	.068
		2.5	307	.172	.93	.072
		5.0	159	.138	1.2	.047
		7.5	31.3	.075	2.1	.017
2.5% C_{16-51}	9.4	1.0	526	.190	.84	.112
		2.5	566	.195	.82	.116
		5.0	395	.198	.80	.081

† Frequency at which $G'(\omega)=G''(\omega)$

Table 6.5: Viscoelastic Properties of Latexes That Contain Model Associative Polymer and Butyl Carbitol

Concentration of: AP	Latex (wt%)	D_p (nm)	[BC] (wt%)	η_o (Poise)	λ (sec)	$\omega^\dagger$ (Hz)	ν (x 10^3M)
2.5% C_{16-51}	0.0	180	5.0	30.3	.023	6.9	.053
	4.2	180	5.0	35.0	.018	9.1	.081
			10.0	0.92	.005	35	.008
	9.4	180	5.0	45.0	.020	7.9	.090
			10.0	.75	.005	30	.006
	4.2	324	5.0	30.1	.017	9.4	.071

† Frequency at which $G'(\omega)=G''(\omega)$

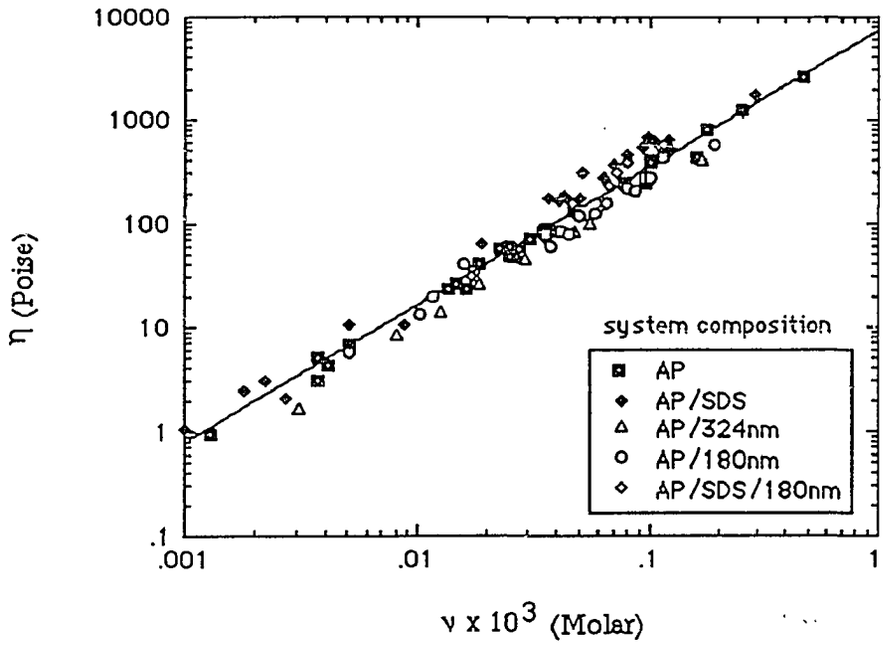

Figure 6.45: Correlation between low shear viscosity and the molar density of association network junctions for 1-5% hexadecyl terminated associative polymer of all molecular weights in solutions and latexes that contain surfactant or cosolvent. See Table 6.2 - 6.4 for system compositions.

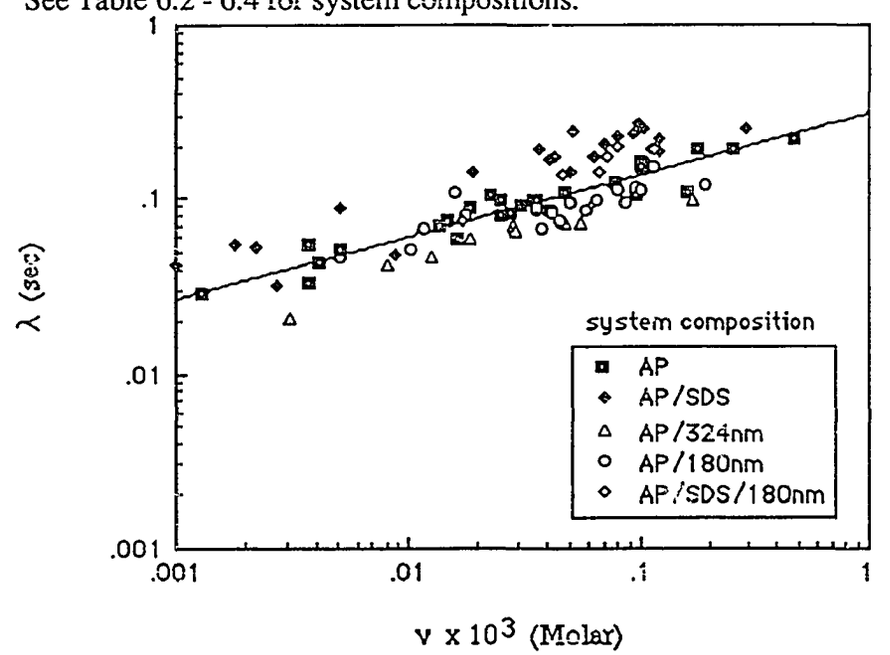

Figure 6.46: Correlation between relaxation time constant and the molar density of association network junctions for 1-5% hexadecyl terminated associative polymer of all molecular weights in solutions and latexes that contain surfactant or cosolvent. See Table 6.2 - 6.4 for system compositions.

from frequency dependence of the solution's linear viscoelastic properties (Tables 6.2 through 6.5). Figures 6.45 and 6.46 show that the correlation also holds for latex systems, provided that the concentration of associative polymer and the strength of interaction between the associative polymer's hydrophobic groups and the surface of the latex particle are large enough to protect the latex from bridging flocculation. These figures include data from 180 nm and 324 nm monodisperse polystyrene latexes at 4.2% and 9.4% solids content, with and without 1 through 7.5 milliMolar sodium dodecyl sulfate for all six polymer molecular weights from 16,600 through 100,400 in 1.5% to 2.5% concentration in latex, and in 1% to 5% concentration in solution. So, even though these are highly interacting systems, the similarity between the viscosity profiles of the latexes thickened by associative polymers and those of associative polymer solutions suggest that the molar density of network junctions created by association in the dispersion medium can adequately explain the rheological properties of latexes that contain associative polymer.

Conclusions

The strength of interaction between the hydrophobic groups of the associative polymer and the latex particle surface dictates the colloidal stability of latexes that contain associative polymer; the hexadecyl terminated model associative polymers flocculate the latex by bridging when the concentration of associative polymer is less than that required to fully cover the latex particles. At larger associative polymer concentrations, such as those found in conventional latex paints, the dispersions are stable, and the aqueous phase network controls the rheological properties of the dispersion. Even though the backbone associative polymer possibly adsorb to the latex surface, the rheological data suggest that the particles primarily reside at the hydrophobic junctions of the network, and become part of the dynamic network created by Brownian processes (Figure 6.47). The dominant

effect of added surfactants or cosolvents on the rheological properties occurs from changes these ingredients cause in aqueous phase network, although they will also effect the degree of adsorption of the associative polymer on the latex (Figure 6.48).

Future investigations should focus on sizing and characterizing the floc formed by the bridging action of the associative polymer, and on the nature of the associative polymer/surfactant complex. Competitive adsorption experiments and colloidal stability experiments should elucidate what happens at the interface of particles when surfactants and cosolvents are added. Standard characterization techniques, such as surface tension, electrophoretic mobility, and light scattering measurements, can investigate the interactions between the hydrophobic and hydrophilic components of the associative polymer and surfactants and electrolytes in solution. These studies should encompass anionic, cationic, and nonionic surfactants whose hydrophobic components vary in size, from less than to greater in length than the hydrophobic groups of the associative polymer, and encompass the influence of the counter-ion valency and ionic strength of electrolytes. Furthermore, the results of these experiments should be related to the influence these formulation components exert on the rheological properties of associative polymer solutions and latexes that contain associative polymers.

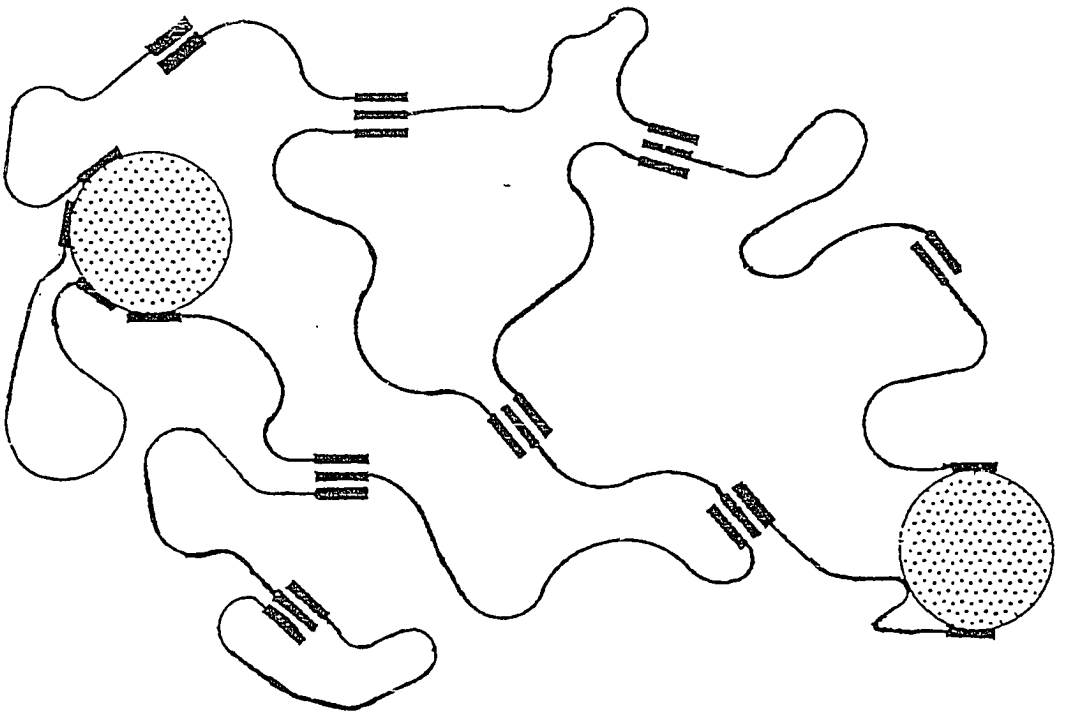

Figure 6.47: Schematic representation of the associative network at rest in a latex dispersion.

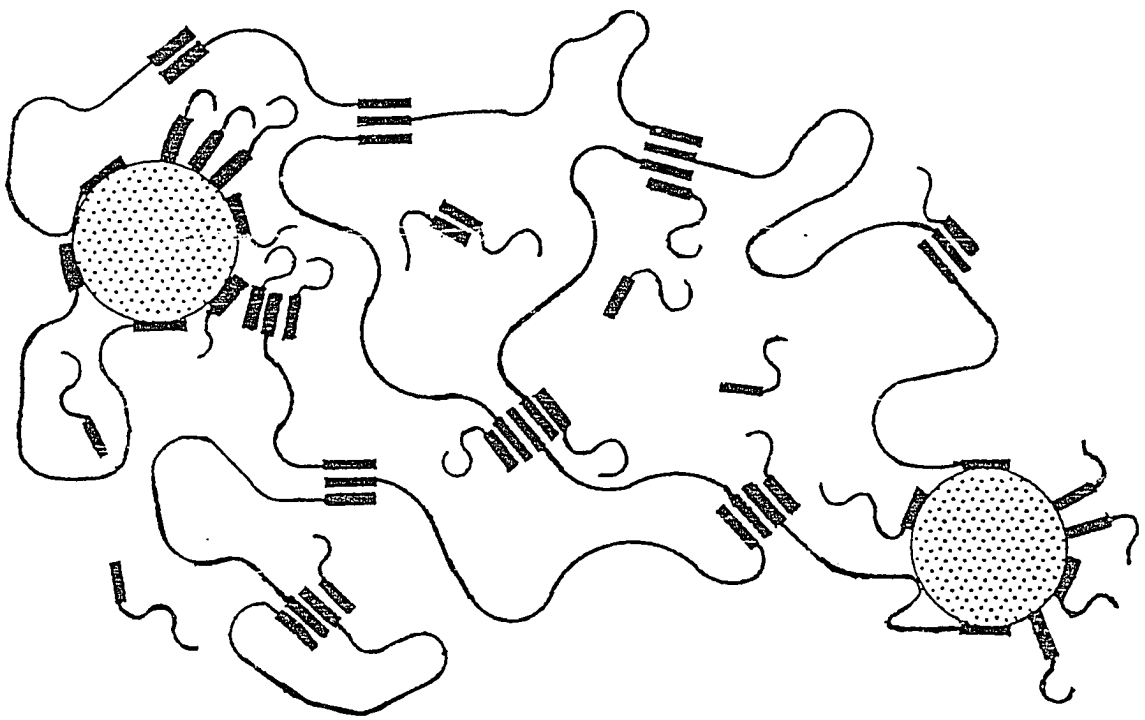

Figure 6.48: Schematic representation of the association network at rest in a latex that contains surfactant.

Chapter VII

Recommendations for Further Research

The ultimate goal of any research with model associative polymers is to understand, from fundamental principles, how the interactions among associative polymers and paint formulation components control the rheology of latex paints. Due to the large number of components in a latex paint, and the multiplicity of interaction among these components, this is not an easy task, nor one that a single dissertation can handle easily. Thus, we have chosen to examine a smaller subset of key systems in some detail rather than study a large number of complex systems in a cursory manner. Although this work has not been all encompassing, we hope that it lays a solid foundation upon which future research can build.

The obvious extension of this dissertation is to repeat the work described herein with model associative polymer of different architectures: vary the placement and size of hydrophobes on the backbone (trimers, combs); vary the structure of the hydrophobe (double - hydrophobes, phenolic hydrophobes); and include acid functionality or ionic groups in the backbone. Only slightly less obvious is the additional research with linear model associative polymers that would broaden the scope of the dissertation. The discussion on this subject is divided into four topics: molecular characterization, adsorption, phase behavior, and rheology.

Molecular Characterization

By molecular characterization, we mean experiments and analysis that will yield information on the individual polymers and its state in solution. First, we need to measure what fraction of the associative polymer backbones, if any, have not been capped with

hydrophobic groups. The hydroxyl number, or some other kind of end - group determination method, would reveal this information. Second, we need additional techniques to measure the molecular weight and molecular weight distribution of the model associative polymers, such as light scattering, membrane osmometry, and water based size exclusion chromatography. These experiments should be conducted in cosolvent mixtures, like mixtures of Butyl Carbitol and water, so that the dimensions of the molecularly dispersed associative polymer can be measured. The second virial coefficients obtained by light scattering and osmometry could be compared to those calculated in Chapter II of this dissertation. These experiments should be conducted on the model polymer samples in their current state, and after they have been fractionated to resolve the influence of the polydispersity of the associative polymer on solution properties.

We also desire direct measurements of the size and strength of the association complex in solution. Light scattering measurements in water and surfactant mixtures directly follow how the aggregate size builds up with concentration, and how surfactants influence the aggregation process. Techniques to measure the free energy of the self-association of the model polymers in the aqueous phase have remained elusive. One possibility is calorimetry to directly measure the enthalpy change of association (although this may not be easy). The morphology and nature of the association cluster or junction site has also remained a mystery. Some people have suggested that the association domains are really crystalline domains. Differential scanning calorimetry of the solutions and solid polymer, and cryogenic electron microscopy , may yield some answers to these questions.

Adsorption and Interactions with Latex Particles

First, the obvious extension of the adsorption studies detailed in this dissertation is to interface the adsorption apparatus with a computer. This should be a straightforward

task, as the computer software is commercially available, and most differential refractometers (and many other detectors) have analog- to- digital convertors built in. The computer will permit on - line monitoring and calculation of the adsorption isotherm, and increase the speed and precision of the apparatus. Second, we studied only polystyrene surfaces in this dissertation, although the method applies equally as well to adsorption of the model associative polymers to other kinds of latexes, (such as vinyl acrylics and acrylates), to latexes sterically stabilized with grafted chains, and to pigments as well.

We can easily generalize the adsorption method developed in Chapter V to measure the adsorption isotherms of multi - component systems where several species adsorb simultaneously, such as the competitive adsorption of surfactants and associative polymers. To perform the true competitive adsorption experiment between associative polymers and surfactants, a naked colloid is subjected to a step change in the concentrations of the surfactant and the associative polymer, and the adsorption isotherms of each species is monitored. Essentially, this experiment has two unknowns, the amounts of the associative polymer and the surfactant bound to the particle surface, and we therefore need two methods of detection (i.e., refractive index, UV adsorption, or fluorescence). One detector is needed to monitor the concentration of associative polymer in the effluent stream, and one is needed to monitor the concentration of the surfactant stream, or any combination of the two. A mass balance on each component then yields the adsorption isotherms. An alternate experiment is to pre- adsorb either the surfactant or associative polymer to the latex surface, and monitor whether the remaining component can desorb it or not. A practically infinite number of systems composed from combinations of latex particles, pigments, associative polymers, and surfactants that can be studied by this technique.

If it is not possible to use two detectors, perhaps due to the low UV activity of the current model associative polymers, one can still infer the influence of surfactants and

cosolvents on the adsorption of associative polymers with the apparatus described in Chapter V. All that is needed is to treat the surfactant or cosolvent solution as a pseudo - solvent. This means using a reference stream that contains an identical concentration of the surfactant or cosolvent as the associative polymer feed stream contains, and pre-adsorbing the surfactant to the latex surface before the experiment. (With the cosolvent, the latex should be pre-swollen.) In this way, the concentration of surfactant or cosolvent in the serum replacement cell should remain nearly constant, and a single detector can monitor the adsorption of the associative polymer. By performing several experiments where all is equal except the concentration of surfactant or cosolvent in the system, one could infer the nature of the competitive adsorption between the surfactant the associative polymer.

Other experiments that the adsorption apparatus of Chapter V can perform include "off- line" desorption experiments, and examination the adsorption of aggregates. In Chapter V, the desorption experiment immediately followed the adsorption experiment; performing the two experiments in series had certain advantages, but the precision of the desorption suffered due to the propagation of errors in the baseline from the adsorption experiment into the desorption experiment. To assess how important such errors were, we should perform the desorption experiment separately. This is now possible because we now know what the upper associative polymer feed stream concentration limit is for a given membrane pore size. Since the upper concentration limit in the associative polymer feed stream is governed by the ability of the membrane to pass the associative polymer, we can also examine the adsorption of aggregates, as opposed to the adsorption of nearly molecularly dispersed associative polymers that we studied in Chapter V, if we use extremely large particles and pore size membranes. Intuitively, we expect that the aggregates will adsorb with a different structure than the molecularly dispersed associative

polymer, and may exhibit a strong time dependence in the conformation of the adsorbed layer.

Other experimental techniques to investigate the interaction between latex particle and associative polymers include nuclear magnetic resonance, electrophoresis, fluorescence emission spectra, calorimetry, surface tension, and intrinsic viscosity. Nuclear magnetic resonance may be the best technique for monitoring the adsorption of aggregates, because it monitors the adsorption in situ, and does not require a separation of the latex and its sera. It may be one of the few ways to measure the adsorption of associative polymers to pigments, which sometimes have particle diameters that are smaller than the size of the associative polymer coil in solution. Electrophoresis could also measure how the associative polymers adsorb to charged surfaces, and how surfactants influence the adsorption, much in the same way that electrophoresis monitors the the adsorption of proteins to latex. Measurements of the florescence emission spectra can determine the spatial distribution of the association junctions sites, both in solution and in latex systems, at rest and under shear, and how polymer structure and latex formulation variables change this distribution. As far as we know, no one has used this technique to examine the effect of associative polymer molecular weight, latex surface characteristics, the influence of surfactants and cosolvents, and so on, and the thickener - latex interaction. We also need a direct measurement of the energy of adsorption that does not depend on an adsorption model. (Unfortunately, a model is needed to determine of the energy of adsorption from an adsorption isotherm.) One way might be calorimetry of associative polymers in the presence of latex. Surface tension measurements in the presence of latex would also yield the strength of the binding of the associative polymer to the latex surface from the Gibbs Equation. Even though we would need to uncouple the contributions from the activity of the associative polymer at the air- water interface from the interactions at the particle

interface, surface tension measurements would still provide a good relative measure of the strength of the latex - thickener interaction. In the same way, measurements of the surface tension of associative polymer solutions that contain surfactants can provide information on the strength of binding between the surfactant and associative polymer in solution. And finally, we should determine the hydrodynamic thickness of the adsorbed layer of associative polymer on latex particles from intrinsic viscosities measurements. These measurements would compliment current light scattering studies.

We need new models for the adsorption behavior of the model associative polymers; the classical adsorption models do not explain all of the features seen in the adsorption isotherm. Such models should start from first thermodynamic principles, and take into consideration the statistical nature of the associative polymer. Perhaps the current statistical mechanical models have been developed for the adsorption of block copolymers to surfaces can be extended to associative polymers.

Colloidal Stability

Most of the latex systems examined in Chapter VI contained enough associative polymer to apparently stabilize them against flocculation; we did very little work on the rheological behavior of latexes flocculated with associative polymer. The influence of surfactants and cosolvents on such systems would probe the resistance of the thickener - latex interaction to other formulation components. We should use microscopy of latex systems to determine if the "restabilized" latexes were truly restabilized in the thermodynamic sense, or simply stable in the kinetic sense. We had relied on the research of others to conclude that the latexes were truly thermodynamically stable.

We need to better understand the influence of associative polymer architecture on the phase stability of colloidal systems that contain associative polymers. In addition to the structure of the model associative polymer, such a study should consider the influence of

latex particle size, surface acid content, the kind of polymer that the particles are made from, and the concentrations of electrolyte, surfactants and cosolvents. The most critical step in the success of this study, and in the measurement of the thermodynamic phase diagrams, is the development of an assay method for the compositions of the colloid rich and colloid poor phases. Gravimetry can determine the fraction of colloidal particles in each phase, although this method cannot determine the distribution of floc sizes and structures. One rather crude method to determine the concentration of associative polymer in the colloid rich and colloid poor phases is to separate the serum and solids via centrifugation, and measurement of the concentration of associative polymer in the serum with differential refractometry or colorimetric titration.

Rheology of Latexes and Solutions

This work considered the effect of an anionic surfactant on the rheological properties of solutions and polystyrene latexes that contain model associative polymer; it is not difficult to to extend the work to include other formulation components that are found in commercial latex paints. Thus, this additional research on the rheology of model associative polymer systems should examine the influence of other anionic, cationic, and nonionic surfactants, and the influence of pH, electrolyte concentration and type, and mixed systems of electrolyte and surfactant. The effect that these variables have on the number and shear sensitivity of the aqueous phase network junctions is important.

Although the open literature contains some work on the rheology of fully formulated latex systems, experimental data from a set of model polymers that very systematically in molecular weight and hydrophobe length in fully formulated and pigmented latex systems obtained following the approach outlined in this dissertation can still make an unique contribution to an understanding of the association mechanism. The rheology of latex systems of compositions other than polystyrene should be studied, as

well as the rheology of pigmented latexes. Latex and pigment particle size distributions, surface acid content, and surfactant content are but a few of key variables controlling the rheology of such systems.

And finally, the statistical mechanical modelling presented in Chapter IV should be generalized to include the effect of the latex particles on the flow field, and the current model should be solved for an oscillatory strain.

Conclusion

This dissertation has highlighted only a few of the interactions that one could study rheologically or otherwise in latex systems that contain associative polymer. The large number of formulation variables, such as surfactant type, latex particle size and surface characteristics, and associative polymer architecture, make for an incredible number of systems permutations to study. Although this work raises as many questions as it answers, we hope that the work in this dissertation will serve as a control group to help illuminate the association mechanism in these more complicated systems.

Bibliography

[1] Patton,T.C. Paint Flow and Pigment Dispersion;John Wiley: New York, (1979), p.355.

[2] Glass, J.E., "Dynamics of Roller Spatter and Tracking III: Importance of Extensional Viscosities", Journal of Coatings Technology, 50(641), (1978), p. 56.

[3] Croll,S.G., and Kleinlein, R.L., "Influence of Cellulose Ethers on Coatings Performance", Chapter 17 in Water- Soluble Polymers: Beauty with Performance, Advances in Chemistry Series 213, American Chemical Society: Washington DC, J.E. Glass, Editor, (1986), p.333.

[4] Blake, D.H. "Effect of Molecular Weight On Performance of Cellulose Thickened Latex Paints", Journal of Coatings Technology, 55(701), (1983), p.33.

[5] Evani, S., and Rose,G.D.,"Water Soluble Hydrophobe Association Polymers", Proceedings of the American Chemical Society Division of Polymeric Materials: Science and Engineering, 57, (1987), p.477.

[6] Strivens, T. A., "Basis of Rheological Additives", Polymers Paint Colours Journal, 176(4161), (1986), p. 466.

[7] Hall,J.E.,"Titanium Chelates–A Novel Approach To Rheological Control in Latex Paints", Journal of Coatings Technology, 59 No.749, (1987), p.51.

[8] Boxall,J."Advances in Protective Coatings: Additives for Water–Bourne Paints", Polymers Paint Colours Journal, 176 No.4169 ,(1986), p.470.

[9] Schaller, E.J., Rheology Modifiers for Water Borne Paints", Surface Coatings Australia, 22(10), (1985), p. 6.

[10] Shay, G.D., "Alkali- Swellable and Alkali- Soluble Thickener Technology", Chapter 25 in Polymers in Aqueous Media: Performance Through Association, Advances in Chemistry Series 223, American Chemical Society: Washington DC, J.E. Glass, Editor, (1989), p.457.

[11] Hoy,K.L.,and Hoy,R.C. United States Patent 4,426,485 issued to Union Carbide Corporation, (1984).

[12] Sau, A.C., and Landoll, L.M.,"Synthesis and Solution Properties of Hydrophobically Modified (Hydroxyethyl) Cellulose", Ch 18. in Polymers in Aqueous Media: Performance Through Association, Advances in Chemistry Series 223, American Chemical Society: Washington DC, J.E. Glass, Editor, (1989), p.343.

[13] Goodwin,J.W.,Hughes,R.W.,Lam,C.K., Miles,J.A., and Warren,B.C.H.,"The Rheological Properties of a Hydrophobically Modified Cellulose", Chapter 19 in Polymers in Aqueous Media: Performance Through Association, Advances in Chemistry Series 223, American Chemical Society: Washington DC, J.E. Glass, Editor, (1989), p.365.

[14] Lesota,S., Lewandowski,E.W., and Schaller, E.J.,"Hydrophobically Modified Alkali-Soluble Emulsions as Thickeners for Exterior Latex Paints", Chapter 26 in Polymers in Aqueous Media: Performance Through Association, Advances in Chemistry Series 223, American Chemical Society: Washington DC, J.E. Glass, Editor, (1989), p.543.

[15] Thibeault,J.C.,Sperry,P.R.,and Schaller,E.J."Effect of Surfactants and Cosolvents on the Behavior of Associative Thickeners in Latex Systems", Chapter 20 in Water Soluble Polymers: Beauty with Performance, Advances in Chemistry Series 213, American Chemical Society: Washington DC, J.E. Glass, Editor, (1986), p.375.

[16] Sperry, P.R., Hopfenberg, H.B., and Thomas, N.L.,"Flocculation of Latex by Water- Soluble Polymers: Experimental Confirmation of a Nonbridging, Nonadsorptive Volume- Restriction Mechanism", Journal of Colloid and Interface Science, 82, (1981), p. 62.

[17] Sperry, P.R., "A Simple Quantitative Model for the Volume Restriction Flocculation of Latex by Water- Soluble Polymers", Journal of Colloid and Interface Science, 87, (1982), p. 375.

[18] Sperry, P.R., "Morphology and Mechanism in Latex Flocculated by Volume Restriction", Journal of Colloid and Interface Science, 99, (1984), p. 97.

[19] Sperry,P.R., Thibeault,J.C., and Kostansek,E.C.,"Flocculation and Rheological Characteristics of Mixtures of Latexes and Water Soluble Polymeric Thickeners", Proceedings of the Eleventh International Conference in Organic Coatings Science and Technology, Technomic Publishing Company: Lancaster, A.V. Patsis, Editor, (1985), p.371.

[20] Glass, J.E., Fernando, R.H., Egland-Jongewaard, S.K., and Brown, R.G. , "The Influence of Associative Thickeners on Coatings Performance. Part 1: Small Particle All-Acrylic Latex Studies", Journal of Oil Colours Chemists Association, (1984), 67(10), p. 256.

[21] Hall, J.E., Hodgson, P., Krivanek, L., and Malizia, P., "Influence of Rheology Modifiers on the Performance Characteristics of Latex Paints ", Journal of Coating Technology, (1986), 58(738), p. 65.

[22] Simpson, L.A., "Factors Controlling Gloss of Paint Films", Progress in Organic Coatings, 6, (1978), p.1

[23] Schwab, F.G., "Advantages and Disadvantages of Associative Thickeners in Coatings Performance", Chapter 19 Water Soluble Polymers: Beauty with Performance, Advances in Chemistry Series 213, American Chemical Society: Washington DC, J.E. Glass, Editor, (1986), p.369.

[24] Anwari, F.M., and Schwab, F.G., "Optimizing Latex Paint Rheology with Associative Thickeners", Chapter 27 in Polymers is Aqueous Media: Performance Through Association, Advances in Chemistry Series 223, American Chemical Society: Washington DC, J.E. Glass, Editor, (1989), p.527.

[25] David R. Bassett, Union Carbide Corporation, South Charleston, West Virginia, personal communication.

[26] Hall,J.E.,Hodgson,P.,Krivanek,L.,and Malizia, P.,"Influence of Rheology Modifiers on the Performance Characteristics of Latex Paints", Journal of Coating Technology, 58 No.738, (1986), p.65.

[27] Nguyen,B.D., and Rundin,A."Polyvinylacetate Emulsion Design and Rheological Performance in Latex Paints",Journal of Coating Technology, No. 736, (1986), p.53.

[28] Blake,D.M.,"Effect of Molecular Weight On Performance of Cellulosic Thickeners in Latex Paints", Journal of Coating Technology, No.701,(1983), p.33 .

[29] Glancy,C.W., "New Associative Thickeners Advance Latex Paint Technology", American Paint and Coatings Journal, August 6, (1984).

[30] Schaller, E.J.,"A Systems Approach to Rheology Control", Proceedings of the American Chemical Society Division of Polymeric Materials: Science and Engineering, 61, (1989), p.619.

[31] Bieleman, J.H., Riesthuis, F.J.J., and Van Der Velden, P.M., "The Application of Urethane Based Polymeric Thickeners in Aqueous Coating Systems", Polymers Paint Colours Journal, 176(4169), (1986), p. 450.

[32] Glass,J.E.,"Influence of Water Soluble Polymers on Rheology of Pigmented Latex Coatings", Chapter 21 in Water Soluble Polymers: Beauty with Performance, Advances in Chemistry Series 213, American Chemical Society: Washington DC, J.E. Glass, Editor, (1986), p. 391.

[33] Graessley,W.W., "The Entanglement Concept in Polymer Rheology", Fortschritte de Hochpolymer-Forschung, Springer-Verlag: Berlin, Volume 16, (1974), p.40.

[34] Frish,H.L., and Simha,R, "The Viscosity of Colloidal Suspensions and Macromolecular Solutions", in Rheology, F. R. Erich editor, Volume 1, Chapter 14 , (1956), p. 525.

[35] Simha,R., and Utracki, L.A. ," The Viscosity of Concentrated Polymer Solutions: Corresponding States Principles", Rheologica Acta 12, (1973), p. 455.

[36] Simha, R. ,"Effect of Concentration on the Viscosity of Dilute Solutions", Journal of Research of the National Bureau of Standards 42, (1949), p. 409.

[37] Gelman,R.A, and Barth, H.G.,"Viscosity Studies of Hydrophobically Modified (Hydroxyethyl)cellulose", Advances in Chemistry Series 213, Chapter 6, (1986), p. 101.

[38] Cornet, C.F. "The Determination of Unperturbed Dimensions of Polymer Molecules by Viscometry of Moderately Concentrated Solutions", Polymer 6, (1965) ,p. 373.

[39] Simha, R., and Zarkin,J.L., "Compression of Flexible Chain Molecules in Solution", Journal of Chemical Physics 33(6), (1960), p. 1791.

[40] de Gennes, P.G., Scaling Concepts in Polymer Physics, Cornell University Press: Ithaca, (1979), p. 40.

[41] Amu, T.C., "The Unperturbed Molecular Dimensions of Poly(ethylene oxide) in Aqueous Solutions from Intrinsic Viscosity Measurements and the Evaluation of the Theta Temperature", Polymer 23, (1982), p. 1775.

[42] Koleske, J.V., and Lundberg,R.D.,"Lactone Polymers. II. Hydrodynamic Properties and Unperturbed Dimensions of Poly-ε-caprolactone", Journal of Polymer Science Part A-2, 7, (1969), p.897.

[43] Beech,D.R., and Booth,C. ,"Unperturbed Dimensions of Poly(ethylene oxide)",Journal of Polymer Science Part A-2, 7, (1969), p.575.

[44] Crowie,J.M.G., "Studies on Amylose and Its Derivatives III. The Effect of Temperature on the Intrinsic Viscosities of Amylose in Several Solvents", Die Mackromolekular Chemie, 53, (1962), p. 13 .

[45] Kurata,M., and Stockmayer,W.H.,"Intrinsic Viscosities and Unperturbed Dimensions of Long Chain Molecules", Fortschritte der Hochpolymeren-Forschung, Bd. 3. ,(1963), p. 196.

[46] Stockmayer,W.H., and Fixman,M.,"On the Estimation of Unperturbed Dimensions from Intrinsic Viscosities", Journal of Polymer Science Part C, 1, (1963), p. 137.

[47] Flory,P.J., Principles of Polymer Chemistry, Second Edition, Cornell University Press:Ithaca, (1953), Chapters 12 and 14.

Flory,P.J.,and Fox,T.G., "Treatment of Intrinsic Viscosities", Journal of the American Chemical Society, 73, (1951), 1904.

[48] Ballard,M.J., Bushcall,R., and Waite, F.A., "The Theory of Shear-Thickening Polymer Solutions", Polymer 29, (1988) ,p. 1287.

[49] McGary,C.W., "Degradation of Poly(ethylene Oxide)", Journal of Polymer Science 46, (1960), p. 51.

[50] Elias, H.G., Macromolecules, Volume 1, second edition, Plenum Press: New York, (1984).

[51] Professor H. Daniel Ou-Yang, Department of Physics, Lehigh University, Bethlehem Pennsylvania, personal communication.

[52] Karunasena,A., Brown, R.G., and Glass, J.E., "Hydrophobically Modified Ethoxylated Urethane Architecture: Importance for Aqueous and Dispersed Phase Properties", Advances in Chemistry Series 223, Chapter 26, (1989), p.495.

[53] Bock,J., Siano,D.B., Valint,P.L., Pace,S.J., "Structure and Properties of Hydrophobically Associating Polymers", Chapter 22 in Polymers in Aqueous Media: Performance Through Association, Glass, J.E., ed.; Advances in Chemistry Series 223; American Chemical Society: Washington, D.C., (1989), p. 411.

[54] Brown,R.G., and Glass, J.E.,"Solution Properties of Hydrophobically Modified Ethoxylate–Urethane Polymers I: Star Polymers", Proceedings of the Polymeric Materials Science and Engineering Division of the American Chemical Society, 57, (1987), p. 709.

[55] Bailey,F.E., and Koleske,J.V.,"Configuration and Hydrodynamic Properties of the Polyoxyethylene Chain in Solution", in Nonionic Surfactants: Physical Chemistry ,Ch. 16, M.J. Schick editor, Marcel Dekker, (1987).

[56] Moacanin, J.A., "Diisocyanate-Linked Polymers. I. Dilute-Solution Properties of Toluene Dissocyanate-Extended Polypropylene Glycol", Journal of Applied Polymer Science, 1(3) (1959), p. 272.

[57] Newman,S., Krigbaum,W.B., Lauger,C., Flory,P.J., "Molecular Dimensions in Relation to Intrinsic Viscosities", Journal of Polymer Science 14, (1954), p. 451.

[58] Kurata,M.,Tsunashima,Y., Iwama,M., and Kamada,K.,"Viscosity-Molecular Weight Relationships and Unperturbed Dimensions of Linear Chains", Chapter IV in Polymer Handbook, second edition, J. Brandup, E.H. Immergut, and W. McDowell, editors, (1975).

[59] Bailey, F.E., and Callard,R.W., "Some Properties of Poly(ethylene oxide) in Aqueous Solution", Journal of Applied Polymer Science 1(1), (1959), p. 56.

[60] Debye,P., and Bueche,A.M.,"Intrinsic Viscosity, Diffusion, and Sedimentation Rate of Polymers in Solution" , Journal of Chemical Physics, 16, (1948), p.573.

[61] Kirkwood,J.G., and Riseman,J.,"The Intrinsic Viscosities and Diffusion Constants of Flexible Macromolecules in Solution",J. Chem Phys. 16(6), (1948), p. 565 .

[62] Peterlin,A. "Viscosity and Sedimentation of Linear Macromolecules Exhibiting Partial Solvent Immobilization",J. Poly. Sci 5(4), (1950), p.473.

[63] Kurata,M., and Yamakawa,H.,"Theory of Dilute Polymer Solution.II. Osmotic Pressure and Frictional Properties",Journal of Chemical Physics, 29(2), (1958), p.311.

[64] Polymer Handbook, second edition, J. Brandup, E.H. Immergut, and W. McDowell, editors, (1975), p. IV- 82.

[65] Weissberg,S.G., Simha, R., and Rothman,S. "Viscosity of Dilute and Moderately Concentrated Polymer Solutions", Journal of Research of the National Bureau of Standards, 47(4), (1951), p. 298.

[66] Zimm,B.H., and Stockmayer,W.H.,"The Dimensions of Chain Molecules Containing Branches and Rings", Journal of Chemical Physics, 17(12) , (1949), p. 1301.

[67] Lundberg, D.J.,Glass,J.E., and Eley,R.R., "Model - HEUR/Surfactant/Model Latex Matrix Rheology Studies", Proceedings of the Polymeric Materials Science and Engineering Division of the American Chemical Society, 1989, 61, (1989), p.533.

[68] Flynn, C.E., and Goodwin,J.W., "Some Solution Properties of Acrylamide Dodecyl Methacrylate Copolymers", Proceedings of the Polymeric Materials Science and Engineering Division of the American Chemical Society, 61, (1989), p. 522 .

[69] Maerker,J.M.; Sinton,S.W., "Rheology Resulting from Shear-Induced Structure in Associating Polymer Solutions", Journal of Rheology, 30(1), (1986), p.77.

[70] Walters, K., Rheometry, Chapman and Hall Ltd: London, (1975).

[71] Darby, R., Viscoelastic Fluids: An Introduction to Their Properties and Behavior, Macrel Dekker: New York, (1975).

[72] Ferry, J.D. , Viscoelastic Properties of Polymers, second edition, John Wiley and Sons: New York, (1970).

[73] Witten,T.A.; Cohen,M.H., "Cross - Linking in Shear-Thickening Ionomers", Macromolecules, 18, (1985), p. 1915.

[74] Lundberg,D.J., Ma, Z., Glass,J.E, "Elasticity Behavior and High Shear Viscosities Among Commercial and Model HEUR-Thickeners", Proceedings of the Polymeric Materials Science and Engineering Division of the American Chemical Society, 63, (1990), p. 440.

[75] Georgelos,P.N., and Torkelson, J.M., "The Role of Solution Structure in Apparent Thickening Behavior of Dilute PEO/Water systems", Journal of Non-Newtonian Fluid Mechanics, 27, (1988), p.191.

[76] Vrahopoulou, E.P., and McHugh, A.J., "A Consideration of the Yamamoto Network Theory with non-Gaussian Chain Segments", Journal of Rheology, 31(5), (1987), p.371.

[77] Bird,R.B.; Armstrong,R.C.; Hassager,O., Dynamics of Polymeric Liquids, Volume 1: Fluid Mechanics; Wiley and Sons: New York, (1977) p.355.

[78] Graessley, W.W.,The Entanglement Concept in Polymer Rheology; Springer-Verlag: Berlin, (1974), p.58.

[79] Richey,B., Kirk,A.B. ,Eisenhart,E.K., Fitzwater,S., and Hook,J.W., "The Interactions of Associative Thickeners With Paint Components As Studied By The Use of A Fluorescently Labeled Model Thickeners", Journal of Coating Technology, to appear, (1991).

[80] de Gennes, P.G., Scaling Concepts in Polymer Physics, Cornell University Press: Ithaca , (1979) p.54.

[81] Bird, R.B.,Hassager,O.,Armstrong,R.C., and Curtiss,C.F. , Dynamics of Polymeric Liquids; Volume 2: Kinetic Theory; Wiley and Sons: New York, (1977) ,Chapter 10.

[82] Yamamoto,M., "The Viscoelastic Properties of Network Structure. I. General Formalism", Journal of the Physical Society of Japan, 11(4), (1956), p. 413.

[83] Yamamoto,M.,"The Viscoelastic Properties of Network Structure. II. Structural Viscosity" , Journal of the Physical Society of Japan, 12(10), (1957), p. 1148.

[84] Yamamoto,M., "The Viscoelastic Properties of Network Structure. III. Normal Stress Effect (Weissenberg Effect)" , Journal of the Physical Society of Japan, 13(10), (1958), p. 1200.

[85] J. M. Schultz, Polymer Materials Science, Prentice Hall, Englewood Cliffs, NJ, (1974), p.307.

[86] A. Peterlin, "Hydrodynamics of Linear Macromolecules", Journal of Pure Applied Chemistry, 12 , (1966), p. 563.

[87] Fuller, G.G., and Leal,L.G., "Network Models of Concentrated Polymer Solutions Derived from the Yamamoto Network Theory", Journal of Polymer Science: Polymer Physics Edition, 19, (1981), p.531.

[88] Phan-Thien,N., and Tanner,R.I., "A New Constitutive Equation Derived from Network Theory", Journal of Non-Newtonian Fluid Mechanics, 2, (1977), p.353.

[89] Lodge, A.S., "Constitutive Equations from Molecular Network Theories for Polymer Solutions", Rheologica Acta, 7, (1968), p.379.

[90] Bird,R.B., "Kinetic Theory and Rheology of Solutions of Rigid Rodlike Macromolecules", Journal of Non-Newtonian Fluid Mechanics,14, (1984), p.85.

[91] Fuller,G.G., and Leal,L.G., "Flow Birefringence of Dilute Polymer Solutions in Two-Dimensional Flows", Rheologica Acta, 19 , (1980), p. 580.

[92] Fuller,G.G., and Leal,L.G.,"The Effects of Conformation-Dependent Friction and Internal Viscosity on the Dynamics of the Nonlinear Dumbbell Model for a Dilute Polymer Solution", Journal of Non-Newtonian Fluid Mechanics, 8, (1981), p. 271.

[93] Phan-Thien,N., Atkinson,J.D., and Tanner, R.I., "The Langevin Approach to the Dumbbell Kinetic Problem in Rheology", Journal of Non-Newtonian Fluid Mechanics, 3, (1978), p. 309.

[94] A. Peterlin,"Gradient Dependence of Intrinsic Viscosity of Freely Flexible Linear Macromolecules"Journal of Chemical Physics, 33(6), (1960) , p.1799.

[95] Hinch, E.J., Proc. Symp. Polym. Lubrification, Brest, (1974).

[96] Phan-Thien,N., Manero, O., and Leal,L.G., "A Study of Conformation-Dependent Friction in a Dumbbell Model for Dilute Solutions", Rheologica Acta, 23, (1984), p.151.

[97] Glancy, C.W, and Bassett, D.R.,"Effect of Latex Properties on the Behavior of Nonionic Associative Thickeners in Paint", Proceedings of the Polymeric Materials Science and Engineering Division of the American Chemical Society, 51 (1984), p. 348.

[98] Santore,M.M., "The Effect of Hydrophobically Modified Water-Soluble Polymer on the Phase Behavior of Colloidal Dispersions", Dissertation, Princeton University, (1990).

[99] Santore,M.M., Russel,W.B., and Prud'homme,R.K., "A Two-Component Model for the Phase Behavior of Dispersions Containing Associative Polymer", Macromolecules, 22 (1989), p. 1317.

[100] Graham, D.E., and Phillips,M.C., "Proteins at Liquid Interfaces: I. Kinetics of Adsorption and Surface Denaturation", Journal of Colloid and Interface Science, 70(3), (1979), 403.

[101] Ahmed, S.M., El-Aasser, M.S.,Pauli, G.H.,Poehlein, G.H., and Vanderhoff,J.W., "Cleaning Latexes for Surface Characterization by Serum Replacement", Journal of Colloid and Interface Science, 73(2), (1980), p.388.

[102] Kronberg,B.,Käll,L.,and Stenius,P.,"Adsorption of Nonionic Surfactants on Latexes", Journal of Dispersion Technology, 2(2&3), (1981), p. 215.

[103] Ahmed, S.M.,"Preparation and Characterization of Latexes", Dissertation, Lehigh University, (1979).

[104] Ahmed,M.S., El-Aasser,M.S., and Vanderhoff,J.W., "Adsorption-Desorption Behavior of Polyvinyl Alcohol on Polystyrene Latex Particles", American Chemical Society Symposium Series 240, (1984), p.77.

[105] Bisio , P.D., Cartledge,J.G., Keesom,W.H., and Radke, C.J., "Molecular Orientation of Aqueous Surfactants on a Hydrophobic Solid ", Journal of Colloid and Interface Science, 78(1), (1980), p. 225.

[106] Baker,J.A., Pearson,R.A., Berg,J.C. "Influence of Particle Curvature on Polymer Adsorption Layer Thickness", Langmuir, 5, (1989), p. 339.

[107] Clunie,J.S., and Ingram, B.T., "Adsorption of Nonionic Surfactants", Chapter 3 in Adsorption from Solution at the Solid/Liquid Interface: Academic Press, New York, G.D. Parfitt and C.H. Rochester editors, (1983).

[108] Hemker, D.J., Kookheon,C.,Hideko,T.O., Gast,A.P, and Frank, C.W., "Macromolecular Complex Formation and Polymer Adsorption on Colloidal Particles in Aqueous Solution", Advances in Chemistry Series 223, Chapter 13, (1989), p. 263.

[109] Silberberg, A.,"Multilayer Adsorption of Macromolecules", Journal of Colloid and Interface Science, 38(1), (1972), p. 217.

[110] Fuller,G.G., and Lee, J, "Flow-Enhanced Desorption of Adsorbed Flexible Polymer Chains", American Chemical Society Symposium Series 240, (1984), p.67.

[111] Cohen Stuart, M.A., Scheutjens,J.M.H.M., Fleer, G.J., "Polydispersity Effects and the Interpretation of Polymer Adsorption Isotherms", Journal of Polymer Science: Polymer Physics Edition, 18, (1980), p. 559.

[112] Kronberg,B., "Thermodynamics of Adsorption of Nonionic Surfactants on Latexes", Journal of Colloid and Interface Science, 96(1), (1983), p. 55.

[113] Bergh, J.S., Lundberg,D.J., and Glass, J.E., "Rheology of Associative Thickener Pigment and Pigmented Commercial Latex Dispersions", Progress in Organic Coatings, 17, (1989), p. 155.

[114] Karunsena, A., and Glass, J.E.,"Interactions in Associative Thickener 220 nm Methyl Methacrylate Latex Dispersions., "Progress in Organic Coatings, 17, (1989), p. 301.

[115] Abe, M., and Ogino, K., "Thermodynamic Studies of 1 - Dodecanol and SDS in Aqueous Solutions", Journal of Colloid and Interface Science, 80(1), (1981), p. 146.

[116] Jack Thibeault, Rohm and Haas Company, Spring House, Pennsylvania, personal communication.

[117] Goddard,E.D.,"Polymer-Surfactant Interaction. Part I. Uncharged Water - Soluble Polymers and Charged Surfactants", Colloids and Surfaces, 19, (1986), p. 255.

[118] Jones, M.N.,"The Interaction of Sodium Dodecyl Sulfate with Polyethylene Oxide", Journal of Colloid and Interface Science , 23 , (1967), p.36.

[119] Cabane,B,"Organization of Surfactant Micelles Absorbed on a Polymer Molecule in Water: A Neutron Scattering Study", Journal de Physique, 43 ,(1982), p. 1529.

[120] Nagarajan, R. "On the Nature of Interactions Between Polymers and Surfactants in Dilute Aqueous Solutions", Polymer Preprints , 22(2) ,p. 30 (1982).

[121] Bassett, D.R. ,and Glancy,C.W.,"Interactions of Associative Polymer with Surfactants in Aqueous Media", paper #31, Division of Colloid and Surface Chemistry, ACS National Meeting, Miami Beach, September 1989.

[122] Mukerjee, P., Mysels, K.J., "Critical micelle concentrations of aqueous surfactant systems", National Bureau of Standards Reference Data System, (1971).

[123] Durali, M. "Structure and Breakup of Flocs Subjected to Fluid Stresses", Graduate Research Progress Report Number 34, Emulsion Polymers Institute, Lehigh University, (1990).

[124] Schaller,E.J.,"Formulating Latex Paints with Associative Polymers", Advances in Emulsion Polymerization and Latex Technology: 20th Annual Short Course, M.S. El-Aasser editor, Lehigh University, June 1989.

[125] Karunsena,A., and Glass, J.E. , "Matrix Interaction in Water - Bourne Latex Coatings", Proceedings of the Polymeric Materials: Science and Engineering Division of the American Chemical Society, 58, (1988), p. 1125.

[126] McCormick,C.L., and Johnson, C.B., "Synthetically Structured Water- Soluble Copolymers. Associations by Hydrophobic or Ionic Mechanism", Polymers in Aqueous Media: Performance Through Association, American Chemical Society Advances in Chemistry Series 223, J.E. Glass, editor, (1989) p. 437.

Appendix A

Molecular Weight Determinations of Model Associative Polymers

Introduction

This appendix details some experiments that have been designed to verify the correctness of the model associative polymer molecular structure. The target structure is a linear backbone of poly(oxyethylene) of number average molecular weight between 16,000 and 100,400, terminated at the ends with either a hydroxyl, dodecyl, or hexadecyl alkyl group through a urethane linkage (see Table 2.1 of Chapter II). The backbone is composed of blocks of poly(oxyethylene) of 8200 number average molecular weight that have been connected through urethane linkages. The model polymer samples, and the results from the quality control tests and chromatography experiments that follow, were kindly provided by Union Carbide Corporation [25].

Although Union Carbide did not reveal to us all of the details of the model associative polymer synthesis, the procedure can be briefly summarized as follows. Catalyst and stoichiometric amounts of isophorone diisocyanate and a condensation alcohol are added batch - wise to a melt of Carbowax® 8000 (Union Carbide Corporation). The mixture is stirred until the melt becomes too viscous to allow further stirring, and the reaction mixture is then cured in an oven for several hours. By the nature of the reaction, all of the polymer chains should be terminated with the alkyl end-group from the alcohol. After curing, the beaker is broken away to reveal the solid model polymer. Because the reaction is diffusion controlled, a polymer with a statistical distribution of molecular weights results.

Results and Discussion

Quality Control

A convenient and simple quality control test to determine if the target structure has been achieved is described as follows. First, the viscosity of solutions of associative polymer of 20% solids in 20/80 solvent mixture by weight of Butyl Carbitol and water are measured with Brookfield viscometer. Butyl Carbitol is a trade name for a diethylene glycol monobutyl ether manufactured by Union Carbide Corporation. The Brookfield viscometer measures a low shear viscosity at an ill defined shear rate that is on the order of 1 to 10 sec^{-1}. The Butyl Carbitol cosolvent impairs the associative character of the model polymers, and the viscosity of the solutions should then increase as the molecular weight of the model polymer increases. Figure A.1 shows that the Brookfield viscosity increases as molecular weight increases for all hydrophobe types. However, the curves for the various end- groups do not superimpose. As we show in the following discussion, the molecular weights of polymers lie close to their target molecular weights irrespective of end- group type, so that the difference between the curves in Figure A.1 is due to the association phenomenon. Second, the solutions used for Figure A.1 are diluted with water from 20% to 2% solids content, which dilutes the cosolvent mixture from a Butyl Carbitol/ water ratio of 20/80 to 1.6/ 98.4. Figure A.2 shows how the viscosities of these diluted solutions vary inversely with thickener molecular weight, which is reminiscent of the low shear viscosity data presented in Figure 3.13. The viscosities of dodecyl and hexadecyl terminated polymers are much larger than viscosities of the model polymers in the 20% Butyl Carbitol solvent mixture, despite a ten fold decrease in the concentration of associative polymer, due to association among the thickener hydrophobes.

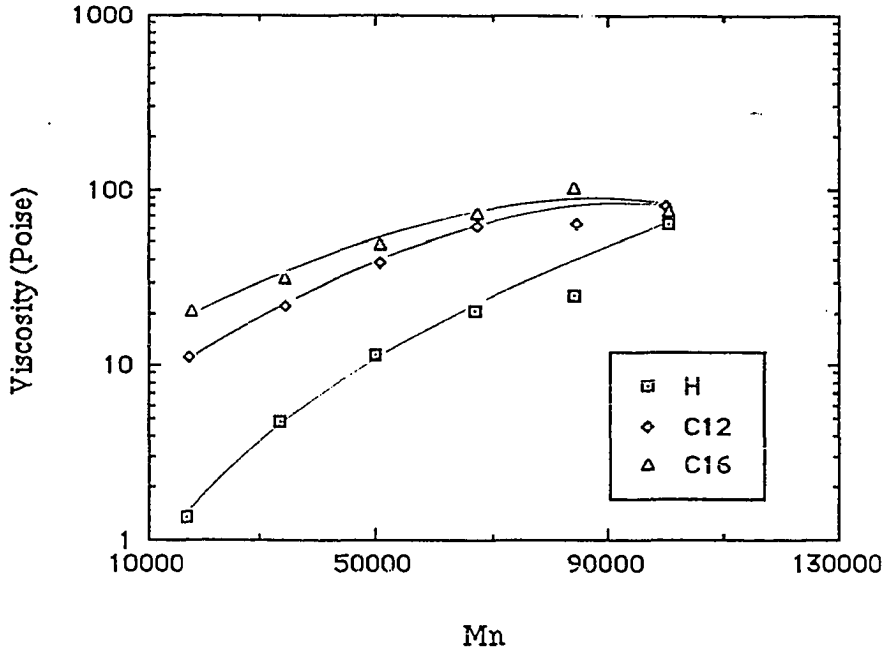

Figure A.1: Brookfield viscosities of 20% solids model associative polymers in a solvent mixture composed of 20% Butyl Carbitol and 80% water by weight at 23°C. Data courtesy of reference [25].

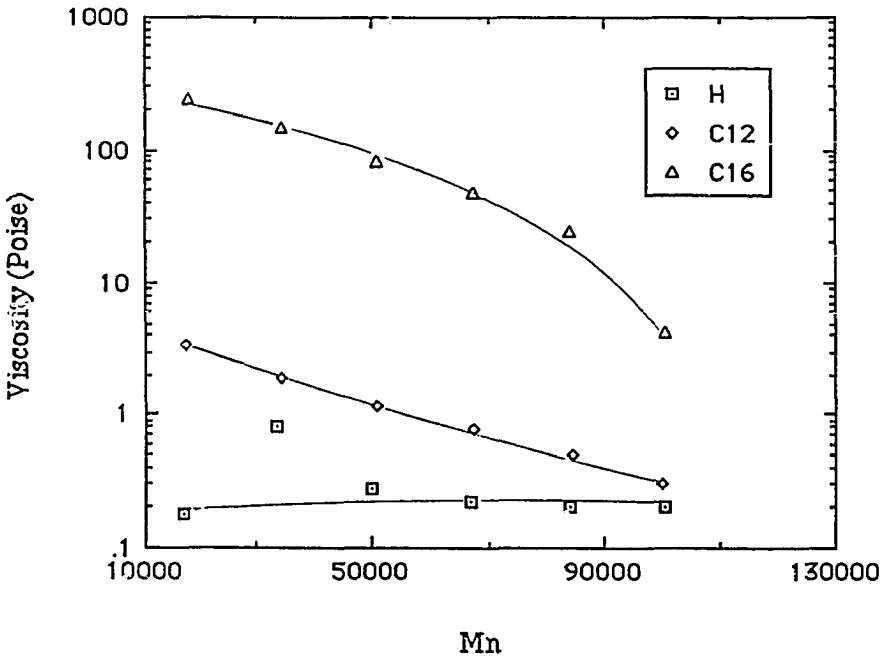

Figure A.2: Brookfield viscosities at 23°C of the solutions used for Figure A.1 diluted to 2% solids with water. Data courtesy of reference [25].

As expected for non-associative polymers, the viscosities of the hydroxyl terminated polymers increases as molecular weight increases. (In Figure A.2, note the difficulty in obtaining accurate data with the Brookfield for low viscosity fluids.) These tests quickly verify that the molecular weights increase as expected within a given series of molecular weights of polymers terminated with a given hydrophobic end- group, and verify that the polymers have indeed been capped with the appropriate hydrophobic groups.

Of course, these tests yield no information on the molecular weight distributions of a given model polymer, nor they do they guarantee that every backbone has been capped with a hydrophobe. Such information must come from chromatography and from end-group analyses.

Size Exclusion Chromatography

The model associative polymers were dissolved as 0.5 weight percent solutions in tetrahydrofuran, which were filtered with a large pore sized membrane to remove residual catalyst. The size exclusion column was calibrated with poly(oxyethylene) standards at ambient temperature, and had a resolution of 14,000 plates. Figures A.4 through A.21 present the resulting chromatograms. The figures are referenced both in our nomenclature from Table 2.1 and in the Union Carbide notebook nomenclature.

All of the chromatograms have two features in common. First, the molecular weight distributions are quite large with long low molecular weight tail, which is expected from the synthetic method. The molecular weight distributions of commercial associative polymers are likewise broad, and we suspect that the model polymers synthesized through urethane chemistry by other researchers also have broad molecular weight distributions. Bailey and Koleske [55] have reviewed several studies that have shown that poly(oxyethylene) can degrade mechanically in tetrahydrofuran while in a size exclusion

Table A.1: Summary of the Molecular Weights of Model Associative Polymers As Obtained From Various Methods

Reference		Calculated*	Size Exclusion Chromatography					Intrinsic Viscosity	
	R†	Mn	Mn	Mw	Mv§	Mz	PDI	Mn	Mv
$C_{0\text{-}16}$	H	16,600	15,600	38,600	34,400	72,700	2.5	10,200	23,100
$C_{0\text{-}33}$	H	33,400	29,300	77,800	69,400	146,000	2.6	18,400	44,000
$C_{0\text{-}50}$	H	50,200	29,400	105,000	93,000	208,000	3.6	20,500	67,000
$C_{0\text{-}67}$	H	67,000	31,300	128,000	112,000	263,000	4.1	22,700	82,200
$C_{0\text{-}84}$	H	84,000	36,000	140,000	123,000	285,000	3.9	26,400	95,400
$C_{0\text{-}100}$	H	100,400	40,200	168,000	146,000	348,000	4.2	30,800	117,000
$C_{12\text{-}17}$	C12	17,400	22,000	51,700	47,200	82,100	2.4	20,600	45,600
$C_{12\text{-}34}$	C12	34,200	27,700	77,800	70,900	122,000	2.8	25,900	66,700
$C_{12\text{-}51}$	C12	50,400	23,700	87,400	78,400	148,000	3.7	25,400	85,300
$C_{12\text{-}68}$	C12	67,700	29,100	101,000	91,800	158,000	3.5	30,200	96,000
$C_{12\text{-}85}$	C12	84,500	30,000	107,000	96,800	169,000	3.6	32,000	102,000
$C_{12\text{-}100}$	C12	99,900	28,800	109,100	98,900	173,000	3.8	36,000	124,000
$C_{16\text{-}18}$	C16	17,500	20,100	54,500	49,400	89,900	2.7	22,800	56,500
$C_{16\text{-}34}$	C16	34,200	13,500	65,300	58,500	108,000	4.9	15,300	68,100
$C_{16\text{-}51}$	C16	51,000	35,100	97,000	88,200	155,000	2.8	31,000	79,700
$C_{16\text{-}68}$	C16	67,600	13,100	93,000	81,600	167,000	7.1	15,800	99,600
$C_{16\text{-}84}$	C16	84,300	31,000	113,000	103,000	177,000	3.7	32,600	118,000
$C_{16\text{-}100}$	C16	100,400	29,300	105,000	95,800	164,000	3.6	35,800	117,000

* Calculated from reaction stoichiometry

† Type of end-group on polymer backbone

§ The Mark - Houwink exponent for poly(oxyethylene) is used to calculate the viscosity average molecular weight.

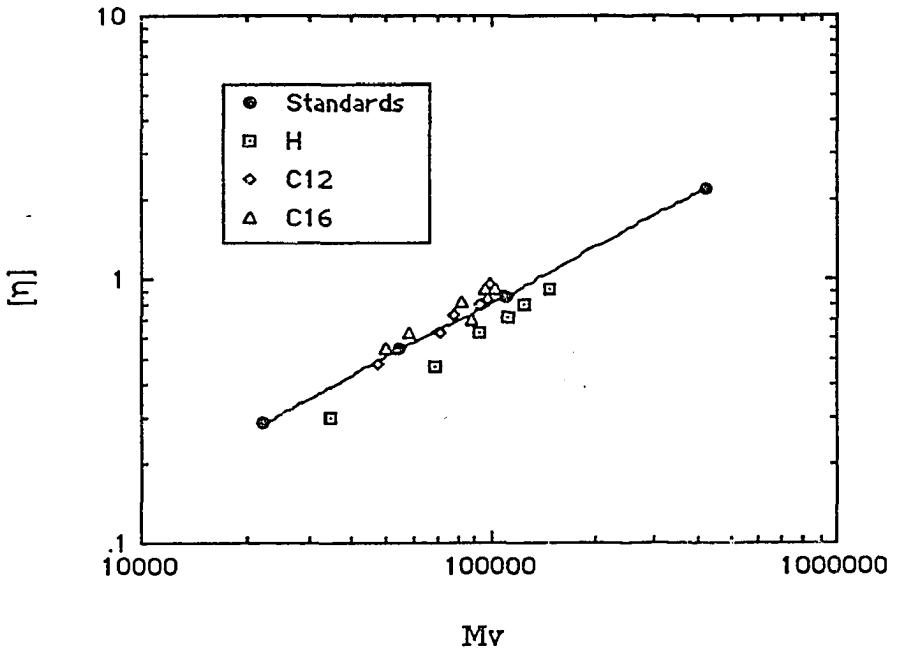

Figure A.3: Intrinsic viscosities of model associative polymers and poly(oxyethylene) standards obtained in a cosolvent mixture of 40% Butyl Carbitol and 60% water at 30°C. Data are plotted against viscosity average molecular weights obtained by size exclusion chromatography.

Table A.2: Molecular Weight Characteristics of Poly(oxyethylene) Standards**

Batch Number	Mn By SEC	Mw By SEC	Mn By MO	Mw By LALLS	Average PDI
23000	20,443	22,072	20,400	22,100	1.08
56300	51,814	54,337	54,000	58,100	1.07
105000	102,989	109,212	102,500	109,200	1.06
400000	390,210	419,886	392,000	408,500	1.06

** Pressure Chemical Company, Pittsburgh Pennsylvania

SEC denotes size exclusion chromatography
MO denotes membrane osmometry
LALLS denotes low angle laser light scattering
PDI denotes polydispersity index Mw/Mn

column. According to Beech and Booth [43], such degradation does not occur if a 50/ 50 mixture of ethanol and water is used to elute the poly(oxyethylene). This makes us wonder if the model polymers are indeed as polydisperse as the chromatograms indicate. Even though the samples are broad, one can easily discern a trend with respect to the peak molecular weight of the chromatogram, which corresponds closely to the viscosity average molecular weight. Second, the chromatograms have a shoulder, or a second peak for some of the lower molecular weight model polymers, that corresponds to a molecular weight of about 10,000. The shoulder grows smaller as the target molecular weight of the polymer increases. This suggests that the shoulder possibly results from some unreacted poly(oxyethylene) starting material. A small amount of unreacted starting material will, of course, influence intrinsic viscosity measurements, but should not significantly affect rheological measurements in larger concentrations where an association network exists.

Table A.1 compiles the molecular weight averages that are calculated from the chromatograms. We wanted to choose a benchmark molecular weight for each sample, but the breadth of the molecular weight distributions makes the selection of a characteristic molecular weight somewhat difficult. We shall use the number average molecular weight calculated from reaction stoichiometry for several reasons. First, it lies close to the peak molecular weight in the chromatograms, and seems to best represent the trends in the molecular weight progression in the model polymer series. Second, no other molecular weight average appears to serve any better. Third, we wish to retain uniformity of nomenclature with our previous publications, which used the number average molecular weight calculated from reaction stoichiometry, and with other research groups who have received the same samples from Union Carbide that we have. In any event, none of the general conclusions presented in this dissertation are affected by an error in the absolute

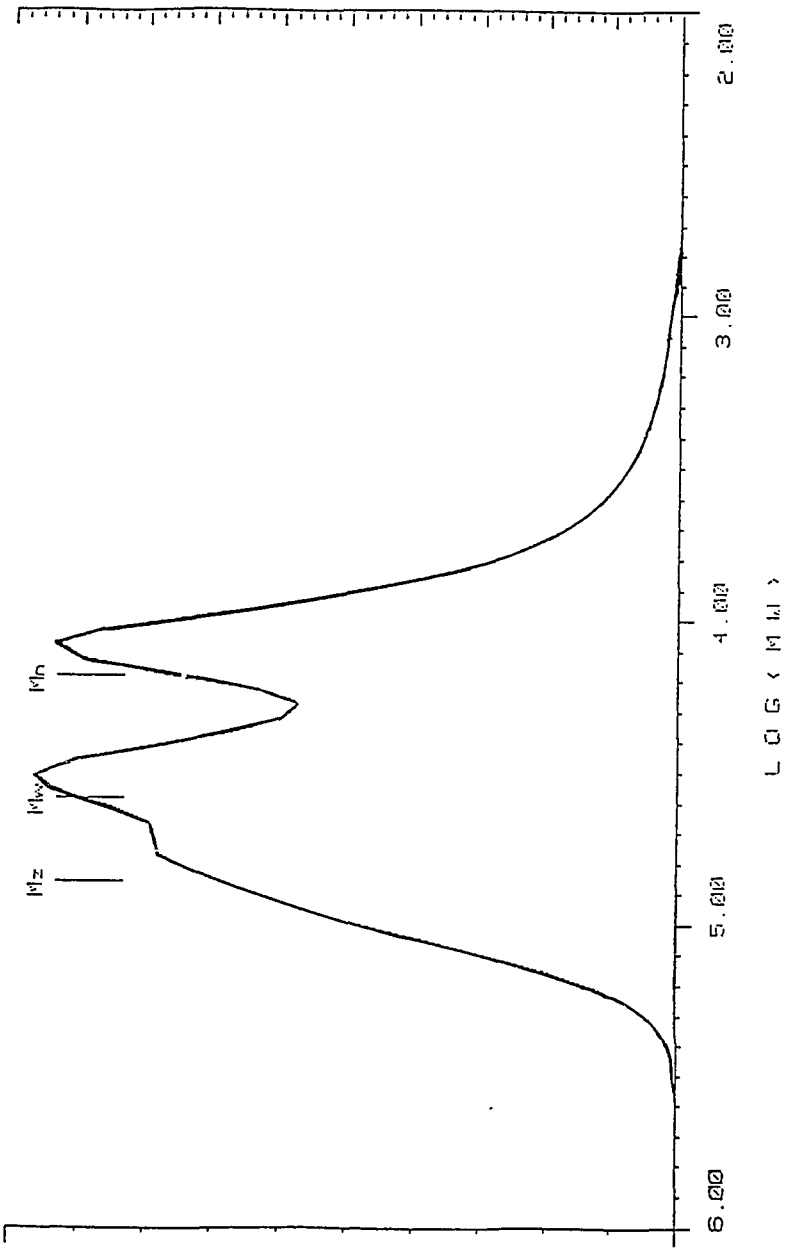

Figure A.4: Size exclusion chromatogram of sample 46-RCH-X-23-1, a hydroxyl terminated model associative polymer of 16,600 number average molecular weight as calculated from reaction stoichiometry ($C_{0\text{-}17}$).

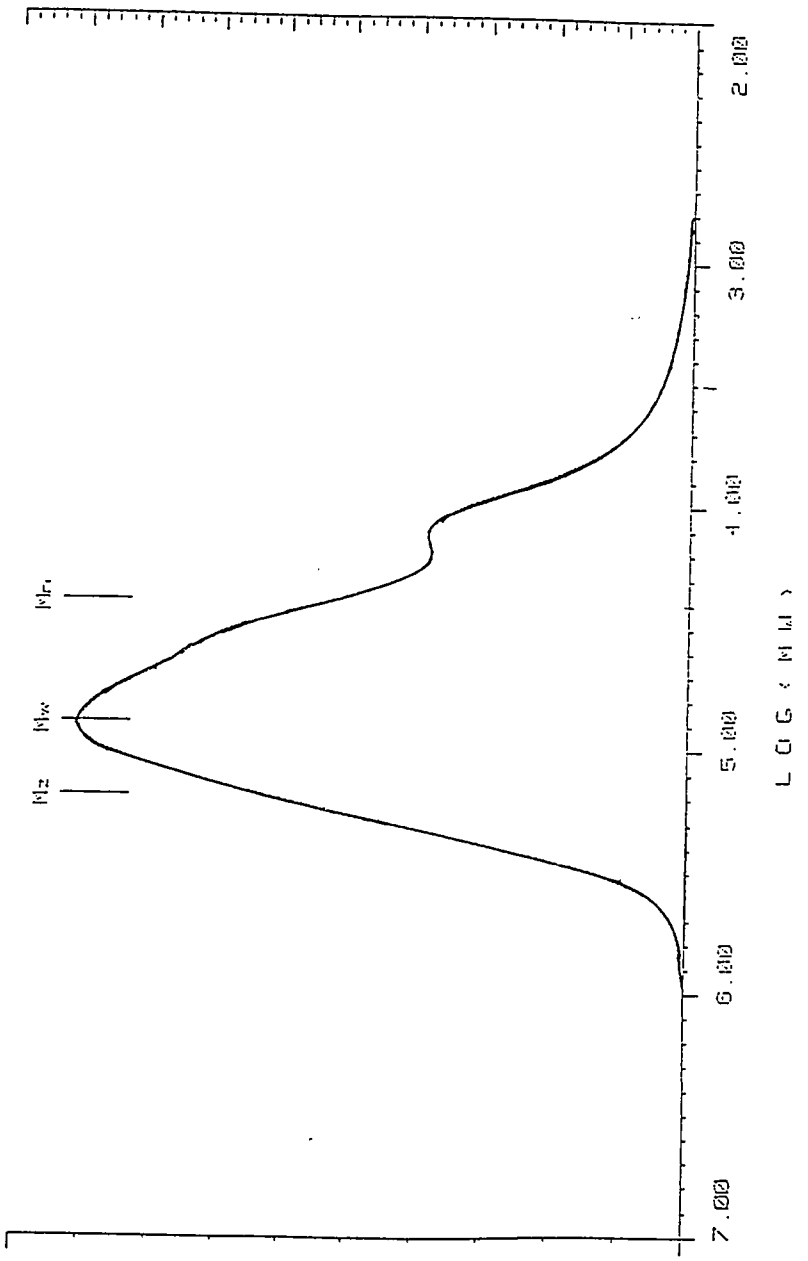

Figure A.5: Size exclusion chromatogram of sample 46-RCH-X-23-2, a hydroxyl terminated model associative polymer of 33,400 number average molecular weight as calculated from reaction stoichiometry ($C_{0\text{-}33}$).

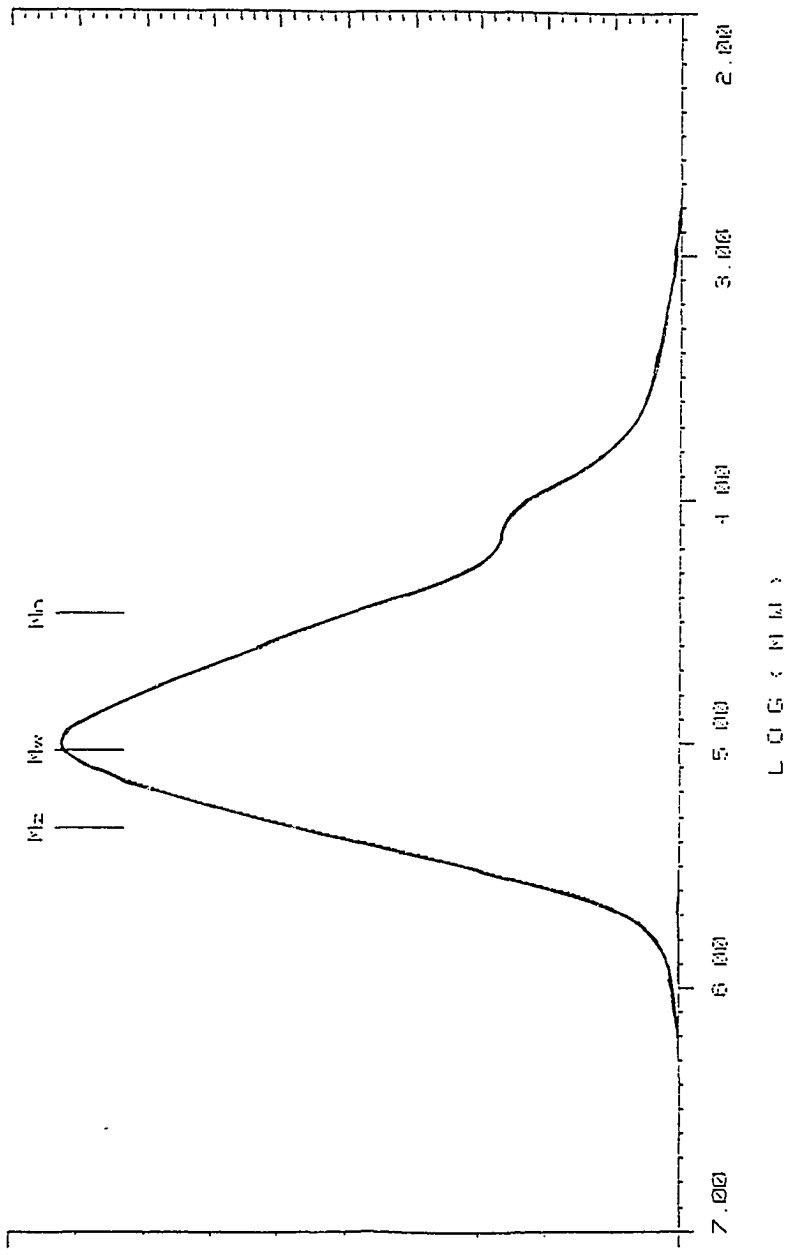

Figure A.6: Size exclusion chromatogram of sample 46-RCH-X-23-3, a hydroxyl terminated model associative polymer of 50,200 number average molecular weight as calculated from reaction stoichiometry ($C_{0\text{-}50}$).

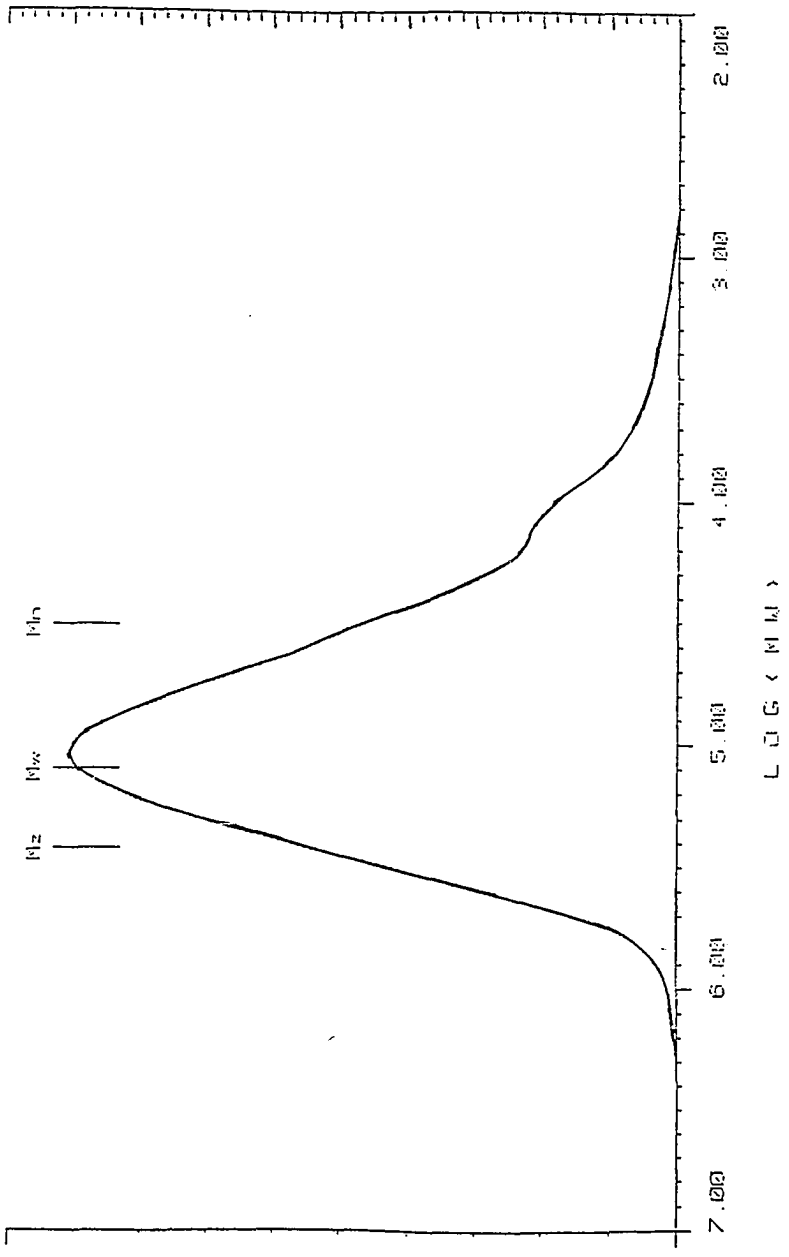

Figure A.7: Size exclusion chromatogram of sample 46-RCH-X-23-4, a hydroxyl terminated model associative polymer of 67,000 number average molecular weight as calculated from reaction stoichiometry ($C_{0\text{-}67}$).

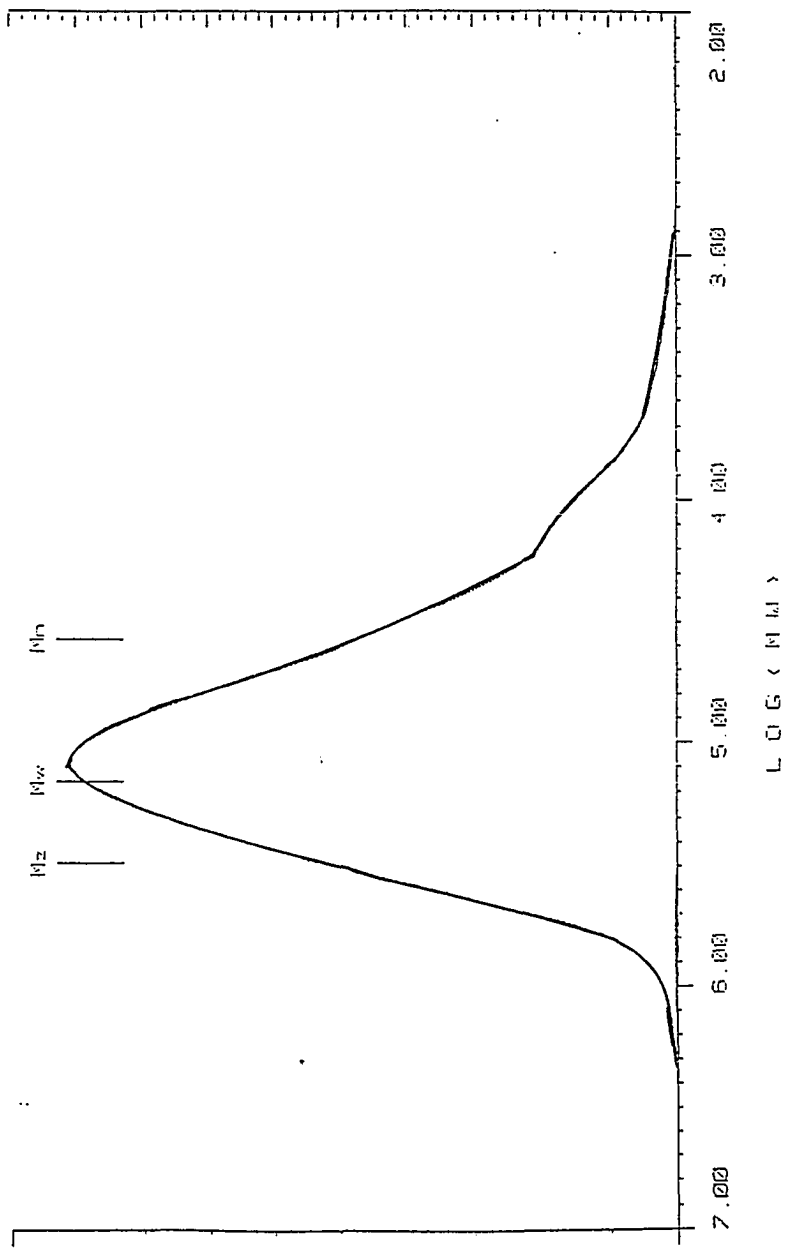

Figure A.8: Size exclusion chromatogram of sample 46-RCH-X-23-5, a hydroxyl terminated model associative polymer of 84,000 number average molecular weight as calculated from reaction stoichiometry ($C_{0\text{-}84}$).

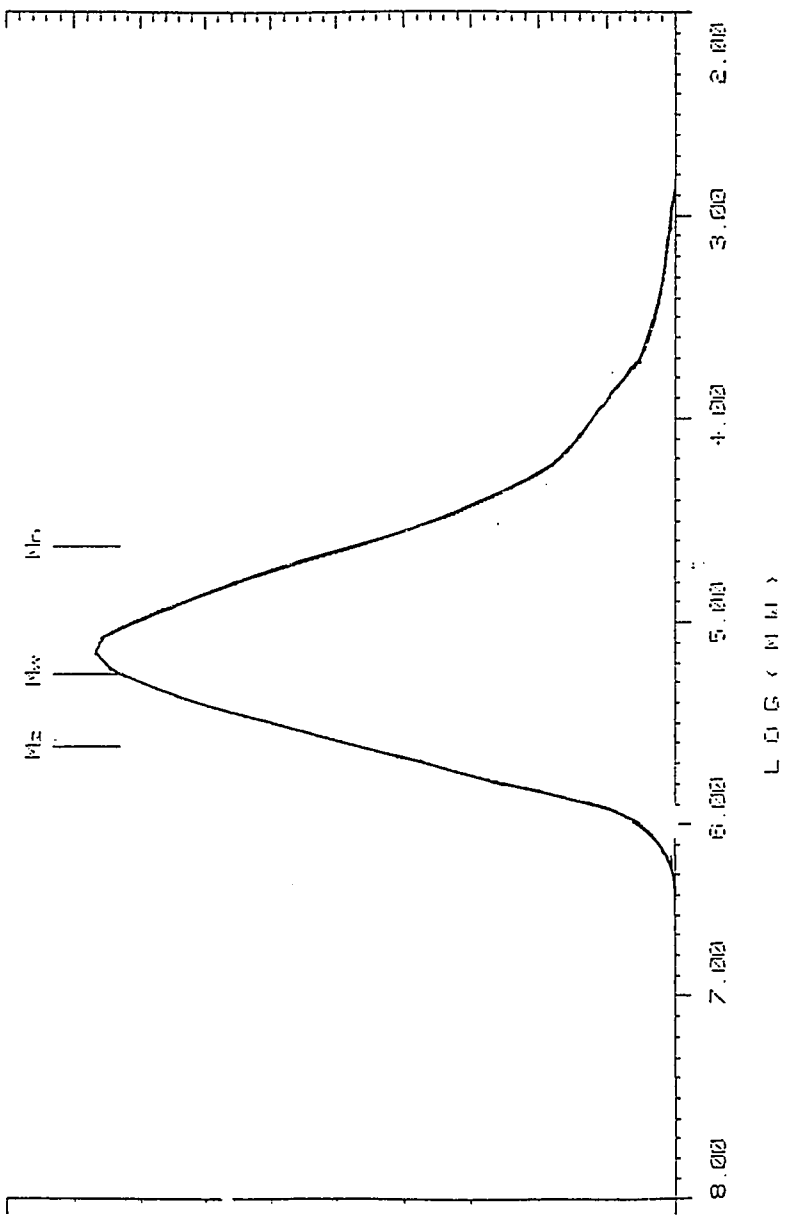

Figure A.9: Size exclusion chromatogram of sample 46-RCH-X-23-6, a hydroxyl terminated model associative polymer of 100,400 number average molecular weight as calculated from reaction stoichiometry ($C_{0\text{-}100}$).

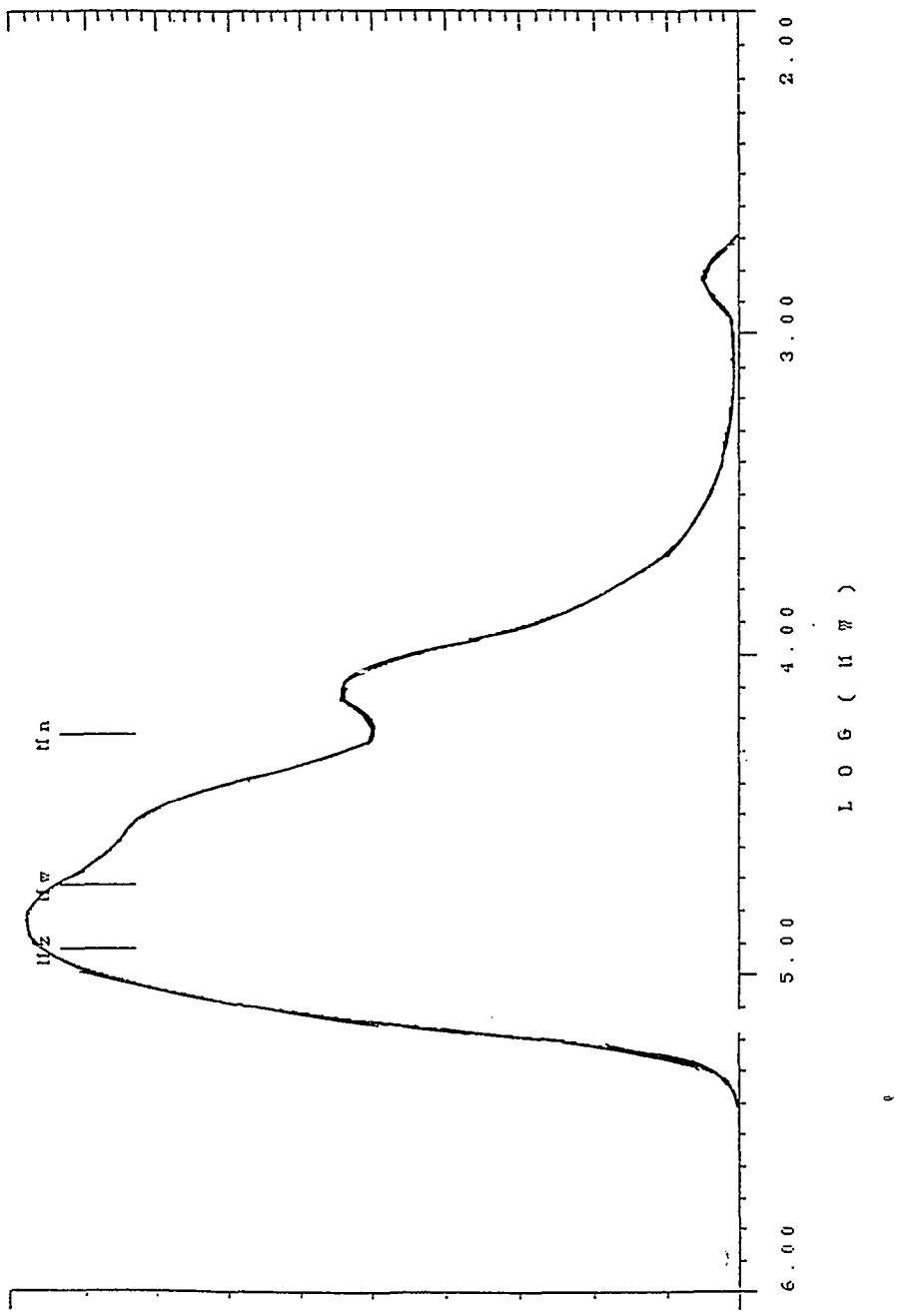

Figure A.10: Size exclusion chromatogram of sample 46-RCH-X-16-1, a dodecyl terminated model associative polymer of 17,400 number average molecular weight as calculated from reaction stoichiometry (C_{12-17}).

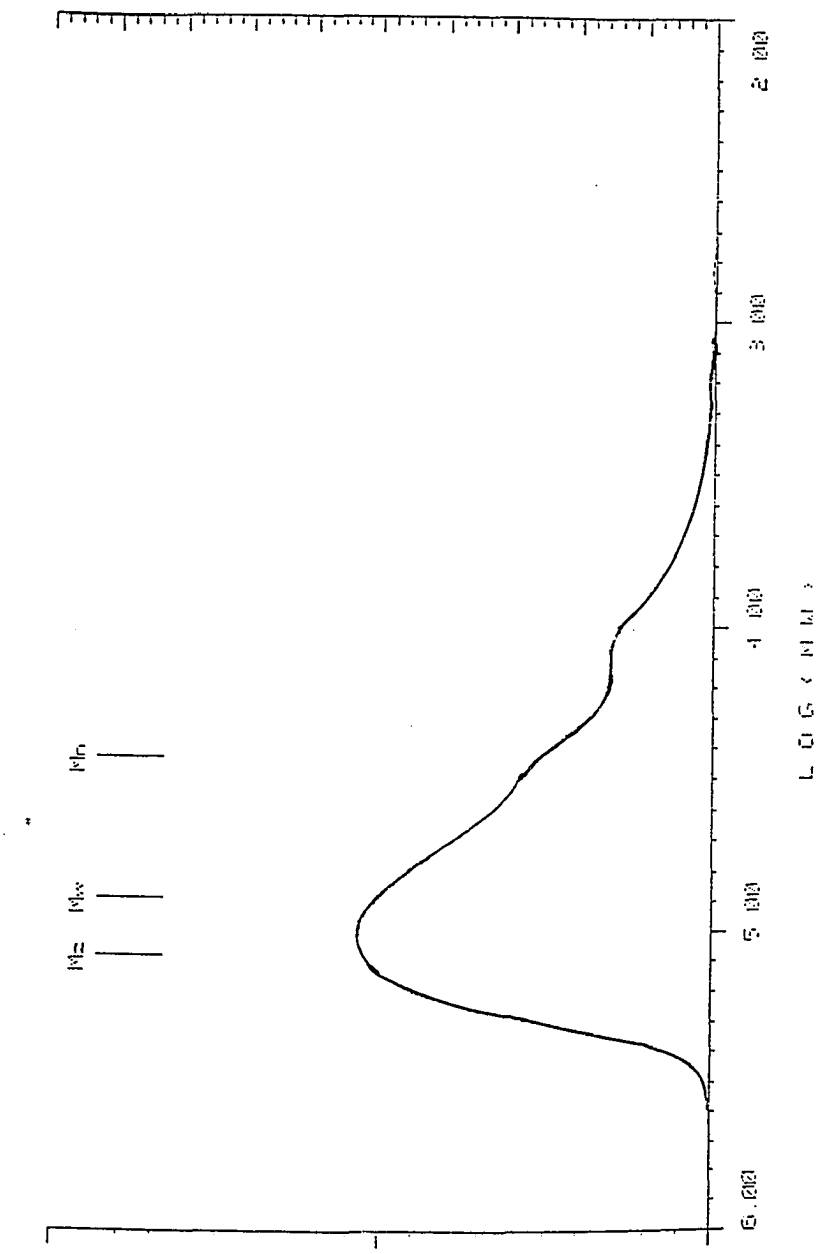

Figure A.11: Size exclusion chromatogram of sample 46-RCH-X-16-2, a dodecyl terminated model associative polymer of 34,200 number average molecular weight as calculated from reaction stoichiometry (C_{12-34}).

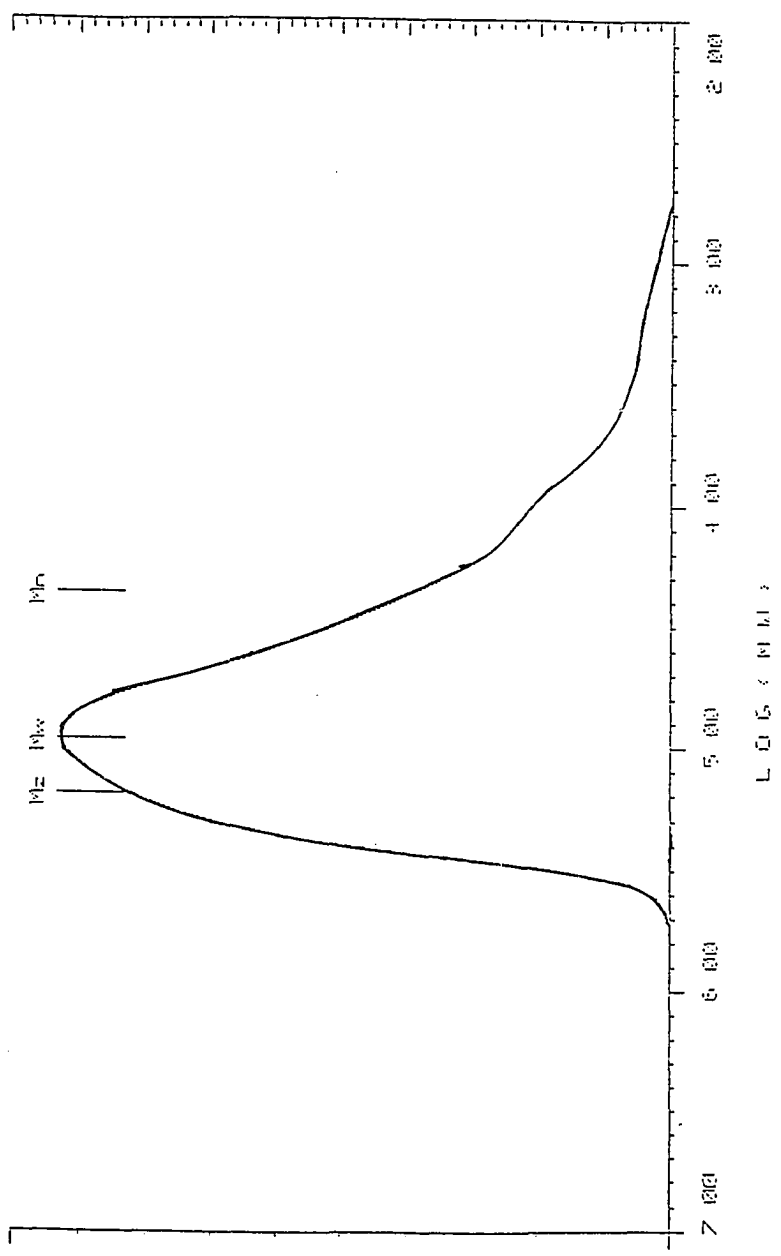

Figure A.12: Size exclusion chromatogram of sample 46-RCH-X-16-3, a dodecyl terminated model associative polymer of 50,700 number average molecular weight as calculated from reaction stoichiometry (C_{12-51}).

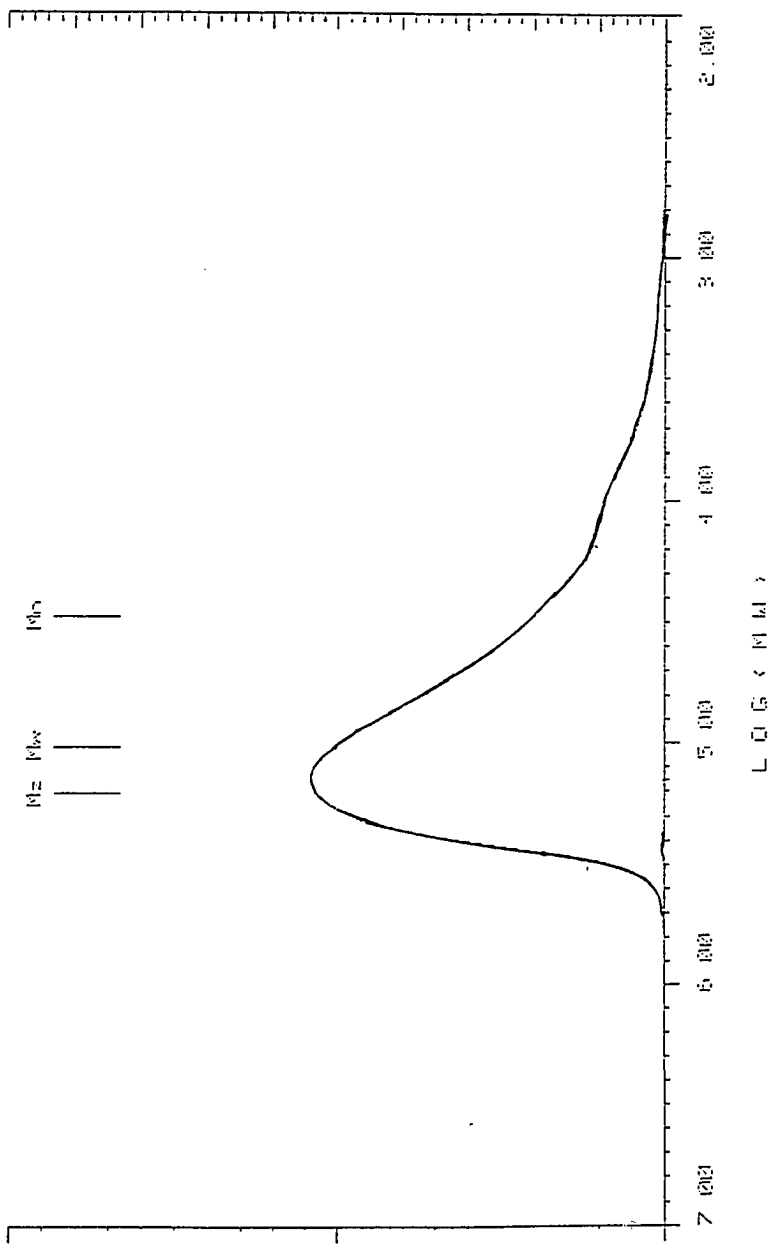

Figure A.13: Size exclusion chromatogram of sample 46-RCH-X-16-4, a dodecyl terminated model associative polymer of 67,700 number average molecular weight as calculated from reaction stoichiometry ($C_{12\text{-}68}$).

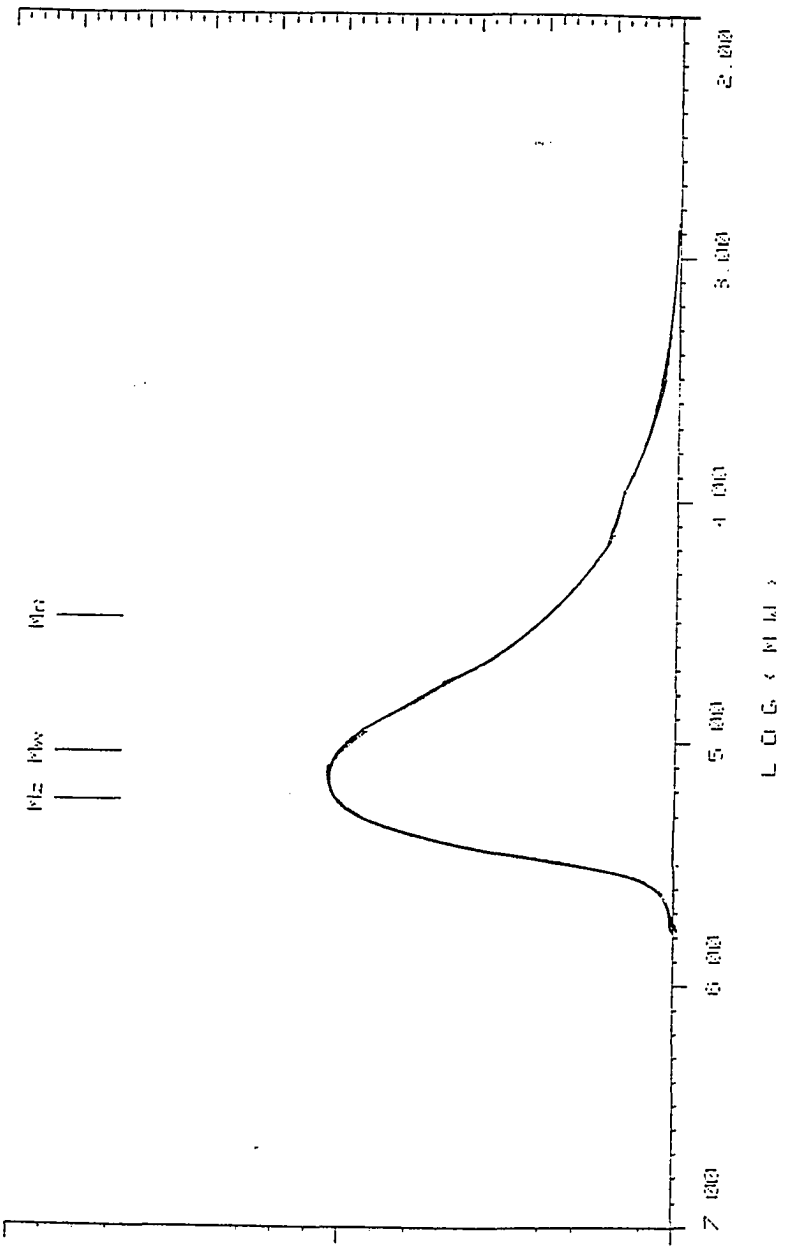

Figure A.14: Size exclusion chromatogram of sample 46-RCH-X-16-5, a dodecyl terminated model associative polymer of 84,500 number average molecular weight as calculated from reaction stoichiometry (C_{12-85}).

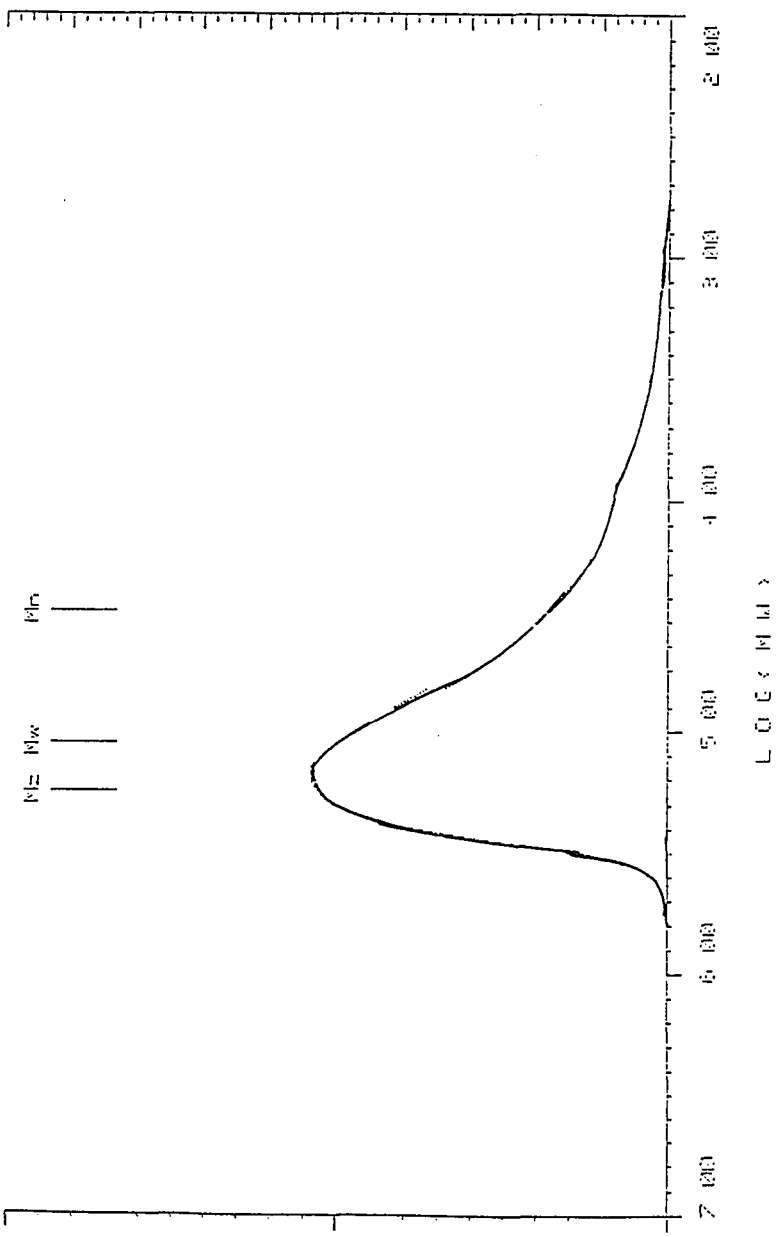

Figure A.15: Size exclusion chromatogram of sample 46-RCH-X-16-6, a dodecyl terminated model associative polymer of 99,900 number average molecular weight as calculated from reaction stoichiometry ($C_{12\text{-}100}$).

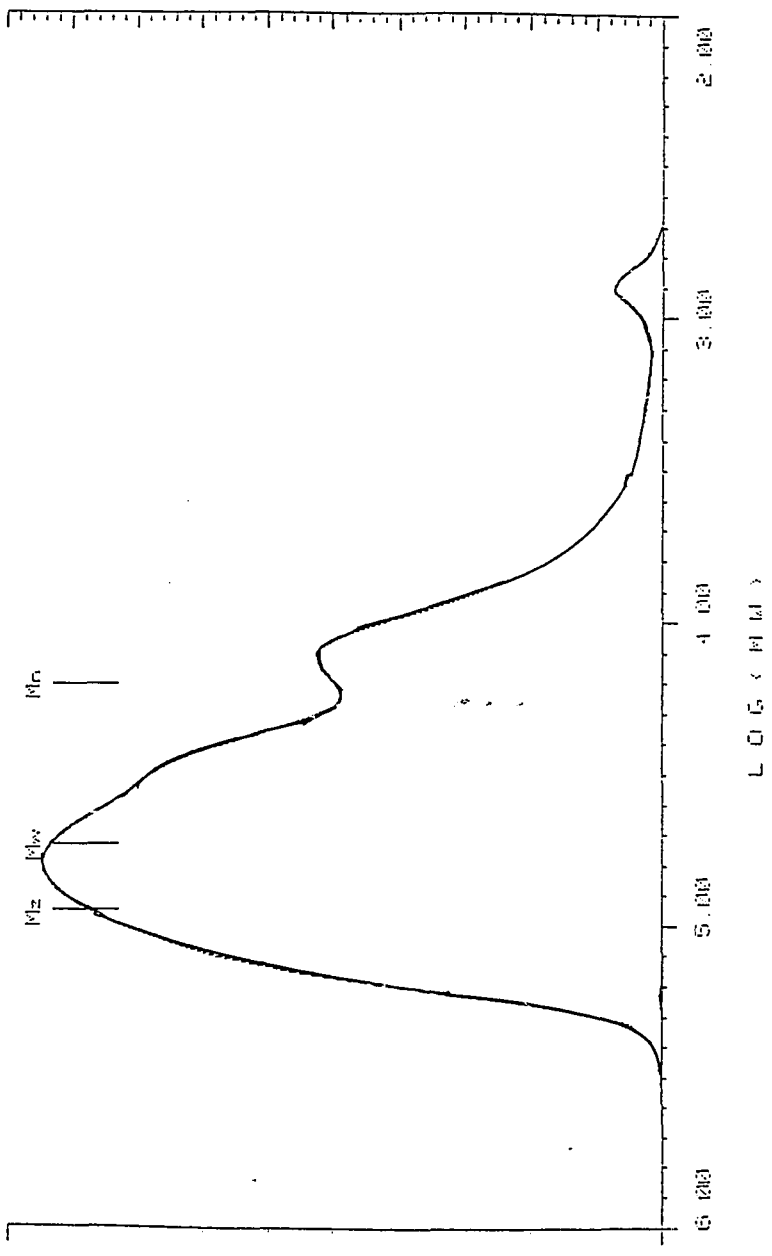

Figure A.16: Size exclusion chromatogram of sample 46-RCH-X-22-1, a hexadecyl terminated model associative polymer of 17,500 number average molecular weight as calculated from reaction stoichiometry (C_{16-18}).

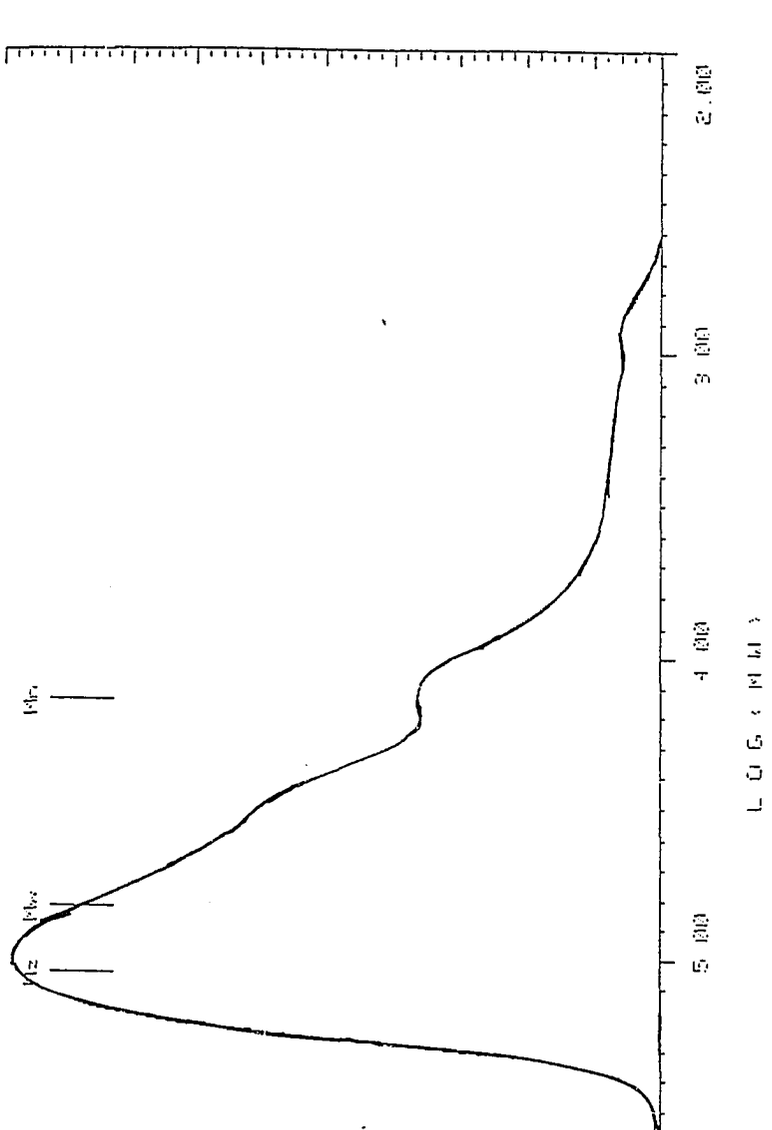

Figure A.17: Size exclusion chromatogram of sample 46-RCH-X-22-2, a hexadecyl terminated model associative polymer of 34,200 number average molecular weight as calculated from reaction stoichiometry (C_{16-34}).

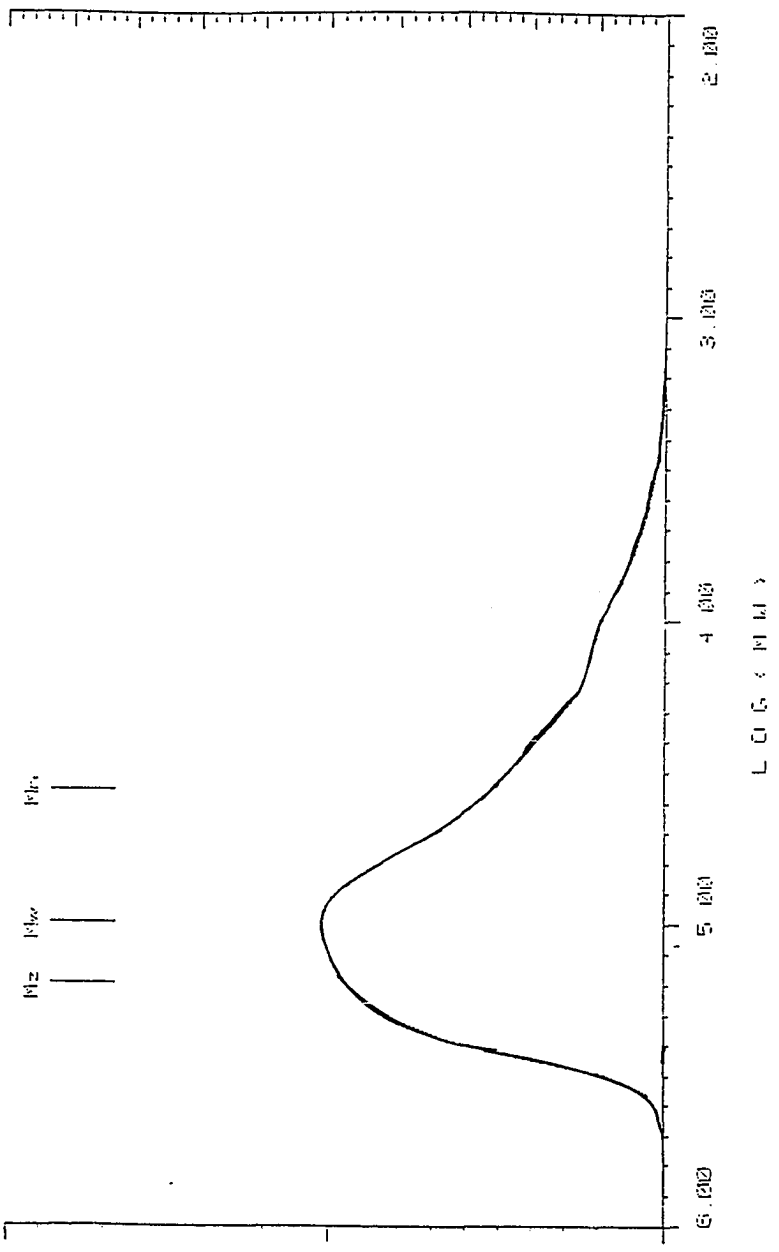

Figure A.18: Size exclusion chromatogram of sample 46-RCH-X-22-3, a hexadecyl terminated model associative polymer of 51,000 number average molecular weight as calculated from reaction stoichiometry ($C_{16\text{-}51}$).

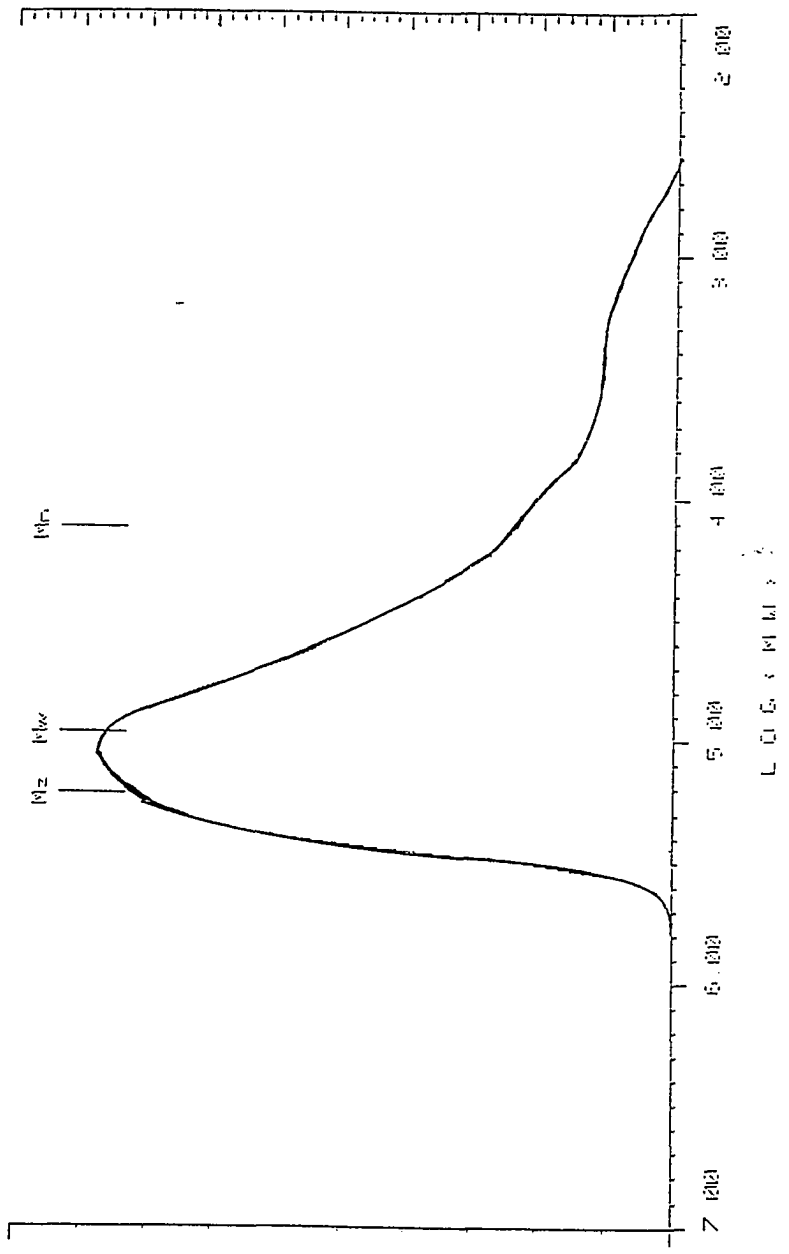

Figure A.19: Size exclusion chromatogram of sample 46-RCH-X-22-4, a hexadecyl terminated model associative polymer of 67,600 number average molecular weight as calculated from reaction stoichiometry (C_{16-68}).

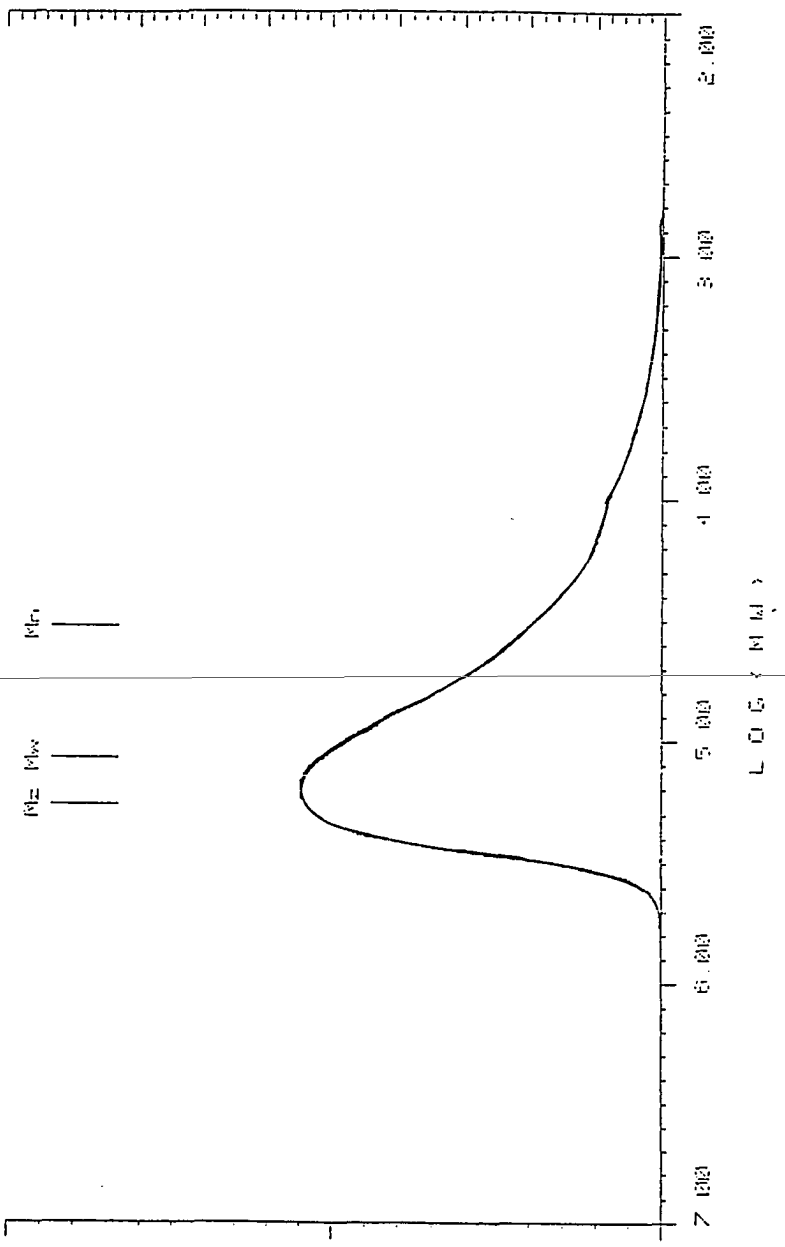

Figure A.20: Size exclusion chromatogram of sample 46-RCH-X-22-5, a hexadecyl terminated model associative polymer of 84,300 number average molecular weight as calculated from reaction stoichiometry ($C_{16\text{-}84}$).

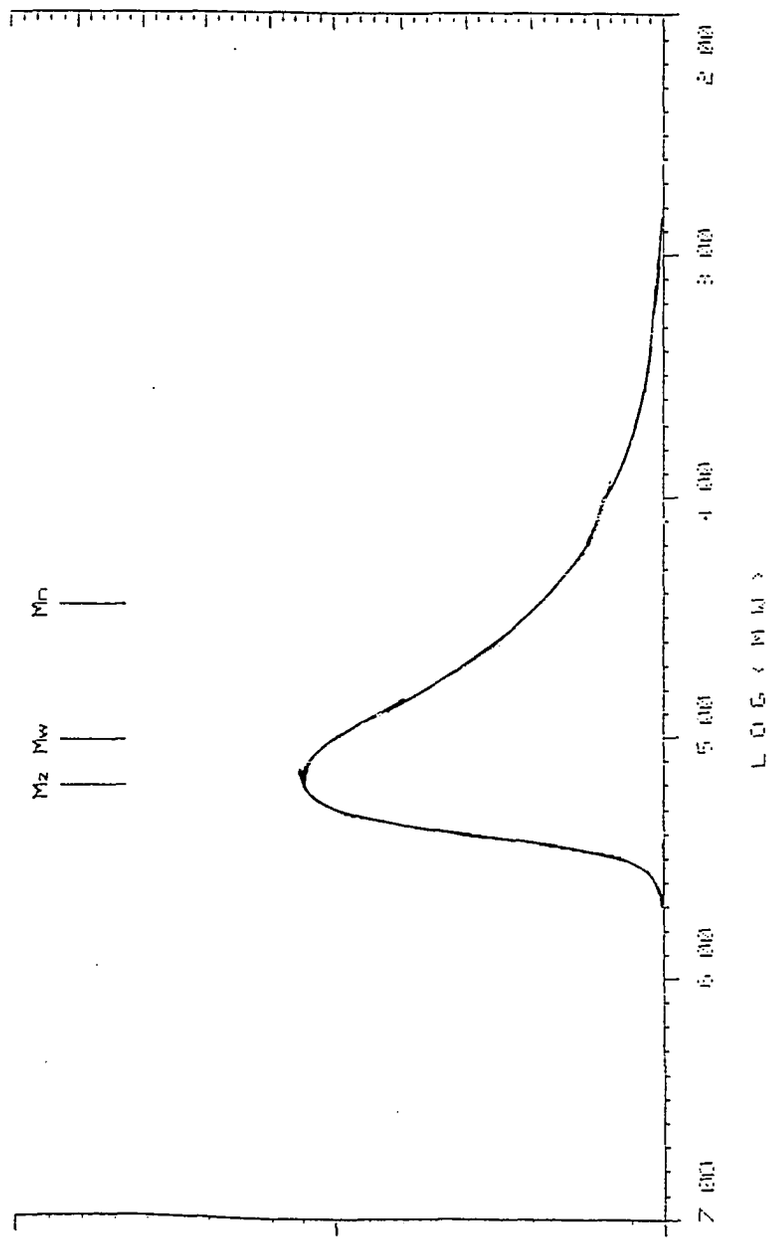

Figure A.21: Size exclusion chromatogram of sample 46-RCH-X-22-6, a hexadecyl terminated model associative polymer of 100,400 number average molecular weight as calculated from reaction stoichiometry ($C_{16\text{-}100}$).

magnitude of the benchmark molecular weight that we choose. It is enough for most purposes that the molecular weights within a given polymer series increase systematically.

Intrinsic Viscosities in Solvent Mixtures of Butyl Carbitol and Water

To independently verify the molecular weights of the model associative polymers, we measured their viscosity average molecular weights in a 40/60 mixture of Butyl Carbitol and water. Butyl Carbitol can eliminate the interactions among associative polymer hydrophobic groups in solution. The proof is in Figures 2.7 and 2.8 of Chapter II, which show that the specific viscosities of associative polymer solutions of a few weight percent solids decrease dramatically in mixtures of Butyl Carbitol and water, and that the viscosities of dilute solutions of associative polymers of equivalent molecular weight are the same regardless of hydrophobe type. Also, the Huggins parameter of all of the model polymers have a "normal" value of 0.4 in the cosolvent mixture, and a plot of the reduced viscosity against concentration is linear for all of the model polymers. These results also indicate that the cosolvent mixture has blocked the formation of an association network. Figure A.3 plots the intrinsic viscosities of the model thickeners and of poly(oxyethylene) standards against their viscosity average molecular weights as obtained by size exclusion chromatography. Table A.2 summarizers the molecular weight distributions of the poly(oxyethylene) standards; use of the poly(oxyethylene) standards to calibrate the Mark - Houwink Equation (Equation (2.8)) yields $[\eta] = 2.84 \times 10^{-4} M_V^{.692}$. Table A.1 shows that the viscosity average molecular weights obtained by intrinsic viscosity compare quite favorably to those obtained by size exclusion chromatography.

The average molecular weight calculated from intrinsic viscosity is very sensitive to the molecular weight distribution of the sample. Hence, we must correct the Mark - Houwink parameter K, which multiplies the viscosity average molecular weight in the

expression given in the previous paragraph, for the molecular weight distribution if we wish to calculate the number average molecular weight of the polymer from intrinsic viscosity data. Kurata et al. [58] and Newman et al. [57] both give methods to calculate this correction. The magnitude of the correction depends both on the magnitude of Mark-Houwink exponent and on the polydispersity index. We know both of these from the intrinsic viscosity data for poly(oxyethylene), and from the size exclusion chromatography. As an example of a typical value of the correction for the model polymers, when the Mark-Houwink exponent equal to 0.7, and when the polydispersity index equals 3, the correction K_n/K_{exp} equals 2.0, where K_n is used to calculate the number average molecular weight of the polymer, and K_{exp} is the experimentally measured value of the Mark-Houwink parameter. Table A.1 shows that the number average molecular weights calculated from this method agree fairly well from the number average calculated from size exclusion chromatography.

Conclusions

This appendix has shown that the model associative polymers have rather broad molecular weight distributions, and that the number average molecular weight of the model polymer calculated from reaction stoichiometry serves as a convenient benchmark molecular weight. The polydispersity of the samples is an unavoidable consequence of the synthetic method. Although the breadth of the distribution hinders some of the calculations from the intrinsic viscosity experiments, it does not invalidate any of the conclusions presented in this dissertation. Nonetheless, future experimental work with these particular model polymers should use fractionated samples, obtained perhaps by dialysis or by precipitation using Moacanin's method [56].

Appendix B

Degradation and Aging of Model Associative Polymers in the Solid State and in Solution

Introduction

Although all of the data presented in Chapters II through VI were collected on one set of model associative polymers, we have actually performed experiments on several different sets; we learned the hard way that the model polymers can degrade when in the solid form and when in solution. This appendix describes our data for the degradation of the polymers, its affect on solution rheology, and how we combated the problem. We also detail the procedure by which we make our stock solutions of model associative polymer. We bother to present this information in some detail because the properties of the model latex systems and solutions can apparently depend upon the procedure used to make them, and their age.

Results and Discussion

Chemical Degradation

We consider two series of model thickeners: an "old" set (labelled series 57,58,59) and a "new" set (labelled series 16,22,23). The structure and nomenclature of the old and new series of model thickeners are presented in Tables B.1 and 2.1 respectively, and the data presented in Chapters II through VI were obtained with the new series. Figures B.1 and B.2 show that the response of the two series of thickeners just after synthesis to the quality control test (as described in Appendix A) are nearly the same, so we conclude that

Table B.1: Structure and Nomenclature of the Old Model Associative Polymer Series§

R-O-(DI-PEG)Y-DI-O-R **

Union Carbide Notebook Name	Reference*	Structure R	Y	Calculated† Mole. Wt.
32-RCH-X-57-1	C_{12}-55	$C_{12}H_{25}$	6	54,400
32-RCH-X-57-2	C_{12}-71	$C_{12}H_{25}$	8	71,300
32-RCH-X-57-3	C_{12}-90	$C_{12}H_{25}$	10	89,600
32-RCH-X-57-4	C_{12}-108	$C_{12}H_{25}$	12	107,700
32-RCH-X-58-1	C_{16}-54	$C_{16}H_{33}$	6	54,400
32-RCH-X-58-2	C_{16}-72	$C_{16}H_{33}$	8	72,300
32-RCH-X-58-3	C_{16}-90	$C_{16}H_{33}$	10	90,200
32-RCH-X-58-4	C_{16}-108	$C_{16}H_{33}$	12	108,000
32-RCH-X-59-1	C_0-53	H	6	53,400
32-RCH-X-59-2	C_0-71	H	8	71,400
32-RCH-X-59-3	C_0-89	H	10	89,300
32-RCH-X-59-4	C_0-107	H	12	107,100

§ Kindly provided by Union Carbide Corporation.

** DI is isophorone diisocyanate, and PEG is Carbowax® 8000 with a nominal molecular weight of 8200.

* The first subscript indicates the length of the alkyl endgroup, denoted R, and the second subscript indicates the molecular weight of the model associative polymer in thousands.

† Number average molecular weight calculated from reaction stoichiometry [25].

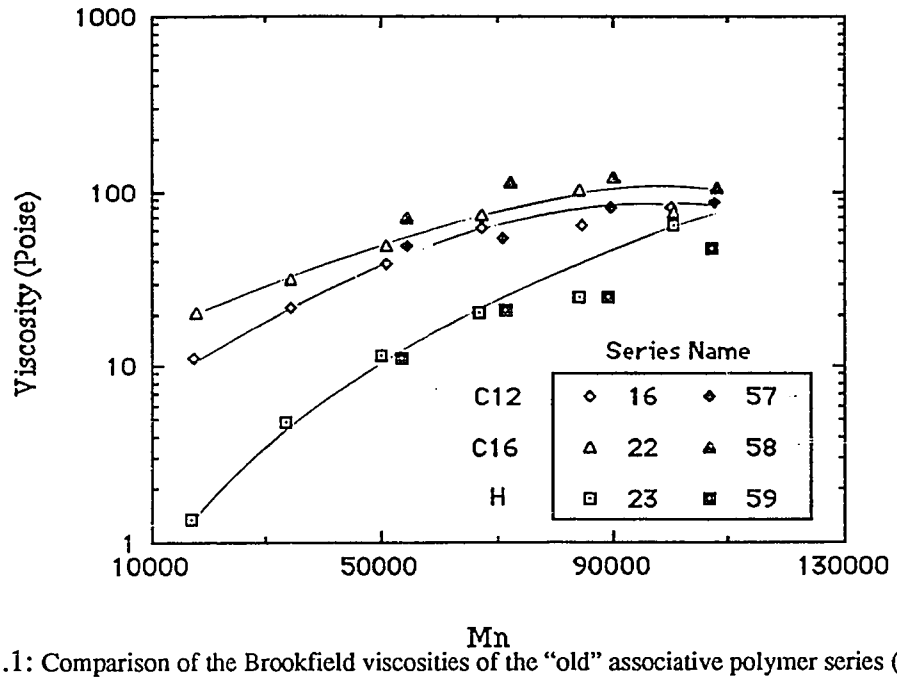

Figure B.1: Comparison of the Brookfield viscosities of the "old" associative polymer series (57, 58, 59) to the "new" associative polymer series (16, 22, 23). Solutions are 20% solids by weight in a 20%/80% by weight Butyl Carbitol and water solvent mixture at 23°C. Diamonds, triangles, and squares denote dodecyl, hexadecyl, or hydroxyl end - groups respectively. Open and filled symbols denote the new and old series, respectively. Data courtesy of reference [25].

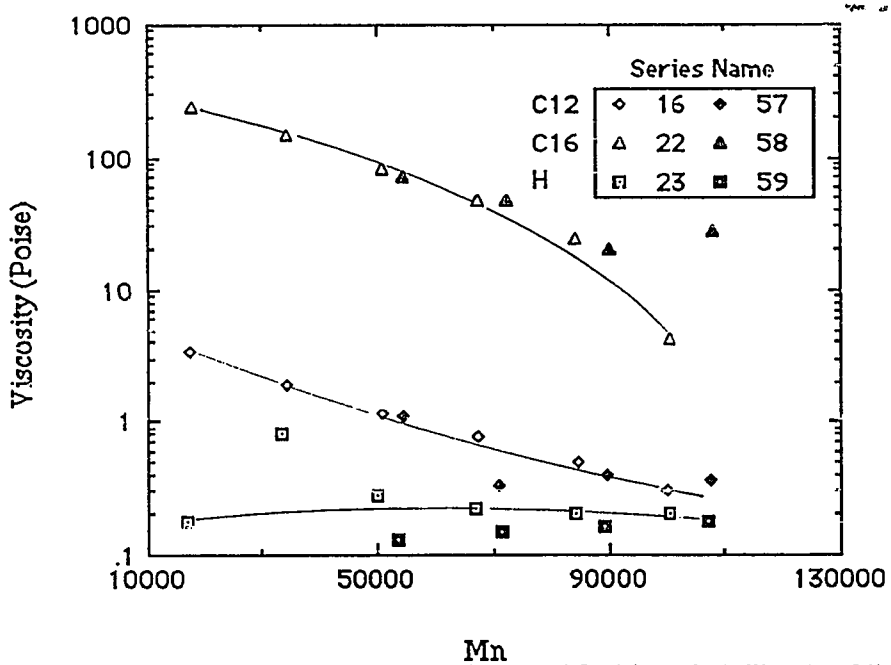

Figure B.2: Brookfield viscosities at 23°C of the solutions used for Figure B.1 diluted to 2% solids with water. Symbols have the same meaning as in Figure B.1. Data courtesy of reference [25].

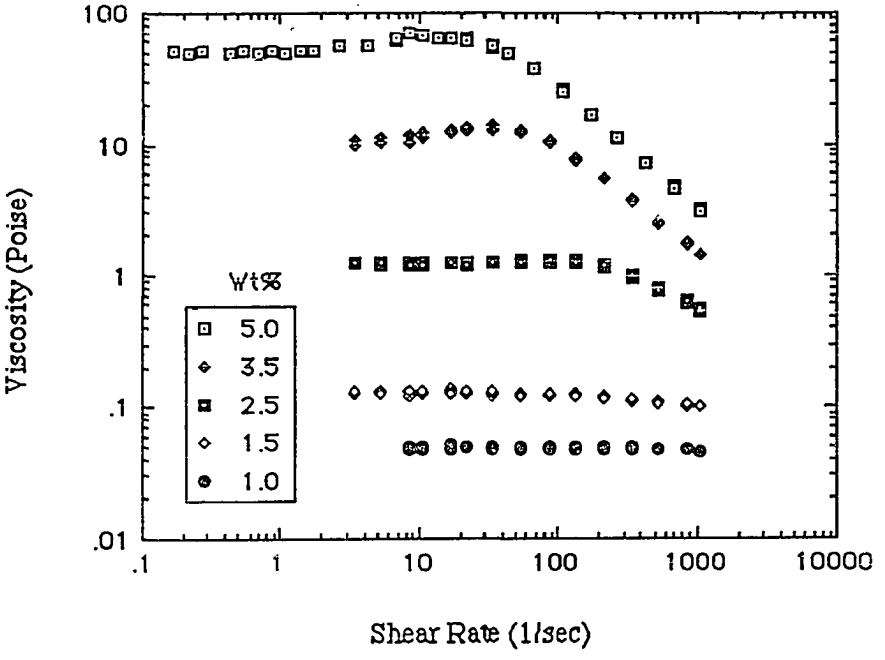

Figure B.3: Steady shear viscosity profiles of aqueous solutions of a degraded hexadecyl terminated model associative polymer with an original number average molecular weight of 54,400.

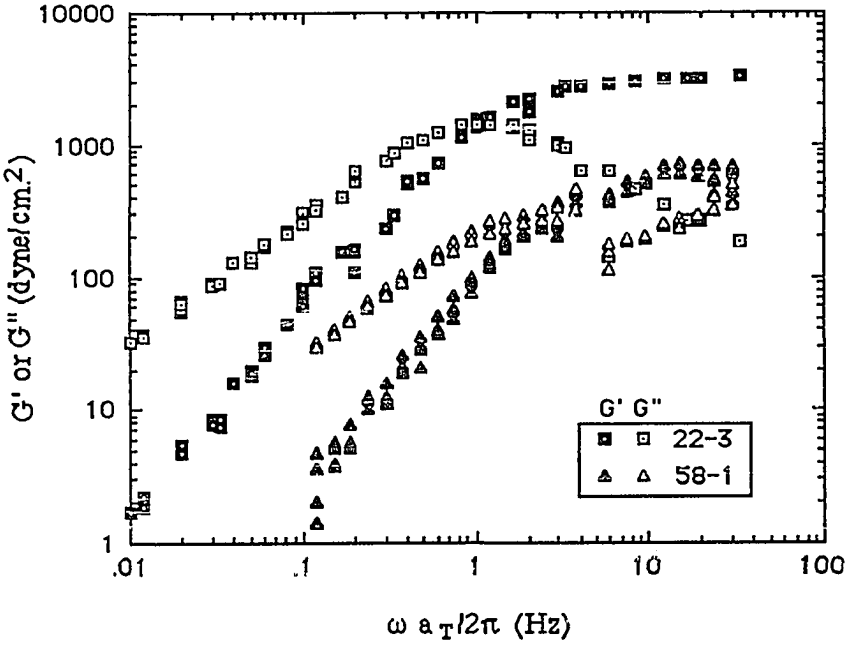

Figure B.4: Dynamic shear moduli of 5% aqueous solutions of hexadecyl terminated polymers of approximately 51,000 number average molecular weight just after synthesis. Solutions are both one week old.

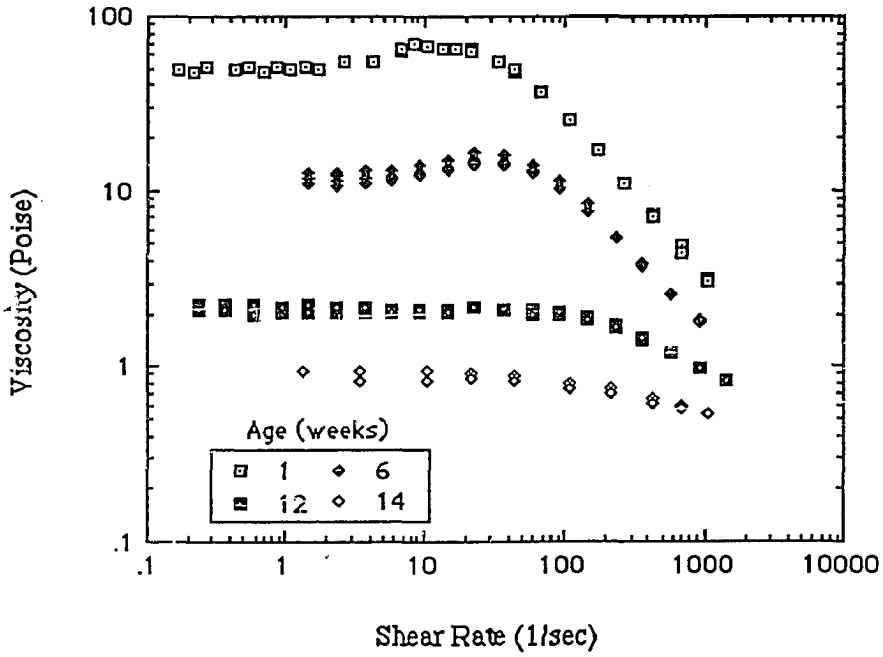

Figure B.5: Degradation of a 5% aqueous solution of a hexadecyl terminated model associative polymer with an original number average molecular weight of 51,000.

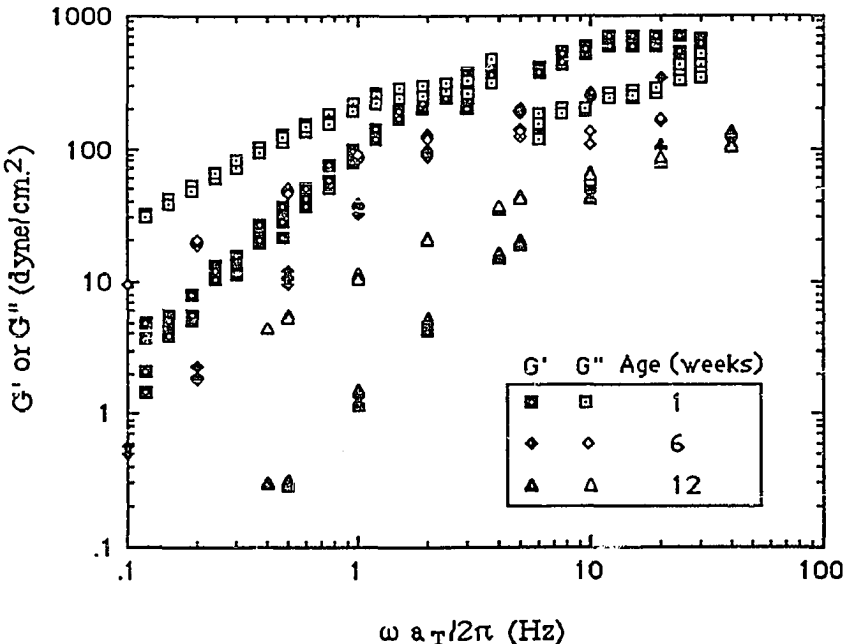

Figure B.6: Influence of aging on the dynamic shear moduli of a 5% aqueous solution of a hexadecyl terminated model associative polymer with an original number average molecular weight 54,400.

the two series of model thickeners were virtually identical at birth. The difference between the new set and the old set is that the old set degraded while in the solid form, and since the two series were nearly identical at birth, we can take advantage of our misfortune to learn how chemical degradation affected the solution properties of model associative polymers.

Poly(oxyethylene) degrades primarily via a free radical auto- oxidation process which decomposes the polymer by chain cleavage [49], and although 100 ppm of butyl hydroxy toluene (BHT) antioxidant had been added to the solid polymer of the old associative polymer series, it was not mobile enough in the solid polymer enough to inhibit the formation of peroxides. In addition, the solid polymer of the old associative polymer series had been flaked to promote dissolution, and this exposed a large surface area of polymer to the oxygen in the atmosphere to exasperate the degradation process. The result is a decrease in the rheological properties of solutions that are made from the same solid polymer as it ages. For example, a 5% solution of a hexadecyl terminated polymer with an original number average molecular weight of 54,400 (i.e., sample 32-RCH-X-58-1) had a low shear viscosity of 50 Poise in June of 1987, and a 5% solution made from the same solid polymer in March of 1988 had a low shear viscosity of only 20 Poise. Nonetheless, these polymers are still capable of forming an association network in solution. Like their counterparts made from undegraded polymers, solutions of the old model polymer exhibit the characteristic shear - thickening region in the steady shear viscosity profile, and have low shear viscosities that depend strongly on the concentration of associative polymer (Figure B.3), although both of these effects are less pronounced than in solutions of the undegraded polymer. It is clear that the inhibitor that was added to the old series of solid model polymer did not do its job.

The influence of degradation on the association is perhaps better reflected in the viscoelastic properties of solutions. Figure B.4 compares the viscoelastic properties of 5%

solutions made from 32-RCH-X-58-1 and 46-RCH-X-22-3 of the old and new series, respectively. These model polymers both have hexadecyl hydrophobes and have about the same molecular weight (54,400 as compared to 51,000). Of course, chemical degradation lowers the magnitude of the moduli and broadens the relaxation spectrum of the solution. This is seen as an inflection in the loss modulus at high frequencies of the sample marked 58-1 in Figure B.4. (Recall from Chapter III that, to the zeroth order approximation, the frequency dependence of the loss modulus has the same functional dependence that the relaxation spectrum has on the relaxation time constant, and that the relaxation time constant scales with the reciprocal of frequency). This broadening in the relaxation spectrum is expected because degradation should broaden the molecular weight distribution of the associative polymers in solution.

Figures B.5 and B.6 demonstrate the decrease in the steady shear viscosity and the dynamic moduli, and the loss of the entanglement plateau in the storage modulus, with age of a solution of the hexadecyl terminated model associative polymer 32-RCH-X-58-1 . We made two experiments to confirm whether this was due to chemical degradation or physical aging. First, we dried the 5% thickener solution of Figures B.5 and B.6 at room temperature until no change in mass was detected in the remaining solids, and recovered the associative polymer. This polymer was redissolved in a five milliMolar sodium dodecyl sulfate solution: if the solution properties returned to their original state, then the change was due to physical processes; if not, then some type of chemical change must have occurred. The intrinsic viscosity of the recovered polymer in the sodium dodecyl sulfate solution at 50°C was 0.21, which when compared to the intrinsic viscosity of 0.41 for 32-RCH-X-58-1 in a freshly made solution indicates that considerable chemical degradation of the polymer in solution had occurred. Second, because poly(ethylene glycol) degrades through a free radical mechanism, we added potassium iodide to the thickener solutions.

Any free radicals that exist in the solution will decompose the potassium iodide and turn the solution yellow. The solutions used in Figure B.5 and B.6 turned yellow. Thus, the associative polymers also degrade when it is in solution, unless it is protected from peroxides.

Even though the associative polymer solutions degrade, their rheological properties are similar to solutions of the undegraded samples described in the previous portion of the dissertation. The samples retain some of their ability to network, as evidenced by the entanglement plateau and shear-thickening, and the rheological properties of these degraded polymers still scale with the number density of association junctions. The data for these solutions would fall on the lines in Figures 3.22 and 3.23 of Chapter III. The effect of methanol, ethanol, Butyl Carbitol, and other cosolvents have the same effect on the solutions of degraded polymers as they do for solutions of the undegraded polymers, both in concentrated and dilute solution.

Solution Preparation

To protect the "new" series of model associative polymer against degradation while in the solid form, Union Carbide doubled the concentration of BHT in the solid polymer to 200 ppm. We stored the polymer under a nitrogen atmosphere in a refrigerator at 4°C, and used the model polymer as supplied without further purification. Stock solutions of 5% model associative polymer by weight were prepared by adding a weighed amount of polymer to double distilled deionized water. Once in water, the polymer swelled to form a gel–like layer at the bottom of the glass container. The time period required to swell the polymer was inversely proportional to the molecular weight of the dissolved polymer, and could take up to a month. The gel–like layer was dispersed by periodic gentle agitation during the swelling period to produce a cloudy and viscous solution which appeared

homogeneous to the unaided eye. Because we were concerned about mechanical degradation, we chose not to roll the solution in a tumbler to accelerate the dissolution process. We added 5 - 15 ppm of hydroquinone, and stored the stock solutions out of light to add extra protection against chemical degradation. The solutions were not stored in the refrigerator since they exhibited a lower critical solution temperature. All solutions were made by dilution of these stock solutions.

Because of the possibility of chemical degradation, we chose to make up batches of 300 grams of the 5% stock solutions as needed, rather than to make up one large stock solution. In this way, we could conserve what precious little model associative polymer we had, and we could minimize the quantity of associative polymer solution that would age and possibly degrade.

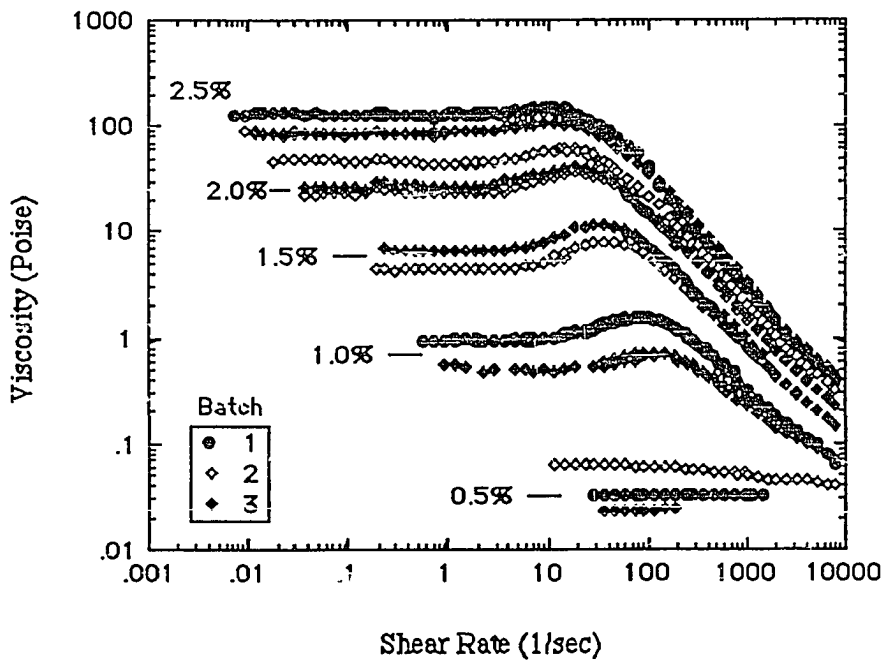

Figure B.7: Batch - to - batch variations in the viscosity profiles of aqueous solutions made from three different stock solutions of a hexadecyl terminated model associative polymer with a number average molecular weight of 51,000.

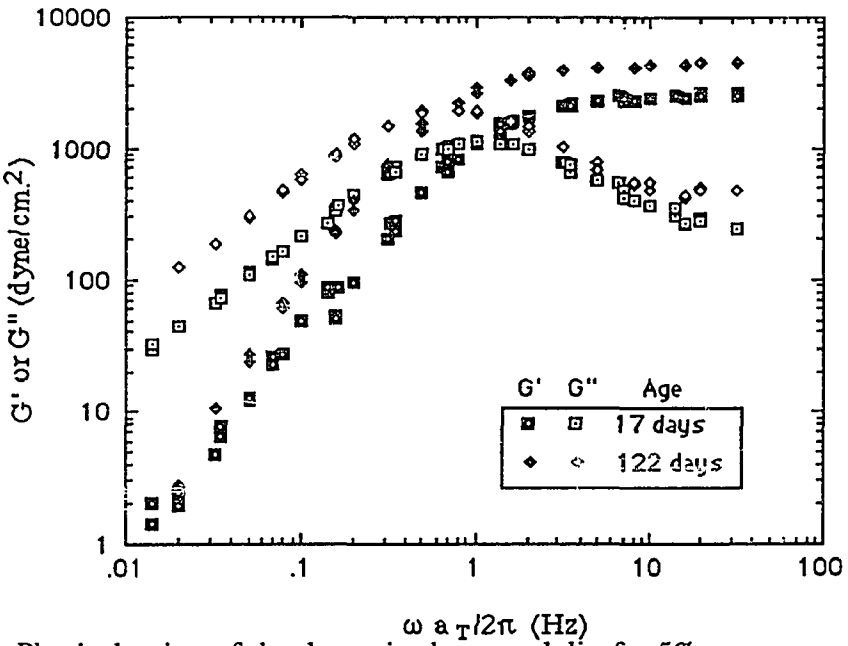

Figure B.8: Physical aging of the dynamic shear moduli of a 5% aqueous solution of a hexadecyl terminated model associative polymer of 67,600 number average molecular weight. The solution has been protected against chemical oxidative degradation by hydroquinone.

However, this created an unexpected problem with the stock solutions of the hydrophobically terminated model polymers: batch - to - batch variations in the viscosity of the stock solutions. In total, we made two to three batches of each model polymer. Figure B.7 presents the viscosity profiles of the batches made of the hexadecyl terminated polymer with a number average molecular weight of 51,000. Although the profiles are similar from batch to batch, small variations do exist. It is not clear whether this is simply an aging phenomenon, or the result of the dissolution history of the stock solution. We had not attempted to study this feature, as we tried to keep the dissolution history from batch to batch as constant as possible. (We discovered the problem in hindsight). The small batch-to -batch deviations confound any comparisons that we could make between systems made from different stock solutions. Thus, it is imperative to always repeat the control experiments for solution rheology for each and every stock solution. Likewise, all of the

measurements of model latex systems made from a given stock solution should all be made at one given instant in time. Although this is slightly inconvenient, this prevents the batch - to -batch variations from invalidating any of the conclusions that we draw in this dissertation.

Depending on the concentration of associative polymer that is added to a latex, the latex would either remain stable, or would apparently flocculate. For example, diluting the stock solutions first and adding the latex would produce a stable dispersion, whereas adding the same quantity of associative polymer in its concentrated form would produce a lumpy and apparently flocculated latex. Thus, the stability and rheological properties of latexes that contain associative polymer can be a product of process. This might be important in latex systems that contain surfactants, where the relative order of the addition of associative polymer and surfactant could dictate how much of each species adsorbs at the particle interface. Although this is something that deserves more study, we chose to simply add all of the ingredients of the model latex systems reported in Chapter VI simultaneously, and let nature take its course.

Physical Aging

Solutions of associative polymers that have been protected against chemical and mechanical degradation have rheological properties that increase with storage time. McCormick and Johnson [126] observed that it often took many weeks for their solutions of hydrophobically modified N-alkylacrylamide-acrylamide copolymers to reach a constant apparent viscosity. Figure B.8 shows how the viscoelastic properties of a stock solution of a hexadecyl terminated model associative polymer with a molecular weight of 67,600 increased with age. Likewise, the low shear viscosity increased from 386 Poise at 17 days of age to 800 Poise after 127 days of age (four months and one week!), and the intrinsic

viscosity of the polymers in the stock solution increased from 0.981 at 17 days of age, to 1.40 after 127 days of age. These results indicate that the association network can build continuously, and can take many months to reach equilibrium. Because all of the rheological measurements were made on model systems that were of nearly the same age, and because we do not compare model systems made from stock solutions of different ages, the effect of aging does not influence any of the comparisons that we make in this dissertation.

Conclusions

To stabilize the model associative polymers against chemical degradation, store solutions and the model polymer in a cool, dark place, and always use a water soluble anti - oxidant when dissolving the solid polymer. It also helps to minimize surface area of solid polymer, and to store it in an inert atmosphere. Variations can occur from batch - to - batch of the associative polymer stock solutions, so it is mandatory to repeat the control experiments with each stock solution. Although formulation ingredients have the same qualitative effects on all of the stock solutions, sometimes minor quantitative differences can exist, so we can only compare model systems that have been made from the same stock solution. The dissolution history and age of the associative polymer solution can influence its rheological properties, which suggests that the associative polymers are aggregated when in the solid form, and that both aggregates and single associative polymer chains dissolve to form the solution.

Vita of Richard D. Jenkins

Richard D. Jenkins was born the eldest son of Don and Jeanne Jenkins in Logansport Indiana, on June 26 in 1964. They moved many times during his childhood, but they settled briefly in Texas. There he matriculated from Plano Senior High School in 1982, and from Texas A&M University with a Bachelor of Science degree in chemical engineering in the spring of 1986. Also in 1986, Richard was elected to the Tau Beta Pi and Omega Chi Epsilon national engineering honor societies. While at A&M, Richard was designated a University Undergraduate Research Fellow, and conducted research on turbulent drag reduction under the guidance of Ron Darby. This work resulted in a senior honors thesis entitled Turbulent Drag Reduction Modelling.

After graduation from A&M, Richard emigrated to Pennsylvania to complete his graduate studies in chemical engineering at Lehigh University. He held a number of departmental and graduate school sponsored fellowships and scholarships, including the Air Products Company Distinguished Fellowship from 1986-1987, and the Byllesby Fellowship for 1989-1990. He conducted research on associative polymers, and on the modelling of capillary hydrodynamic chromatography, and he wrote proposals and received externally funded grants in these research areas. He received the Hoechst - Celanese award for excellence in polymer science for his work on associative polymers in November of 1988. He also made presentations at a number of national meetings of the American Chemical Society and American Institute of Chemical Engineers in Los Angeles, Houston, Miami Beach, and Bethlehem, and also attended the NATO ASI short course on polymer colloids in Strasbourg France in the summer of 1988. During the summer of 1990, he held the post of visiting lecturer in chemical engineering at Lehigh, and taught an undergraduate course on mathematical modelling and process control. After graduation from Lehigh with a Doctor of Philosophy in chemical engineering, Richard was employed by Union Carbide Corporation at their research and development facilities in Charleston, West Virginia.

Richard married the former Mary Rayl of Dallas, Texas, in the summer of 1984, and they were blessed with an exceptional son, Collin, in the spring of 1990.